

# **Soil-Atmosphere Exchange of PAHs: The Determination of Concentration Gradients with Passive Samplers**

DISSERTATION

der Mathematisch-Naturwissenschaftlichen Fakultät  
der Eberhard Karls Universität Tübingen  
zur Erlangung des Grades eines  
Doktors der Naturwissenschaften  
(Dr. rer. nat.)

vorgelegt von  
**JANA MEIERDIERKS**  
aus Lilienthal

Tübingen  
2019



Gedruckt mit Genehmigung der Mathematisch-Naturwissenschaftlichen Fakultät der  
Eberhard Karls Universität Tübingen.

Tag der mündlichen Qualifikation: 24.06.2019

Dekan:	Prof. Dr. Wolfgang Rosenstiel
1. Berichterstatter:	Prof. Dr. Peter Grathwohl
2. Berichterstatter:	Jun. Prof. Dr. Christiane Zarfl





FÜR PAUL



## Abstract

Polycyclic aromatic hydrocarbons (PAHs) as a group of ubiquitously occurring organic pollutants are released into the atmosphere by combustion processes of organic materials. Parallel to the beginning of industrialisation (1870), PAH accumulation in soils is clearly evident. With increasing environmental protection, about one century later, the emission and thus concentrations of PAH in the atmosphere decrease. Variations in the atmosphere significantly influence the relationship and equilibrium conditions of PAH between soil and air. Accordingly, low emissions can induce a change in the function of soils as pollutant sinks towards a secondary source. The aim of this study is to identify the current pollutant flux of PAHs between atmosphere and soil as well as potential temporal variations. Figure 0.1 illustrates the different distribution processes of PAH in atmosphere and soil and thus the complexity of respective net fluxes.

Passive samplers serve as chemometers, i.e. equilibrium concentrations of PAHs in the samplers reflect their activity in the respective sampled medium. In this way, concentrations on the samplers can be directly compared to identify the current direction of PAH flow between atmosphere and soil. As a control on equilibrium concentrations on the passive samplers, active sampling in air was conducted and sorption behaviour of PAHs in the examined soils was measured. At three sites in the rural surroundings of Tübingen, soil profiles were sampled and seasonal monitoring of PAH concentrations in the atmosphere in the gas phase and bulk deposition was carried out. The individual sites are very comparable in both soil characteristics and in PAH concentrations in atmosphere, deposition and soil. Differences result mainly from the agricultural use at two sites and the associated regular mixing of the plough horizon. Seasonal monitoring in the atmosphere shows a clear correlation of (up to 5-fold) higher PAH concentrations during the indoor heating period in autumn and winter compared to spring and summer. In the atmospheric bulk deposition this seasonal variation is even more pronounced with a factor of 30. Temperature-dependent sorption and lower summer emissions imply temporary fluctuations with short-term outgassing of semi-volatile components (up to pyrene) from soils. Stable PAH distribution patterns at the three sites as well as for the different monitorings indicate a good air mixing and constant source profiles in the investigated region. Constant concentration ratios among all analyzed substances allow the use of a single substance as a reference compound for the calculation of concentrations of the other target substances. Identical distribution patterns were determined for atmospheric particles and within the bulk soil confirming particle-bound deposition of PAHs as the main input into the soil. This results in a continuous flux of PAHs from the atmosphere into the soil, and consequently defines soils overall as long-term sinks for this group of substances.

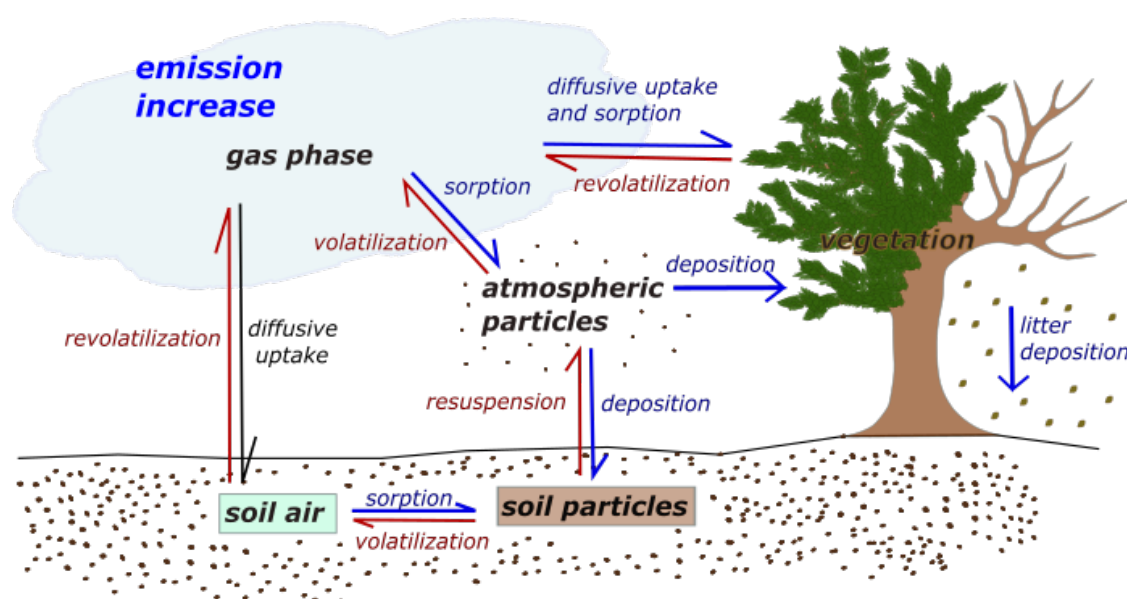


Figure 0.1: Scheme of redistribution processes of PAHs in the environment with respect to the gas phase in atmosphere and soils, particles in atmosphere and soils as well as vegetation. Temperature dependent fluxes are indicated with colours: blue arrows depict the flux direction for cold temperatures and red arrows mark the flux direction for warm temperatures.

## Zusammenfassung

Polyzyklische Aromatische Kohlenwasserstoffe (PAK) als Gruppe ubiquitär auftretender, organischer Schadstoffe werden durch Verbrennungsprozesse von organischen Materialien in die Atmosphäre freigesetzt. Parallel zum Beginn der Industrialisierung (1870) zeigt sich eine deutliche Anreicherung von PAK in Böden. Mit zunehmendem Umweltschutz, etwa ein Jahrhundert später, verringern sich die Emissionen von PAK und damit ihre Konzentrationen in der Atmosphäre. Variationen in der Atmosphäre beeinflussen maßgeblich das Verhältnis von PAK in Boden und Luft. Dementsprechend können niedrigere Emissionen eine Änderung der Funktion von Böden als Schadstoffsенke hin zu einer sekundären Quelle induzieren. Das Ziel dieser Studie liegt in der Identifizierung des aktuellen Schadstoffflusses der PAK zwischen Atmosphäre und Boden sowie potentiellen zeitlichen Variationen. Figure 0.1 illustriert die verschiedenen Verteilungsprozesse von PAK in Atmosphäre und Boden und damit die Komplexität dieser Stoffflüsse.

Passivsammler wurden als Chemometer genutzt; Gleichgewichtskonzentrationen der PAK im Sammler reflektieren deren Aktivität in dem jeweilig beprobten Medium. Auf diese Weise können Konzentrationsgradienten auf dem Sammler direkt verglichen werden, um die aktuelle Stoffflussrichtung von PAK zwischen Atmosphäre und Boden zu identifizieren. Zur Kontrolle von Gleichgewichtskonzentrationen auf dem Sammler wurden Aktivsammler in der Luft genutzt und das Sorptionsverhalten von PAK in den beprobten Böden gemessen. An drei Standorten im ländlichen Umland von Tübingen wurden dazu Bodenprofile aufgenommen und saisonale Monitorings von PAK-Konzentrationen in der Atmosphäre für die Gasphase und Gesamtdeposition durchgeführt. Die einzelnen Standorte sind sowohl in Bodencharakteristik als auch an PAK-Konzentrationen in Atmosphäre, Deposition und Boden sehr vergleichbar. Unterschiede ergeben sich hauptsächlich durch die landwirtschaftliche Nutzung an zwei Standorten und die damit einhergehende regelmäßige Durchmischung des Pflughorizonts. Saisonale Monitorings in der Atmosphäre zeigen eine deutliche Korrelation von (bis zu 5-fach) höheren PAK-Konzentrationen während der Heizperiode im Herbst und Winter im Vergleich zu Frühjahr und Sommer. In der atmosphärischen Gesamtdeposition ist diese saisonale Variation noch deutlicher ausgeprägt mit einem Faktor von 30. Temperaturabhängige Sorption und geringere Emissionen im Sommer implizieren temporäre Schwankungen mit kurzzeitiger Ausgasung von semi-volatilen Komponenten (bis hin zu Pyren). Stabile Verteilungsmuster der PAK an den drei Standorten sowie für die verschiedenen Monitorings weisen auf eine gute Durchmischung der Luft und konstante Quellen in der untersuchten Region hin. Konstante Verhältnisse der Stoffe untereinander ermöglichen die Nutzung eines einzelnen Stoffs als Referenzkomponente zur Berechnung von Konzentrationen der weiteren Zielsubstanzen. Identische Verteilungsmuster auf Partikeln in der Atmosphäre und im Boden bestätigen partikelgebundene Deposition als Haupteintragspfad von PAK in den Boden. Daraus ergibt sich ein konstanter Stofffluss von PAK aus der Atmosphäre in den Boden, der weiterhin als Langzeitsenke für diese Stoffgruppe agiert.

## Acknowledgments

An dieser Stelle möchte ich mich bei all den Menschen bedanken, die auf vielfältigste Art und Weise zu dem Gelingen dieser Arbeit beigetragen haben:

An erster Stelle gebührt mein Dank Prof. Dr. Peter Grathwohl, der mir dieses Projekt übertrug und mir dabei die Freiheit ließ meine eigenen Ideen und Ziele zu verfolgen. Vielen Dank dafür und vielen Dank für das gründliche Hinterfragen und Drehen an den wackeligen Schrauben, beides hat diese Arbeit sehr voran gebracht! Ebenso dankbar bin ich für die stets aufmunternde Unterstützung von Jun. Prof. Dr. Christiane Zarfl, die mit ihrer positiven Art immer für ihre Doktoranden da ist. Für die ausgesprochen hilfreiche Unterstützung mit meinen Matlab Codes und vor allem die geduldigen Erklärungen zu fitting-Prozessen bin ich Prof. Dr. Olaf Cirpka sehr dankbar.

Vielen Dank an Prof. Dr. Beate Escher sowie Dr. Annika Jahnke am UFZ Leipzig, die einen produktiven Kontakt zu Dr. Sabine Schäfer und Julia Bachtin bei der BfG geknüpft haben. Und damit natürlich auch vielen Dank an Prof. Dr. Gesine Witt an der HAW Hamburg, die mir die Teilnahme an einem spannenden Methodenaustausch ermöglicht hat.

Mein besonderer Dank gilt dem ZAG-Labor, durch das diese Arbeit überhaupt erst möglich wurde und in dem es soviel Spaß macht zu arbeiten. Vielen Dank für eure Unterstützung in allen Belangen! Eure hilfsbereite Art, euch in meine Probleme hineinzudenken, mir Arbeit abzunehmen, Methoden zu erklären oder einfach mal nur zuzuhören, ich weiß es sehr zu schätzen! Damit ihr auch wisst, dass ich euch meine: Vielen Dank Renate Seelig, Bernice Nisch, Sara Cafisso, Thomas Wendel, Annegret Walz und Stefanie Nowak. Außerdem möchte ich mich bei meinen Hiwis für die unterstützenden Hände bei der Probenahme und -aufbereitung bedanken.

Vor allem die gute Stimmung und die Hilfsbereitschaft unter den *Leidensgenossen* im ZAG weiß ich sehr zu schätzen. Vielen Dank an alle Gegenleser, vor allem Stefan hat mir hier extrem geholfen! Und natürlich die *Hobbithöhlenmitbewohner*: Vielen Dank für eure Unterstützung, hilfreiche Diskussionen und unermüdliches Auffüllen von Kaffee- und Zuckervorräten.

Ein großes Dankeschön geht außerdem an meine Familie, die in dem letzten Jahr viel auf mich verzichten musste und trotzdem aus der Ferne immer für mich da war mit einem beständigen "Du schaffst das schon".

Zuguterletzt vielen Dank an meine Lieblingsmenschen in Tübingen, vielen Dank fürs füreinander da sein und die Zeit vergessen. Vielen Dank Micha, Britta, Eva, Valle und Lars.

Ganz offiziell möchte ich mich natürlich auch bei der Deutschen Forschungsgesellschaft für die Finanzierung dieses Projektes bedanken.

---

# Contents

<b>1</b>	<b>Introduction</b>	<b>1</b>
1.1	Background and Motivation . . . . .	1
1.2	Thesis aim and objectives . . . . .	5
1.3	Quality assurance . . . . .	8
<b>2</b>	<b>Characterization of study sites - land use and soil properties</b>	<b>14</b>
2.1	Study sites and land use . . . . .	14
2.2	Methods . . . . .	15
2.2.1	Soil properties . . . . .	15
2.2.2	Sorption properties; Distribution coefficients . . . . .	16
2.2.3	$C_{w,eq}$ and desorption enthalpies from static leaching tests . . . . .	18
2.3	Results: Soil properties . . . . .	20
2.3.1	Grain size and fraction of organic carbon . . . . .	20
2.3.2	Concentrations of PAHs in vertical soil profiles . . . . .	21
2.3.3	Distribution coefficients and sorption isotherms for Phenanthrene . . . . .	23
2.4	Results: Aqueous concentrations . . . . .	29
2.4.1	Aqueous leachates and desorption enthalpies . . . . .	29
2.4.2	Equilibrium concentrations in pore water . . . . .	30
2.5	Diagnostic ratios and source allocation . . . . .	32
2.6	Discussion . . . . .	36
2.7	Conclusion . . . . .	38
<b>3</b>	<b>Background theory of passive sampling</b>	<b>39</b>
3.1	Double film diffusion model; exemplarily in the atmosphere . . . . .	39
3.2	Numerical model . . . . .	43
3.2.1	Temperature dependent parameters . . . . .	44
3.2.2	Sherwood numbers . . . . .	45
3.2.3	Comparison of calibration approaches . . . . .	46
<b>4</b>	<b>Development of an appropriate sampling set-up in the field</b>	<b>49</b>
4.1	Atmospheric Monitorings - general methodology . . . . .	49
4.2	Preliminary test on diverse sampling-set-ups . . . . .	50
4.2.1	Study design . . . . .	52
4.2.2	Results and discussion . . . . .	54
4.2.3	Discussion . . . . .	65
4.2.4	Conclusion . . . . .	67
4.3	Validation with active sampling . . . . .	68
4.3.1	Method . . . . .	68
4.3.2	Results . . . . .	69
4.3.3	Discussion . . . . .	71

4.3.4	Conclusion . . . . .	72
4.4	Atmospheric uptake: PE sheets vs. PDMS coated jars . . . . .	73
4.4.1	Method . . . . .	74
4.4.2	Results and discussion . . . . .	75
4.4.3	Conclusion . . . . .	85
<b>5</b>	<b>Correlation of PAH concentrations, uptake kinetics and environmental parameters</b>	<b>86</b>
5.1	Sampling set-up and data evaluation . . . . .	87
5.2	Results and discussion . . . . .	88
5.2.1	Comparison of study sites based on numerical and analytical data evaluation . . . . .	88
5.2.2	Seasonal variations of passive air sampling kinetics . . . . .	92
5.2.3	Variability of PAH concentrations in the atmosphere and on PE considering smaller scales . . . . .	95
5.2.4	Diurnal fluctuation of Phe on the passive air sampler . . . . .	98
5.2.5	Seasonal variations of $C_g$ and the use of representative compounds	99
5.3	Conclusions . . . . .	102
<b>6</b>	<b>Concentration gradients of PAHs within the atmosphere</b>	<b>103</b>
6.1	Sampling and data evaluation . . . . .	104
6.2	Results and discussion . . . . .	104
6.2.1	Uptake kinetics at the two sampling heights . . . . .	104
6.2.2	Temporal variations of atmospheric PAH concentrations . . . . .	106
6.2.3	Evaluation of potential concentration gradients in the atmosphere	110
6.3	Conclusion . . . . .	115
<b>7</b>	<b>Characteristic ratios and source appointment</b>	<b>116</b>
7.1	Background and objectives . . . . .	116
7.2	Data evaluation . . . . .	116
7.3	Results and discussion . . . . .	117
7.4	Conclusion . . . . .	121
<b>8</b>	<b>Passive sampling in soils</b>	<b>122</b>
8.1	Concept and Objectives . . . . .	122
8.2	Theoretical Background . . . . .	124
8.2.1	Redistribution of contaminants in multiple phases . . . . .	124
8.2.2	Rate constants and characteristic times . . . . .	128
8.3	Set-up Batch tests (soil slurries) . . . . .	131
8.4	Results and discussion: Accurate passive sampling of PAHs in soils . . . . .	132
8.4.1	Loss and uptake rate constants for batches with PE . . . . .	132
8.4.2	Uptake of target compounds onto PE sheets . . . . .	136



8.4.3	Uptake onto PDMS coated jars . . . . .	139
8.4.4	Passive samplers as mirror for natural organic carbon . . . . .	140
8.5	Results and discussion: $C_{w,eq}$ within the three soil profiles . . . . .	143
8.5.1	Vertical concentration profiles of PAHs determined with PE pas- sive samplers . . . . .	148
8.5.2	Distribution pattern and specific relations of individual compounds	149
8.5.3	Diagnostic ratios for PAHs on PE . . . . .	153
8.6	Conclusion . . . . .	157
<b>9</b>	<b>Soil-atmosphere exchange</b>	<b>158</b>
9.1	Theoretical background . . . . .	158
9.1.1	Theoretical background for the mathematics of the different ap- proaches . . . . .	159
9.2	Sampling and extraction . . . . .	161
9.3	Data analysis . . . . .	162
9.4	Results and discussion . . . . .	163
9.4.1	Phe concentrations in soil air . . . . .	163
9.4.2	Seasonally varying concentrations gradients across the soil-atmosphere interface . . . . .	166
9.4.3	Compound specific relations between soil and atmosphere . . . . .	170
9.4.4	Atmospheric bulk deposition . . . . .	172
9.4.5	Distribution patterns of PAHs comparing gas phase, passive sam- pler, bulk deposition and bulk soil . . . . .	176
9.4.6	Sources of PAHs – diagnostic ratios . . . . .	177
9.5	Summary and Conclusion . . . . .	182
<b>10</b>	<b>Summary and outlook</b>	<b>183</b>
<b>A</b>	<b>Appendix</b>	<b>186</b>
A.1	Characterization of study sites . . . . .	186
A.2	Passive sampling . . . . .	188
A.3	Passive sampling in the atmosphere . . . . .	190
A.4	Passive sampling within soils . . . . .	201
A.5	Soil-Atmosphere Exchange of PAHs . . . . .	206
	<b>References</b>	<b>213</b>

## List of Figures

0.1	Scheme of redistribution processes of PAHs in the environment with respect to the gas phase in atmosphere and soils, particles in atmosphere and soils as well as vegetation. Temperature dependent fluxes are indicated with colours: blue arrows depict the flux direction for cold temperatures and red arrows mark the flux direction for warm temperatures. . . . .	ii
2.1	Map of the surroundings of west Tübingen, showing the sampling sites Entringen, Poltringen, Tailfingen. . . . .	14
2.2	Grain size distribution shown as cumulative curves for each soil horizon.	20
2.3	Profiles of a) foc [-] and b) ratio of C/N as indicator for soil maturity determined for the three locations. . . . .	21
2.4	Comparison of distribution pattern of 15 U.S. EPA Priority PAHs (excluding Any) within the top soils of Entringen, Poltringen and Tailfingen as a) bulk concentrations and b) OC normalized values. . . . .	22
2.5	OC-normalized concentration profiles of Phe, Pyr and Fth at the three locations (Entringen, Poltringen and Tailfingen). . . . .	23
2.6	Scatter plot comparing empirical estimations of $K_d$ values (based on $K_{ow}$ versus $S_{sub}$ ) for each soil horizon and all sampling sites. . . . .	24
2.7	Sorption isotherms of Phe determined for the top soil of Entringen, Poltringen and the root horizon 1 in Tailfingen. . . . .	25
2.8	Scatter plot of measured versus estimated (Equation 2.3) distribution coefficients of Phe for each soil horizon at each study site. . . . .	26
2.9	Aqueous concentrations of a) Phe b) Fth and c) Pyr in van't Hoff plots for Entringen; diamonds show measured concentrations for the uppermost cm (green), 0-3 cm (orange), 3-6 cm (blue) and 6-9 cm (grey), extrapolated for 10°C and 20°C (black) as well as calculated according to sorption isotherms (red); only temperature between 65 and 100°C resulted in concentrations above the limit of detection. . . . .	31
2.10	Equilibrium concentrations of all 16 U.S. EPA Priority PAHs in water, calculated for the soil profiles in Entringen, Poltringen, and Tailfingen, based on solubility normalized Freundlich coefficients. . . . .	33
2.11	Scatter plot for diagnostic ratios relating a) Ant, Phe, Fth and Pyr and b) Indeno, BghiP, BaA and Chr to each other, comparing Entringen, Poltringen and Tailfingen. . . . .	36
3.1	Scheme of the double film diffusion model. . . . .	39
3.2	Characteristic uptake curve onto passive sampler, classified in three uptake modes; linear, non-linear and equilibrium conditions. . . . .	42
3.3	Measured (crosses) and calculated (lines) loss of Ant-D10 as PRC at the different locations Entringen, Poltringen and Tailfingen during May 2016, standard deviation is shown in bars for the measurement and shaded areas for the numerical model. . . . .	47

---

3.4	Sensitivity analysis of the air side boundary layer, estimated with the use of Sherwood numbers for different wind speeds. . . . .	47
3.5	Measured loss of Ant-D10 (red crosses) in comparison to calculated loss (black lines with grey area as respective standard deviation) comparing empirical with theoretical calibration of the samplers. . . . .	48
4.1	Different sampling set ups in the field; comparing black and transparent sheets with and without cover. . . . .	53
4.2	Comparison of <i>PRC</i> loss (Ant-D <sub>10</sub> ) during preliminary testing in Entringen comparing transparent and black PE sheets, deployed in the field covered and uncovered. . . . .	55
4.3	Measured and calculated <i>PRC</i> -loss for the different set-ups in the field, comparing the numerical model accounting for temperature variations (the grey area represents the respective standard deviation of 10 % for $C_p$ ) to the analytical solution. . . . .	56
4.4	Comparison of Ant-D10 and Pyr-D10 as <i>PRCs</i> during May and August 2016 in Entringen; combination of measured concentrations and the numerical model with according standard deviation (solid line with grey shading). . . . .	58
4.5	Uptake of the four representative PAHs onto PE sheets, comparing the different field set-ups in a preliminary test in Entringen. . . . .	60
4.6	Measured uptake of the four representative PAHs onto transparent, covered PE sheets in combination with the fitted numerical model, the grey area illustrates the standard deviation for the model. . . . .	61
4.7	Uptake curves of representative compounds onto the passive samplers during August 2017, comparison of measured (crosses) to calculated (lines) concentrations, additionally b) considering photodegradation as loss process (lower plot). . . . .	64
4.8	Comparison of PAH concentrations on PE at the end of the day versus at the end of the night, regarding the 16 U.S. EPA Priority PAHs, sampled in two different heights in Entringen, November 2017. . . . .	65
4.9	<i>PRC</i> -loss exemplary for one of the seasonal monitorings illustrating the successfully adjusted spiking of the sheets in advance of deployment by showing excellent triplicates for each location. . . . .	67
4.10	Atmospheric concentrations [ng/m <sup>3</sup> ] of Fl <sub>n</sub> , Phe, Fth and Pyr, determined in triplicates with active samplers at the end of monitoring campaigns in August '17 and November'17 and in duplicates during February'18. Error bars indicate a general standard deviation of 10% as measurement uncertainty. . . . .	70
4.11	Set up of the PDMS coated jars (backyard of the Centre for Applied Geosciences in Tübingen) . . . . .	75

4.12	PRC-loss (Ant-D <sub>10</sub> ) measured on PDMS coated jars for three thicknesses of PDMS coating, including $\lambda$ , which is calculated based on the linear loss during the first 9 hours of sampling. The error bars account for 20% standard deviation. . . . .	76
4.13	Measured uptake curves of four representative PAHs in PDMS coated jars with different thicknesses as well as on PE (with 9 replicates) combined with the numerical model for uptake onto PE sheets (accounting for temperature changes). Error bars for PDMS indicate variation of 20%. . . . .	78
4.14	Uptake of four representative PAHs in PDMS coated jars with different thicknesses, combined with calculated uptake curves on 4 $\mu$ m coating (including the analytical solution as well as the numerical model). . . . .	79
4.15	Double logarithmic plot of masses of the target compounds (Fln, Phe, Fth and Pyr) versus mass of the PDMS for sampling after 8, 12, 17 and 25 days. With a linear regression as equilibrium concentration, only data sets with $R^2 \geq 0.7$ are included. Error bars illustrate 20% variation. . . . .	82
4.16	Comparison of atmospheric concentrations of Fln, Phe, Fth and Pyr based on different PDMS thicknesses, assuming short equilibration times, including $C_g$ determined with PE sheets (dashed line). . . . .	84
5.1	Measured uptake of Fln, Phe, Fth and Pyr onto PE at the study sites in May 2016; solid lines: predicted uptake based on the numerical model including the previously fitted air-side boundary layer and the fitted $C_g$ , black dashed line: predicted uptake based on the analytical solution considering Entringen as exemplary site, error bars indicate standard deviation of triplicates and the grey areas show confidence intervals for the numerical model of Entringen, again exemplarily. . . . .	89
5.2	Concentrations of four representative PAHs on PE for the last sampling of the seasonal monitorings (May, August and November 2016 and February 2017) in Entringen, Poltringen and Tailfingen. Error bars illustrate the measured standard deviation of triplicate samplers. . . . .	92
5.3	Measured and numerically fitted uptake curves of Phe for each of the seasonal monitorings, considering the three locations individually. The grey area indicates the standard deviation of the numerical model. . . . .	94
5.4	Uptake of representative PAHs onto the PE sheets during May 2016 in Entringen; measured data: symbols; numerical model with variable $C_g$ in two time-intervals (0-10 and 10 -30 days). The grey area illustrates the standard deviation of the numerical model. . . . .	97
5.5	Atmospheric concentrations of the representative target compounds in Entringen, fitted with the numerical model during two predefined time spans (filled: 0-10 days, lined: 10-30 days). Errorbars indicate standard deviation calculated with the numerical model, as aforementioned standard deviation increases for the second time span due to fewer data. . . . .	98

5.6	Diurnal variation of Phe on PE sheets covering 24 hours on 10.-11.7.16 (unpubl. data, provided by Bettina Rüdiger). Comparison of measured concentrations to a numerical solution based on a constant $C_g$ of 6 ng/m <sup>3</sup> and varying temperature. The grey area illustrates the standard deviation of the numerical model. . . . .	100
5.7	Fitted atmospheric concentrations of the four representative PAHs during seasonal monitorings (May, August, November and February) at each study site. Error bars demonstrate the standard deviation measured for triplicate samplers . . . . .	101
5.8	Atmospheric concentrations of Fl <sub>n</sub> , F <sub>th</sub> and Pyr for all seasons and all locations calculated from Phe and the average distribution patterns during August 2016. The red circle denotes outliers during May 2016. . . . .	102
6.1	Measured and modelled uptake curves of Fl <sub>n</sub> , Phe, F <sub>th</sub> and Pyr onto the passive sampler at a) 0.1 m and b) 1.2 m height during May 2017, considering the three locations individually. The grey area illustrates the standard deviation of the numerical model. . . . .	105
6.2	Measured and modelled uptake curves of Phe onto the passive sampler at a) 0.1 m and b) 1.2 m height for each of the seasonal monitorings during the second year of sampling, considering the three locations individually. The grey area illustrates the standard deviation of the modelled uptake. . . . .	108
6.3	Atmospheric concentrations of the four representative PAHs fitted to measured uptake and therefore averaging over each seasonal monitoring, respectively. Error bars indicate standard deviation of triplicate samples. . . . .	109
6.4	Double logarithmic scatter plot comparing concentrations of a) Fl <sub>n</sub> , b) Phe, c) F <sub>th</sub> and d) Pyr at 1.2 m height to concentrations right above ground at each station for seasonal sampling campaigns. Error bars indicate the standard deviation of triplicate samplers, the solid line demonstrates a reference line with a ratio of 1:1 and the dashed lines define a confidence interval of 20%. . . . .	111
6.5	Double logarithmic scatter plot comparing concentrations of a) Fl <sub>n</sub> , b) Phe, c) F <sub>th</sub> and d) Pyr at 1.2 m height to temperature-corrected concentrations right above ground at each station for seasonal sampling campaigns. Error bars indicate the standard deviation of triplicate samplers, the solid line demonstrates a reference line with a ratio of 1:1 and the dashed lines define a confidence interval of 20%. . . . .	113
7.1	Scatter plot of diagnostic ratios for atmospheric concentrations for each location and seasonal monitoring, based on Ant, Phe, F <sub>th</sub> and Pyr. Encircled data points illustrate ratios observed during November monitorings of both years. . . . .	118

7.2	Distribution pattern of eight PAHs (Any, Ace, Fl <sub>n</sub> , Phe, Ant, Fth, Pyr and BaA) on PE, measured for the last sampling of each seasonal monitoring during both years of sampling campaigns; covering May 2016 - March 2018. Error bars indicate the standard deviation determined for triplicate samplers. . . . .	120
8.1	Measured loss of Ant-d <sub>10</sub> during three months of equilibration combined with the calculated loss, following the first order kinetic model and for desorption from PE alone; slow uptake in soil limits kinetics. . . . .	133
8.2	Comparison of measured and calculated uptake of Phenanthrene from soil slurries onto the passive samplers to the observed loss of Ant-D <sub>10</sub> and the respective characteristic times to reach 90 % equilibrium. Error bars indicate the determined standard deviation of triplicate samples. . . . .	134
8.3	Uptake of Phe onto PE in soil slurries comparing the two fitted rate constants $\lambda$ for Ant and Phe. . . . .	135
8.4	Uptake of target compounds onto PE sheets out of soil slurry comparing Fl <sub>n</sub> , Phe, Fth, and Pyr (left plot) and LMWC Nap, Any to Fl <sub>n</sub> (right plot). Error bars indicate the observed standard deviation of triplicate batches. . . . .	137
8.5	Masses of Phe, Fth, and Pyr plotted against mass of PDMS in the respective jars after a) 4 weeks (4 $\mu$ m coating not yet in equilibrium) and b) 6 weeks of equilibration. . . . .	140
8.6	Distribution patterns of the 16 U.S. EPA Priority PAHs comparing a) OC-normalized concentrations in the bulk soil and b) PE in soil batches (error bars reflecting triplicates) after 1,2,3,4 and 12 weeks. . . . .	141
8.7	Distribution pattern of the 15 U.S. EPA Priority PAHs in soil, comparing a) the bulk soil with OC-normalized concentrations and b) PDMS batches, extracted after 6 weeks of equilibration. . . . .	143
8.8	Measured versus estimated concentrations on the passive sampler of Phe after 4.5 months of equilibration, comparing Entringen, Poltringen, and Tailfingen. Error bars show the measured standard deviation of triplicate samples. . . . .	145
8.9	Scatter plot of concentration ratios of Phe in the bulk soil, normalized to OC and PE plotted against the ratio of the expected $K_{oc}$ values and $K_{pw}$ of Phe, shown for the soil profiles of Entringen, Poltringen, and Tailfingen. Error bars are set as 10 % assumed standard deviation. . . . .	145
8.10	$C_{w,eq}$ of Phe calculated according to the measured Freundlich sorption isotherm as well as based on the batch tests with PE for each soil sample in Entringen, Poltringen, and Tailfingen; the yellow diamond was calculated from PDMS. The solid line illustrates a ratio of 1:1 as reference, and dashed lines indicate $\pm 10$ % as confidence interval. . . . .	147
8.11	Comparison of $C_{w,eq}$ , determined for the 16 U.S. EPA Priority PAHs with PE passive samplers in soil batches and calculated according to measured $K_{Fr}$ , exemplarily for Entringen. . . . .	147

---

8.12	Concentration profiles of Phe, Pyr, and Fth at the three locations, measured on PE-sheets after the <i>ex situ</i> batch tests. . . . .	148
8.13	Distribution patterns of the 16 U.S. EPA Priority PAHs in each soil horizon in Entringen, determined for the bulk soil and comparing expected to observed patterns on PE passive samplers. . . . .	149
8.14	Distribution patterns of 16 U.S. EPA Priority PAHs determined for the top soils of Entringen, Poltringen, and Tailfingen regarding a) the bulk soil and b) the PE-sheets after shaking for 4.5 months. . . . .	150
8.15	Linear relation determined for a) BaP and b) Phe to the sum of the measured U.S. EPA Priority PAHs considering all soil samples of Entringen, Poltringen and Tailfingen with error bars indicating the standard deviation of measurements in triplicates. . . . .	151
8.16	Comparison of measured concentrations of the 16 U.S. EPA Priority PAHs in bulk soil a) and PE b) to values predicted based on Phe and the distribution patterns. . . . .	152
8.17	Diagnostic ratios relating a)Ant, Phe, Fth and Pyr and b) Indeno, BghiP, BaA and Chr to each other; determined for bulk soil samples (I), considering Entringen, Poltringen, and Tailfingen. Error bars indicate the measured standard deviation for triplicate samples. . . . .	155
8.18	Diagnostic ratios relating a)Ant, Phe, Fth and Pyr and b) Indeno, BghiP, BaA and Chr to each other; determined for PE sheets from batch tests (II), considering Entringen, Poltringen, and Tailfingen. Error bars indicate the measured standard deviation for triplicate samples. . . . .	156
9.1	Comparison of Phe concentrations in the soil air (for 20°C) based on measured Freundlich coefficients versus PE equilibrated with soil slurries, determined for Entringen, Poltringen and Tailfingen individually. . . . .	165
9.2	Comparison of Phe in the soil air based on the hot-water extraction and measured sorption isotherms, both referring to 20° C as soil temperature during summer. Error bars indicate 20% standard deviation.. . . . .	165
9.3	Phe concentration profiles in gas phase, in the atmosphere measured by passive sampling and in the soil calculated from the bulk soil concentration and measured Freundlich coefficients comparing summer (with 20 °C) and winter (5 °C) at the different locations. . . . .	167
9.4	Seasonal concentration gradients of Phe across the soil-atmosphere interface, directly comparing passive samplers deployed in both compartments at each of the study sites during the second year of monitoring campaigns. . . . .	168

9.5	Double logarithmic scatter plots of seasonal atmospheric concentrations of Fln, Phe, Fth and Pyr to estimated concentrations of the soil air in the topsoil, both based on passive samplers. Concentrations on the sampler within the atmosphere were extrapolated during November and February (of both years) to obtain equilibrium conditions. Error bars indicate the measured standard deviation for triplicate samples, the reference line depicts a ratio of 1:1 and the confidence interval includes 20 % deviation.	171
9.6	Seasonal deposition rates [ng/m <sup>2</sup> /day] of the four representatives, sampled at the three study sites during the second year of monitoring (May 2017- May 2018).	173
9.7	Seasonal distribution patterns (in %) of the atmospheric deposition for Fln, Phe, Fth and Pyr comparing the three study sites to an additional location, close to the city centre of Tübingen.	173
9.8	Percentage contribution of Fln, Phe, Fth and Pyr, comparing the gas phase (active sampler) and particles (passive sampler) in the atmosphere, bulk atmospheric deposition and soil exemplarily for Entringen.	177
9.9	Diagnostic ratios for atmospheric bulk deposition comparing Entringen, Poltringen and Tailfingen during the individual seasons.	178
9.10	Diagnostic ratios of HMW PAHs calculated for the atmospheric bulk (wet and dry) deposition (May2017 - May 2018). The encircled data points reflect the atmospheric deposition during November 2017- February 2018.	179
9.11	Diagnostic ratios of HMW PAHs calculated in the bulk soil of the different study sites.	180
9.12	Diagnostic ratios of a) Ant/(Ant+Phe) and b) Indeno/BghiP in the rather undisturbed soil profile in Entringen, indicating a temporal evolution of these ratios.	181
A.1	Concentration profiles of Phe, Pyr and Fth in the bulksoil at the three locations Entringen, Poltringen and Tailfingen (not normalized to OC).	187
A.2	Measured uptake of the four representative PAHs (Fln, Phe, Fth and Pyr) onto transparent, uncovered PE sheets (upper plot) and onto black, covered PE sheets (lower plot) in combination with the fitted numerical model; the grey area illustrates the standard deviation for the model.	190
A.3	Measured uptake of the four representative PAHs (Fln, Phe, Fth and Pyr) onto black, uncovered PE sheets in combination with the fitted numerical model; the grey area illustrates the standard deviation for the model.	191
A.4	Meteorological influences, including hourly measurements of wind speed (black), precipitation (blue) and temperature (red) during all seasonal sampling campaigns. Data are obtained from the German Weather Survey (measured in Stuttgart, Echterdingen).	193



A.5	Diffuse solar and global radiation [ $\text{J}/\text{cm}^3$ ] for seasonal monitorings during the first year. Data are obtained from the German Weather Survey (measured in Stuttgart, Echterdingen). . . . .	194
A.6	Measured and numerically fitted uptake curves of Fln (upper plots) and Fth (lower plots) for each of the seasonal monitorings, considering the three locations individually. The grey area depicts the standard deviation of the numerical model. . . . .	195
A.7	Measured and numerically fitted uptake curves of Pyr for each of the seasonal monitorings, considering the three locations individually. The grey area depicts the standard deviation of the numerical model. . . . .	196
A.8	Distribution pattern of eight PAHs (Any, Ace, Fln, Phe, Ant, Fth, Pyr and BaA) on PE, comparing Entringen, Poltringen and Tailfingen for the first half of the monitoring during February 2017. Error bars indicate the standard deviation determined for triplicate samplers. . . . .	197
A.9	Relations of Mt/Meq to Fourier numbers ( $\text{Dat}/a^2$ ) within a finite bath for different values of $\beta$ (figure taken from Grathwohl (2012)). . . . .	201
A.10	Measured concentrations of the 16 U.S. EPA Priority PAHs within the bulk soil before and after the batch experiment, shown here exemplarily for Entringen. . . . .	202
A.11	Ratio of PAH concentration normalized to the organic carbon content within the soil to the measured concentration on the polymer comparing a) PE and b) PDMS, illustrates no correlation to the size of the compound. . . . .	202
A.12	Comparison of $C_{w,eq}$ , determined for the 16 EPA PAHs with PE passive samplers in soil batches and calculated according to measured $K_{Fr}$ for Poltringen. . . . .	203
A.13	Comparison of $C_{w,eq}$ , determined for the 16 EPA PAHs with PE passive samplers in soil batches and calculated according to measured $K_{Fr}$ for Tailfingen. . . . .	203
A.14	Distribution patterns of the 16 EPA PAHs in each soil horizon in Poltringen (upper plot) and Tailfingen (lower plot), determined for the bulk soil and comparing expected to observed patterns on PE passive samplers. . . . .	204
A.15	Comparison of Phe concentrations in the soil air based on measured Freundlich coefficients versus PE equilibrated with soil slurries, determined for Entringen, Poltringen and Tailfingen individually and adapted to a temperature of $5^\circ\text{C}$ . . . . .	206
A.16	Phe concentration profiles in gas phase, in the atmosphere measured by passive sampling and in the soil calculated from the bulk soil concentration and measured Freundlich coefficients comparing summer (with $20^\circ\text{C}$ ) and winter ( $5^\circ\text{C}$ ) at the different locations. . . . .	207

A.17	Seasonal concentration gradients of Phe across the soil-atmosphere interface, directly comparing passive samplers deployed in both compartments at each of the study sites during the first year of monitoring campaigns. . . . .	207
A.18	Extrapolation of Fth on PE passive sampler in the atmosphere during August 2017 (upper plot) and November 2017 (lower plot), based on three different $\delta_g$ and resulting $C_g$ values, leading to explicitly different equilibrium concentrations on PE. . . . .	208
A.19	Extrapolation of Pyr on PE passive sampler in the atmosphere during August 2017 (upper plot) and November 2017 (lower plot), based on three different $\delta_g$ and resulting $C_g$ values, leading to explicitly different equilibrium concentrations on PE. . . . .	209
A.20	Double logarithmic scatter plots of seasonal atmospheric concentrations of Fln, Phe, Fth and Pyr to estimated concentrations of the soil air in the topsoil, both based on passive samplers. Concentrations on the sampler within the atmosphere were extrapolated during November and February to obtain equilibrium conditions. Error bars indicate the measured standard deviation for triplicate samples, the reference line depicts a ratio of 1:1 and the confidence interval includes 20 % deviation. . . . .	210
A.21	Concentration profiles of BaP and Phe determined at each study site as a direct indicator on biodegradation with Phe being more biodegradable than BaP. . . . .	211
A.22	Development of road traffic in Germany 1954 – 2012 (statistics provided by Federal Road Research Institute). . . . .	211

## List of Tables

1.1	Physicochemical properties of U.S. EPA Priority PAHs; molecular weight ( $M_{mol}$ ), water solubility ( $S^1$ ), subcooled liquid solubility ( $S_{sub}^2$ ), Henry's law constant ( $H^1$ ) and octanol-water partition coefficients ( $K_{ow}^2$ ). With <sup>1</sup> taken from <i>New Jersey Department of environmental protection</i> and <sup>2</sup> taken from <i>EPISUITE</i> . . . . .	7
2.1	List of sampled horizons and respective depth (in cm ) for each study site including topsoil, root horizons (1, 2, 3) as well as sub soils (1,2,3). . .	16
2.2	Temperatures and equilibration times for the explicit extraction steps of the hot water extraction at the ASE. . . . .	19
2.3	A) Distribution coefficients estimated on $K_{oc} * f_{oc}$ in [ L/kg ], based on <sup>a)</sup> $K_{ow}$ , according to Karickhoff (1981) and <sup>b)</sup> $S_{sub}$ , following Razzaque & Grathwohl (2008). And B) Freundlich coefficients and Freundlich exponents determined for Phe on measured sorption isotherms. . . . .	28
2.4	Distribution and partition coefficients adjusted for the low concentrations of Phe in the bulk soil samples. . . . .	28
2.5	Desorption enthalpies [kJ/mol] determined for the uppermost 9 centimetres in Entringen for Phe, Fth and Pyr in [kJ/mol] and the respective coefficients of determination. . . . .	29
4.1	Calculated air-side boundary layers $\delta_g$ and characteristic times to reach 63 % equilibrium for <i>PRC</i> -loss in each set-up. . . . .	55
4.2	Calculated loss rates $\lambda_{loss}$ [day <sup>-1</sup> ] for <i>PRCs</i> in different set-ups, comparing the analytical and numerical evaluation. . . . .	57
4.3	Comparison of loss rate constants ( $\lambda$ [s <sup>-1</sup> ]) and accordingly calculated air-side boundary layers ( $\delta_g$ [mm]) based on Ant-D <sub>10</sub> and Pyr-D <sub>10</sub> as Performance Reference Compounds. . . . .	57
4.4	Characteristic properties of Fl <sub>n</sub> , Phe, Fth and Pyr as representative PAHs, comparing their respective molar volume and mass as well as the diffusion coefficients in gas and partition coefficients $K_{pg}$ (25°C). . . . .	59
4.5	Uptake rate constants ( $\lambda$ [day <sup>-1</sup> ]) of the four representative PAHs, comparing the different settings in the field during preliminary trial. . . . .	59
4.6	Atmospheric concentrations [ng/m <sup>3</sup> ] fitted with the numerical model for each field set up. . . . .	62
4.7	Fitted air-side boundary layer [mm] and atmospheric concentrations [ng/m <sup>3</sup> ] for the representative compounds, comparing results with and without consideration of photodegradation. . . . .	63
4.8	Comparison of atmospheric concentrations [ng/m <sup>3</sup> ] for the four representative PAHs determined with passive and active sampling during August and November 2017 as well as during February 2018, including standard deviation. . . . .	70

4.9	Characteristic times [days] to reach 63% equilibrium on passive samplers, calculated for the four representative compounds during August, November 2017 and February 2018. . . . .	71
4.10	Partition and diffusion coefficients (in [L/kg] and [m <sup>2</sup> /s]) between polymer and gas phase for PE and PDMS at 25°C and 20°C, resp. With <sup>a</sup> Lohmann (2012), <sup>b</sup> Rusina et al. (2010), <sup>c</sup> K <sub>PDMS-water</sub> taken from <sup>b</sup> and adapted for gas phase . . . . .	77
4.11	Calculated uptake rate constants for each coating thickness and characteristic times to reach 90% equilibrium. . . . .	77
4.12	Partition coefficients ( $K_{PDMS-air}$ [L/kg]) of Fln, Phe, Fth and Pyr, adapted for different time spans (dependent on the temperature), depending on the approach to determine atmospheric concentrations (numerically, analytically and assuming equilibrium). . . . .	80
4.13	Atmospheric concentrations [ng/m <sup>3</sup> ] of Fln, Phe, Fth and Pyr, determined with PDMS coated jars, based on scatter plots as equilibrium validation, again only including data sets with $R^2 \geq 0.7$ . . . . .	81
4.14	Atmospheric concentrations [ng/m <sup>3</sup> ] of Fln, Phe, Fth and Pyr, determined with PDMS coated jars fitted from the analytical solution, based on equilibrium conditions at the end of the sampling campaign and fitted from the numerical model for each thickness of the coatings; for comparison concentrations determined with PE sheets are shown sampled a) after the first half of the monitoring and b) at the end of the sampling campaign. .	83
5.1	Air-side boundary layers [mm] for the seasonal monitorings in May, August and November 2016 and February 2017 and characteristic times [days] to reach 63 % equilibrium on the sampler, calculated for Fln, Phe, Fth and Pyr. . . . .	88
5.2	Mean values for log K <sub>p</sub> [L/kg] of the four representative compounds during seasonal monitorings of the first year of sampling. . . . .	90
5.3	Atmospheric concentrations [ng/m <sup>3</sup> ] and respective standard deviations of the representative PAHs determined with the numerical model, analytical solution and under equilibrium conditions in May 2016. . . . .	91
5.4	Partition coefficients (Log K <sub>pg</sub> [L/kg]) of Fln, Phe, Fth and Pyr, adapted for different time spans, depending on the approach to determine atmospheric concentrations (numerically, analytically and assuming equilibrium). . . . .	91
5.5	Average environmental parameters (Temp in °C, wind speed in m/s) during the different monitorings, air-side boundary layers [mm] determined from PRC-loss, concentration ranges of Phe on the sampler [ng/g] and in the atmosphere [ng/m <sup>3</sup> ], numbers in brackets are average values covering the time period used for calibrating $\delta_g$ . . . . .	95

6.1	Atmospheric boundary layers during the second year of sampling, calibrated for both sampling heights at each of the study sites individually (except for May 2017: PRC-loss for M <sub>A</sub> y 2017 was derived from measurements in August 2017). . . . .	106
6.2	Comparison of $C_g$ [ng/m <sup>3</sup> ] of Fl <sub>n</sub> , Phe, Fth and Pyr in the atmosphere. . .	114
8.1	Log $K_p$ [L/kg] for the representative compounds between water and the two polymers PE and PDMS (at 20°C). . . . .	124
8.2	Characteristic times of Ant-D <sub>10</sub> and Phe to reach 90 % equilibrium in batches comprising PE and PDMS respectively, considered mass transports are film and intraparticle diffusion ( <sup>1</sup> parameters for intraparticle diffusion were defined as $\varepsilon = 0.7$ and $r_s = 0.05$ mm). . . . .	130
8.3	Comparison of the fitted rate constants, polymer-water partition coefficients, concentration dependent distribution coefficients and equilibrium concentrations in the bulk soil as relevant parameters for the uptake of LMW PAHs (Nap, Any and Fl <sub>n</sub> ), compared to the regular representative PAHs onto PE passive samplers within the batches. . . . .	138
8.4	Percentage equilibrium status determined for each batch based on the loss of Ant-D <sub>10</sub> from PE as PRC, after 4.5 months of equilibration and a liquid to solid ratio of 1.5. . . . .	144
8.5	Contribution [%] of the four representative compounds Fl <sub>n</sub> , Phe, Fth and Pyr to $\Sigma_{16}$ U.S. EPA Priority PAHs, averaging for the individual soil horizons. . . . .	153
9.1	Concentration ratios of Phenanthrene in the gas phase (atmosphere/soil) determined with respect to sampling at 1.2 m height for each atmospheric monitoring at each location individually for both years of sampling. . .	169
9.2	Concentration ratios of Phenanthrene on PE passive samplers (atmosphere/soil) at 1.2 m sampling height for each atmospheric monitoring at each location individually for both years of monitoring. . . . .	169
9.3	Average ambient temperatures [°C] during the seasonal atmospheric monitorings, covering both years of sampling, data taken from <i>German Weather Survey</i> . . . . .	169
9.4	Average soil temperatures [°C] in different depths during each of the seasonal monitorings, data taken from <i>German Weather Survey</i> . . . . .	170
9.5	Comparison of measured PAH deposition rates for $\Sigma_{12}$ PAHs (excluding LMW PAHs) with literature studies. . . . .	175
A.1	Partition coefficients and solubilities of the 16 U.S. EPA Priority PAHs at 25°C: log $K_{ow}$ (EPI Suite), log $S_{sub}$ (Chiou et al., 2005), log $K_{pw}$ (Smedes et al, 2009) as well as calculated log $K_{oc}$ ( <sup>1</sup> following Karickhoff (1981), and <sup>2</sup> according to Razzaque & Grathwohl (2008)), all in [L/kg], except log $S_{sub}$ with [kg/L]. . . . .	186

List of Tables

---

A.2	Partition and diffusion coefficients of the 16 EPA-PAHs at 25°C: Log $K_{pe-air}$ (Lohmann, 2011), $D_{pe}$ (Lohmann, 2012), $D_g$ and $D_w$ ( <i>New Jersey Department of environmental protection</i> ). . . . .	188
A.3	Seasonal atmospheric concentrations [ $ng/m^3$ ] of the representative compounds during the first year of sampling campaigns, numerically fitted for each location including respective standard deviations. . . . .	198
A.4	Seasonal atmospheric concentrations [ $ng/m^3$ ] of the representative compounds during the second year of sampling campaigns, numerically fitted for each location and both sampling heights (0.1 m and 1.2 m) including respective standard deviations. . . . .	199
A.5	diagnostic ratios, considering Ant, Phe, Fth and Pyr, including both years of sampling campaigns and determined for each season and each study site individually. . . . .	200
A.6	Contribution [%] of the four representative compounds Fln, Phe, Fth and Pyr to the sum of the 16 EPA PAHs and the according standard deviation [%] of their concentrations from triplicate analysis. . . . .	205
A.7	Phe concentrations in the atmosphere [ $ng/m^3$ ] determined for each location during seasonal monitorings in 2016/2017. . . . .	206
A.8	Phe concentrations in the atmosphere [ $ng/m^3$ ] determined for each location during seasonal monitorings in 2017/2018, including both sampling heights (0.1 m and 1.2 m). . . . .	206

## Nomenclature

### Abbreviations

ABL	Atmospheric boundary layer
AC	Activated carbon
ASE	Accelerated Solvent Extractor
DOC	Dissolved organic carbon
GC	Gaschromatograph
HMW	High molecular weight
LMW	Low molecular weight
MeOH	Methanol
MS	Massspectrometer
OC	Organic carbon
PAH	Polycyclic Aromatic Hydrocarbons
PBDE	Polybrominated Diphenyl Ethers
PCB	Polychlorinated Biphenyls
PDMS	Polydimethylsiloxane
PE	Polyethylene
POP	Persistent organic pollutant
PRC	Performance Reference Compound
PUF	Polyurethane foam
R <sup>2</sup>	Coefficient of determination
US EPA	United States Environmental Protection Agency
SVOC	Semi-volatile organic compounds

### Compounds

ACE	Acenaphthene
ANT	Anthracene
ANY	Acenaphthylene
B(a)A	Benz(a)Anthracene
B(a)P	Benz(a)Pyrene
B(b)f	Benz(b)Fluoranthene
B(ghi)P	Benz(ghi)Perylene
B(k)f	Benz(k)Fluoranthene
CHR	Chrysene
D(ah)A	Dibenzo(ah)Anthracene
FLN	Fluorene
FTH	Fluoranthene
NAP	Naphthalene
PHE	Phenanthrene

List of Tables

---

PYR

Pyrene

Symbols

$A^{\circ}$	Specific surface area	$[m^2/kg]$
$A_p$	Surface of polymer	$[m^2]$
$C_{ini}$	Initial concentration	$[\mu g/L]$
$C_{eq}$	Equilibrium concentration	$[\mu g/L]$
$C_w$	Concentration in water	$[\mu g/L]$
$C_{pe}$	Concentration on polyethylene	$[\mu g/kg]$
$C_{PDMS}$	Concentration on polydimethylsiloxane	$[\mu g/kg]$
$C_{bulk}$	Concentration in bulksoil	$[\mu g/kg]$
$C_s$	Concentration on soilsolids	$[\mu g/kg]$
$C_g$	Concentration in gasphase	$[ng/m^3]$
$d$	Diameter of polymers	$[m]$
$D_a$	Apparent Diffusion coefficient (concentration dependent)	$[m^2/s]$
$D_e$	Effective Diffusion coefficient	$[m^2/s]$
$D_g$	Diffusion coefficient in air	$[m^2/s]$
$D_w$	Diffusion coefficient in water	$[m^2/s]$
$D_p$	Diffusion coefficient in polymer	$[m^2/s]$
$\delta_g$	air-side boundary layer	$[m]$
$\delta_p$	polymer-side boundary layer	$[m]$
$\Delta H_{DES}$	Desorption enthalpy	
$\Delta H_{vap}$	Evaporation enthalpy	
$\varepsilon$	Porosity	$[-]$
$f_{oc}$	Fraction of organic carbon	$[-]$
$H$	Henry's Law Coefficient	$[-]$
LDPE	Low Density Polyethylene	
$M_{mol}$	Molecular weight	$[g/mol]$
$m_{soil}$	Mass of soil	$[kg]$
$m_p$	Mass of polymer	$[kg]$
$p$	Pressure	
$1/n$	Freundlich exponent	
$\eta$	Kinematic viscosity air	$[m^2/s]$
$k$	Mass transfer coefficient	$[m/s]$
$K_d$	Distribution coefficient	$[L/kg]$
$K_d^*$	Distribution coefficient, adapted for low concentration in bulksoil	$[L/kg]$
$K_{Fr}$	Freundlich coefficient	$[L/kg]$
$K_{Fr}^*$	Freundlich coefficient, unit-equivalent	$[-]$



---

$K_{oc}$	Organic carbon-water partition coefficient	[L/kg]
$K_{oc}^*$	OC-water partition coefficient, adapted for low concentrations in bulksoil	[L/kg]
$K_{ow}$	Octanol-water partition coefficient	[L/kg]
$K_{pg}$	Partition coefficient polymer-gasphase	[L/kg]
$K_{pw}$	Partition coefficient polymer-water	[L/kg]
$\lambda$	Rate constant	[s <sup>-1</sup> ]
$r$	Radius of spheres	[m]
$R$	Ideal gas constant	[J/kgK]
$Re$	Reynolds number	[-]
$\rho$	density	[kg/m <sup>3</sup> ]
$S$	Water solubility	[mg/L]
$S_{sub}$	Subcooled liquid solubility	[mg/L]
$Sc$	Schmidt number	[-]
$Sh$	Sherwood number	[-]
$T$	Temperature	
$t$	Time	[s]
$V_{air}$	Molecular volume of air	[m <sup>3</sup> /mol]
$V_w$	Volume of water	[L]
$V_p$	Volume of polymer	[m <sup>3</sup> ]
$V_{PAH}$	Molecular volume of PAHs	[m <sup>3</sup> /mol]
$\nu$	dynamic viscosity	[kg/ms]



---

# 1 Introduction

## 1.1 Background and Motivation

### **Polycyclic aromatic hydrocarbons: occurrence, origin and environmental input pathways**

Polycyclic Aromatic Hydrocarbons (PAHs) form a large group of several hundreds of organic contaminants that all have at least two benzene rings in common (Abdel-Shafy & Mansour, 2016). Generally, water solubility of PAHs decreases with the number of condensed benzene rings and of course hydrophobicity increases proportional to the size and molecular weight of the compound. Higher condensed compounds, in particular *Benz(a)Pyrene (BaP)*, *Benz(a)Anthracene (BaA)*, *Dibenz(a,h)Anthracene (DahA)* and *Indeno(1,2,3-cd)Pyrene (Indeno)*, are known to be mutagenic and carcinogenic (Wild & Jones, 1995, Dat & Chang, 2017), which awakened societal as well as scientific concerns. Natural sources of PAHs exist, e.g. wild fires or volcano eruptions, nevertheless those inputs are of minor importance for the overall emission rate in comparison to anthropogenic sources (Aichner *et al.*, 2007, Aydin *et al.*, 2017). The anthropogenic generation of PAHs has been determined as a result of incomplete combustion of organic matter and fossil fuels. Consequently, typical emission sources are industrial processes, waste burning, domestic heating and traffic (Wijayarathne & Means, 1984, Jones *et al.*, 1989, Howsam & Jones, 1998, Roux *et al.*, 2008). In principal, PAHs do not occur as single compounds within the environment, but as a mixture of several compounds. Several studies have been conducted to identify specific patterns and fingerprints in the composition of PAH occurrence that would help to establish relationships between emission sources and emitted PAHs (Khalili *et al.*, 1995, Dickhut *et al.*, 2000, Kavouras *et al.*, 2001, Larsen & Baker, 2003, Kakareka *et al.*, 2005, Lee *et al.*, 2005). In general, combustion of organic material can be differentiated between pyrogenic and petrogenic combustion. Pyrogenic combustion includes biomass and organic matter like coal and wood, whereas petrogenic combustion refers to petroleum and thus vehicular emission (Mostert *et al.*, 2010, Tobiszewski & Namieśnik, 2012). Due to higher temperatures during petrogenic combustion, PAHs emitted by this process are characterized by higher condensation and consequently higher molecular weight (Hwang *et al.*, 2003). Different studies identify traffic exhaust gases, domestic heating or industrial processes as main emission sources, which may also vary seasonally (Harrison *et al.*, 1996, Simpson *et al.*, 1996, Larsen & Baker, 2003, Dvorská *et al.*, 2011). Hence, identification of specific emission sources remains difficult, in particular, since numerous environmental influences and varying stabilities of individual compounds generate altering patterns over time (Biache *et al.*, 2014). However, aiming for the reduction of pollution, an accurate characterization and quantification of specific sources and pathways is important (Prevedouros *et al.*, 2004).

Within the atmosphere, PAHs may generally be differentiated as gaseous and particle bound PAHs. The latter are emitted already bound to particles during incineration (e.g. soot particles) (Rogge *et al.*, 1993). Gaseous PAHs, on the other hand, have shown to sorb onto dust particles after emission within the atmosphere as well (Finizio *et al.*, 1997, Dachs & Eisenreich, 2000, Akyüz & Çabuk, 2010). Bucheli *et al.* (2004) relate gas phase PAHs to long range transport opposed to particle-bound PAHs, which get deposited close to their emission source. This is mainly due to the size and the solubility or volatility of the respective compounds; heavier compounds are characterized by lower solubility and therefore stronger binding to particles, which in turn leads to rather fast deposition. In contrast, smaller compounds are more volatile, remain in the gas phase longer, and as a result are transported over longer distances before deposition. Additionally, Gouin *et al.* (2004) describe the *Grasshopper effect* as an adequate process for PAHs in the environment: this defines deposition and revolatilization as ongoing process, including numerous ‘hops’ of the respective compound. As a result of continuous exchange between the gas phase and sorbing surfaces, PAHs may also get transported over longer distances. Within the atmosphere, PAHs may undergo additional processes like dissolution into water droplets, oxidation by photochemical radicals or scavenging by precipitation (Atkinson, 1994, Franz & Eisenreich, 1998, Xiao & Wania, 2003, Ravindra, Wauters *et al.*, 2008, Ringuet *et al.*, 2012, Wang *et al.*, 2015, Li *et al.*, 2016). Overall, deposition and therefore input into the soil is the major pathway following emission (Ribes *et al.*, 2003, Gocht *et al.*, 2007, Bozlaker *et al.*, 2008).

Based on their hydrophobicity, PAHs may be characterized by rather strong sorption to organic materials like organic carbon in soils and sediments (Verma *et al.*, 2017). Hence, soils are widely accepted as the major terrestrial reservoir for PAHs and other common organic pollutants. Once a PAH compound has entered the soil, additional processes, such as biodegradation and adsorption, affect the fate of PAHs, whereas potential leaching with subsequent transport to subsoil horizons may bypass biodegradation (Harner *et al.*, 2001, Kuppusamy *et al.*, 2017, Harmsen & Rietra, 2018). However, sorption of PAHs to the soil solids may be identified as the most relevant factor, since it defines the available fraction of PAHs for degradation and transport processes. Sorption of PAHs strongly depends on soil properties, in particular on the organic matter content of the soil (Wijayarathne & Means, 1984, Yang, Tao, *et al.*, 2010, Yang, Zhang, *et al.*, 2010). Several studies relate distribution and partition coefficients of PAHs to the fraction of organic carbon (Karickhoff *et al.*, 1979, Razzaque & Grathwohl, 2008). Moreover, the quality of organic carbon has been identified as a significant parameter for PAH-sorption in soils. Thus, soot and black carbon illustrate substantially strong sorption capacities (Ribes *et al.*, 2003, Brändli *et al.*, 2008). Degrendele *et al.* (2016) describe the properties of soil organic matter as much too diverse to identify direct relations between the concentrations of organic contaminants and the amount of organic carbon. Additionally, not only the soil properties, but also the land use as well as the plant cover of the soil considerably affect transport processes of PAHs and therefore their fate in the environment (McLachlan

& Horstmann, 1998, Barber *et al.*, 2004, Komprda *et al.*, 2013). Furthermore, owing to the long range transport, PAHs can be found ubiquitously in the environment, even in remote areas like Antarctica and Arctic (Halsall *et al.*, 1997, Hung *et al.*, 2005). Therefore PAHs are *substances of very high concern* (defined by the European Chemical Agency), particularly in combination with their mutagenic and carcinogenic impacts. The U.S. EPA defined 16 isomers out of this big group as *priority pollutants*, which are listed in Table 1.1 together with their structure and characteristic parameters.

### **Temporal development: emission, accumulation and redistribution**

With natural emission sources contributing only to a minor extent to the overall emission of PAHs, an explicit “starting” point for substantially increasing PAH emission can be identified with the beginning of the industrialization around 1880 (Gschwend & Hites, 1981, Bao *et al.*, 2015). Obviously, industrial burning processes, incineration, power plants (using coal), as well as traffic increased substantially with the industrial development and the growth of cities. Since soils generally act as sinks for organic contaminants, a continuous accumulation may be observed in undisturbed soil profiles (Jones *et al.*, 1989). Highest concentrations and highest deposition rates of PAHs were determined around 1960, followed by a notable decline (Sanders *et al.*, 1993, Jones, 1994). Gocht (2005) reports an enrichment factor of PAHs in soil and sediment profiles, which varies as a function of time. In particular, at the end of the 20<sup>th</sup> century several European states, the US, Canada and the former Soviet Union agreed on a number of conventions aiming to reduce ongoing air pollution. Subsequent courses of action were introduced including filters and catalysts for incineration and vehicular combustion to obtain a decrease of atmospheric concentrations for a broad range of pollutants (e.g. PCBs, PAHs, heavy metals, nitric oxides). This effect of regulatory measures may be observed widespread in the environment, as reported in several studies (Brun *et al.*, 2004, Hung *et al.*, 2005, Ravindra, Sokhi, *et al.*, 2008, Hung *et al.*, 2016, Liu *et al.*, 2017). Accordingly, a significant decrease of PAH emission of 60% has been determined within the EU between 1990 and 2008 (reported by the European Environment Agency).

Based on the close interrelation between atmosphere and soil, concentration changes within one compartment cause direct responses within the other. Consequently, decreasing atmospheric concentrations change the concentration gradients across the soil-atmosphere interface and may therefore induce a shift of the respective flux direction. Donald and Anderson (2017) define the uppermost centimetre of the topsoil as exchange layer, providing the potential for fast reaction and adaption to changes of ambient conditions. Accordingly, formerly accumulated pollutants within the topsoil may revolatilize back into the atmosphere responding to a decline of atmospheric concentrations (Harner *et al.*, 2000, Cabrerizo *et al.*, 2011a, b, Bao *et al.*, 2015). Moreover, global climate change has been identified as an additional influence on atmospheric concentrations of persistent organic pollutants; higher temperatures (combined with drier soils) enhance

the revolatilization of formerly accumulated compounds in soils (Ren *et al.*, 2019). The temperature-dependency of gas-particle partitioning may also influence the exchange between soil and atmosphere (Pankow, 1987). Therefore, the flux direction of organic pollutants across the soil-atmosphere interface may vary throughout the day or throughout the year due to its coupling to temperature fluctuations (Lee *et al.*, 1998, Bao *et al.*, 2016).

Due to significant regional variations of emission sources and influencing parameters on the transport, deposition and degradation, further studies are needed focussing on the fate of PAHs in the environment. Global inventories and characterization of recent developments are of major importance, particularly with respect to regulatory policies. Consequently, the primary goal of ongoing studies is the identification, estimation and quantification of continuing emissions as well as of the redistribution processes of PAHs between different environmental compartments. Therefore, one objective of current studies is the impact of different land uses and soil characteristics as well as meteorological influences and the role of climate change on pathways and exchange processes of organic pollutants in air and soil (Ghirardello *et al.*, 2010, Komprda *et al.*, 2013, Herkert *et al.*, 2016). A comprehensive understanding of crucial processes and parameters allows transferring explicitly characterised relations to model the ongoing exchange processes and ultimately quantify recent fluxes.

### **Passive sampling for an environmental pollutant inventory**

Investigation of exchange processes across the soil-atmosphere interface regarding semi-volatile organic compounds is so far mainly based on two approaches: i) calculating fugacity ratios (Harner *et al.*, 2001, Backe *et al.*, 2004, Masih *et al.*, 2012, Tasdemir *et al.*, 2012) or ii) direct measurements of air equilibrated with the topsoil by the use of fugacity samplers (Meijer *et al.*, 2003, Cabrerizo *et al.*, 2009, Koblížková *et al.*, 2009, Wang, Luo, *et al.*, 2015). The calculation of fugacity ratios is mainly based on estimated partition coefficients between solid and gaseous phase. Several approaches to obtain the respective coefficients may be found in literature, leading to values ranging over several orders of magnitude and therefore generating contrasting flux directions (Ribes *et al.*, 2003). To this end, this method introduces vast uncertainty into data evaluation and the determination of the fate of Persistent Organic Pollutants (POPs) in the environment. For the estimation of fugacity ratios, discrete soil profiles are taken in the field and analysed further in the laboratory by exhaustive extraction of target compounds. Fugacity samplers, on the other side, are designed to sample air, which is assumed to be in equilibrium with the underlying soil (Donald & Anderson, 2017). If equilibrium is not reached, significant errors may be introduced into data evaluation. Another drawback of this sampling approach is the uncertainty of the reflected soil horizon. Since fugacity samplers are deployed in the field right above the top soil they cannot distinguish for the soil depth. Hence, this method merely samples a rather undefined topsoil horizon and

lacks the opportunity to determine a concentration (or fugacity) gradient within the soil.

Therefore, an alternative approach may be applied based on passive samplers. Passive samplers have been successfully applied to determine concentrations of hydrophobic, organic pollutants in the atmosphere, aqueous phase as well as soils and sediments (Lohmann *et al.*, 2001, Kot-Wasik *et al.*, 2007, Hawthorne *et al.*, 2011, Tuduri *et al.*, 2012, Estoppey *et al.*, 2016). Several advantages of passive sampling opposed to active sampling are reported in literature, such as low costs, no energy consumption as well as easy deployment and handling. Besides, the sensitivity as well as the spatial and temporal resolution may easily be adapted to the needs of the research question. A broad range of different passive samplers is described in literature, like Polyurethane Foam (PUF) disks, Ethylene Vinyl Acetate (EVA) coatings, Polydimethylsiloxane (PDMS) sheets or coatings, XAD resins, Low Density Polyethylene (LDPE) sheets, as well as semipermeable membrane devices comprising a defined sampling phase (Bartkow, Hawker, *et al.*, 2004, Bartkow, Huckins, *et al.*, 2004, Farrar *et al.*, 2006). One characteristic attribute of passive samplers refers to the integration over several days or months, which compensates short-term fluctuations in the atmosphere or water body (Vrana *et al.*, 2005). In particular, within sediments, soils, and water an additional advantage of passive sampling refers to the direct measurement of freely dissolved or (bio-)available concentrations (Jahnke *et al.*, 2012, Smedes *et al.*, 2013). Hence, passive samplers are used to reflect concentrations of contaminants in organisms acting as indicator for bioaccumulation (Bergknut *et al.*, 2007, Mäenpää *et al.*, 2011). Corresponding to this attempt, the activity of target compounds within the sampled medium may be determined directly as well, and the samplers may be applied as 'Chemometers' (Reichenberg *et al.*, 2008). Therefore, diffusive fluxes of PAHs within soil and sediments as well as across compartments can be examined by the use of passive samplers (Belles *et al.*, 2017). The passive sampling approach has successfully been applied to measure the activity of target compounds as well as to establish the pollutant flux across different compartments, e.g. sediment-water and water-atmosphere exchange, respectively (Morgan & Lohmann, 2008, Sobek *et al.*, 2013).

## 1.2 Thesis aim and objectives

The overall aim of this thesis is the determination and quantification of concentration gradients of PAHs across the soil-atmosphere interface. Based on such gradients, the recent flux direction of PAHs may be determined. Moreover, relevant environmental parameters like soil properties and air temperature are monitored to analyse potential correlations. The study was conducted at three different locations to allow for an appropriate comparison of different soil types, plant covers and land uses. The scope of this work is subdivided into four specific objectives:

1. Development of an appropriate passive sampling method for the atmosphere

This includes a detailed study on uptake kinetics of PAHs from the atmosphere onto Polyethylene (PE) sheets, elimination of sampling artefacts like photodegradation as well as a comparative monitoring campaign for PE sheets and Polydimethylsiloxane (PDMS) coated jars as passive samplers. Verification of the chosen method and the respectively determined atmospheric concentrations was obtained by the use of active samplers and the application of a numerical model.

2. Application of the chosen method for seasonal monitoring campaigns.

Following the development of an adequate passive sampling method for the atmosphere, PAH concentrations in the air were determined at the three study sites (based on PE sheets). Seasonal monitoring campaigns during two subsequent years were performed to identify both spatial and temporal variations within the atmosphere. Additionally, a potential concentration gradient within the atmosphere as well as bulk deposition of PAHs was investigated.

3. Comparison of four approaches investigating freely available PAH concentrations in soils.

Since passive sampling in the soil has been performed in ex-situ batch tests, the according uptake kinetics were also examined within a preliminary kinetic test for the respective set-up of the batches. Adjacent to this kinetic test, freely available concentrations of PAHs were obtained for each of the soil profiles. Besides, an equivalent comparison of batch tests comprising PE sheets and PDMS coatings was conducted.

4. Identification of the recent flux direction of PAHs across the soil-atmosphere interface.

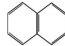
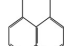
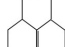
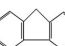
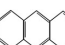
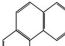
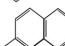
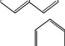
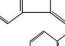
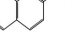
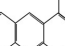

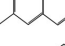
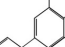

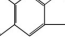
Ultimately, based on equilibrium concentrations of PAHs on passive samplers and in the gas phase in both atmosphere and soil, concentration gradients were obtained for each study site as indicator on the recent flux direction.

Finally, with the outcome of this study three papers are in progress, according to the defined objectives, including:

- a) Validation and application of PE passive samplers for a quantitative determination of atmospheric PAH concentrations at three sites in Southern Germany
- b) A comparative study on the determination of freely available PAH concentrations in soils
- c) Identification of the recent flux direction of PAHs across the soil-atmosphere interface



**Table 1.1: Physicochemical properties of U.S. EPA Priority PAHs; molecular weight ( $M_{mol}$ ), water solubility ( $S^1$ ), subcooled liquid solubility ( $S_{sub}^2$ ), Henry's law constant ( $H^1$ ) and octanol-water partition coefficients ( $K_{ow}^2$ ). With <sup>1</sup> taken from *New Jersey Department of environmental protection* and <sup>2</sup> taken from *EPISUITE***

Compound	Structure	$M_{mol}$ [g/mol]	$S^1$ [mg/L]	$S_{sub}^2$ [mg/L]	$H^1$ [-]	$\text{Log } K_{ow}^2$ [L/kg]
Naphthalene ( $C_{10}H_8$ )		128	31	124.8	1.98E-02	3.17
Acenaphthylene ( $C_{12}H_8$ )		152	16	25.25	4.51E-03	3.94
Acenaphthene ( $C_{12}H_{10}$ )		154	4.24	22.05	6.36E-03	4.15
Fluorene ( $C_{13}H_{10}$ )		166	1.98	9.81	2.61E-03	4.18
Anthracene ( $C_{14}H_{10}$ )		178	4.34E-02	4.34	2.67E-03	4.35
Phenanthrene ( $C_{14}H_{10}$ )		178	1.10	4.34	9.43E-04	4.35
Pyrene ( $C_{14}H_{10}$ )		202	0.14	0.84	4.51E04	4.93
Fluoranthene ( $C_{16}H_{10}$ )		202	0.21	0.84	6.6E-04	4.93
Chrysene ( $C_{18}H_{12}$ )		228	1.6E-03	0.14	3.88E-03	5.52
Benzo(a)-anthracene ( $C_{18}H_{12}$ )		228	9.4E-03	0.14	1.37E-04	5.52
Benzo(a)-pyrene ( $C_{20}H_{12}$ )		252	1.62E-03	0.03	4.63E-05	6.11
Benz(b)-fluoranthene ( $C_{20}H_{12}$ )		252	1.5E-03	0.03	4.55E-03	6.11
Benz(k)-fluoranthene ( $C_{20}H_{12}$ )		252	8.0E-04	0.03	4.55E-03	6.11
Benz(ghi)-perylene ( $C_{22}H_{12}$ )		276	2.6E-04	0.005	5.74E-06	6.7
Indeno(1,2,3-cd)perylene ( $C_{22}H_{12}$ )		276	2.2E-05	0.005	6.03E-07	6.99
Dibenzo(a)-anthracene ( $C_{22}H_{14}$ )		278	2.5E-03	0.004	6.56E-05	6.7

### 1.3 Quality assurance

Several precautions were taken to provide a reliable dataset, this applies to the work in the field and in the lab as well as to the analysis of the measured peak areas. To consider potential cross-contamination within the lab, blanks were produced differentiating between procedure-blanks, lab and field blanks. Procedure-Blanks are generated without any sample material to control possible contamination or alteration of extracts caused during the extraction process. In this study lab blanks serve as surveillance for passive sampler and IRA material, checking on accidentally sampled target compounds during exposure times within the lab. Additionally, field blanks are produced for passive and active air sampling campaigns, surveying potential contamination during transport from the field to the lab and unintentional passive sampling for the active air samplers. As a measure of reproducibility samples were at least taken in duplicates, preferred was sampling in triplicates if possible. The sensitivity and accuracy of GC/MS measurements were regularly controlled by the use of external standards to ensure stable conditions. Variations over the course of longer measurements were taken into account by repeated triplicate measurements of the external standards.

#### ASE (Accelerated Solvent Extractor)

Three different kinds of procedure blanks were generated as a control on the ASE: empty cells were extracted at the ASE as well as cells exclusively filled with mixing materials like diatoms or quartz sand which are used to ensure homogeneous samples without preferential flow paths during the extraction process. In general, very low concentrations of target compounds were detected within the procedure blanks of the ASE with slightly higher concentrations determined for the diatomaceous earth compared to quartz sand with 1.2 ng/g Phenanthrene on diatoms and 0.3 ng/g on quartz sand. Highest concentrations within these blanks were detected for Naphthalene and Phenanthrene, leading to background concentrations determined at the ASE of up to 5% of the concentrations detected for each compound within the soil samples. Concentrations detected at the ASE were corrected by accounting for mass determined in procedure blanks and the weight proportion of the used mixing material. Naphthalene additionally was excluded from the data set on which following discussions and conclusions are based on because of cross-contamination issues.

The observed reproducibility differs for each target compound depending on concentrations. Phenanthrene, Fluoranthene and Pyrene illustrate a good reproducibility in general, validating their use as representative compounds. Calculated standard deviation depends on the concentration range detected for the samples: Low concentrations, close to the limit of quantification lead to a broader spreading and therefore higher standard deviation than high concentrations. Additionally, soil samples were homogenized best possible, yet natural differences occurring within the soil create varying concentrations for the extracts. Standard deviations calculated for the individual soil profile differ between up to 10% for Entringen, 20% for Poltringen and up to 30% in Tailfingen. Yet, all triplicates

depict the same general trend for the soil profiles.

#### Sorption tests

Three sets of blanks or controls were produced to check on potential contamination or underestimation of sorbed material and to validate the input of sorbent. Therefore, vials were filled in triplicates with Millipore water to check on potential contamination caused by the glassware or during the extraction; Millipore water and soil was used to exclude potential leaching out of the soils, besides triplicates were also filled with the working solution, including Phenanthrene, to determine the amount of sorbent actually available for sorption processes. Concentrations measured at the procedure blanks are generally below detection limit with exception of two sets of blanks providing concentrations of Phenanthrene of up to 0.16 µg/L which is less than 0.1% of the equilibrium concentration detected in the water phase in the sorption test. The sorption tests indicate a very good reproducibility with a standard deviation calculated for the triplicates of each equilibrium concentration around 3% with only few exceptions reaching up to 10%.

#### Passive sampling

Procedure blanks for passive samplers were conducted with the standard-extraction of PE sheets, irrespective of the sheets. Masses of PAHs extracted by this method were below 0.5 ng except for Nap with values up to 2 ng and Phenanthrene with values up to 1.2 ng. Considering the measured concentrations of target compounds at the end of each monitoring campaign, the procedure blanks account for less than 10 % of the detected masses on the sheets.

#### I. Passive sampling in soils

Lab blanks were done in triplicates for the passive soil sampling, including preloaded passive samplers, Millipore water and NaN<sub>3</sub>. These blanks were handled identically to the regular batches including the soil to check on potential contamination throughout the whole process of the batch experiment and the extraction of the samplers. In general, concentrations on the blank passive samplers were below 1.5 ng/g and therefore quite close to the limit of quantification. Exceptions were Naphthalene and Phenanthrene with concentrations around 3-5 ng/g and in one case up to 11 ng/g. As for the bulk soil samples, Naphthalene was excluded from the discussion and conclusion due to its comparably high background concentration. Considering Phenanthrene, on the other side, measured concentrations on the blanks were expected to be at the utmost 10% of the concentrations determined in combination with soil. This holds true for most of the soil samples, except for the lowest horizons in each soil-profile due to the particular low concentrations of PAHs within these horizons. Thus, the lowest horizons are mainly excluded from discussion and interpretation.

Considering the soil profile in Entringen, a clear correlation can be seen considering the horizons and the reproducibility. In general, a standard deviation of 10 % was calculated for all target compounds except Naphthalene, which reaches up to 40 %. Higher

variations of up to 40 % were also detected for other compounds within the deepest horizon with the lowest concentrations of PAHs and the turf, which included plant material and was potentially very heterogeneous. Batches including soil samples from Poltringen show standard deviations that depend on the size of the target compound, with lower deviation for high molecular weight compounds. More precisely, small compounds vary up to 50%, Flt and Phe indicate deviation between 4 and 24%, whereas bigger PAHs illustrate deviation around 10%. On the other end, this profile is explicitly homogeneous with depth leading to a number of 15 replicates instead of triplicates. Considering the whole set of samples provides a similar trend with standard deviation of up to 40% for smaller compounds (Nap – Ace), around 25% for Flt and Phe and less than 13% for bigger compounds. The soil profile taken in Tailfingen produces the biggest variation on the passive samplers with standard deviation up to 50% for Phenanthrene and up to 80% for Fluoranthene. Besides, no clear correlation can be determined considering the individual target compounds or horizons of the soil profile. Observed variations can be explained with difficulties during the process of homogenization due to high water content of the soil samples.

### II. Passive sampling in air

Lab blanks for atmospheric passive samplers were extracted in triplicates subsequent to the loading step and in advance of the installation in the field to determine starting concentrations of the performance reference compound, on the one side, and to check on potential pre-existing concentrations of target compounds on the sheets, independent of the transport to the field sites and back. Additionally, triplicate field blanks were extracted for every location to determine the concentrations of target compounds at the starting time of the monitoring at each location. Concentrations of all PAHs are below 1 ng/g for all compounds at the beginning of each monitoring and generally close to the limit of detection. Exceptions are Naphthalene with concentrations up to 5 ng/g and Phenanthrene with up to 3 ng/g on the lab and the field blanks. Lab blanks were close to the detection limit and subtracted from concentrations on the samplers after field exposure.

Since low PAH concentrations on the passive samplers during the uptake phase led to high standard deviations, only measurements after at least ten days of sampling are taken into account. May 2016: A generally low standard deviation of less than 10% was observed with only exception for Pyrene detected in Poltringen, reaching up to 15% standard deviation. August 2016: During this monitoring campaign in general very low concentrations of less than 10 ng/g generate high variation of detected concentrations of up to 100%. Higher concentrations immediately decrease the observed standard deviation to less than 10%. November 2016: The observed standard deviation varies between 1 and 20% with higher variation of the detected concentrations for the bigger compounds. February 2017: Entringen and Tailfingen illustrate a very good reproducibility with standard deviation of up to 8%. Poltringen, on the other side, depicts rather high variation

of up to 40%. May 2017 (1. Sampling with two heights): Standard deviation was low for both heights at all stations, reaching at maximum 18%, except for the compounds detected close to the limit of quantification; those illustrate variation higher than 100%. August 2017: At 0.1 m height a strong correlation can be observed for detected concentrations with standard deviation, with concentrations around 0.1 – 1.5 ng/g illustrating a standard deviation up to 30% whereas higher concentrations generate standard deviation between 5 and 15%. At 1.2 m height, on the other side, comparably high variation can be observed regardless of the compound and the concentration of up to 30%. November 2017: The lowest standard deviation can be observed for 1.2 m height in Entringen and Poltringen with variation below 8%, whereas in Tailfingen concentrations deviate slightly greater around 13%. At 0.1 m height the lowest variation was detected for Entringen below 10%, while in Poltringen and Tailfingen concentrations vary up to 15%. February 2018: At 0.1 m height generally low standard deviation < 10% was detected; only very low concentrations on the sampler (e.g. *Bbf-BkF*) result in higher standard deviation up to 50%, however, those values were excluded from further evaluation and interpretation. Sampling at 1.2 m height in Entringen and Poltringen depicts slightly higher standard deviations reaching 15%. In Tailfingen, higher variation throughout the course of the sampling was obtained reaching up to 40%.

#### Active air sampling

Concentrations measured with active air samplers were corrected based on measured field blanks. Field blanks were handled identically to the active samplers except for pumping air, in order to passively sample air masses that all of the samplers are exposed to during transport and charging events. Background concentrations of target compounds reached 10 to 30% of the masses measured on the active sampler, depending on the seasonal monitoring. For Naphthalene and Phenanthrene these amounts reach up to 75% of the masses on the samplers. Procedure blanks were close to or below the limit of detection with highest masses detected for Phenanthrene with up to 0.9 ng relating to less than 3% of the masses detected in the sampler.

Active air sampling was only done at one location (Entringen) and therefore conducted in triplicates as a measure for reliability. Starting with the second monitoring, two subsequent time spans were sampled to increase the number of replicates. During August 2017, concentrations were quite reproducible with a standard deviation of 5-10%. Runtime-issues of the active samplers occurred at colder temperatures, caused by the battery. This leads to notable uncertainties of sampled air masses and to standard deviations of up to 30% for Fth during November 2017. For February 2018, one of the samplers had to be excluded altogether. Duplicate samples agree quite well with a maximum deviation of 8%.

#### Sampling of atmospheric bulk deposition

As control on the deposition sampler, procedural and lab blanks were used to correct the

detected masses of target compounds on the sorbing material. Therefore, the standard extraction method was conducted on empty glassware to check on potential contamination. Low masses for all of the compounds were found with the highest values for Naphthalene at 0.6 ng and Phenanthrene at 0.15 ng, which amounts to 10% of the masses detected on the lab blanks. Lab blanks consist of cartridges prepared identically to the ones installed in the field but kept in the lab unexposed to air throughout the time of the monitoring and then extracted concurrent to the samples. Again, Naphthalene and Phenanthrene were the dominant PAHs detected on the blanks with masses up to 8 and 5.5 ng per cartridge, providing up to 4% of the masses detected on the samples. In general, the masses of target compounds on the lab blanks were below 1.5 ng per cartridge resulting in less than 2% of the masses detected on the samples. Yet, sampled masses were corrected for both the procedure as well as for the lab blank.

Although only one depositional sampler was set up per location, standard deviations could be calculated, since PAH concentrations in other respects were quite comparable at the three locations. During the first two monitorings one of the locations (Tailfingen) needed to be excluded, leading to duplicates instead. Masses detected for the first monitoring, covering May – August 2017 were quite comparable for Entringen and Poltringen. Yet, low values between 0.5 and 15 ng for the different compounds lead to a spreading of up to 100 %. Considering the second monitoring from August to November 2017 100% variation was still detected for Acenaphthene, all other compounds indicate variation of less than 10%. The lowest variation, including all three stations, were measured during November 2017 – February 2018 and February - May 2018 with a general standard deviation of less than 10%, except for Fth and Pyr, reaching up to 15%.

Altogether, procedural and field blanks indicate no cross-contamination by sample transportation and preparation in the lab with concentrations generally below 10% of concentrations in the respective samples. Only Naphthalene and Phenanthrene form an exception with respect to PUF filters used for active air sampling. Besides, a very good reproducibility was determined with standard deviations generally below 30 %. Here, exceptions with higher standard deviations are obviously caused by low concentrations, which is mainly compound-related.

### Chemicals and devices

All chemicals used for extraction of the different materials (soil, water, polymers) were supplied by Merck Millipore (Darmstadt, Germany). Generally suprasolv solvents were used with a certified purity of 99.8%. This includes Acetone, Toluene, Ethylacetate and Cyclohexane. Millipore water was obtained by a water purification system (*Gen Pure Pro UV-TOC, Thermo Scientific*). Reference solutions for the quantification of target compounds within the extracts were obtained by *Dr. Ehrenstorfer GmbH* as internationally standardized references; *PAH MIX 31* and *PAH MIX 14* were used as internal and external standards, respectively. *PAH MIX 31* includes Naphthalene-D<sub>8</sub>, Acenaphthene-D<sub>10</sub>, Phenanthrene-D<sub>10</sub>, Chrysen-D<sub>12</sub> and Perylene-D<sub>12</sub>, while *PAH MIX 14* comprises all U.S. Environmental Protection Agency 16 Priority PAHs.

Devices regularly needed for the concentration of extracts in advance of the measurements include: A rotational evaporator for volumes up to 200 ml, supplied by *Heidolph* and an evaporation device (*Vapotherm mobil*) for volumes  $\leq$  10 ml, supplied by *Barkey*.

### Measurement at the GC/MS

The concentrations of the 16 U.S. EPA Priority PAHs as target compounds were determined by gas chromatography and coupled mass spectrometry (*Hewlett Packard (HP) 68909 and HP 5973*). The separation was attained within a 25 m long capillary column (25  $\mu$ m in diameter), coated with a 0.25  $\mu$ m thick film of 5% Phenyl- and 95% of Dimethylpolysiloxane (*J&W Scientific*). Samples were injected in pulsed splitless mode. The temperature program started with an initial temperature of 65 °C for 4 minutes. Subsequently, temperature increased with 10 °C per minute up to 270 °C, which was held constant for 10 minutes, before continuing the increase up to a second constant temperature of 310 °C for 6 minutes. Helium was used as inert carrier gas with a constant flow rate of 0.7 mL/min. The mass spectrometer was operated in single ion mode. Both external (*PAH Mix 14*) and internal (*PAH Mix 31*) standards were used for quantification of target compounds.

## 2 Characterization of study sites - land use and soil properties

### 2.1 Study sites and land use

This study was conducted at three sites in a rural, but not remote, area located in south-western Germany in the hinterland of Stuttgart. Sampling locations were chosen with respect to main influences on PAH concentrations within air, considering no influence of primary as well as secondary sources and feasibility. Thus, local point sources were avoided. The different study sites were in close vicinity to each other with a maximum distance of 12 km but characterized by different soil types and land use. The different types of soil were expected to influence the exchange of PAHs between soil and atmosphere to varying degrees leading to site-specific fluxes across the soil-atmosphere interface. Characterization of the study sites focuses on determining the soil and atmosphere parameters relevant for pollutant fluxes and their direction.



Figure 2.1: Map of the surroundings of west Tübingen, showing the sampling sites Entringen, Poltringen, Tailfingen.

The selected sites are near small villages in the south of Stuttgart, namely Entringen, Poltringen and Tailfingen. The sampling site Entringen lies within a water protection zone, which was agriculturally used until ca. 50 years ago, and since then preserved as fenced-in meadow (not agriculturally used). Entringen is the site with the lowest elevation of 363 m a.s.l., close to a federal road on one side and a railway line used by a diesel engine train on the other side. The site in Poltringen is set up on an agricultural field with alternating vegetation of maize and clover. 15 years ago the farmer in charge switched



from conventional to organic farming. It is located on top of a hill at 394 m a.s.l. outside of the village with a small airport for gliding planes in close vicinity. The sampling site Tailfingen is also outside of the village, lying within an open plain of agricultural fields at a height of 402 m a.s.l.; the vegetation here varies between beets and other crops. Nearby are a federal road as well as a motorway (A81). Both Poltringen and Tailfingen are ploughed at least once a year to an estimated depth of 30 – 40 cm.

At all sampling sites, precise soil profiles were taken and soil samples for different horizons were characterised in terms of grain size distribution, organic carbon content and sorption behavior. Further characterization of the soil horizons includes PAH concentrations. Besides, soils were classified by the *Landesamt für Geologie, Rohstoffe und Bergbau* (LGRB-Kartenviewer; soil –survey 1:200 000, (BÜK 200)). According to that, soils within the valley plain of Entringen are brown alluvial soils including gley to some extent. The underlying geology in Poltringen belongs to the *Lettenkeuper* and soils are generally described as brown soils. Soils around Tailfingen developed on loess and are described as luvisols (LGRB-Kartenviewer; geological-survey 1:300 000 (GÜK300)).

## 2.2 Methods

### 2.2.1 Soil properties

#### Sampling in the field

Soil profiles in the field were taken by digging on a square meter to discrete depth, to minimize local heterogeneity. Each horizon was homogenized manually in the field to obtain representative samples for the individual horizons (see Table 2.1). Depending on depth interval, 1 – 2.5 kg per sample were collected in galvanized steel buckets and stored in the lab at 4 °C until further preparation. Particles larger than 2 mm were removed in the lab by sieving.

#### Grain size distribution

Homogeneous subsamples of each soil horizon of 40 g were dispersed in 60 mL of Millipore water in glass bottles and kept on a horizontal shaker for at least 48 hours before the measurement. Grain size distribution was determined by laser granulometry based on wet sample dispersion, with a pumping rate set to 3000 rpm (*Mastersizer 2000* coupled to *Hydro 2000S*, Malvern). Grain sizes are calculated from refraction of laser light according to the *Mie-Theory*.

#### Organic carbon content

Measurement of organic carbon and nitrogen content was performed at the element analyser (*vario EL*, *Elementar*). The first step of sample preparation included freeze-drying of 20 g of soil for each horizon and subsequent pulverisation in a planet ball mill. Carbonates were removed with hydrochloric acid (16 %), followed by neutralization of soil

samples with Millipore water and drying at 60 °C. 20-30 mg of the prepared soil were pressed into tin capsules and burnt at 950 °C. The subsequent release of CO<sub>2</sub> was determined with a thermal conductivity detector.

### Extraction of bulk soils

The extraction of PAHs from bulk soil samples was performed in a two-step extraction procedure using Accelerated Solvent Extraction (ASE 300, Dionex) with acetone and toluene as subsequent solvents. Therefore, 20 g of soils were mixed manually with 80 g of quartz sand or diatomaceous earth and filled into 66 mL cells. Clean mixing material was used to ensure sufficient permeability and good contact of the solvent with soil particles and prevent preferential flow paths within the cell. Quartz sand beds and glass fibre filters were used to hold back fine material released from the sample. The ASE used 100 bars pressure at 100 °C for extraction with acetone and 150 °C for toluene. To optimize the yield of target compounds in the extracts, two consecutive extraction cycles were performed for each solvent. One cycle included 10 minutes of static extraction time at the respective temperature and pressure. After the first cycle, 50 % of the solvent was released and then fresh solvent pumped into the cell. Following the second cycle, the solvent was displaced from the cells by purging with nitrogen for 60 seconds. toluene extracts were subsequently reduced to ca. 1 mL and measured at the gas-chromatograph with coupled mass spectrometer. acetone extracts needed to be transferred over Millipore water into cyclohexane and reduced to about 150 µL under gentle stream of nitrogen with simultaneous heating to 40 °C ahead of the measurement at the GC/MS.

**Table 2.1: List of sampled horizons and respective depth (in cm ) for each study site including topsoil, root horizons (1, 2, 3) as well as sub soils (1,2,3).**

Soil horizon	Entringen	Poltringen	Tailfingen
Topsoil	0 – 2.5	0 – 2	0 – 3
Root horizon 1	2.5 – 10	2 – 10	3 – 8
Root horizon 2	10 – 15	10 – 15	8 – 13
Root horizon 3		15 – 20	13 – 18
Subsoil 1	15 – 35	20 – 30	18 – 33
Subsoil 2	35 – 50	30 – 40	33 - 48
Subsoil 3			48 – 60

### 2.2.2 Sorption properties; Distribution coefficients

Sorption of neutral organic compounds in soils is primarily dependent on the amount and type of soil organic matter. Therefore, distribution coefficients ( $K_d$  in [L/kg]) for PAHs

between soil and water may be estimated based on the organic carbon content ( $f_{oc}$  [-]) of each soil sample and compound properties, like the organic carbon partition coefficients ( $K_{oc}$  [L/kg]):

$$K_d = \frac{K_{oc}}{f_{oc}} \quad (2.1)$$

Respective values of  $K_{oc}$  were estimated according to well-established empirical relationships (Karickhoff, 1981, Razzaque & Grathwohl, 2008). In particular, the octanol/water partition coefficients ( $K_{ow}$  in [L/kg]) or the subcooled water solubility ( $S_{sub}$  in [kg/L]) may be used:

$$\log K_{oc} = 0.989 \log K_{ow} - 0.346 \quad (2.2)$$

$$\log K_{oc} = -0.92 \log S_{sub} - 0.72 \quad (2.3)$$

$K_{ow}$  values were taken from literature (EPI –Suite) as listed in the appendix (Table A.1) and subcooled liquid solubilities were taken from Razzaque and Grathwohl (2008). Uncertainties of estimated partition coefficients are widely discussed in literature (Ran *et al.*, 2007, Allen-King *et al.*, 2002, Pan *et al.*, 2007, Yang *et al.*, 2010). Therefore, sorption isotherms were measured using Phenanthrene (Phe) exemplarily, to obtain more precise  $K_d$  values. Soil samples for aqueous batch tests were freeze dried and ground to ensure homogeneity on small scale. Spiked aqueous solutions contained  $\text{CaCl}_2$  and  $\text{NaN}_3$  providing a stable pH and minimizing bacterial activity during equilibration. Two sets of sorption tests were conducted, each aiming for a specific concentration range. The higher concentration range tests were conducted with 40 mL aqueous solution and a constant starting concentration of Phe of 0.7 mg/L or 0.07 mg/L depending on the targeted equilibrium concentration. Masses of soil varied, spanning a range of 5-200 mg depending on the desired equilibrium concentrations in water from 0.02 mg/L to 0.6 mg/L, adjusted to the individual soil sample. The second sorption test was based on the results of the first one, but aimed at very low concentration ranges and here the solid to water ratio was kept constant while the spiked concentrations were varied. Batch tests included 1 g of soil and 100 mL aqueous solution with varying starting concentrations of 0.026  $\mu\text{g/L}$ , 0.1  $\mu\text{g/L}$ , 0.5  $\mu\text{g/L}$ , 2.5  $\mu\text{g/L}$ , 12.5  $\mu\text{g/L}$  and 25.5  $\mu\text{g/L}$ . All batches were kept in the dark on a horizontal shaker with 150 rpm at 20 °C throughout the whole equilibration time. Kleineidam *et al.* (1999) suggested 7 days as sufficient equilibration time period for pulverised solids with particle sizes in the tens of  $\mu\text{m}$  range. To be on the safe side, equilibration time was set to 12 days with 10 days of constant shaking. Afterwards batches were left to rest for 2 days, allowing for a clear separation of the two phases. The cleared supernatant water was sampled and extracted with cyclohexane. Deuterated Phenanthrene was used as internal standard for quantification. Up to 95 %

of the spiked Phenanthrene was sorbed, depending on the respective  $K_d$ . This would have led to equilibrium concentrations in the water phase below the limit of detection for the very low concentration levels. Hence, the extracts were concentrated by a factor of 3000 (extraction of ca. 90 mL water with 5 mL cyclohexane and subsequent reduction of the cyclohexane to 30-50  $\mu\text{L}$ ). Calculation of equilibrium concentrations within the solid phase ( $C_{s,eq}$  [ $\mu\text{g}/\text{kg}$ ]) is based on mass balances taking into account the initial ( $C_{ini}$  [ $\mu\text{g}/\text{L}$ ]) and the equilibrium ( $C_{w,eq}$  [ $\mu\text{g}/\text{L}$ ]) concentration in the water phase as well as the previously determined background concentration within the bulk soil sample ( $C_{bulk}$  [ $\mu\text{g}/\text{kg}$ ]) following:

$$C_{s,eq} = \frac{(C_{ini} V_w + C_{bulk} m_{soil}) - C_{w,eq} V_w}{m_{soil}} \quad (2.4)$$

$V_w$  [L] and  $m_{soil}$  [kg] denote the respective volume of water and mass of the solids. Sorption to components of the batch system (glass vials, septa) was negligible, as measured on control batches including the spiked solution only. The respective loss was generally below 3 %; only samples with the highest initial concentrations show a loss of up to 9 %.

### 2.2.3 $C_{w,eq}$ and desorption enthalpies from static leaching tests

$K_d$  values from empirical relationships or from measured sorption isotherms for single compounds allow to calculate concentrations to be expected in water under equilibrium condition from solid phase concentrations. In order to determine  $C_w$  directly in seepage water, leaching experiments in columns were conducted. Since concentrations to be expected in water are very low, potentially below the detection limit, the temperature was increased stepwise which results in lower  $K_d$  values and thus higher aqueous concentrations. This also allows to determine the compound-specific desorption enthalpy  $\Delta H_{DES}$  (ten Hulscher & Cornelissen, 1996, Henzler, 2004, Madelener, 2003). Provided that equilibrium conditions prevail and the entropy is constant (and not temperature dependent) the van't Hoff equation may be used:

$$\Delta H_{DES} = -R \frac{d \ln \left( \frac{1}{K_d} \right)}{d \left( \frac{1}{T} \right)} \quad (2.5)$$

$T$  and  $R$  denote temperature [K] and the ideal gas constant [ $\frac{\text{J}}{\text{kg} \cdot \text{K}}$ ], respectively. Assuming no depletion within the solid phase reduces this to:

$$\Delta H_{DES} = -R \frac{d \ln(C_w)}{d \left( \frac{1}{T} \right)} \quad (2.6)$$

Thus, desorption enthalpies can be easily obtained by plotting  $\ln(C_w)$  vs.  $1/TR$ . This

also allows to extrapolate relatively high aqueous concentrations determined at elevated temperatures to field conditions where  $C_w$  may be below detection limit as described previously by Henzler (2004). Leaching tests were conducted using the ASE, following a protocol of 8 extraction steps at a constant pressure of 100 bars with step-wise increasing temperature and sufficiently long equilibration times (static conditions), as listed in Table 2.2. As a control whether hot water extracts display equilibrium concentrations, two separate extraction steps were performed twice with constant temperature (55 °C and 100 °C); the first with varying static times of 30 and 60 minutes, and the second with identical settings.

**Table 2.2: Temperatures and equilibration times for the explicit extraction steps of the hot water extraction at the ASE.**

Temperature [°C]	Equilibration time [min]
40	60
55	30
55	60
65	90
75	90
85	90
100	90
100	90

In order to facilitate percolation of the fine grained samples, silica (diatomaceous earth) was mixed into soils at a ratio of 1:2. Additionally, a layer of ca. 2.5 cm ground silica was placed at the bottom of the ASE cell on top of two glass fibre filters (0.45 µm pore size) to allow an even distribution of the flow. The aqueous leachates obtained from the ASE were extracted with 5 mL cyclohexane; 5 µL internal standard (*PAH Mix 31, with 200 mg/L*) were added to the aqueous phase and kept on the shaker for 30 minutes. After leaving the extracts to rest for 2-3 days in the dark, the two phases were separated and the cyclohexane was withdrawn and reduced gently under a stream of nitrogen at 40 °C to 150 µL before measurement by GC/MS. Due to low concentrations determined for temperatures below 65 °C, only five out of eight extraction steps delivered concentrations above the detection limit.

## 2.3 Results: Soil properties

### 2.3.1 Grain size and fraction of organic carbon

Figure 2.2 shows the grain size distributions measured individually for the different horizons of each location. Grain size distributions are quite comparable for the different horizons as well as for the different locations and around 90 % of the particles were smaller than fine sand ( $< 63 \mu\text{m}$ ). In Entringen and Poltringen ca. 45 % of the particles were smaller than medium sized silt and less than 20 % belong to clay sized particles. Tailfingen can be differentiated due to a higher amount of medium-coarse sized silt with only 30 % of the particles being smaller than medium silt and ca. 10 % of clay particles. Considering Poltringen and Tailfingen only slight variations were observed for the different horizons, indicating well mixed plough horizons. Entringen on the other side shows a more distinct grain size distribution with a higher fraction of coarser materials in the top layer. This is due to remains of grass and roots of the meadow within the sampled topsoil.

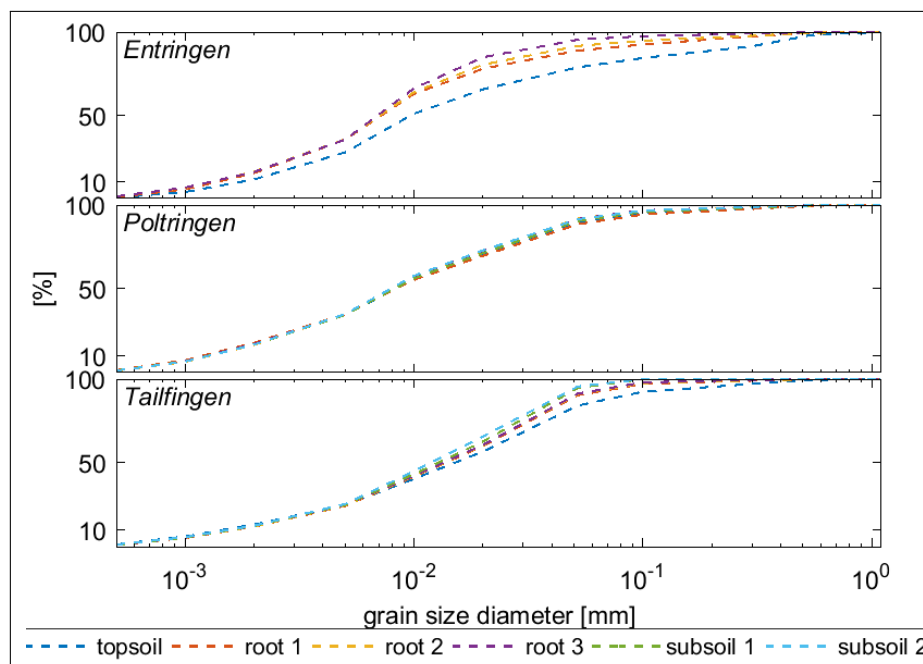


Figure 2.2: Grain size distribution shown as cumulative curves for each soil horizon.

Figure 2.3 shows the vertical distribution of the fraction of organic carbon  $f_{oc}$  and the ratio of carbon to nitrogen as an indicator for soil maturity. Organic matter essentially consists of carbon and nitrogen with explicitly higher amounts of carbon compared to nitrogen. In general, the decomposition of carbon chains with according release of  $\text{CO}_2$  is faster than binding and release processes of N. Therefore, C/N ratios evolve over time towards lower values and ratios can be used as an indicator for fresh versus matured

organic material in soils. In this study, C/N ratios are included as additional factor with respect to the comparability of the individual study sites. Poltringen and Tailfingen show low and homogeneous concentrations of organic carbon, resulting in  $f_{oc}$  ranges of 0.01 to 0.02 at each depth. In Entringen  $f_{oc}$  decreases from 0.1 in the topsoil to 0.02 at 20 cm depth. This comparison illustrates the strong influence of agricultural ploughing on the soil composition; with the end of ploughing in Entringen (ca. 50 years ago) accumulation of organic matter in the top soil can be observed. A similar trend is observed in soil maturity: A distinct decrease with depth can be observed for Entringen with a C/N ratio of 15 in the topsoil and 5 at 20 cm depth. In contrast to that, C/N ratios are almost stable in profiles of Poltringen and Tailfingen. In Tailfingen a slight decrease can be detected with a C/N value of 11 in the topsoil and 7 at 45 cm depth while in Poltringen the ratio stays 8.5 throughout the profile.

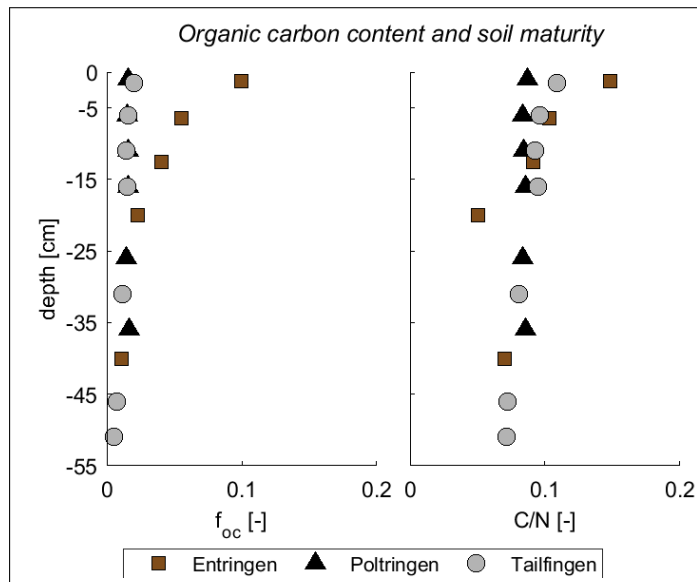


Figure 2.3: Profiles of a)  $f_{oc}$  [-] and b) ratio of C/N as indicator for soil maturity determined for the three locations.

### 2.3.2 Concentrations of PAHs in vertical soil profiles

Figure 2.4 shows a) PAH concentrations measured for the bulk soil samples after exhaustive extraction using ASE (with acetone and toluene) as well as b) organic carbon normalized concentrations. Illustrated are distribution patterns for 15 U.S. EPA Priority PAHs comparing the top soils exemplarily for the three study sites. Acenaphthylene is excluded here, due to analytical uncertainties. Benzo(b)fluoranthene (Bbf) and Benzo(k)fluoranthene (BkF) could not be separated and are therefore combined as Bbf-BkF. One characteristic distribution pattern can be observed for all three locations with highest concentrations for Fth and Bbf-BkF, followed by Pyr and further 4-6 ring PAHs;

Phe on the other side shows the highest concentration of the 2-3 ring PAHs, generally in the same range as Benz(a)anthracene (BaA), Benz(a)pyrene (BaP) and Indeno[1,2,3-cd]pyrene (Indeno). The sum of PAH concentrations in bulk soils from Entringen and Poltringen are in the same range with 5-25  $\mu\text{g}$  of PAHs per gram organic carbon, whereas Tailfingen depicts slightly higher concentrations of up to 65  $\mu\text{g}/\text{g}$  OC. Concentrations in soils not normalized to organic carbon show low (background) concentrations of 0.1-0.2  $\mu\text{g}/\text{g}$  in Poltringen, 0.2-0.7  $\mu\text{g}/\text{g}$  in Entringen and 0.03-0.7  $\mu\text{g}/\text{g}$  in Tailfingen.

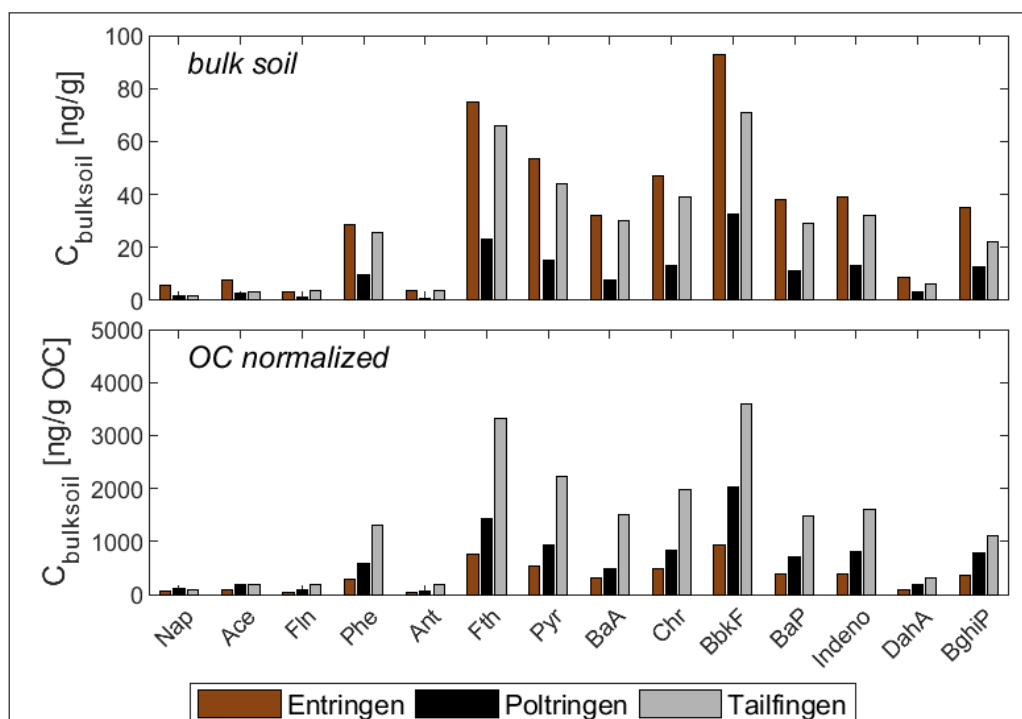


Figure 2.4: Comparison of distribution pattern of 15 U.S. EPA Priority PAHs (excluding Any) within the top soils of Entringen, Poltringen and Tailfingen as a) bulk concentrations and b) OC normalized values.

Elevated concentrations in Entringen and Tailfingen in comparison to Poltringen may be explained by additional influences due to federal roads and the diesel engine railroad trains in close vicinity of the sampling sites. Figure 2.5 shows OC-normalized concentration profiles of Phe, Fth and Pyr at each location. All three locations show quite homogeneous concentrations down to a depth of about 30 cm with the exception of the lowest soil sample in Tailfingen. This low concentration below 30 cm depth most likely indicates the end of the plough horizon. For each location identical trends were observed for the different compounds, illustrating constant distribution patterns for the individual depths. In Entringen all three compounds demonstrate a slight increase of the concentrations over the first 15 cm, followed by rather stable concentrations, with a slight decrease at 25 cm depth. Highest concentrations were measured for Fth with 0.75 - 4.8  $\mu\text{g}/\text{g}$  OC,



while Phe shows the lowest concentrations of 0.27 - 0.96  $\mu\text{g/g OC}$ . In Poltringen almost homogeneous PAH concentrations were detected throughout the profile with values of 0.5 - 0.75  $\mu\text{g/g}$ , 0.85 - 1.0  $\mu\text{g/g}$  and 1.3 - 1.5  $\mu\text{g/g OC}$  for Phe, Fth and Pyr, respectively. One exception can again be observed at 25 cm depth, which depicts a minor increase. Tailfingen, on the other hand, illustrates a notable increase of concentrations up to a depth of ca 10 cm, followed by a slow decrease and identical values for 15 and 30 cm depth. The measured concentrations at the three study sites are within a quite comparable range, indicating lowest concentrations for Phe (0.3 - 3  $\mu\text{g/g OC}$ ) and highest values for Fth (0.8 - 12  $\mu\text{g/g OC}$ ). Profiles measured on the bulk soil (not normalized to OC) illustrate even higher homogeneity with depth (Figure A.1), particularly with respect to Entringen. Here, the substantial decrease of OC with the depth of the profile leads to a clear increase of PAH/g OC.

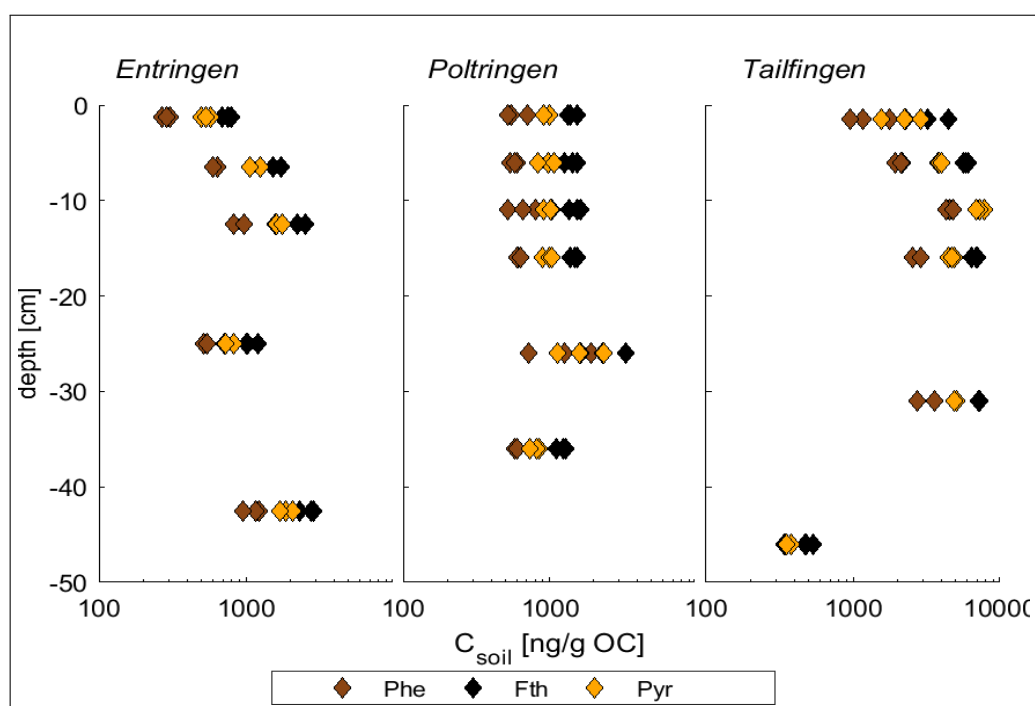


Figure 2.5: OC-normalized concentration profiles of Phe, Pyr and Fth at the three locations (Entringen, Poltringen and Tailfingen).

### 2.3.3 Distribution coefficients and sorption isotherms for Phenanthrene

As introduced above, different approaches exist for the determination of soil-water distribution coefficients for PAHs, e.g. related to their physicochemical properties like  $K_{ow}$  or  $S_{sub}$ . Based on the measured  $f_{oc}$ , distribution coefficients were calculated for all soil horizons according to Equation 2.2 and Equation 2.3, as listed in Table 2.3. Per definition, the respective distribution coefficients decrease with soil depth in Entringen, correlating

## 2 Characterization of study sites - land use and soil properties

to the decline of  $f_{oc}$ . Correspondingly, in Poltringen and Tailfingen rather stable values were determined independent of the soil depth. Results of both approaches are compared in Figure 2.6 illustrating a systematic offset towards higher coefficients based on  $S_{sub}$  than  $K_{ow}$  (for 0.2 log units). This offset confirms the uncertainty of empirical relationships for characterizing sorption properties of soils and thus the need for accurate measurements of sorption tests.

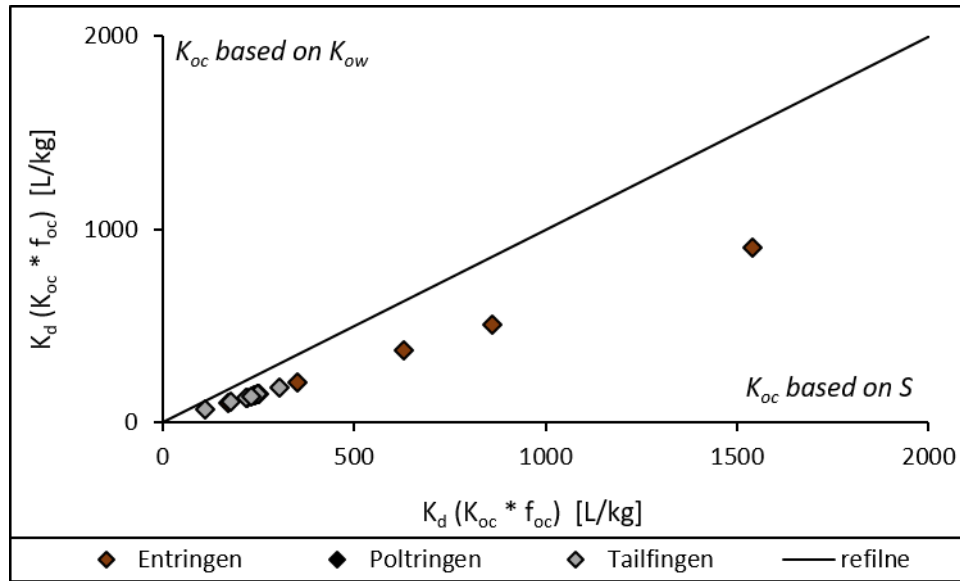


Figure 2.6: Scatter plot comparing empirical estimations of  $K_d$  values (based on  $K_{ow}$  versus  $S_{sub}$ ) for each soil horizon and all sampling sites.

Figure 2.7 shows sorption isotherms measured for Phe in the top soils of each location. Lowest equilibrium concentrations in the aqueous phase were 0.04  $\mu\text{g/L}$  in Poltringen and highest levels were 580  $\mu\text{g/L}$  in Poltringen and up to 780  $\mu\text{g/L}$  in Entringen. Corresponding solids concentrations in the soil range from 40 - 300 000  $\mu\text{g/kg}$  for Entringen and 10 - 100 000  $\mu\text{g/kg}$  and 40 - 80 000  $\mu\text{g/kg}$  in Poltringen and Tailfingen, respectively. All isotherms show a slight, but significant nonlinear behaviour. This nonlinear relation is most pronounced within the low-concentration range of  $C_{w,eq}$  below 1  $\mu\text{g/L}$ . Equilibrium soil concentrations are calculated based on simple mass balances (Equation 2.4). Therefore, the total mass in the batches was determined based on measurements of the native concentration in the soil and the initially spiked concentration of the aqueous solution ( $C_{w,ini}$ ). After equilibration, concentrations in the aqueous phase ( $C_{w,eq}$ ) were measured, which leaves the equilibrium concentration of the soil solids as only unknown. At low concentrations close to the limit of detection, the uncertainty of measurements increases. Based on their good reproducibility, the respective data are still included within the shown regression.

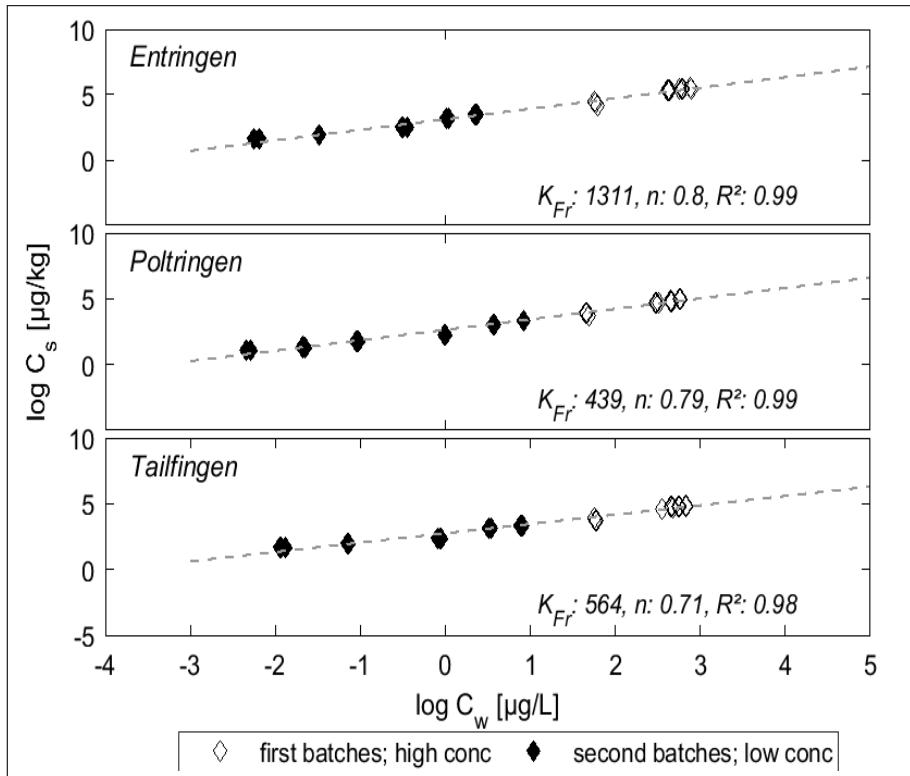


Figure 2.7: Sorption isotherms of Phe determined for the top soil of Entringen, Poltringen and the root horizon 1 in Tailfingen.

Distribution of organic compounds between soil and water may depend on concentrations and therefore follow a nonlinear relation between  $C_{w,eq}$  and  $C_{s,eq}$ . Allen-King *et al.* (2002 - and references therein) describe adsorption as a relevant process at low concentrations and partitioning predominating at high concentrations. Therefore, sorption data can be described best by Freundlich isotherms, following:

$$C_s = K_{Fr} C_w^{1/n} \quad (2.7)$$

This provides  $\log K_{Fr}$  values in the range of 2.3 - 3.1 L/kg for the studied soils. Freundlich isotherms are used widely to evaluate sorption tests, since broad concentration ranges can be covered within one correlation (Allen-King *et al.*, 2002, Luthy *et al.*, 1997). Independent of the sampling location, very good coefficients of determination ( $R^2$ ) were obtained when combining two sets of sorption tests, as illustrated in Figure 2.7. In Poltringen and Tailfingen, samples show quite comparable trends with  $K_{Fr}$  values of 440 and 560 L/kg. A maximum  $K_{Fr}$  value of 1300 L/kg was determined for the topsoil in Entringen with the highest  $f_{oc}$  of all soil samples. The respective Freundlich exponents are identical in Entringen and Poltringen with values of 0.8. In Tailfingen, nonlinear-

ity is slightly more pronounced with an exponent of 0.7. The whole set of measured Freundlich coefficients and exponents for all soil samples is listed in Table 2.3. Due to the very good fit of measured sorption isotherms to the Freundlich relation, further data evaluation is based on corresponding Freundlich coefficients ( $K_{Fr}$ ) and exponents ( $n$ ). Measured Freundlich coefficients may be used to calculate specific distribution coefficients for the low concentrations of Phe in the bulk soil. Regarding the considerably strong sorption determined for all soil horizons the measured  $C_{bulksoil}$  can be accepted as  $C_{s,eq}$  and used within Equation 2.7 providing  $C_{w,eq}$ . Subsequently, the equilibrium concentrations in water and solid phase can be applied to calculate the distribution coefficient for measured background concentrations:

$$K_d^* = \frac{C_{s,eq}}{C_{w,eq}} \quad (2.8)$$

A comparison of experimentally determined  $K_d^*$  values to the empirical prediction based on measured  $f_{oc}$  values, including  $S_{sub}$  (Equation 2.3) is shown in Figure 2.8. Measured  $K_d^*$  exceed the estimations based on empirical correlations by a factor of two in Poltringen and Tailfingen and a factor of four in Entringen. This observation underlines the considerable nonlinear sorption behaviour as well as the strong sorption capacity of the examined soil samples.

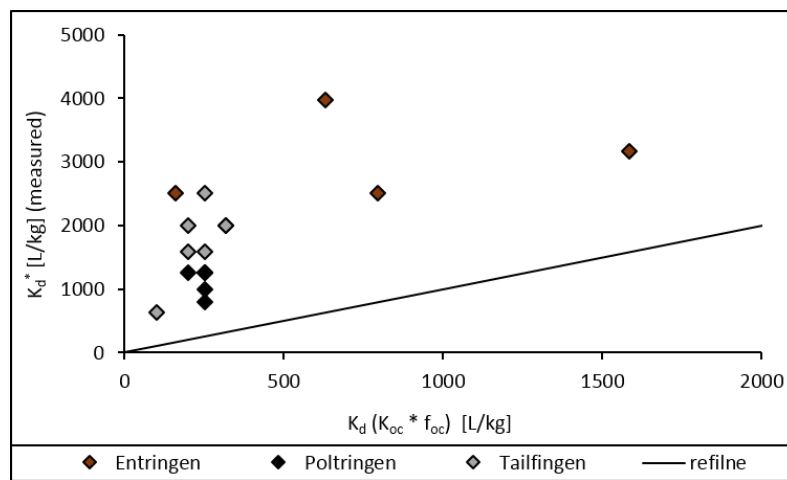


Figure 2.8: Scatter plot of measured versus estimated (Equation 2.3) distribution coefficients of Phe for each soil horizon at each study site.

Finally, in accordance to the correlation of  $K_d$  to organic carbon in soils (Equation 2.1),  $K_{oc}$  values may be adapted to the low concentrations measured in the bulk soil as well:

$$K_{oc}^* = \frac{K_d^*}{f_{oc}} \quad (2.9)$$

Adapting partition coefficients to the observed non-linear sorption behaviour of the studied soils leads to significantly high values, exceeding literature about one order of magnitude, as listed in Table 2.4. The top soil in Entringen, which comprises the highest amount of organic carbon illustrates the best fit for the different approaches. In accordance to that, the biggest offset can be observed for the lowest soil horizon in Tailfingen (subsoil 2), which is characterized by the lowest  $f_{oc}$ . Yet, with respect to nonlinear sorption, properties of organic material like structure and maturity influence the sorption capacity of soils as well. Distribution coefficients illustrate a notable correlation to the observed C/N ratio (as indicator for soil maturity), most pronounced in Entringen. Regarding Poltringen and Tailfingen rather constant values of  $K_{oc}^*$  were determined, independent of the soil depth demonstrating a range of  $10^{4.7} - 10^{4.9}$  in Poltringen and  $10^{5.0} - 10^{5.3}$  L/kg in Tailfingen. In Entringen the topsoil illustrates the lowest  $K_{oc}^*$  with  $10^{4.5}$  [L/kg] corresponding to the highest C/N ratio with a value of 15. In parallel to a decrease of the C/N ratio, an increase of the oc-normalized sorption coefficient was determined, up to a Log  $K_{oc}^*$  of 5.3 for the lowest soil horizon in Entringen with a C/N ratio of 5. Accordingly, stronger sorption of PAHs to soils was related to organic carbon demonstrating higher maturity. These findings are consistent with a clear correlation of higher  $K_{oc}$ -values for more condensed organic matter, illustrated by Grathwohl (1990) and Kleineidam *et al.* (1999). Similarly, Zhou *et al.*, 2010 and Sun & Li, 2005 report stronger sorption and therefore lower availability of sorbed compounds with respect to aged organic material compared to fresh organic matter. In general, fresh organic material accumulates in topsoils, with time and depth this fresh material ages and alters towards higher condensation and thus higher sorption coefficients, as observed in Entringen. Regarding agricultural soils (like Poltringen and Tailfingen) instead, regular mixing of soils hinders such a development with time by generating regularly stable conditions within the whole profile. Structural effects of organic matter in soils cannot be captured by the empirical correlations of  $K_d$  to  $f_{oc}$  as they merely refer to the amount and not the type of organic carbon. Hence, Freundlich coefficients and exponents combine both information: Freundlich coefficients refer to the amount of organic carbon while the exponent, as a measure for non-linearity, reflects the structure or condensation of the organic material with higher non-linearity of more condensed material. Consequently, highest Freundlich coefficients in the upper soil horizons in Entringen correspond to high amounts of organic carbon in parallel to comparably high Freundlich exponents. With depth, and thus higher maturity, non-linear sorption gets more pronounced (lower values of  $1/n$ ), while in parallel values of  $K_{Fr}$  decline.

## 2 Characterization of study sites - land use and soil properties

**Table 2.3: A) Distribution coefficients estimated on  $K_{oc} * f_{oc}$  in [ L/kg ], based on <sup>a)</sup> $K_{ow}$ , according to Karickhoff (1981) and <sup>b)</sup>  $S_{sub}$ , following Razzaque & Grathwohl (2008). And B) Freundlich coefficients and Freundlich exponents determined for Phe on measured sorption isotherms.**

Location/soil horizon	Entringen		Poltringen		Tailfingen	
A) Distribution Coefficients	Log $K_d^a$	Log $K_d^b$	Log $K_d^a$	Log $K_d^b$	Log $K_d^a$	Log $K_d^b$
Topsoil	3.0	3.2	2.2	2.4	2.3	2.5
Root horizon 1	2.7	2.9	2.2	2.4	2.2	2.4
Root horizon 2	2.6	2.8	2.2	2.4	2.1	2.3
Root horizon 3			2.2	2.4	2.2	2.4
Subsoil 1	2.3	2.5	2.1	2.3	2.1	2.3
Subsoil 2	2.0	2.2	2.2	2.4	1.8	2.0
B) Freundlich Parameter	Log $K_{Fr}$	1/n	Log $K_{Fr}$	1/n	Log $K_{Fr}$	1/n
Topsoil	3.1	0.8	2.6	0.8	2.5	1.0
Root horizon 1	3.1	0.8	2.7	0.8	2.8	0.7
Root horizon 2	3.1	0.8	2.6	0.8	2.8	0.7
Root horizon 3			2.6	0.8	2.9	0.7
Subsoil 1	2.7	0.7	2.6	0.8	2.9	0.7
Subsoil 2	2.6	0.7	2.6	0.8	2.3	0.8

**Table 2.4: Distribution and partition coefficients adjusted for the low concentrations of Phe in the bulk soil samples.**

location	Entringen		Poltringen		Tailfingen	
Soil sample	Log $K_d^*$	Log $K_{oc}^*$	Log $K_d^*$	Log $K_{oc}^*$	Log $K_d^*$	Log $K_{oc}^*$
Topsoil	3.5	4.5	3.1	4.9	3.3	5.0
Root horizon 1	3.4	4.6	3.1	4.9	3.2	5.0
Root horizon 2	3.6	5.0	3.1	4.9	3.3	5.1
Root horizon 3			3.0	4.8	3.4	5.2
Subsoil 1	3.3	5.0	3.1	4.9	3.3	5.3
Subsoil 2	3.4	5.3	2.9	4.7	2.8	5.0

## 2.4 Results: Aqueous concentrations

### 2.4.1 Aqueous leachates and desorption enthalpies

Aqueous concentrations of selected PAHs and their desorption enthalpies were determined exemplarily for the uppermost 9 cm in Entringen using hot water extraction, as described above (ASE). Phe, Fth and Pyr were chosen as representative compounds since their respective water solubilities reflect the medium range of the 16 U.S. EPA Priority PAHs with 1.29, 0.26 and 0.14 mg/L (Chiou *et al.*, 2005) as well as subcooled liquid solubilities of 4.3, 0.84 and 0.84 mg/L (EPI SUITE), respectively. In combination with relatively low background concentrations in the bulk soil, reliable aqueous concentrations well above the limit of quantification are only obtained at high temperature leachates. Figure 2.9 shows aqueous concentrations of a) Phe, b) Fth and c) Pyr in van't Hoff plots determined for each horizon, each in triplicate, indicating a good reproducibility of the extractions. The different depth horizons sampled in a high resolution of 3 cm indicate nearly the same concentrations. The slope of the van't Hoff plots provides the desorption enthalpy for the examined soil sample. Desorption enthalpies and respective coefficients of determination are shown in Table 2.4.1, illustrating high linearity for all samples except the uppermost centimetre. This leads to a rather small range of desorption enthalpies for the individual soil horizons. Hence, it seems valid to combine the data set of the whole soil profile for each compound for further evaluation, merely excluding the top-soil sample. The following almost identical desorption enthalpies for Phe, Fth and Pyr were observed:  $83 \pm 11$  kJ/mol,  $98 \pm 10$  kJ/mol and  $99 \pm 24$  kJ/mol. The uppermost centimetre is characterized by the broadest spreading of grainsizes, due to coarser, organic particles (plant residues) and thus highest amounts of organic carbon. Additionally, the C/N ratio indicates lowest maturity of this soil horizon, which is confirmed by the lowest  $K_{oc}^*$  values. As a result, the lowest desorption enthalpies (41 - 57 kJ/mol for Phe, Fth and Pyr) were determined for this specific soil horizon, confirming primarily weak sorption sites for this soil horizon. Hot water extraction at the ASE performed for soil samples from the Poltringen and Tailfingen sites failed due to difficulties caused by the wash-out of fine materials and filter clogging.

**Table 2.5: Desorption enthalpies [kJ/mol] determined for the uppermost 9 centimetres in Entringen for Phe, Fth and Pyr in [kJ/mol] and the respective coefficients of determination.**

Soil horizon	Phe	R <sup>2</sup>	Fth	R <sup>2</sup>	Pyr	R <sup>2</sup>
1 cm	41 ± 14	0,47	56 ± 10	0,59	57 ± 10	0,6
0-3 cm	71 ± 1	0,93	97 ± 4	0,9	98 ± 5	0,91
3-6 cm	91 ± 6	0,93	95 ± 6	0,95	99 ± 3	0,96
6-9 cm	85 ± 9	0,97	99 ± 8	0,98	99 ± 7	0,97
<b>overall</b>	<b>83 ± 11</b>	<b>0,92</b>	<b>98 ± 10</b>	<b>0,95</b>	<b>99 ± 24</b>	<b>0,94</b>

### 2.4.2 Equilibrium concentrations in pore water

Extrapolation of the determined regression on hot water leachates to lower (environmentally relevant) temperatures of 10 ° and 20 °C was performed accounting for all measurements except the uppermost cm, as illustrated in Figure 2.9. At the last extraction step, with the highest temperature, lower concentrations than expected were measured. Depletion of the extracted soil samples can be excluded since only 10 % of the total mass of target compounds within the cell were extracted during the complete hot-water-extraction. The procedure with several extraction cycles including several flushing and purging steps for each cell may strongly influence other parameters such as the leaching of dissolved organic carbon (DOC). This was indicated by coloration of the extracts at higher temperatures. DOC within aqueous leachates generates exceedingly high concentrations of PAHs in water. Wang *et al.* (2007a) report an attempt to correct measured concentrations of PAHs in the aqueous phase by accounting for the fraction of dissolved organic carbon ( $f_{DOC}$ ). Unfortunately,  $f_{DOC}$  was not determined within this study. However, the measured concentrations of Phe in the aqueous phase and in the bulk soil result in  $\log K_d$  values of 3.2 at 65°C and around 2 for 100°C. Adapting these values to 20°C for comparison to measured  $K_d^*$  yields  $\log K_d$  in the range of 4.7 to 5.3, exceeding the measured coefficients for up to 2 log units. These values may therefore be interpreted as an indication for the substantial influence of DOC on PAH concentrations in the eluats. Such methodical issues potentially lead to an overestimation of concentrations in the aqueous leachates. Consequently, extrapolating to environmental relevant temperatures might lead to an underestimation of equilibrium concentrations in the aqueous phase. One possible explanation for low concentrations in the last extraction step may be a depletion of weak sorption sites or DOC within the bulk-soil. The combination with water as a weak solvent for the hydrophobic PAHs presumably results in low concentrations at later extraction steps.

Figure 2.9 predicts the equilibrium concentration of the target compounds in water calculated with measured Freundlich coefficient and exponent (marked in red). Substantially higher value of 8.4, 5.4 and 3.5 ng/L based on the Freundlich sorption isotherm were determined compared to 0.25, 0.07 and 0.03 ng/L extrapolated from hot water extraction regarding Phe, Fth and Pyr, respectively. Furthermore, equilibrium concentrations of Phe in pore water were calculated following the empirical correlations based on literature  $K_{oc}$  and  $f_{oc}$  in soils yielding rather high concentrations in water with 31.5 and 18.6 ng/L based on literature values of  $K_{ow}$  and  $S_{sub}$ , respectively. All of these approaches refer to 20°C as underlying temperature and are therefore directly comparable.



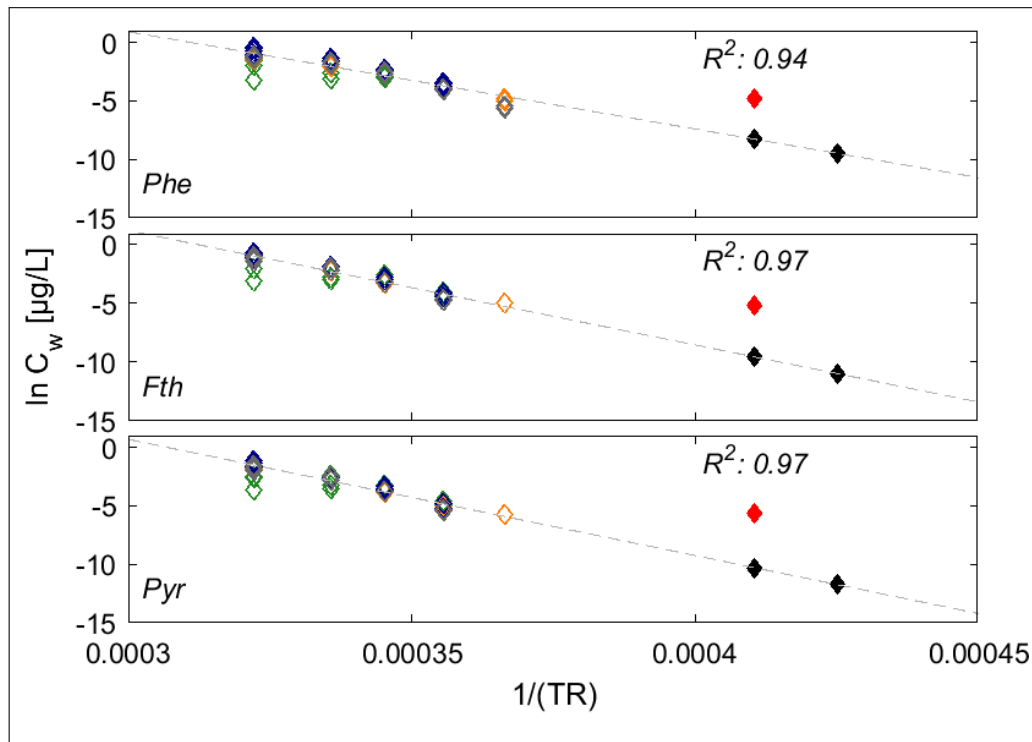


Figure 2.9: Aqueous concentrations of a) Phe b) Fth and c) Pyr in van't Hoff plots for Entringen; diamonds show measured concentrations for the uppermost cm (green), 0-3 cm (orange), 3-6 cm (blue) and 6-9 cm (grey), extrapolated for 10°C and 20°C (black) as well as calculated according to sorption isotherms (red); only temperature between 65 and 100°C resulted in concentrations above the limit of detection.

However, empirical relationships in general are developed for specific conditions and assumptions. Prerequisites for partitioning, e.g.  $K_{oc}$  values, are high concentrations of PAHs, since at low concentrations adsorption may prevail. As the soil samples within this study show low concentrations of contaminants nonlinear isotherms are revealed. Consequently, the conditions for estimating reasonable partitioning coefficients are not fulfilled for the study sites. Besides, aqueous leachates are not reliable, as discussed above, due to methodical issues during hot-water extraction with partial loss of the extracts as well as wash-out of particles and clogging of filters. Yet, in the measured sorption isotherms two data sets are combined for each soil sample which agree reasonably well with coefficients of determination around 0.98. Therefore, distribution coefficients determined with sorption isotherms can be accepted as most reliable method to characterize the sorption behaviour of the surveyed soils.

Ultimately, measured Freundlich coefficients of Phe may be applied for the whole range of PAHs (Kleineidam *et al.*, 2002, Carmo *et al.*, 2000). Accordingly,  $K_{Fr}$  values of Phe need to be normalized by the respective subcooled liquid solubility of Phe yielding an

unit-equivalent coefficient ( $K_{Fr}^*$ ):

$$K_{Fr}^* = K_{Fr,Phe} S_{Phe}^{1/n} \quad (2.10)$$

Subsequently, applying this relation vice versa with subcooled liquid solubilities of the target compounds yields their  $K_{Fr}$ , respectively:

$$K_{Fr,i} = \frac{K_{Fr}^*}{S_i^{1/n}} \quad (2.11)$$

Based on these relations precise equilibrium concentrations of all PAHs in water may be calculated for known concentrations in soils. Results calculated for the individual soil horizons at each study site are shown in Figure 2.10. The respective distribution patterns for all U.S. EPA Priority PAHs in the aqueous phase show an enrichment of low molecular weight PAHs (Nap – Phe), as well as for Fth and Pyr. Such a pattern agrees well with respectively higher water solubilities for low and medium weight PAHs (see Table A.1).

In general, aqueous concentrations and distribution patterns in Entringen and Poltringen demonstrate a notable conformity. Tailfingen on the other side depicts slight variations with lower concentrations of Nap and Ace in parallel to higher concentrations of Phe, Fth and Pyr in water. Considering the very comparable distribution patterns determined for all bulk soil samples, these variations for the aqueous phase may be due to higher nonlinearity (lowest values of  $1/n$ ) determined for all soil samples in Tailfingen, in particular.

### 2.5 Diagnostic ratios and source allocation

The main source of naturally and anthropologically emitted PAHs is incomplete combustion of organic material (Abdel-Shafy & Mansour, 2016, Zhang & Tao, 2009, Mantis *et al.*, 2005). Depending on the raw organic material and the temperature during incineration, different PAHs get emitted. Tobiszewski and Namieśnik (2012) as well as Yunker *et al.* (2002) summarize several studies on source-specific ratios of different PAHs, illustrating the use of such indicative relations to determine corresponding emission sources. Unfortunately, contrasting interpretations of identical ratios can be found within different studies: E.g. Ant/Phe ratio of 0.17, 0.18 and 0.19 are reported as indicator for coal tar, wood, and grass combustion, respectively (Yunker *et al.*, 2002)- (and references therein). Furthermore, some studies demonstrate the potential to differentiate between traffic emission, coal and wood combustion related to single compounds (Ravindra *et al.*, 2008, De La Torre-Roche *et al.*, 2009, Pies *et al.*, 2008, Alsberg *et al.*, 1989, Larsen & Baker, 2003). Yet, several studies define the same specific compounds as reference for different emission sources. According to Alsberg *et al.* (1989) and Larsen

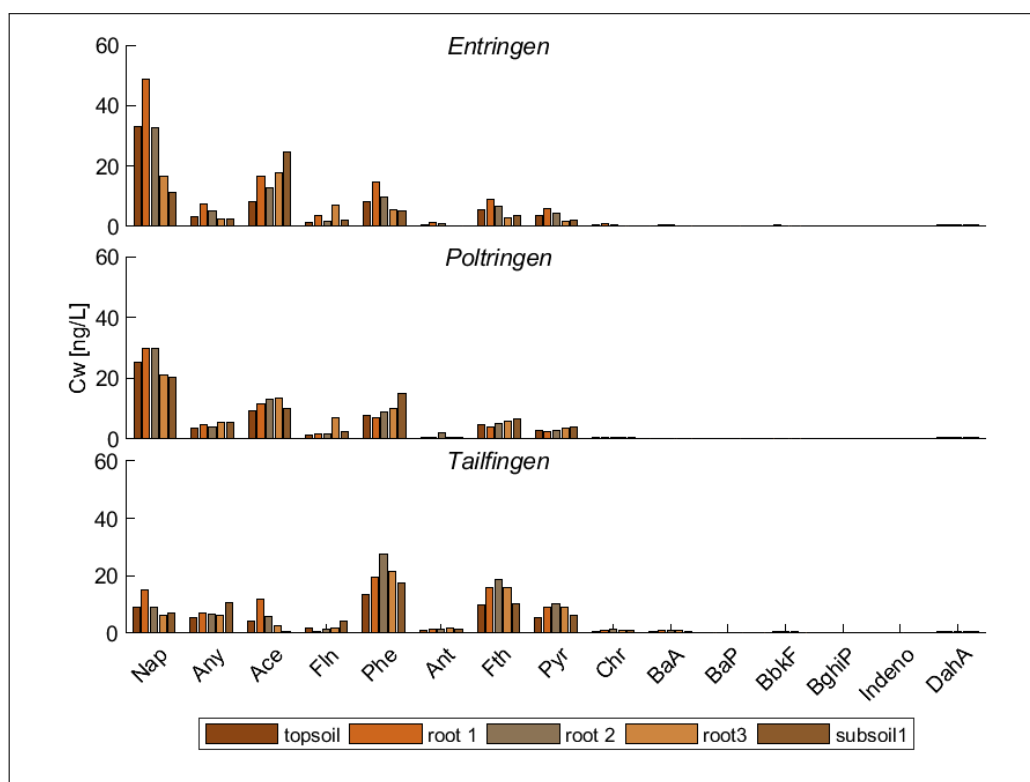


Figure 2.10: Equilibrium concentrations of all 16 U.S. EPA Priority PAHs in water, calculated for the soil profiles in Entringen, Poltringen, and Tailfingen, based on solubility normalized Freundlich coefficients.

and Baker (2003), Pyr might be used to differentiate between diesel and gasoline vehicle emission with higher amounts of Pyr in diesel exhaust. Opposed to that, Aydin *et al.* (2014) and Tian *et al.* (2009) use Pyr as a marker for coal combustion. Such contrasting interpretations may be caused by the highly variable composition of organic material and correspondingly emitting compounds. Additionally, a rapid mixing within the atmosphere hinders the exact identification and attribution of individual compounds to certain sources (Mostert *et al.*, 2010). Hence, Khalili *et al.* (1995) relate explicit groups of PAHs as fingerprints to different burning processes and suggest the relation of individual compounds to a reference value like the sum of 20 PAHs. Thus, defining less specific respective relations leads to a wider agreement. Therefore, Soclo *et al.* (2000) as well as Aydin *et al.* (2014) describe Phe as a compound of higher stability compared to Anthracene (Ant) generating higher Phe/Ant ratios in petrogenic than pyrogenic emission. Cetin *et al.* (2018) report high molecular weight (HMW) PAHs like Benzo[ghi]perylene (BghiP) and Dibenz[a,h]anthracene (DahA) as dominant in vehicle exhaust. One fundamental relation is widely accepted in literature with heavier and more condensed PAHs being produced at higher temperatures and therefore during petrogenic combustion (Aydin *et al.*, 2014, Aichner *et al.*, 2007, Hwang *et al.*, 2003, Pies *et al.*, 2008, Wilcke,

2000a). Accordingly, Hwang *et al.* (2003) suggest the use of Fth-BghiP in relation to U.S. EPA Priority PAHs to determine the contribution of petrogenic emission to the signal of the total amount of PAHs. Besides, it is generally agreed on that complexity results from various influences contributing to the sum of PAHs in different matrices as well as potential degradation processes altering the original source-related signal (Mantis *et al.*, 2005, Pies *et al.*, 2008, Butler & Crossley, 1981, Ringuet *et al.*, 2012).

Due to the differences found in literature, several ratios may be combined in scatter plots, including a direct measure for uncertainties into the source appointment. Therefore, two diagnostic ratios were taken from Tobiszewski and Namieśnik (2012) referring to the concentrations of four compounds which were reliably detected within this study, independent of the sampling or extraction method:

- (1)  $\frac{\text{Ant}}{(\text{Ant}+\text{Phe})} < 0.1 \rightarrow \text{petrogenic} > 0.1 \rightarrow \text{pyrogenic}$
- (2)  $\frac{\text{Fth}}{(\text{Fth}+\text{Pyr})} < 0.4 \rightarrow \text{petrogenic}, 0.4-0.5 \rightarrow \text{fossil fuel combustion}, > 0.5 \rightarrow \text{grass, wood, coal combustion}$

With respect to particle associated PAHs, Dickhut *et al.* (2000) suggest the use of HMW PAH concentrations for diagnostic ratios. Those are in particular Benz(a)anthracene (BaA), Chrysene (Chr) as well as Indeno and BghiP. Within a comparative study the authors sampled vehicular emission as well as wood and coal burnings and characterized specific source-related ratios, such as:

- (3)  $\frac{\text{BaA}}{\text{Chr}} \sim 0.5 \rightarrow \text{automobile}, \sim 0.8 \rightarrow \text{wood}, \sim 1.1 \rightarrow \text{coal}$
- (4)  $\frac{\text{Indeno}}{\text{BghiP}} < 0.3 \rightarrow \text{wood}, > 0.3 \rightarrow \text{automobile}, \sim 1.1 \rightarrow \text{coal}.$

The respective ratios (1) and (2) are combined for the soil profiles of each study site in Figure 2.11a) while ratios (3) and (4) are shown in Figure 2.11b). Taking account of Ant, Phe, Fth and Pyr, no significant difference can be observed for the different soil horizons at the individual sampling sites. All stations plot equally at a ratio of Fth/(Fth+Pyr) above 0.5 indicating combustion of coal and softwood as main source. Additionally, a constant ratio of Ant/(Ant+Phe) around or above 0.1 was determined, also referring to combustion of organic material. In general, low concentrations of Ant were determined for all soil samples, inducing the potential for considerable uncertainty of the respective ratios. However, with a high reproducibility of these low values observed for all sampling depths and all triplicates, resulting ratios including Ant may also be accepted as reliable.

The ratios according to Dickhut *et al.* (2000), however, result in distinctively varying patterns for the different locations. Poltringen plots consistently at a ratio  $< 1.1$  for Indeno/BghiP, which refers to wood and vehicular combustion, and around 0.6 for BaA/Chr

indicating a distinctive influence of wood combustion. Entingen plots also at a ratio of BaA/Chr around 0.6 but at higher values for Indeno/BghiP above 1.1, therefore relating to coal combustion. In Tailfingen the broadest spreading can be observed with a ratio of Indeno/BghiP between 0.9 - 1.6 as well as a range of 0.6-0.9 for BaA/Chr, which refers to wood and coal combustion as well as to vehicular emission. Thus, this figure clearly illustrates the mentioned uncertainty of such ratios and the difficulty of identifying one specific emission source by the use of one or two individual compounds. However, one general signal can be identified confirming the combustion of wood and coal as major source for the PAHs in the soil profiles and thus fits the expectation of domestic heating as major emission of PAHs into the atmosphere. This is in good agreement with several comparable studies for soils in rural areas (Bucheli *et al.*, 2004, Peng *et al.*, 2016, Lee *et al.*, 2005).

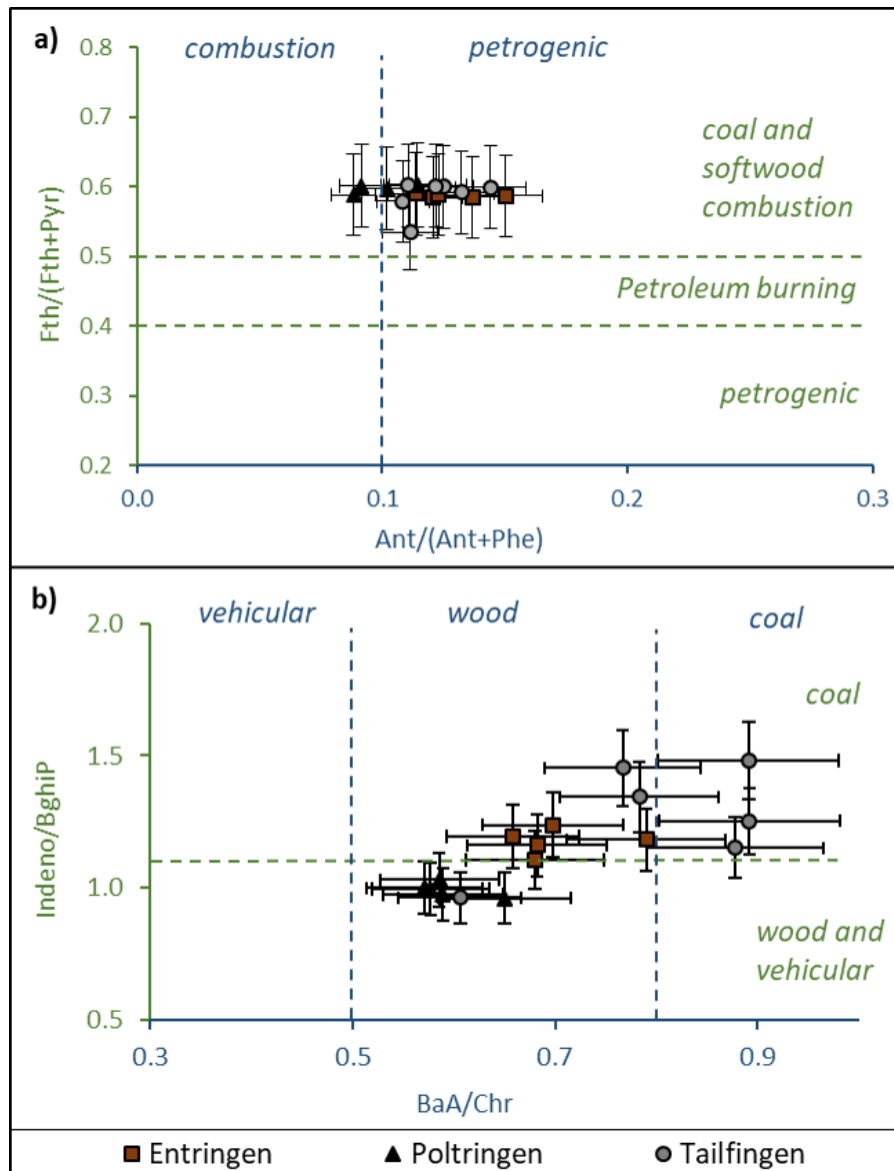


Figure 2.11: Scatter plot for diagnostic ratios relating a) Ant, Phe, Fth and Pyr and b) Indeno, BghiP, BaA and Chr to each other, comparing Entringen, Poltringen and Tailfingen.

## 2.6 Discussion

A comparison of the different locations, taking account of each of the determined parameters, depicts the study sites as quite comparable with only slight variation. Poltringen can be described as location with the most homogeneous soil profile, regardless of the determined parameter. In contrast, Entringen illustrates the most distinct gradient within the soil profile. This was expected since Entringen is in a water protection zone and the soil was undisturbed for at least 50 years while ploughing of agricultural fields in Poltrin-

gen and Tailfingen caused annual mixing down to 30 – 40 cm. The conducted sorption tests show nonlinear isotherms, especially if low concentration ranges are included. If only a narrow concentration range e.g. at high concentration is considered a linear relation might fit the data. Yet, extrapolation into lower concentrations cannot be maintained. Nonlinear sorption is mainly obvious in the low-concentration range with  $C_{w,eq}$  measured between 5 ng/L and 100 ng/L. Within this range, strong sorption was observed. This may be due to adsorption as relevant process at low concentrations, opposed to partitioning at higher concentrations. Sorption isotherms can be described appropriately by the Freundlich model, taking account of this nonlinearity. Numerous studies have been conducted on correlations regarding nonlinear sorption behaviour of PAHs for different organic materials (Cornelissen & Gustafsson, 2004, Cornelissen *et al.*, 2006, Gao *et al.*, 2007, Guo *et al.*, 2010). One general conclusion of the different studies is a strong dependency of sorption in soils and sediments on amount and type of organic matter. Sorption behaviour of Phenanthrene as representative PAH is also studied for a broad spectrum of organic materials like carbonaceous sediments, humic acids, or black carbon, providing an accordingly wide range of Log  $K_{Fr}$  between 2.64 and 8.08. Kleineidam *et al.* (2002) depict a good overview of Freundlich coefficients for Phe on different organic matter like peat, lignite, different forms of coal and activated carbon. Respective values of log  $K_{Fr}$  vary between 3.5 for peat and 6.18 for activated carbon. As often reported in literature (Jonker & Koelmans, 2002), calculation of  $K_d$  values based on empirical  $K_{oc}$  relationship and measured  $f_{oc}$  may lead to significant overestimation of equilibrium concentrations in the aqueous phase, as observed within this study. The  $K_{oc}$  values calculated for Phe at the low background concentrations of the soil profiles results in fivefold stronger sorption as expected based on EPI SUITE. The respective Freundlich coefficients determined within this study are in good agreement with values found in the literature regarding natural carbonaceous material (Yang *et al.*, 2008) or rural soils with comparable fractions of organic carbon (Gocht, 2005). Desorption enthalpies show generally high values of -83 – -99 kJ/mol for Phe, Fth and Pyr, combining the individual soil samples in Entringen. Only the uppermost centimetre in Entringen, characterized by freshly accumulated organic material demonstrates substantially lower desorption enthalpies of -41 kJ/mol for Phe and -57 kJ/mol for Fth and Pyr. Corresponding values from literature only range between -23 and -38 kJ/mol for Phenanthrene (Ran *et al.*, 2007, Wang & Grathwohl, 2009, Yang & Hofmann, 2009). This confirms the considerable influence of the type of organic material on the sorption strength with weaker sorption sites provided by fresh organic matter. Consequently, less energy is needed for desorption of PAHs from the root horizon in Entringen compared to lower soil horizons. Additionally, the considerably high values of  $K_{oc}^*$  determined in Poltringen and Tailfingen suggest the content of strongly sorbing components within the soil samples. As described earlier, hot water leachates were impaired by several issues. Especially the wash out of fine material and dissolved organic carbon could cause artificially high concentrations with higher temperatures and desorption enthalpies might have been overestimated. This would be in good agreement with the apparently underestimated equilibrium concentrations in the aque-

ous phase based on the hot water extraction after extrapolation to lower temperatures. In general, Fth, Bbf-BkF, Chry and Pyr contribute most to  $\Sigma$ U.S. EPA Priority PAHs in all soil samples, which agrees well with other studies. For example, Wilcke (2000a) report PAH concentrations measured in 43 soil samples in temperate regions, with a similar distribution pattern as observed here. This also agrees with 23 topsoils in Switzerland studied by Bucheli *et al.* (2004), as well as samples from southern Italy (Qu *et al.*, 2019). Finally, the determined sum of PAH concentrations of 0.1 - 0.7  $\mu\text{g/g}$  in this study is in the same range as the reported median concentrations for top soils in Germany of 0.47  $\mu\text{g/g}$  (Krauss *et al.*, 2000). Furthermore, comparable concentrations were reported for plough horizons in England of 0.66  $\mu\text{g/g}$ , for grassland in the Canadian River floodplain in Oklahoma of 0.03  $\mu\text{g/g}$ , rural areas of Estonia of 0.06-0.3  $\mu\text{g/g}$ , a mean concentration of 0.6  $\mu\text{g/g}$  for 49 sampling sites in Wales, and of 0.16  $\mu\text{g/g}$  as median concentration for 105 observation sites of Switzerland (Jones *et al.*, 1989a, Jones *et al.*, 1989b, Sartori *et al.*, 2010, Wilcke, 2000b, Trapido, 1999, Desaulles *et al.*, 2008). Furthermore, main sources of PAHs were identified to be most likely combustion of coal and biomass, underlining rural emission sources as main influence on the chosen study sites. Thus, strong local point sources within the catchment area of the study sites can be excluded, as assumed in the beginning.

### 2.7 Conclusion

In summary, the chosen study sites are quite comparable with each other and are in line with similar studies found in literature. Sorption behaviour of the soils indicates a good correlation to the amount and maturity of organic carbon. Freundlich sorption isotherms for Phe provide the basis to a proper description of its distribution between solids and aqueous phase. In combination with subcooled liquid solubilities of all U.S. EPA Priority PAHs, measured Freundlich coefficients of Phe may even be applied to calculate  $C_{w,eq}$  for all target compounds. Thus, Phe represents well the U.S. EPA Priority-PAHs and further calculations based on Phe are expected to generate reliable values regarding the targeted fluxes across the soil-atmosphere interface. The observed comparability of the individual study sites provides an opportunity of additional replicates for the following monitoring of concentration gradients across the soil-atmosphere interface. Potential variations within these gradients can therefore be linked directly to differences in the atmospheric influence.



---

### 3 Background theory of passive sampling

#### 3.1 Double film diffusion model; exemplarily in the atmosphere

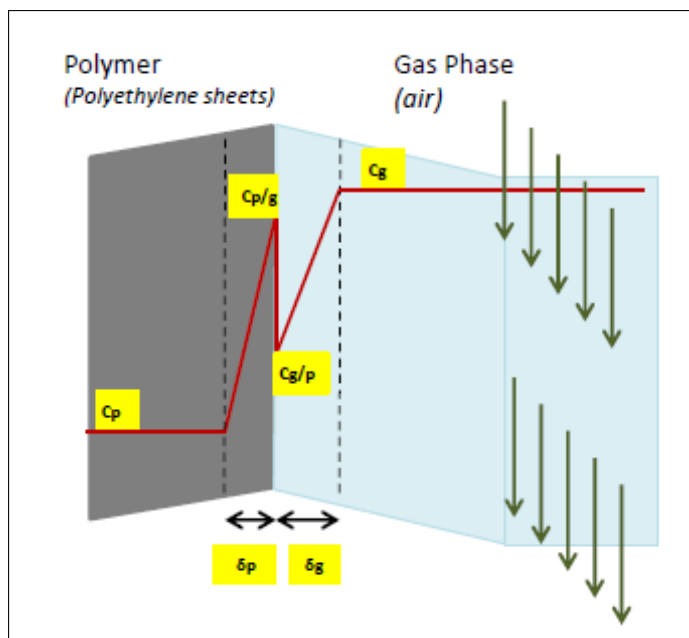


Figure 3.1: Scheme of the double film diffusion model.

The overall concept of passive sampling is based on adding a selective phase into an environmental compartment which provides a significant potential to accumulate target compounds (Mayer *et al.*, 2003). Due to the hydrophobic behaviour of PAHs, a non-polar organic polymer can be used as such an artificial sink. The comprehensive theory of passive sampling is straightforward and well described in literature (Huckins *et al.*, 1993, Shoeib, 2002, Bartkow *et al.*, 2004, Bartkow *et al.*, 2005, Tuduri *et al.*, 2012, Khairy & Lohmann, 2012). Following Whitman's two-film approach (Whitman, 1962), air and passive sampler are defined as two phases within which concentrations are homogeneously distributed. Alternatively, passive samplers may be porous media in which hydrophobic compounds can diffuse (Shoeib, 2002). Right at the interface of the different phases concentration gradients evolve on both sides. Bartkow *et al.* (2005) described in great detail how boundary layers at the air ( $\delta_g$ ) and the sampler ( $\delta_p$ ) side act as mass transfer resistances as illustrated in Figure 3.1. Considering small scale, this double film diffusion model can be explained precisely by taking three (compound-specific) processes into account: (i) diffusion in the air-side boundary layer that is characterized by the diffusion coefficient in air  $D_g$ , (ii) diffusion in the polymer-side boundary layer that is defined by the intrapolymer diffusion coefficient  $D_p$ , and (iii) equilibrium distribution described by the partition coefficient between the gas phase and the polymer phase  $K_{pg}$

[L/kg]. Consequently, the overall kinetic behaviour of passive samplers relates to the characteristic physicochemical properties of target compounds and the materials.

Passive air sampling is a widely accepted method to study the spatial and temporal distribution of specific contaminants as well as to detect concentration gradients across several compartments (Sobek *et al.*, 2014, Niehus *et al.*, 2019, Beckingham & Ghosh, 2013, Liu *et al.*, 2016, Lohmann *et al.*, 2011, Morgan & Lohmann, 2008). However, application within the environment is often semi-quantitative and used to examine fluxes rather than concentrations (Schifman & Boving, 2015, Harner *et al.*, 2006). For the translation of measured concentrations on the passive sampler into reliable atmospheric concentrations, the described processes need to be quantifiable. For that purpose, comprehensive knowledge and characterization of influencing parameters on partitioning as well as diffusion in the corresponding boundary layers is of major relevance. Accordingly, the different influences on uptake kinetics of target compounds need to be characterized (i.e. environmental parameters) for each study individually. Shoeib (2002) report the air-side boundary layer as the controlling factor for the uptake process of semi- and low volatile atmospheric compounds onto the polymer passive samplers, maintaining the sampler-side boundary layer as negligible (Pozo *et al.*, 2009, Tuduri *et al.*, 2012). Therefore, the temperature-dependent  $K_{pg}$  and the wind velocity-related air-side boundary layer  $\delta_g$  control uptake kinetics. High wind speeds result in thinner boundary layers and thus in corresponding faster kinetics and higher sampling rates (Moeckel *et al.*, 2009, Söderström & Bergqvist, 2004). Booij *et al.* (1998) suggest the spiking of passive samplers with Performance Reference Compounds (*PRCs*) as an in-situ calibration of exchange kinetics. Two aspects are the crucial factors for the choice of a compound as a *PRC*; On the one hand, physicochemical properties of the *PRC* should be in line with those of the target compounds. Thus, parameters defining the exchange kinetics between sampler and medium can be determined by the use of *PRCs* and subsequently translated for target compounds. On the other hand, environmental concentrations of the *PRC* should be close to zero, allowing a significant loss of the *PRC* during the sampling period. Since the kinetic of this loss is also controlled by the air-side boundary layer, the use of *PRCs* adjusts for prevailing wind influence (Moeckel *et al.*, 2009, Söderström & Bergqvist, 2004). Analytically, the loss of *PRCs* over time can be described with a simple first-order approach and is characterized by a specific loss rate constant  $\lambda_{loss}$  [ $s^{-1}$ ]:

$$C_{PRC,t} = C_{PRC,0} * e^{(\lambda_{loss}t)} \quad (3.1)$$

with  $C_{PRC,t}$  [ng/g] delineating the current concentration of the *PRC* on the passive sampler at time  $t$  [s] and  $C_{PRC,0}$  [ng/g] as initial concentration. A required decrease of *PRC* concentrations to determine reliable loss rate constants lies between 20 and 80% of the initial concentration (Bartkow *et al.*, 2006). Accordingly, the measured *PRC*-loss can be applied as calibration in two ways:

- i) Assuming the exchange of target compounds between sampler and air as isotropic process allows to directly relate the loss rates to uptake or sampling rates. Therefore, the measured loss rate constant  $\lambda_{loss}$ , simply referring to the slope of the exponential Equation 3.1, can be used as a substitutional overall rate constant  $\lambda$ :

$$\lambda_{loss} = \frac{\left( \ln \frac{C_{PRC,0}}{C_{PRC,t}} \right)}{t} \quad \text{and} \quad \lambda_{loss} = \lambda \quad (3.2)$$

- ii) The air-side boundary can be determined as responsible size for the respective loss rate constants of the *PRC*. As described above, diffusion within the gas phase ( $D_g$ ) as well as partitioning between gas and polymer ( $K_{pg}$ ) are the major processes which need to be taken into account. Additionally, the specific surface area of the passive sampler ( $A_P/V_P$ ) influences the respective kinetics, since exchange occurs across this sampler-air interface:

$$\delta_g = \frac{D_{g-PRC} A_P}{K_{pg-PRC} V_P \lambda_{loss}} \quad (3.3)$$

Therefore,  $\lambda$  simply relates to the observations made on the loss of the *PRC* and can be described as sum parameter. This parameter comprises the respective partition and diffusion coefficient as well as the geometry of the passive sampler and the air-side boundary layer. The kinetic behaviour of PAHs is strongly dependent on the respective partition and intrapolymer diffusion coefficients, which in turn vary over a range of 6 and 2 orders of magnitude regarding the 16 U.S. EPA Priority PAHs, respectively (Lohmann, 2012) (Table A.2). Since uptake rates of target compounds also refer to partitioning, it is not sufficient to apply one rate constant based on one specific *PRC*, to the whole set of PAHs. The simultaneous use of several *PRCs*, spanning a broad range of partition and diffusion coefficients, is described in literature as a common practice (Bartkow *et al.*, 2006, Gouin *et al.*, 2005, Farrar *et al.*, 2005, Jaward *et al.*, 2004). This way few target compounds are merged to be calibrated on the basis of a *PRC* with similar properties. On the other hand, the thickness of the air side boundary layer is assumed to be independent of the target compound. Corresponding individual uptake rate constants  $\lambda [s^{-1}]$  can also be formulated for each target compound (*i*), based on Equation 3.1, provided  $\delta_g$  is known:

$$\lambda_i = \frac{D_{g,i} A_P}{K_{pg,i} V_P \delta_g} \quad (3.4)$$

with  $K_{pg}$  as volumetric partition coefficient.

Three stages of characteristic uptake curves of target compounds can be defined independent of the sampled medium: linear and non-linear uptake as well as equilibrium state,

### 3 Background theory of passive sampling

sketched in Figure 3.2. Depending on the partition coefficients of target compounds, the time to reach equilibrium varies over several orders of magnitude (Wania *et al.*, 2003). To a smaller extent, sampling rates depend on the sampler material, especially for air-side limited uptake.

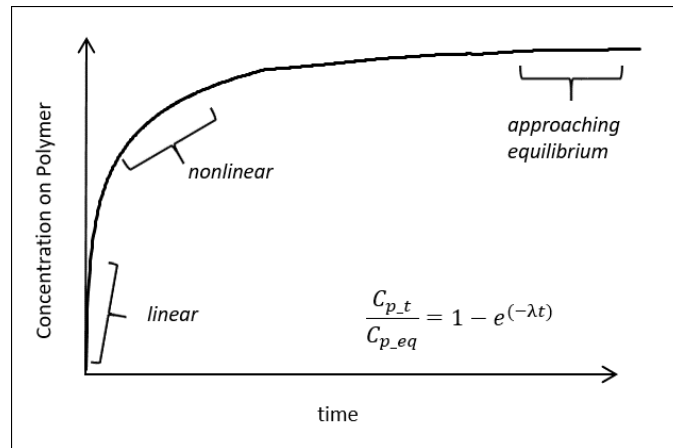


Figure 3.2: Characteristic uptake curve onto passive sampler, classified in three uptake modes; linear, non-linear and equilibrium conditions.

Uptake of target compounds onto the passive sampler can be described by the exponential relation:

$$\frac{C_{p,t}}{C_{p,eq}} = 1 - e^{-\lambda t} \quad (3.5)$$

Relating to  $C_g = C_{p,eq}/K_{pg}$ , corresponding atmospheric concentrations ( $C_g$  in [ng/m<sup>3</sup>]) can be calculated using the following equation:

$$C_g = \frac{C_{p,t}}{(1 - e^{-\lambda t}) K_{pg}} \quad (3.6)$$

Referring to the determined rate constants, characteristic times to reach equilibrium may be estimated as an objective measure for the individual compounds. Basically,  $C_{p,t}/C_{p,eq}$  describes the state of equilibrium reached on the sampler. With  $\ln(0.37) \approx -1$  (Equation 3.1) may be transferred into:

$$t_{0.63} = \frac{1}{\lambda} \quad (3.7)$$

Simultaneous sampling of a group of contaminants instead of specifically targeting one compound generates the issue of single compounds being in different uptake modes

(equilibrium vs. different non-equilibrium states). Therefore, calibrated air-side boundary layers are used together with compound-specific partition coefficients in Equation 3.5. Integrating the relevant parameters over the sampled time is assumed to compensate for the offset to equilibrium state. This analytical approach applies for uptake and exchange kinetics to determine ambient concentrations instead of considering sampling rates used by Lohmann *et al.* (2011). Transferring this simple solution of passive sampling into practice relies on an average  $\delta_g$  and  $K_{pg}$ .  $\delta_g$  is obtained for the time period of depletion of the PCR and  $K_{pg}$  is sensitive to temperature, which to some minor extent also applies to  $D_g$ . In order to account for variable temperatures, a numerical modelling approach is needed to describe uptake in passive samplers as introduced below.

### 3.2 Numerical model

The uptake of the compounds from the sampled medium into the polymer corresponds to a simple mass transfer process, namely diffusion through a stagnant boundary layer. Therefore, Fick's first law can be applied to calculate the uptake rates in the passive sampler. The concentration change over time ( $dC_p/dt$ ), depends on a characteristic mass transfer coefficient ( $D_g/\delta_g$ ), the specific surface area ( $A^\circ$ ) of passive samplers (i.e. the ratio of surface area  $A$  [m<sup>2</sup>] to the mass  $m_p$  [kg] of the passive sampler ( $A/m_p$ )) and the concentration gradient at the sampler-air interface ( $\frac{C_p}{K_{pg}} - C_g$ ), here  $K_{pg}$  is used in [L/kg]:

$$\frac{dC_p}{dt} = -\frac{D_g}{\delta_g} \frac{A}{m_p} \left( \frac{C_p}{K_{pg}} - C_g \right) \quad (3.8)$$

$C_p/K_{pg}$  denotes the gas phase concentration at the polymer/air interface. Solving this equation step-wise provides discrete  $C_p$  values, resulting in an uptake curve of target compounds onto the passive samplers.

$$C_{p,t+1} = \left[ -\frac{D_{g,t}}{\delta_g} \frac{A}{m_p} \left( \frac{C_{p,t}}{K_{pg,t}} - C_g \right) \right] dt + C_{p,t} \quad (3.9)$$

With such a numerical solution, temperature dependent parameters ( $K_{pg}$ ,  $D_g$  and to a minor extent  $\delta_g$ ) may be adjusted for each time step. As the 16 U.S. EPA Priority PAHs span a broad range of partition coefficients, higher molecular weight compounds do not equilibrate during the exposure time and the PE sheets act as kinetic passive samplers. Therefore, Equation 3.9 and Equation 3.6 may be used to predict further uptake onto the passive sampler until equilibrium is reached.

### 3.2.1 Temperature dependent parameters

Since diffusion and partition coefficients are significantly temperature dependent, they need to be adapted to the current temperatures during the sampling period. Temperature dependent partition coefficients can be calculated following the van 't Hoff equation:

$$K_{pg(T2)} = K_{pg(T1)} * \exp \left[ \frac{\Delta H_{\text{vap}}}{R} \left( \frac{1}{T2} - \frac{1}{T1} \right) \right] \quad (3.10)$$

with  $K_{pg(T1)}$  as a partitioning coefficient taken from Khairy and Lohmann (2012) for a well-defined temperature (25°C),  $\Delta H_{\text{vap}}$  describing the evaporation enthalpy (typically around 55 - 130 kJ/mol for the 16 U.S. EPA Priority PAHs) and  $R$  the ideal gas constant ( $8.314 \times 10^{-3}$  kJ/(mol K)).  $T2$  accounts for the ambient air temperature in Kelvin whereas  $T1$  denotes the reference Kelvin temperature of 20° C or 25° C of literature  $K_{pg(T1)}$ . The diffusion coefficient in the gas phase  $D_g$  (in [m<sup>2</sup>/s]) can be calculated for the respective temperature conditions following the Fuller-Schettler-Giddings-Method (*Fuller, 1969*):

$$D_g = \frac{10^{-3} T^{1.75} \sqrt{M_{PAH}^{-1} + M_g^{-1}}}{p * \left( V_{PAH}^{\frac{1}{3}} + V_g^{\frac{1}{3}} \right)} \quad (3.11)$$

with  $T$  as ambient air temperature in Kelvin,  $M$  as the molecular mass [g/mol] of the compound of interest ( $M_{PAH}$ ) and of air ( $M_g$ ), and  $p$  accounting for the pressure (1 atm) and  $V$  for the molecular volume of the compound ( $V_{PAH}$ ) and of air ( $V_g$ ) [m<sup>3</sup>/mol].

By solving Equation 3.9 to Equation 3.11 on the basis of measured air temperatures, the uptake of target compounds onto the passive sampler over time can be calculated for each compound specifically. The combination of modelled uptake curves onto the sampler with measured concentrations allows to check how temperatures will influence uptake kinetics.

Another aim of this numerical model is to include uncertainties connected to varying atmospheric concentrations. This first requires the calibration of the passive samplers, i.e. to fix the air-side boundary layer  $\delta_g$  for each monitoring period. Here, the loss of preloaded Ant-D<sub>10</sub> as *PRC* is monitored during the first few days of each sampling campaign. Deuterium labelled Ant-D<sub>10</sub> does not occur in the atmosphere and allows to calculate  $\delta_g$  as the only unknown parameter within Equation 3.9. A Gauß-Newton type least-square method implemented in the optimization toolbox of Matlab (*lsqcurvefit*) was utilized to correlate the calculated concentrations on the PE to the measured data set by fitting  $\delta_g$ .

### 3.2.2 Sherwood numbers

Assuming an explicit dependency of  $\delta_g$  on environmental parameters provides the opportunity for a theoretical approach of this boundary layer. Based on the exchange kinetics of the *PRC*, the respective air side boundary layer got calibrated for each monitoring and each location individually. In order to transfer calibration to other compounds, empirical relationships based on Sherwood numbers (*Sh*) are used. *Sh* is a dimensionless number describing mass transfer as a relation of effectively transferred mass (characterized by the mass transfer coefficient  $k$  [m/s]) to purely diffusion driven mass transfer (described by the diffusion coefficient  $D$  [m<sup>2</sup>/s]) over a specific length, here the length of the PE sheets ( $l$  [m]):

$$Sh = \frac{kd}{D} \Rightarrow \delta = \frac{l}{Sh} \quad (3.12)$$

Sherwood numbers may be estimated based on empirical correlations from Schmidt *Sc* [-] and Reynolds numbers *Re* [-], e.g.:

$$Sh = 1.9 Sc^{1/3} Re^{1/2} \quad (3.13)$$

The Schmidt number is the ratio between kinematic viscosity of the air ( $\eta$  [m<sup>2</sup>/s]) and gas diffusion coefficient ( $D_g$ ), the kinematic viscosity in turn relates to the dynamic viscosity of air ( $\nu$  [kg/ms]) and the respective density ( $\rho$  [kg/m<sup>3</sup>]):

$$Sc = \frac{\eta}{D_g} = \frac{\nu}{\rho D_g} \quad (3.14)$$

The Reynolds number also considers the kinematic viscosity of the air in combination with the thickness of the passive sampler and the measured wind speed ( $\nu$  [m/s]):

$$Re = \frac{\nu d}{\eta} \quad (3.15)$$

The viscosity of the air as well as the diffusion in air are temperature dependent parameters. Meteorological data were taken from the German Weather Service providing an hourly resolution of measurements at a meteorological station in Stuttgart-Echterdingen, about 25 km distant to the studied areas. Subsequently, this temperature data was used to calculate  $K_{pg}$ ,  $D_g$ ,  $\nu$ , and  $\eta$ . Air side boundary layers were calculated in a resolution of one hour as well as an average over the first three days. Only for low molecular weight (LMW) PAHs with fast kinetics, equilibrium concentrations on the passive sampler are obtained. For high molecular weight (HMW) PAHs, uptake in PE passive samplers is extrapolated to equilibrium conditions based on modelling approaches.

#### 3.2.3 Comparison of calibration approaches

The first step of calculating atmospheric concentrations or extrapolating measured uptake curves is generally the calibration of the passive samplers by monitoring the loss of Ant-D<sub>10</sub> as *PRC*. This needs to be done during the first few days of each monitoring, respectively. Subsequently, the numerical model fits  $\delta_g$  to the measured *PRC*-loss as shown exemplarily in Figure 3.3 for May 2016. The plot illustrates comparable trends for the *PRC*-loss at the individual locations resulting in air side boundary layers of 0.3 mm in Entringen, 0.4 mm in Poltringen and 0.3 mm in Tailfingen. Calculating air side boundary layers on the basis of *Sh* can be used for comparison of these values and to perform a sensitivity analysis with respect to wind speed and temperature. The outcome of this analysis illustrates a clear correlation of the air side boundary layer to prevailing wind speed, as shown in Figure 3.4. In the model *Re*, *Sc* and thus *Sh* are adopted to hourly measures of temperatures and wind speed providing corresponding values for  $\delta_g$  with an equal resolution. Based on this approach, a range of  $\delta_g$  between 0.2 mm and 0.6 mm was determined throughout May 2016, leading to an average value of 0.26 mm regarding the first three days of the monitoring. Subsequently, a comparison of *PRC*-loss calculated for the whole range of  $\delta_g$  including minimum, maximum and mean values is shown in Figure 3.5. The average air side boundary layer thickness determined with empirical *She* correlations is in very good agreement to the measurements of *PRC*-loss. Slight variations within the thickness of this layer of only 0.1 mm, however, already lead to an offset for the calculated *PRC* concentrations on the passive sampler compared to the measured data set. Calculated concentrations of Ant-D<sub>10</sub> after three days vary between 46 and 137 ng/g, based on the range of  $\delta_g$  according to the *Sh*. The respective measured concentration depicts a value of 99 ng/g. Hence, an individual calibration of the exchange kinetics for passive samplers and air is required to account for spatial and seasonal variations of temperature and wind.

A comparison of the respective air side boundary layers indicates almost identical thicknesses independent on the compound. *Sh* calculated for individual compounds lead to almost identical film thicknesses in the range of 0.252 – 0.262 mm considering Fluorene (Fln), Phenanthrene (Phe), Fluoranthene (Fth) and Pyrene (Pyr). Therefore, one air side boundary layer, calibrated by the use of a single *PRC* seems to be sufficient for the range of chosen target compounds.

Besides the numerical model, specific steps regarding the improvement of accuracy in passive sampling of PAHs in the atmosphere were pursued:

- I. Development of an appropriate sampling set-up in the field, including
  - a. A preliminary test on sampler properties
  - b. Quantifying the effect of photodegradation



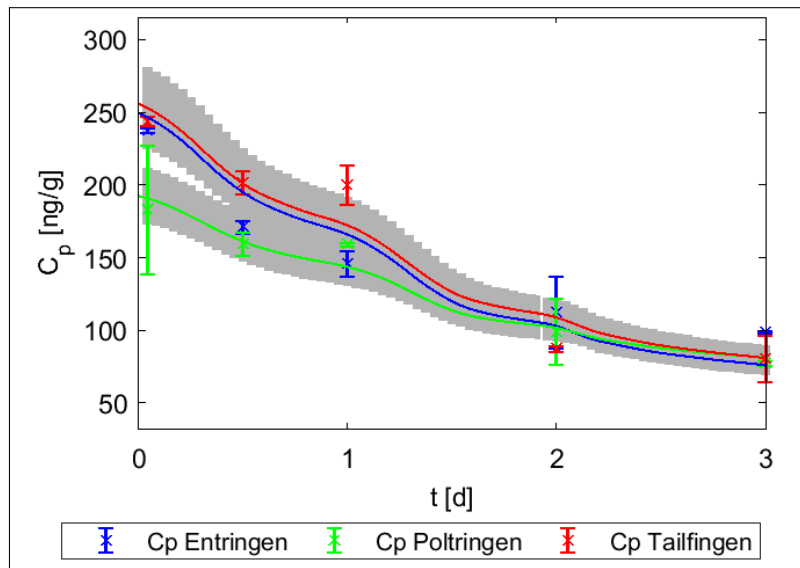


Figure 3.3: Measured (crosses) and calculated (lines) loss of Ant-D10 as PRC at the different locations Entringen, Poltringen and Tailfingen during May 2016, standard deviation is shown in bars for the measurement and shaded areas for the numerical model.

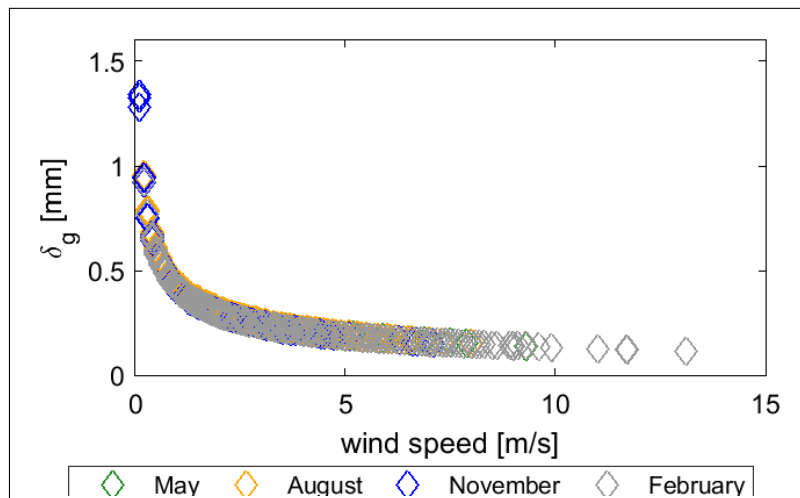


Figure 3.4: Sensitivity analysis of the air side boundary layer, estimated with the use of Sherwood numbers for different wind speeds.

- II. Validation of passive sampling by the use of active samplers and examination of the method's sensitivity
- III. Comparison of different passive sampler types (PE sheets and PDMS coated jars)
- IV. Determination of correlations between PAH equilibrium concentrations, uptake kinetics, and environmental parameters

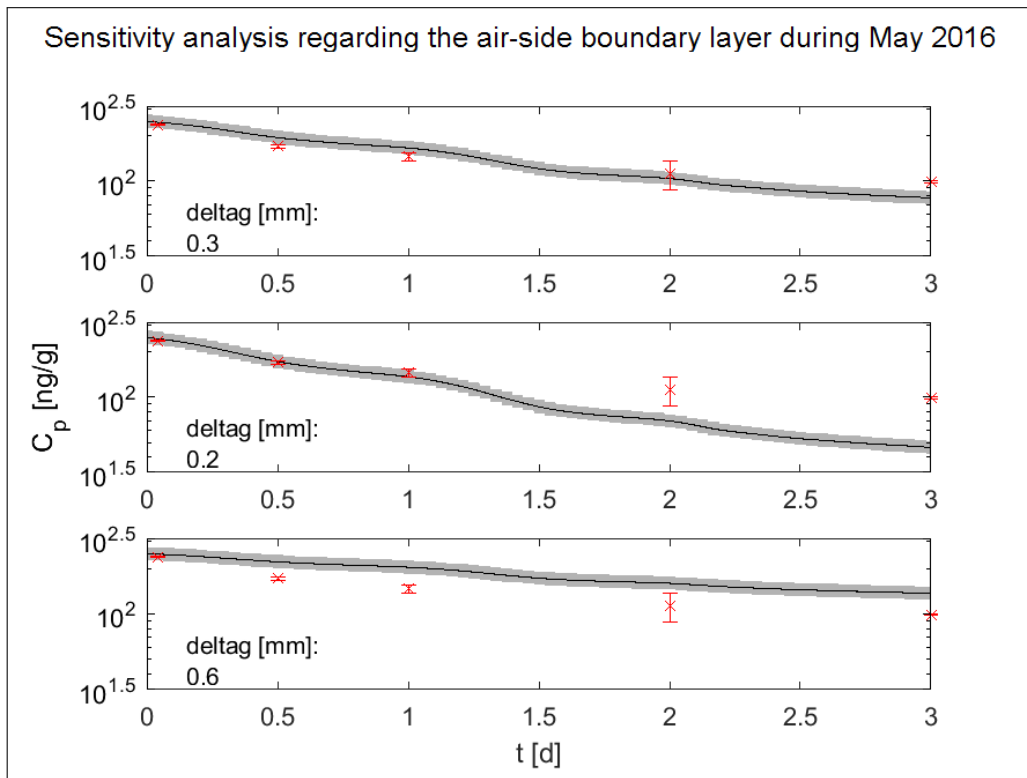


Figure 3.5: Measured loss of Ant-D10 (red crosses) in comparison to calculated loss (black lines with grey area as respective standard deviation) comparing empirical with theoretical calibration of the samplers.

V. Determination of potential concentration gradients within the ground-level atmosphere

---

## 4 Development of an appropriate sampling set-up in the field

### 4.1 Atmospheric Monitorings - general methodology

#### Passive sampler

Low-Density Polyethylene (LDPE, or short: PE) sheets of 30 and 80  $\mu\text{m}$  thickness which consist exclusively of carbon and hydrogen ( $[\text{C}_2\text{H}_4]_n$ ), supplied by a home-improvement store (Hornbach), are used as passive sampler. The sheets were cut into strips of 9x25 cm and prepared with two holes assuring an easy and fast deployment in the field. For cleaning purpose, the sheets were shaken for 24 h in cyclohexane followed by 24 h in Ethyl acetate and several rinsing steps with ultrapure water. In advance of the deployment, PE sheets were spiked with deuterated Anthracene (Ant-D<sub>10</sub>) as *PRC* aiming for a starting concentration  $C_0$  of 0.5- 1  $\mu\text{g/g}$  PE, depending on the monitoring. Ant-D<sub>10</sub> was chosen as *PRC* as it fulfills the requirements with physicochemical properties of target compounds and insignificant environmental concentrations. Additionally, it is characterized by comparably fast kinetics, ensuring the required loss for calibration within a few days. Spiking was performed by shaking PE sheets in an ultrapure water solution containing Ant-D<sub>10</sub> for seven days on an overhead shaker. The prepared sheets were taken out of the spiking solution, wiped perfunctory to eliminate potential left-over Ant-D<sub>10</sub> and wrapped thoroughly in aluminium foil right before the transportation into the field.

#### Set-up in the field, sampling and extraction

Depending on the objective of the respective sampling campaign, the set-up in the field varied slightly and is described in greater detail within the corresponding sections. Independent of the survey, passive samplers were deployed at about 1.2 m height. At the beginning of each monitoring, samples were taken in higher resolution in order to precisely determine the uptake curves of the target compounds. During the sampling process, sheets were rinsed with ultrapure water and wiped dry with lint-free tissue to wash off potential particles. For the extraction, the sheets were shaken with 50 mL of Ethyl acetate twice for 24 hours. Internal standard (*PAH mix 31*) was added to the combined extracts before reducing the volume to 10 mL at the rotational evaporator (at 40°C and 215 mbar). Adjacent, the extracts were mixed with 800 mL ultrapure water before adding additional 10 mL of cyclohexane and shaken for 30 minutes. Subsequently the cyclohexane was transferred into clean vials, heated to 40°C and reduced under a gentle nitrogen stream to 200  $\mu\text{L}$ . Then target compounds were detected at the GC/MS.

### Data analysis

The evaluation of the measured concentrations on the samplers is essentially based on the parallel determined decrease of the *PRC*. Besides, data analysis was generally coupled to the numerical modelling approach introduced above. Therefore, as a first step the numerical model was applied to calibrate the respective air-side boundary layer for each study site during each sampling campaign individually. Based on this boundary layer, atmospheric concentrations were fitted by modelling the uptake curves for target compounds onto passive samplers including partition coefficients adapted to measured temperatures.

### 4.2 Preliminary test on diverse sampling-set-ups

Within a first experiment basic issues were tested before starting the regular seasonal monitorings of PAHs in the atmosphere. More precisely, the type of Polyethylene as well as the set up in the field considering handling, purity of extracts and reproducibility were checked. Particularly, with respect to one major issue regularly brought up in the literature concerning photodegradation of PAHs, a comprehensive control has been conducted for potential loss of target compounds on the passive samplers (Bartkow *et al.*, 2006b, Seethapathy *et al.*, 2008, Kim *et al.*, 2013). Photodegradation of PAHs is described in literature as a major process regarding their loss within the atmosphere. Several studies have been conducted on the reaction of gaseous PAHs with radicals like OH, NO<sub>3</sub> and O<sub>3</sub> (Atkinson & Arey, 1994, Lee & Lane, 2010, Wang *et al.*, 2007). Correspondingly, half-life-times were determined for several compounds in the range of hours to weeks. Besides photolytic reactions of gaseous PAHs with those radicals, photodegradation due to direct UV radiation may be considered as a relevant impact on particle-associated PAHs (Liu *et al.*, 2013, Valerio & Lazzarotto, 1985). Surprisingly few studies can be found regarding photodegradation of PAHs and its impact on passive air sampling. Bartkow *et al.* (2006b) present one comparative study on different set-ups of passive samplers in the atmosphere, using semipermeable membrane devices. They suggest precaution regarding the set-up of passive samplers in the field to eliminate photolytic loss of target compounds. Two settings were tested in the field to overcome the issue of potential loss by photodegradation:

1. Black PE sheets with black carbon for UV-protection by fabrication
2. Stainless steel cover above the PE sheets

All combinations were tested to get the optimal set up: black sheets covered and uncovered as well as transparent sheets covered and uncovered. However, the covered set-up was hypothesized to provide a specifically robust data set, due to comparably stable conditions as well as preventing photodegradation. Further tests to confirm the effect of photodegradation of PAHs on the chosen passive samplers as negligible include:

- I) First of all, Bartkow *et al.* (2006a) suggest the simultaneous use of two different *PRCs* as control on ongoing photodegradation. Respective compounds need to be characterized by significantly distinguishable partition coefficients, since loss rate constants are bound to partitioning. Accordingly, the proportion of different partition coefficients is expected to be identical to the proportion of the respective rate constants for individual compounds. The observation of such a relation at field sites would in turn confirm partitioning between sampler and air as major process for exchange kinetics and support the hypothesis of photodegradation as a negligible effect. Within this study Ant-D<sub>10</sub> and Pyr-D<sub>10</sub> are used as *PRCs* in parallel. Partition coefficients of these compounds differ by one log unit with  $K_{pg}$  of  $10^{7.07}$  for Ant and  $10^{8.06}$  for Pyr (at 25°C). Ravindra *et al.* (2008) list a half-life of Pyr exceeding the half-life of Ant for about a factor of 20 with 4.2 hours at simulated sunlight. With that, they indicate a significant difference within the photosensitivity of both compounds. Pyr-D<sub>10</sub> as additional *PRC* was included during spring and summer monitorings in 2016 to ensure sampling correlation to highest UV-radiation. A solution containing both (Ant-D<sub>10</sub> and Pyr-D<sub>10</sub>) was used for simultaneous spiking of the sampler.
- II) The basic numerical model was applied to the loss of Pyr-D<sub>10</sub> in the same way as introduced for Ant-D<sub>10</sub>, calculating loss rate constants as well as air-side boundary layers. Additionally, the trend of the curve was modelled for the first ten days of the monitoring. As a first attempt this was done without any adaption of the model to an additional process. In case the loss of the surveyed *PRCs* was influenced by photodegradation, distinctively faster kinetics would be observed. Differences between measured and calculated curves could be interpreted as indication on occurring photolysis.
- III) Photodegradation is obviously connected to the influence of light and therefore defined as potential process only during daytime. Stable concentrations of target compounds on the polymer throughout the course of 24 hours relate to consistent influences on passive samplers within the atmosphere. Hence, consecutive sampling during day and night was conducted as control on potential diurnal variation due to UV radiation. Behymer and Hites (1985) list a range of half-lives for 15 U.S. EPA Priority PAHs, bound to silica gel, of 0.7 – 150 hours according to photolysis. Therefore, day versus night sampling should allow to compare respective concentrations of all 16 U.S. EPA Priority PAHs to include a wide range of compounds with considerably different photosensitivity.

Towards the end of the sampling campaign in November 2017 passive samplers were collected after a sunny day at 4:30 PM, shortly before sunset to reflect daytime influences on the sampler. Additional samples were taken after the night 15.5 hours later at 8:00 AM at sunrise. Taking account of the whole range of U.S. EPA Priority PAHs might be used as a control on potential photodegradation in two different ways:

- a) Low molecular weight (LMW) PAHs (Nap-Ace) are characterized by fast exchange kinetics, reaching equilibrium between air and PE within a few hours. Therefore, passive samplers provide a high temporal resolution and the potential to reflect short-term fluctuations within the atmosphere for those LMW PAHs.
  - b) HMW PAHs on the other side demonstrate long equilibration times and don't reach equilibrium during the 4 weeks of monitoring. Yet, some of them are reported as highly photosensitive with half-lives of only a few hours (Behymer & Hites, 1985). Consequently, short-term variation of those compounds on the PE may indicate an induced loss like photodegradation of PAHs on the passive sampler. This day versus night sampling was performed during the second year of monitoring atmospheric concentrations. Within this monitoring campaign two different heights were sampled at 0.1 m and 1.2 m. The samplers at 0.1 m height were also deployed underneath an aluminium cover, hovering right above the ground with only 2-3 cm distance to the ground. This gap between soil surface and cover allows the exchange of air masses but excludes any influence of UV radiation and thus limits losses due to photodegradation.
- IV) Finally, photodegradation in the samplers was exemplarily included into the numerical model as an additional process to support the previous controls. For this application half-lives ( $t_{1/2}$ ) of the representative PAHs with Fl<sub>n</sub>, Phen, Fth and Pyr as 20, 20, 23 and 5 days, respectively were taken from literature (EPI- SUITE). The numerical approach accounts for a simple first order loss rate constant ( $\lambda$ ), with  $\lambda = \frac{\ln(2)}{t_{1/2}}$ .

For comparison, the calibration of PE sheets was performed using Ant-D<sub>10</sub> without consideration of photodegradation. Subsequently, uptake curves onto the passive samplers were also modelled comparing both premises (with and without photodegradation).

#### 4.2.1 Study design

The pre-experiment was done in Entringen, one of the locations chosen for the regular monitorings, closest to the lab. The monitoring covered two weeks between 30<sup>th</sup> of

#### 4.2 Preliminary test on diverse sampling-set-ups

September and 14<sup>th</sup> of October in 2015 with specific sampling times after 12 and 24 hours as well as 3, 6 and 13 days; samples were always taken in duplicate for each setting. Black and transparent sheets were spiked separately, aiming for a starting concentration of 1  $\mu\text{g/g}$  of Ant-D<sub>10</sub>. The different polymer types can additionally be differentiated by their thickness with black sheets of 80  $\mu\text{m}$  and transparent sheets of 30  $\mu\text{m}$ . For the covered deployment an aluminium cover at 1.2 m height was used in which 21 samplers can easily be installed, providing protection from direct sunlight, rain and to some extent wind. Uncovered sheets were attached to a cord, spanned right beside the cover at about 1.6 m height (Figure 4.1).



Figure 4.1: Different sampling set ups in the field; comparing black and transparent sheets with and without cover.

## 4.2.2 Results and discussion

### a) *PRC*-loss

Figure 4.2 illustrates significant differences in the concentrations of Ant-D<sub>10</sub> for the different set-ups during this preliminary test. Highest concentrations were determined on black covered sheets throughout the whole monitoring period. Regarding the starting concentrations ( $C_0$ ) of the *PRC*, considerably lower values can be observed on transparent sheets in comparison to black sheets. This is especially evident for the uncovered sampling set-up. Unfortunately, several uncertainties can't be excluded regarding the spiking process. This incorporates unknown equilibration times for the individual sheets (black vs. transparent). Earlier tests in the lab have shown that the whole mass of Ant-D<sub>10</sub> in the spiking solution was taken up by PE sheets. Therefore, no additional control was performed for initial concentrations on the samplers before deployment in the field or concentrations within the solutions adjacent to the spiking. Furthermore, this test lacks on a control of Ant-D<sub>10</sub> concentrations for the single loading solutions. Besides, varying starting concentrations of Ant-D<sub>10</sub> for black and transparent sheets might be attributed to different sorption kinetics of the black sheets containing black carbon particles. This might produce an offset to equilibrium concentrations for transparent sheets. Black carbon is generally characterized by high sorption capacities for hydrophobic organic contaminants potentially promoting a fast uptake of Ant-D<sub>10</sub> in a batch system of limited volume. Hence, differences in sorption kinetics would generate distinguishable uptake curves for black and transparent sheets during the atmospheric sampling. The measured concentrations of Ant-D<sub>10</sub> on the sheets demonstrate variations above the usual 10 % for the individual sampling times. The best reproducibility can be seen for black uncovered sheets. This, however, might be by chance since samples were only measured in duplicates. Yet, each set-up shows a coherent trend for the *PRC*-loss during this test as well as comparable trends for the different sheets. Data evaluation was based solely on the linear decrease of the *PRC*. This way a potential bias and respective error propagation due to the mentioned uncertainties was expected to be negligible. Thus, determined kinetic parameters are believed to provide a reliable means for further comparison. In practice, this leads to a slight difference of the time span on which the calibration of the samplers is based. Ant-D<sub>10</sub> concentrations measured after 72 hours are taken into account for the transparent uncovered sheets. Whereas for the rest of the samplers the loss of Ant-D<sub>10</sub> after 144 hours is used for calibration. The exponential loss of *PRC*s during the first few hours results in a consistent trend of faster kinetics for uncovered sheets. Characteristic times to reach 63% equilibrium ( $t_{0,63}$ ) were also calculated based on the observed loss rates. Fitted air-side boundary layers as well as characteristic times are listed in Table 4.1. Regarding the calibrated  $\delta_g$  confirms a first impression on similar trends in the *PRC*-loss for the different set-ups. All air-side boundary layers show similar thicknesses within the range of 0.4 - 1.3 mm. Yet, two differences can be observed: Thicker layers were identified concerning the covered set-up, independent of the type of sheets as well



as for transparent sheets independent of the set-up. Considering the outside boundary layer as limiting resistance generates exchange kinetics which are independent of the sampler thickness (Bartkow *et al.*, 2004). Converting the measured loss into respective boundary layers includes the thickness of the polymer (see ‘*theory on double film diffusion model*’). For both types of PE sheets longer equilibration times are determined for the covered set-up. The black covered sheets indicate the slowest equilibration with 63 % equilibrium being reached after 5.8 days while transparent uncovered sheets show the shortest characteristic time of 2.4 days. Such a difference for black and transparent sheets was to be expected, merely based on their respective thicknesses. Shielding of the samplers is provided with the aim to reduce environmental influences on the sampler like wind and UV-radiation. Corresponding thicker air side boundary layers and longer equilibration are expected for the covered deployment. Additionally, geometric properties of the passive sampler strongly correlate to equilibration with longer times for higher masses and bigger volumes of the polymer.

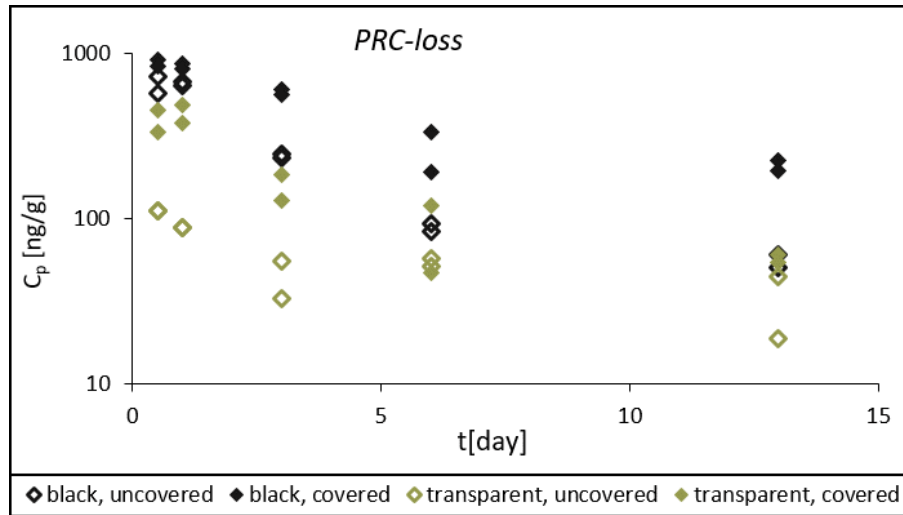


Figure 4.2: Comparison of PRC loss ( $Ant-D_{10}$ ) during preliminary testing in Entringen comparing transparent and black PE sheets, deployed in the field covered and uncovered.

Table 4.1: Calculated air-side boundary layers  $\delta_g$  and characteristic times to reach 63 % equilibrium for PRC-loss in each set-up.

field set-up	$\delta_g$ [mm]	$t_{0.63}$ [days]
black, uncovered	0.4	3.3
black, covered	0.7	5.8
transparent, uncovered	0.9	2.4
transparent, covered	1.3	3.9

#### 4 Development of an appropriate sampling set-up in the field

Figure 4.3 shows the measured loss of Ant-D<sub>10</sub> for each set-up in the field. Trends are calculated according to the numerical model as well as based on the analytical solution. In general, a good fit can be observed for the measurements and the corresponding calculated concentrations on the sampler for both approaches. One exception can be observed with transparent uncovered sheets illustrating notably higher concentrations on the sampler as calculated. This set-up also generates a slight deviation for the numerical and the analytical solution, which is due to the individual calibration of both mathematical approaches. While the numerical model accounts for the complete data set shown here, the analytical solution is based on a loss rate according to only two sampling times. Ensuring a more objective analogy the respective loss rates are provided in Table 4.2 considering the numerical as well as the analytical data evaluation. Examined loss rates are in the range of 0.17-0.37 day<sup>-1</sup> for the different field set-ups, which is in the same range as loss rates determined for Ant-D<sub>10</sub> by Bartkow *et al.* (2006a).

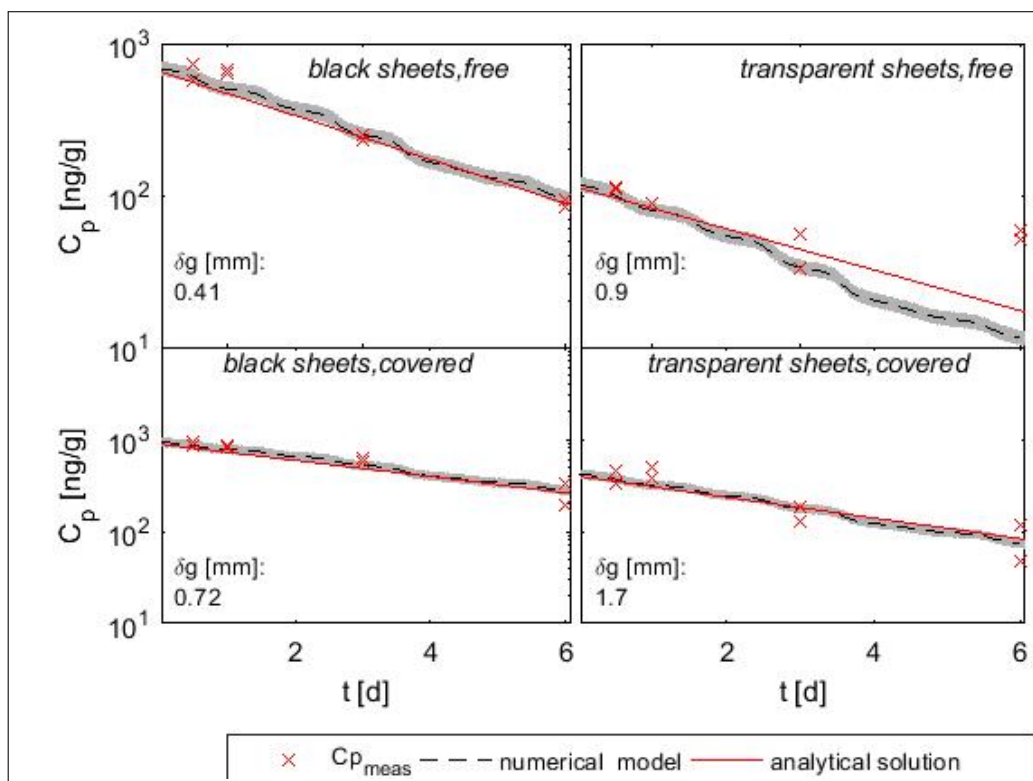


Figure 4.3: Measured and calculated PRC-loss for the different set-ups in the field, comparing the numerical model accounting for temperature variations (the grey area represents the respective standard deviation of 10 % for  $C_p$ ) to the analytical solution.

**Table 4.2: Calculated loss rates  $\lambda_{loss}$  [day<sup>-1</sup>] for PRCs in different set-ups, comparing the analytical and numerical evaluation.**

field set-up	$\lambda_{loss}$ (numerical) [day <sup>-1</sup> ]	$\lambda_{loss}$ (analytical) [day <sup>-1</sup> ]
black, uncovered	0.3	0.33
black, covered	0.17	0.2
transparent, uncovered	0.37	0.31
transparent, covered	0.25	0.26

In general, the numerical and the analytical approach provide equivalent loss rates. This verifies the numerical model as reliable data evaluation and calibration method for the following monitoring campaigns. The transparent uncovered sheets demonstrate minor variation and a faster loss calculated numerically. Considering the transparent sheets without shielding, explicitly lower concentrations are surveyed throughout the whole monitoring. Behymer and Hites (1985) demonstrate Ant as one of the most photosensitive PAHs on particles with half-lives of only a few hours depending on the corresponding substrate Ant is bound to. With respect to black carbon as substrate they report a rather long half-life of 310 hours. Since the black sheets contain black carbon this could explain the significant offset of higher PRC concentrations on black versus transparent sheets. Incomplete spiking of transparent sheets might therefore be not as relevant for the different starting concentrations as a sampler-specific influence of photodegradation on the PRC concentration.

As aforementioned, Pyr-D<sub>10</sub> was included during May and August 2016 as additional PRC with lower photo-sensitivity. Loss rates and air-side boundary layers are calculated individually for both PRCs, as listed in Table 4.3. During both monitorings slower release can be observed for Pyr-D<sub>10</sub>, which in turn generates loss rates of  $3\text{-}4 \cdot 10^{-6} \text{ s}^{-1}$  compared to loss rates of Ant-D<sub>10</sub> around  $2\text{-}3 \cdot 10^{-5} \text{ s}^{-1}$ . This is in perfect agreement with the corresponding partition coefficients, since  $\log K_{pg}$  of Pyr is one order of magnitude higher than  $\log K_{pg}$  of Ant. The individually calibrated air-side boundary layers are quite comparable for Ant and Pyr during May 2016 with 0.3 and 0.2 mm, respectively. In contrast, an offset with a factor of two can be observed during August with  $\delta_g$  of 1.1 mm determined with Ant-D<sub>10</sub> and 0.5 mm based on the loss of Pyr-D<sub>10</sub>.

**Table 4.3: Comparison of loss rate constants ( $\lambda$  [s<sup>-1</sup>]) and accordingly calculated air-side boundary layers ( $\delta_g$  [mm]) based on Ant-D<sub>10</sub> and Pyr-D<sub>10</sub> as Performance Reference Compounds.**

Monitoring	Ant-D <sub>10</sub> : $\lambda_{loss}$	$\delta_g$	Pyr-D <sub>10</sub> : $\lambda_{loss}$	$\delta_g$
May 2016	3E-05	0.3	4E-06	0.2
August 2016	2E-05	1.1	3E-06	0.5

Figure 4.4 shows the release of Ant-D<sub>10</sub> and Pyr-D<sub>10</sub> as PRCs during May and August 2016, exemplarily for Entringen. Measured concentrations on the passive sampler are combined with the numerical model as described earlier. Concentration changes over time are calculated based on the individually fitted air-side boundary layers listed in Table 4.3. Again, a good fit can be observed for calculated and measured concentrations except for the loss of Ant-D<sub>10</sub> during May 2016. In this case calculated concentrations are significantly lower than observed on the sampler after 3 days.

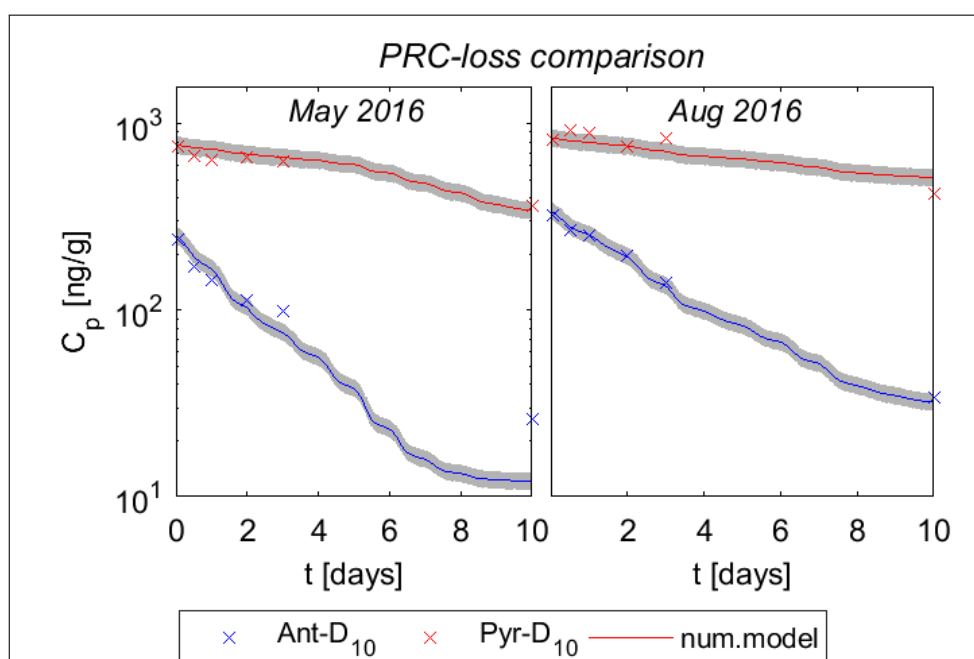


Figure 4.4: Comparison of Ant-D<sub>10</sub> and Pyr-D<sub>10</sub> as PRCs during May and August 2016 in Entringen; combination of measured concentrations and the numerical model with according standard deviation (solid line with grey shading).

#### b) Uptake of target compounds and resulting atmospheric concentrations

Figure 4.5 presents the uptake of four exemplary PAHs onto the passive samplers for the different set-ups. The choice of the representative compounds Fluorene (Fln), Phenanthrene (Phe), Fluoranthene (Fth) and Pyrene (Pyr) is based on their partition coefficients as they cover a broad range of  $K_{pgs}$  of almost two log units (Table 4.4). Additionally, the chosen compounds show comparably high concentrations on the sampler and thus a good reliability of measured data-sets. Pyr is the only high molecular weight PAH which could be detected in sufficient concentrations during all monitoring periods. As expected, the time needed to reach equilibrium increases with increasing  $K_{pg}$ . Fln reached equilibrium already after three to five days and then shows varying concentrations over the rest of the

monitoring. Phe seems to be in equilibrium after two weeks whereas Fth and Pyr concentrations still increase. Uptake rate constants are calculated as objective means for each set-up individually and listed in Table 4.5. They confirm the surveyed compound specific uptake kinetics and illustrate an explicit correlation to the deployment in the field. Besides, an explicitly good agreement of  $\lambda$  for Ant-D<sub>10</sub> as *PRC* and Phe as target compound with almost identical physicochemical properties (Table 1.1) was determined. For shielded samplers the equilibration time increases corresponding to the thickness of the boundary layers. Highest concentrations on the passive sampler can be observed for Phe and Fth followed by Pyr. Regarding the different sampling set-ups, slight differences can be seen with transparent sheets providing almost consistently higher concentrations as determined in black sheets. Moreover, higher concentrations and a better reproducibility were observed for the covered sheets. Considering Pyr, comparably high starting concentrations on the black sheets may indicate an existing (background) contamination present even after the clean-up step. Additionally, the extracts of black sheets include large amounts of impurities, which cause noise, elevated baselines, broad or even disturbing peaks in the chromatograms and therefore complicate an accurate peak detection and data-evaluation.

**Table 4.4: Characteristic properties of Fln, Phe, Fth and Pyr as representative PAHs, comparing their respective molar volume and mass as well as the diffusion coefficients in gas and partition coefficients  $K_{pg}$  (25°C).**

Compound	V [cm <sup>3</sup> /mol]	MW [g/mol]	log D <sub>g</sub> [m <sup>2</sup> /sec]	log K <sub>pg</sub> [L/kg]	ΔH <sub>vap</sub> [J/mol]
FLN	193.9	166.22	-12.36	6.3	72100
PHE	190.2	128.23	-12.44	7.0	78300
FTH	223.2	202.25	-12.96	8.1	87100
PYR	203	202.25	-12.76	8.1	89400

**Table 4.5: Uptake rate constants ( $\lambda$  [day<sup>-1</sup>]) of the four representative PAHs, comparing the different settings in the field during preliminary trial.**

Field set-up	FLN	PHE	FTH	PYR
Black, uncovered	1.67	0.28	0.02	0.02
Black, covered	0.91	0.16	0.01	0.01
Transparent, uncovered	2.0	0.34	0.02	0.02
Transparent, covered	1.43	0.24	0.02	0.02

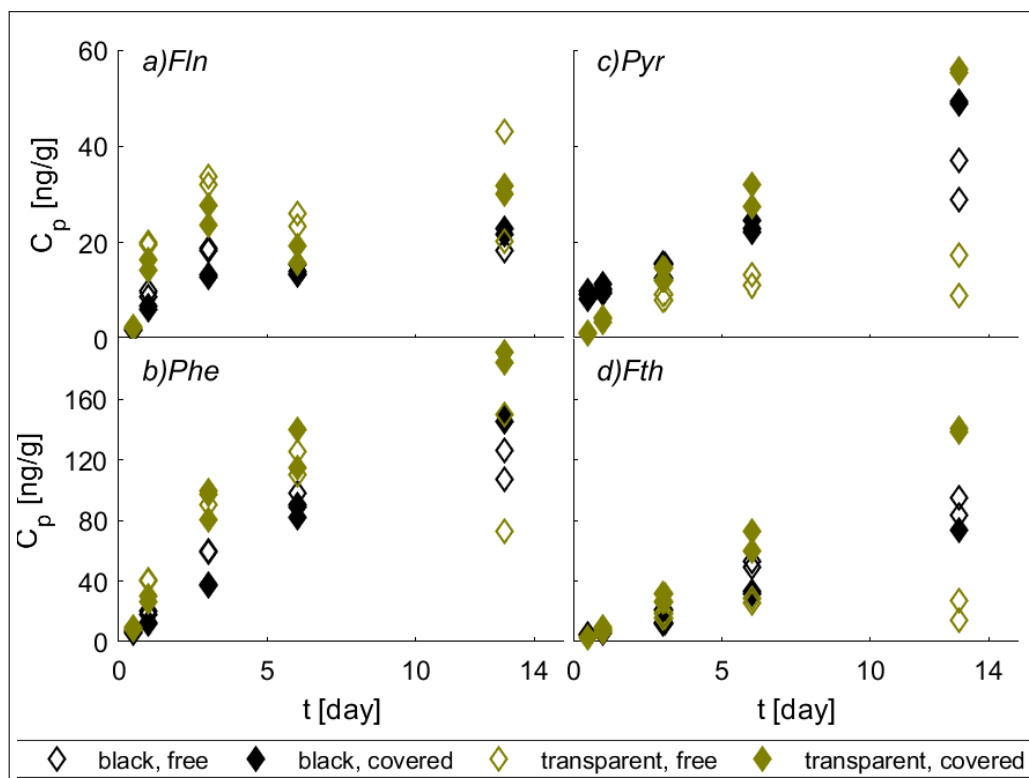


Figure 4.5: Uptake of the four representative PAHs onto PE sheets, comparing the different field set-ups in a preliminary test in Entringen.

Figure 4.6 shows exemplarily modelled uptake curves fitted to measured concentrations on the transparent and covered sheets (Uptake curves for the other settings are shown in Figure A.2 and Figure A.3). This model adapts the partition coefficients to hourly measured ambient temperature and fits a constant value of  $C_g$ . Results obtained for the transparent covered sheets are chosen due to the good quality of the extracts in combination with the better reproducibility for the covered set-up. A very good fit is observed for the calculated and the measured concentrations, for all target compounds, along with low standard deviations of the measurements. As shown in Figure 4.6, Fln reaches equilibrium within a few days. Besides, the numerical model illustrates diurnal varying concentrations as well as quite unstable concentrations over several days. Diurnal varying concentrations on the passive sampler are caused by temperature-variation throughout the day, which strongly influences the partition coefficient. Furthermore, varying concentrations over the course of several days indicate varying atmospheric concentrations day by day, which is captured by the fast equilibrating Fln. In general, atmospheric PAH concentrations seem to increase during this monitoring period, as the same increasing trend can be observed on the samplers regarding Fln and Phe, the latter equilibrates within a week. Fth and Pyr do not equilibrate and therefore accumulate continuously in the PE throughout the sampling. Besides, the diurnal temperature influence is dampened

because of the slow uptake kinetics for compounds with higher molecular weight. The latter has the advantage of long term integration, yielding average atmospheric concentrations during the monitoring period.

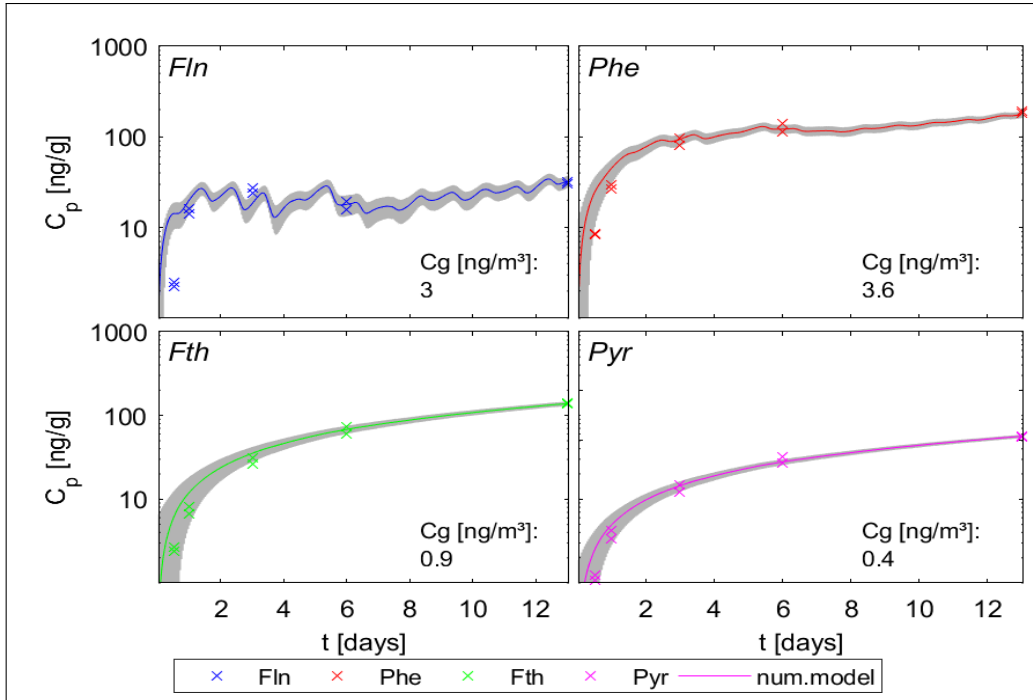


Figure 4.6: Measured uptake of the four representative PAHs onto transparent, covered PE sheets in combination with the fitted numerical model, the grey area illustrates the standard deviation for the model.

One of the main objectives of the numerical model is to determine accurate atmospheric concentrations as listed in Table 4.6. Comparing the different sampling settings only some differences are observed, mainly in form of higher values determined with transparent sheets. Regarding the black sheets separately demonstrates the same concentrations for covered and free samplers. Whereas transparent sheets depict higher concentrations for the covered set-up, except for Flu. In general, the highest concentrations in the atmosphere were calculated regarding Flu and Phe with  $1.7 - 3.6 \text{ ng/m}^3 \pm 0.5 \text{ ng/m}^3$ . Pyr shows the lowest concentration with  $0.1 - 0.4 \text{ ng/m}^3$ , and Fth concentrations vary between  $0.1$  and  $0.9 \text{ ng/m}^3$ ; these low concentrations show proportionally large differences depending on the set-up. Thus, the covered transparent sheets combine the thickest  $\delta_g$  of  $1.3 \text{ mm}$  with highest atmospheric concentrations for Phe, Fth and Pyr of  $3.6$ ,  $0.9$  and  $0.4 \text{ ng/m}^3$ , respectively. Equivalent to the validation of the numerical modelling approach for sampler calibration, atmospheric concentrations are verified by the analytical solution. Overall, a very good agreement is observed with only minor variations. Regarding Fth and Pyr, lower atmospheric concentrations are determined independent of the sampler type and field deployment according to the analytical solution. Flu and Phe just differ

with respect to the type of PE. Black PE shows slightly lower concentrations following the numerical model. The fitting process for transparent sheets results in slightly higher atmospheric concentrations than determined analytically. As mentioned above, calibration of the respective kinetic parameters differs slightly for the two approaches. The analytical solution relies on two sampling times whereas the numerical model accounts for all measurements throughout the linear *PRC*-loss and thus slight variations within the calculated atmospheric concentrations are to be expected. Nevertheless, all values are in the same range, independent of the sampling set-up and data analysis. Hence, the considerably similar uptake curves onto the different types of PE as well as the comparable results for atmospheric concentrations contradicts the suggestion of higher partition coefficients for black PE sheets.

**Table 4.6: Atmospheric concentrations [ $\text{ng}/\text{m}^3$ ] fitted with the numerical model for each field set up.**

Field set-up	FLN	PHE	FTH	PYR
Black, uncovered	$1.7 \pm 0.3$	$2.2 \pm 0.1$	$0.3 \pm 0.03$	$0.2 \pm 0.04$
Black, covered	$1.7 \pm 0.1$	$2.2 \pm 0.3$	$0.3 \pm 0.05$	$0.2 \pm 0.06$
Transparent, uncovered	$3.4 \pm 0.5$	$2.6 \pm 0.4$	$0.1 \pm 0.07$	$0.1 \pm 0.02$
Transparent, covered	$3 \pm 0.3$	$3.6 \pm 0.2$	$0.9 \pm 0.05$	$0.4 \pm 0.01$

As described above, differences in the loss of Ant-D<sub>10</sub> for the varying set-ups in the field might be taken as indication on photodegradation. In that case, explicit differences for the uptake of individual target compounds would be expected related to the compound specific photo-sensitivity. In particular, Ant and Phe are characterized by almost identical properties, except their photo-sensitivity. Literature values demonstrate Ant as considerably less stable in the atmosphere with a half-life of ca. 4 hours, compared to ca. 20 days for Phe (Biache *et al.*, 2014, Tobiszewski & Namieśnik, 2012 - and literature therein). Behymer and Hites (1985) determined respective half-lives for Phe exceeding the values for Ant up to a factor of 50, depending on the investigated material. Based on these findings Phe was expected to illustrate the same uptake behaviour for all settings in the field. Simultaneously, correlations of exchange kinetics between sampler and air should be clearly distinguishable for Ant and Phe. Considering the uptake of the respective target compounds induces a contrasting perspective: Estimated rate constants and characteristic times illustrate the same trend with faster kinetics on uncovered sheets independent of the compound and its reported photo sensitivity. Additionally, shorter equilibration times are surveyed for the transparent PE in comparison to the black PE, again for each compound. These consistent correlations for all examined PAHs contradict the assumption of photodegradation as relevant process for passive sampling. Furthermore, loss rate constants of Ant-D<sub>10</sub> and uptake rate constants of Phe are almost identical for the respective set-ups. Therefore, the observed correlations of kinetics and shielding are rather



caused by influences other than UV radiation. Wind on the other end acts generally as a major influence on exchange kinetics, independent of the target compound, and is also reduced by the covered set-up.

Figure 4.7 depicts a comparison of modelled uptake onto the passive sampler following the basic numerical approach as described earlier and a modelling approach which additionally considers photodegradation as first order loss rate (b). Both approaches are shown in combination with measured uptake of the representative compounds at 1.2 m height during August 2017. In the beginning of the sampling campaign, the observed uptake onto the sampler was explicitly faster as calculated, for both the numerical and the analytical solution. This gets more pronounced for high molecular weight compounds. However, calculated and measured concentrations converge towards the end of the monitoring for all studied compounds. Including photodegradation into the numerical approach generates no significant difference for the uptake curves regarding the shown PAHs. Equivalent to the preliminary test, air-side boundary layer and atmospheric concentrations of target compounds were fitted, including photodegradation as additional influence for comparison. All fitted parameters are listed in Table 4.7, indicating almost identical results for the modelling approach with and without consideration of photodegradation.

**Table 4.7: Fitted air-side boundary layer [mm] and atmospheric concentrations [ng/m<sup>3</sup>] for the representative compounds, comparing results with and without consideration of photodegradation.**

Fitted Parameter	Without photodegradation	Including photodegradation
$\delta_g$	2.02	1.89
$C_g$ Fln	$2.4 \pm 0.5$	$2.4 \pm 0.5$
$C_g$ Phe	$2.7 \pm 0.4$	$2.8 \pm 0.4$
$C_g$ Fth	$0.2 \pm 0.05$	$0.3 \pm 0.05$
$C_g$ Pyr	$0.03 \pm 0.01$	$0.08 \pm 0.02$

#### 4 Development of an appropriate sampling set-up in the field

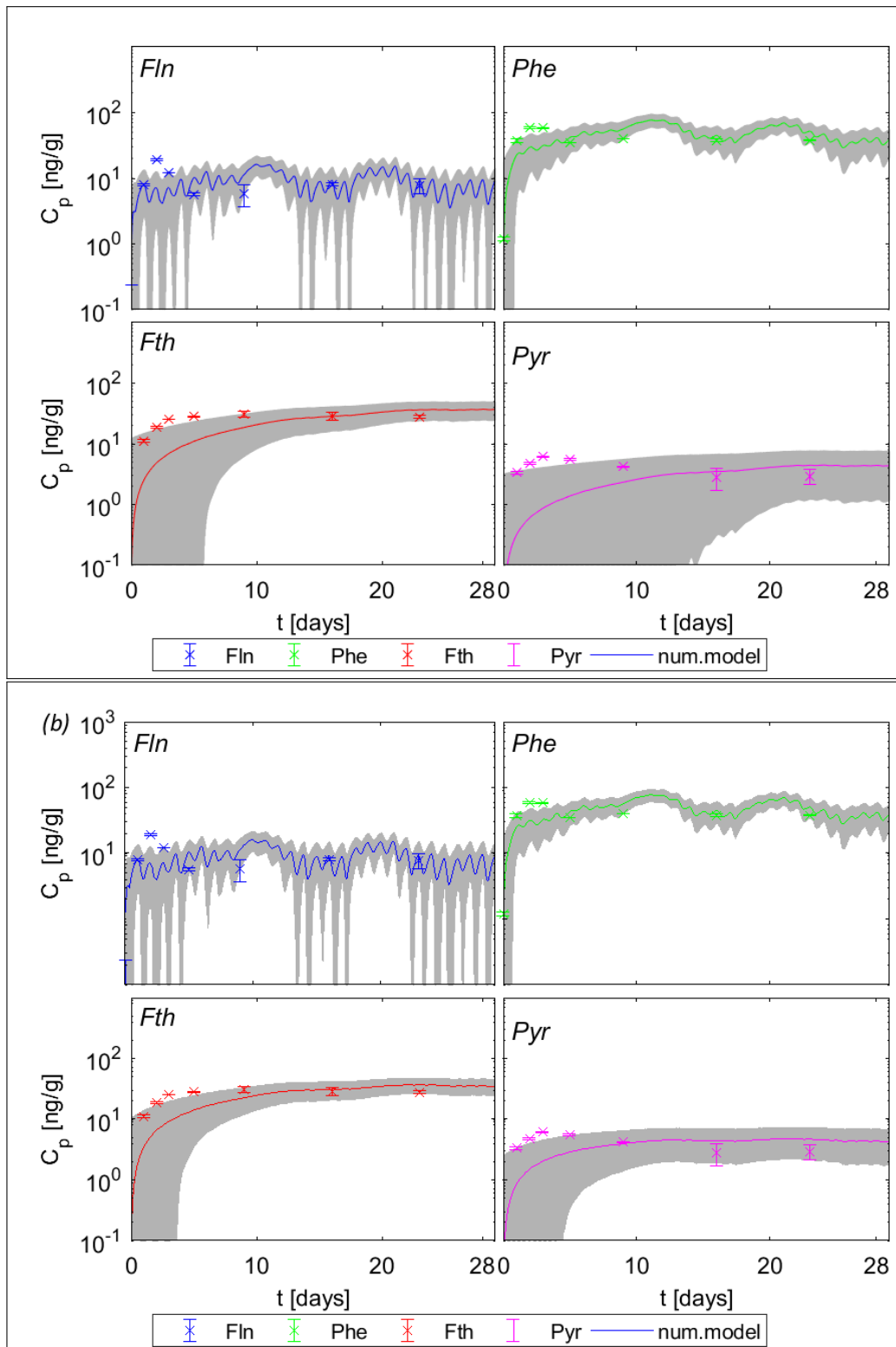


Figure 4.7: Uptake curves of representative compounds onto the passive samplers during August 2017, comparison of measured (crosses) to calculated (lines) concentrations, additionally b) considering photodegradation as loss process (lower plot).

Figure 4.8 shows the comparison of day versus night sampling of PAHs on passive samplers as a last test on photodegradation as relevant influence. Here, all of the 16 U.S. EPA Priority PAHs are included as well as both sampling heights (0.1 m and 1.2 m above ground) during November 2017, using four replicates. An excellent agreement of concentrations on the sampler comparing day and night samples can be observed for almost all of the target compounds. Exceptions were only observed regarding the low molecular weight compounds Nap – Ace, which show considerable higher concentrations on the sampler after the night sampling.

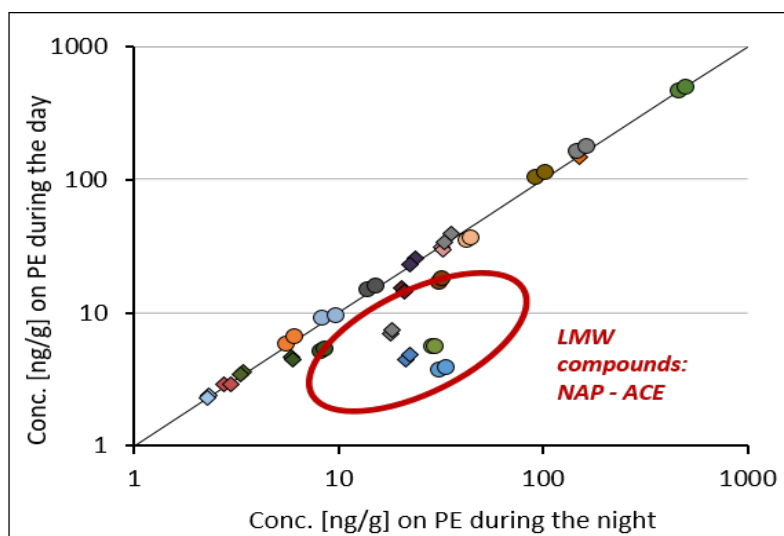


Figure 4.8: Comparison of PAH concentrations on PE at the end of the day versus at the end of the night, regarding the 16 U.S. EPA Priority PAHs, sampled in two different heights in Entringen, November 2017.

### 4.2.3 Discussion

The observed difference in calculated loss rates of Ant-D<sub>10</sub> in comparison to Pyr-D<sub>10</sub> corresponds to their respective partition coefficients. Loss rates as well as partition coefficients differ by a factor of ten with higher partition coefficients for Pyr leading to slower kinetics. Air-side boundary layers were considerably high during August compared to May and Pyr-D<sub>10</sub> shows a notably thinner  $\delta_g$  than Ant-D<sub>10</sub>. The *German Weather Service* provides a comprehensive data set regarding a broad range of meteorological parameter on their Climate Data Centre. Based on this data an evaluation of influencing factors like temperature, wind speed as well as total irradiance has been performed, for seasonal sampling campaigns (Figure A.4 and Figure A.5). Mean temperatures were measured with 13.5 °C and 17.2°C for May and August 2016, generating Log  $K_{pgs}$  of 7.6 and 7.4 for Ant as well as 8.7 and 8.5 for Pyr, respectively. Higher wind speeds during May explain a thinner air-side boundary layer compared to August. Regarding the global ra-

diation only a slight bias towards higher values could be observed during May. Yet, the surveyed temperature and the according shift of the partition coefficients may explain the detected variation in the exchange kinetics. One of the set-ups within the comparative study of Bartkow *et al.* (2006b) consists of passive samplers deployed in an open box, which provides quite comparable loss rates to our study. On the other side, they state contrary trends for the comparison of Ant-D<sub>10</sub> and Pyr-D<sub>10</sub> with loss rates of the same range as well as significant differences for the individual set-ups with respect to target compounds. Both observations are in contrast to the study presented here. While the contrasting outcomes on loss rates seems unclear, differences within concentrations of target compounds are most likely due to a distinguishable influence of field deployments on uptake kinetics. A better comparability of target compounds sampled with different settings could be provided by taking kinetics into account, potentially by calculating respective atmospheric concentrations.

During May 2016 the observed loss of Ant-D<sub>10</sub> from PE sheets was notably faster than calculated based on the air-side boundary layer as main resistance. This offset could serve as an indicator for an additional influence on the exchange kinetics between sampler and air. However, as no influence on the calculated uptake curve can be observed after including photodegradation as additional process, photolysis was no longer considered in fitting  $\delta_g$  and  $C_g$ . As illustrated in Figure 4.8, the concentration of most target compounds on the PE seems independent of day or night as well as on the sampling height. Hence, no correlation can be observed for light intensity, concentrations on the sampler and photosensitivity of target compounds. Significantly higher concentrations on the sampler were only determined during the night for the low molecular weight compounds Nap, Any and Ace. This test was performed as part of the monitoring in November 2017 and temperature fluctuation can be observed on diurnal basis with explicitly higher temperatures during the day. The partition coefficients calculated for the night exceed those estimated for daytime by a factor of two. Regarding the LMW PAHs Nap, Any and Ace, concentrations on the PE are integrated over a few hours (< 1 day), reflecting short-term variations due to changes in temperature and partition coefficients, respectively. Therefore, temperature variation can be interpreted as main impact on diurnal variation of PAHs on passive samplers, which is in good agreement with studies on diurnal variations of PAHs in the atmosphere and bound to particles (Liu *et al.*, 2013, Wu *et al.*, 2010).

Eventually, the implementation of photodegradation into the numerical model served as control on potential loss of PAHs from passive samplers driven by UV radiation. Comparing the two theoretical approaches of analysing the measured data sets provides no significant difference for the air-side boundary layer nor for the modelled uptake curve.

#### 4.2.4 Conclusion

None of the examined aspects shows any significant influence of photodegradation onto passive air sampling of PAHs within the precision of the sampling method. This is independent of theoretical data analysis or practical examination. Neither the numerical model nor the comparison of diverse sampling set-ups, sampling intervals or the use of different *PRC*s provides evidence of photosensitive behaviour of any of the target compounds on the passive sampler. Those findings support the hypothesis of photodegradation as negligible process and confirm the chosen sampling method as valid approach to determine atmospheric concentrations of PAHs. The observed uptake curves onto the passive sampler in different setups are quite comparable for each compound and calculated atmospheric concentrations are in the same order of magnitude. The choice for an appropriate field set-up for the following monitorings is therefore based on reproducibility of data. Black sheets have the disadvantage of providing “dirty” solvent extracts which produce poor chromatograms. Comparing covered and uncovered sheets it appeared reasonable to continue the monitorings with covered sheets, to minimize potential photodegradation of target compounds as well as errors in the calibration of uptake kinetics. Since calibration is based on an accurate *PRC*-loading of the sheets, the loading of the transparent sheets with Ant-D<sub>10</sub> was improved. For equilibration, a Millipore-water:MeOH solution (80:20 volumetric) kept on the overhead shaker for 10 days was used to ensure a complete and consistent spiking of the passive samplers with the *PRC*. As illustrated in Figure 4.9, the reproducibility of the starting concentration of Ant-D<sub>10</sub> was significantly improved with a standard deviation of only 1.5% (regarding the triplicates for each location).

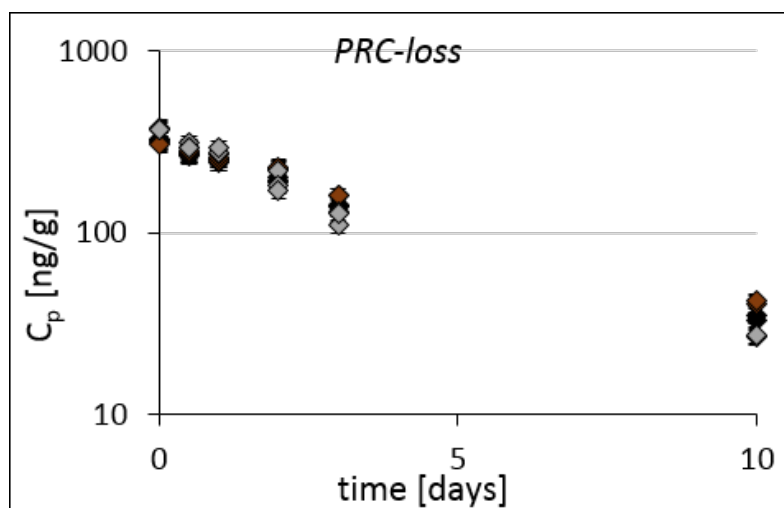


Figure 4.9: *PRC*-loss exemplary for one of the seasonal monitorings illustrating the successfully adjusted spiking of the sheets in advance of deployment by showing excellent triplicates for each location.

### 4.3 Validation with active sampling

As described above, the uptake of target compounds onto the passive sampler is mainly driven by their physicochemical properties and environmental conditions like temperature and wind. Passive samplers integrate atmospheric PAH concentrations over a variety of time spans from hours to years, according to the respective partition coefficient. In addition, atmospheric PAH concentrations may vary with time, again to various degrees on separate time scales. This needs to be kept in mind when calculating and comparing atmospheric concentrations from passive sampling data. Otherwise significant errors are easily produced, in particular for compounds with fast kinetics. Short equilibration times lead to higher uncertainties of reflected time spans. Depending on the target compound, potential sampling of dust particles needs to be excluded if possible, as sampling of particles might lead to an overestimation of gaseous concentrations. However, since this study focuses on low to medium molecular weight PAHs, particles are assumed to be negligible for atmospheric concentrations. As suggested by Tuduri *et al.* (2012), the simultaneous application of a well-established reference method should be used to validate atmospheric concentrations. For a reliable comparison of different sampling methods, an equivalent “reference” volume of air under the same ambient conditions needs to be sampled. Active air sampling of organic contaminants may be used to validate passive sampling of specific target compounds. This method is to a large extent independent of wind and temperature since the sampler does not equilibrate and sampling rates depend solely on air pumping rates.

#### 4.3.1 Method

Active air sampling was conducted in parallel to the end of passive sampling campaigns during August and November 2017 as well as during February 2018 at the study site in Entringen. This way LMW PAHs are expected to have reached equilibrium between air and PE sheets and reliable concentrations on the passive sampler are obtained. Active air sampling was performed with Gilian 5000 – Personal Air Sampling Pumps, set to a flow rate of 1 L/min, which was calibrated by the use of a flow-through-meter (Rotameteror, *Fisher Bioblock*). Cartridges with 2.5 cm in diameter containing three filters were used: a glass fibre filter with 0.45 µm poresize (*Whatman*) to prevent sampling of particles connected to two subsequent polyurethane foam (PUF) filters of 1 cm thickness each as sorbing material (*TISCH Environmental*). Active sampling was performed aiming to sample about 4 m<sup>3</sup> of air, to provide sufficient amounts of gaseous PAHs for reliable quantification. A relatively low sampling rate allowed the integrated monitoring of PAH concentrations for several days to provide optimal conditions for a comparison between active and passive air sampling. Battery recharge was needed after 18-36 hours of sampling (at colder temperatures batteries needed to be recharged more often), leading to sampling gaps of up to 12 hours. The time of those sampling gaps varied with respect to provide representative concentrations reflecting the whole sampling period

of 3-5 days. Active sampling was implemented into seasonal monitorings during August and November 2017 as well as during February 2018. Two separate intervals were sampled in November and February as additional control on stability of atmospheric concentrations during the monitoring campaigns. A clean-up step of PUF filters to be used was done by Soxhlet extraction with acetone for 12 hours before cartridges were assembled. Subsequent to the sampling, all filters were extracted separately with the ASE using ethylacetate as solvent at 85°C during 3 extraction cycles for 20 minutes each. Internal standard (10  $\mu$ l with 20 mg/L of *PAH mix 31*) was added into the extracts before shaking with Millipore water and transferred into 10 ml cyclohexane. Subsequently, the volume of cyclohexane was reduced from 10 ml to 100  $\mu$ l under a gentle stream of nitrogen at 40°C and samples were measured by GC/MS.

#### 4.3.2 Results

Figure 4.10 shows the quite variable atmospheric concentrations of the four representative PAHs (Fln, Phe, Fth and Pyr) determined with active samplers during August and November 2017 and February 2018. Independent of the sampling campaign, highest concentrations were determined for Phe with up to 10 ng/m<sup>3</sup> during August and November and 20 – 30 ng/m<sup>3</sup> in February, respectively. Fln, Fth and Pyr show significantly lower concentrations of 1 – 3 ng/m<sup>3</sup> during August and November and 2 – 12 ng/m<sup>3</sup> in February. As expected, the highest concentrations were determined for all target compounds in the winter monitoring, in particular during the first sampling period in February 2018. However, the second sampling period in February 2018 shows the overall lowest concentrations for Fln, Fth and Pyr with the exception of Phe which still displays about half the concentration of the first February sampling.

A comparison of atmospheric concentrations detected with active air samplers in contrast to passive samplers and their respective standard deviation is listed in Table 4.8. In general, both methods provide concentrations within the same order of magnitude regardless of the compound or the monitoring campaign. Best fits were obtained during November with concentrations varying between 2.9 – 3.3 ng/m<sup>3</sup>, 8.3 – 11.3 ng/m<sup>3</sup>, 2.2 – 2.4 ng/m<sup>3</sup> and 1.3 – 1.9 ng/m<sup>3</sup> for Fln, Phe, Fth and Pyr, respectively. In particular, atmospheric concentrations of Fln indicate a very good reproducibility for both methods during each monitoring campaign. For Phe, Fth and Pyr slightly higher atmospheric concentrations were determined by active samplers during August. Additionally, atmospheric concentrations in February calculated from passive samplers were considerably lower than determined with active samplers. Taking both of the actively sampled periods into account reveals a distinctive decrease of atmospheric PAH concentrations towards the end of February. As introduced for the preliminary test, the days to reach 63% equilibrium on PE sheets are calculated for the representative PAHs during August, November and February respectively, as listed in Table 4.9. Accordingly, characteristic times provide a measure for the reflected time span on the passive sampler and can be used as an indicator on the comparability of active and passive sampling during the individual

#### 4 Development of an appropriate sampling set-up in the field

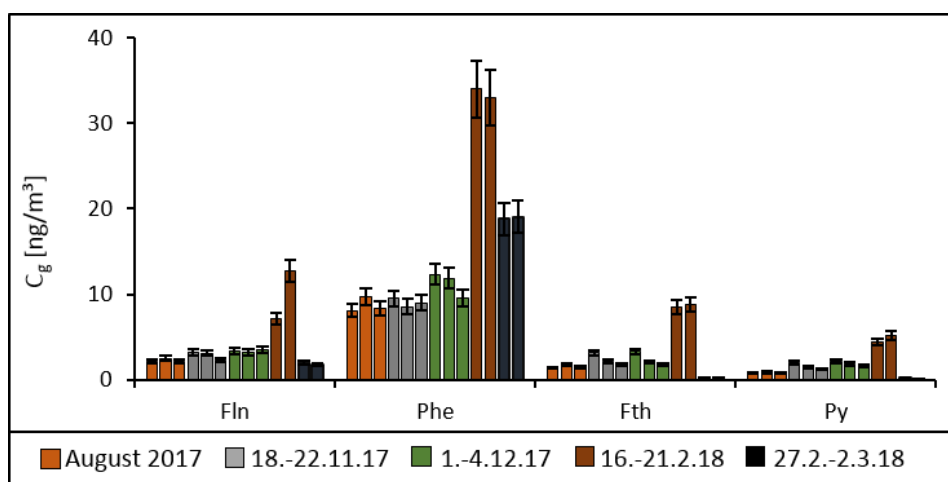


Figure 4.10: Atmospheric concentrations [ng/m<sup>3</sup>] of Fln, Phe, Fth and Pyr, determined in triplicates with active samplers at the end of monitoring campaigns in August '17 and November '17 and in duplicates during February '18. Error bars indicate a general standard deviation of 10% as measurement uncertainty.

monitorings. Fln shows the fastest equilibration with characteristic times between 0.6 and 2.6 days. Opposed to that, it takes about 40-270 days –depending on the monitoring - for Fth and Pyr to reach 63% equilibrium. Those compound specific times illustrate perfectly the proportional relation to the corresponding partition coefficients.

**Table 4.8: Comparison of atmospheric concentrations [ng/m<sup>3</sup>] for the four representative PAHs determined with passive and active sampling during August and November 2017 as well as during February 2018, including standard deviation.**

Monitoring	method	Fln	Phe	Fth	Pyr
August 2017	passive	2.4 ± 0.5	2.7 ± 0.4	0.2 ± 0.04	0.03 ± 0.01
	active	2.3 ± 0.2	8.7 ± 0.7	1.6 ± 0.1	0.8 ± 0.04
November 2017	passive	2.9 ± 0.2	8.3 ± 0.2	2.2 ± 0.1	1.3 ± 0.1
	active (18.-22.11.17)	2.9 ± 0.4	9.0 ± 0.4	2.4 ± 0.6	1.6 ± 0.3
	active (1.-4.12.17)	3.3 ± 0.1	11.3 ± 1.2	2.4 ± 0.7	1.9 ± 0.3
February 2018	passive	1.9 ± 0.3	6.7 ± 0.2	0.1 ± 0.05	0.03 ± 0.03
	active (16.-21.2.18)	8.7 ± 2.8	32.0 ± 2.2	8.5 ± 0.2	4.5 ± 0.5
	active (27.2.-2.3.18)	1.7 ± 0.3	16.1 ± 4.0	0.2 ± 0.1	0.2 ± 0.02



**Table 4.9: Characteristic times [days] to reach 63% equilibrium on passive samplers, calculated for the four representative compounds during August, November 2017 and February 2018.**

Monitoring	Fln	Phe	Fth	Pyr
August 2017	0.6	3.2	42.7	39.6
November 2017	2.6	16.6	271.8	265.6
February 2018	2.5	15.9	260.4	254.5

### 4.3.3 Discussion

Within this study only minor concentrations of few PAHs were detected on the glass fibre filters used as particle traps for active sampling. Thus, sampling of particles was excluded likewise for active and passive samplers complying one of the requirements for an effective method comparison (Tuduri *et al.*, 2012). Another prerequisite for comparison of both methods is the integration over the same time interval. As mentioned above, the active samplers covered varying time spans over 3-5 days, integrating about 40- 80 hours altogether. Considering the chosen target compounds on the passive samplers, only Fln integrates over an equivalent time span. Therefore, Fln allows to effectively compare atmospheric concentrations determined with the different methods, but still on the same time scale. A very good fit between both methods verifies passive sampling as appropriate method to determine atmospheric concentrations of LMW PAHs. One exception can only be observed during February 2018 with the first set of active sampling being conducted two weeks before the end of the regular monitoring with passive samplers. Subsequently, atmospheric concentrations calculated according to passive samplers integrate over a distinctively different period of time as active samplers, which generates the observed differences. The notably lower atmospheric concentrations determined with the second set of active sampling during February 2018 relate to distinctively higher wind speeds during the last week of the monitoring. At first, low wind speeds demonstrate rather stable conditions with respect to the general weather situation, which can be observed during November 2017 and in the beginning of February 2018. Adjacent, an increase of almost 2 m/s higher wind speeds towards the end of February might illustrate a general change of air masses sampled at the study sites (see Figure A.4). Higher wind speeds demonstrate a faster exchange of air masses, inducing higher turbulences and potentially increase the catchment area of the study locations. Therefore, the determined variations with actively sampled PAHs indicate an actual decline of atmospheric concentrations towards the end of the monitoring. In contrast, during November 2017 an excellent fit of atmospheric concentrations determined with both methods regardless of the compound can be observed. This indicates stable atmospheric conditions over a

longer period of time, especially since this conformity of active and passive sampling can be observed for both time spans of active sampling. In August 2017, unexpectedly high atmospheric concentrations were determined with active samplers, providing values within the same range as in November 2017. Usually PAH emission is considerably lower during spring and summer in comparison to autumn and winter. Yet, those high concentrations can be explained by construction work on the sampled field site in Entringen. During summer 2017, a drinking water well was installed with heavy diesel fuel engines, likely causing a local increase of atmospheric PAH concentrations. The comparison to passive samplers shows higher concentrations for Phe, Fth and Pyr. This might be due to a diluting effect generated with passive samplers as they integrate for bigger PAHs (> Fln) over longer periods of time than actively sampled. For those compounds passive samplers reflect additional air parcels, that are not affected by the construction devices. In general, atmospheric concentrations of Phe, Fth and Pyr determined with active samplers exceed passively measured concentrations during less stable atmospheric conditions. This may be due to respectively longer equilibration times and thus integration time scales, compared to Fln. However, this observation is in good agreement with literature data (Gouin *et al.*, 2005, Hayward *et al.*, 2010).

#### 4.3.4 Conclusion

Passive samplers integrate over different time spans dependent on the compound monitored in contrast to active samplers. This gets especially important with variable environmental conditions as observed during August 2017 and February 2018. Optimal conditions for comparing both methods were met for Fln only. In this case, an excellent agreement of atmospheric concentrations determined with active and passive samplers was observed. Therefore, the passive sampling method employed in this study provides reliable atmospheric concentrations. Yet, the integrated time span varies for the individual target compounds depending on their physicochemical properties (mol. weight, vapour pressure and thus  $K_{pg}$ ), which needs to be considered for the evaluation of the results.

#### 4.4 Atmospheric uptake: PE sheets vs. PDMS coated jars

PDMS coated surfaces provide yet another way to passively sample contaminants in any media of interest (Rusina *et al.*, 2007). The theory for uptake processes of target compounds onto the sampler remains identical as described for the PE sheets. Differentiation of the separate polymers is mainly evident in the sampling set-up with PDMS-coated jars being more flexible in their usage considering thickness and volume of the PDMS since the jars are being prepared and coated individually within the lab, generally aiming for thin layers of polymer of only few micrometres. Diffusion coefficients within PDMS are more than 100 times higher compared to PE as reported by Lohmann (2012) and Rusina *et al.* (2010), listed in Table 4.10. Partition coefficients between PDMS and water were also taken from Rusina *et al.* (2010) and transferred into  $K_{PDMS-air}$  by the use of Henry's law constant (provided by *New Jerseys Department of Environmental Protection*). Partition coefficients between PE and gas phase (again taken from Lohmann, 2012) of Flt and Phe are in the same range as for PDMS but exceed  $K_{PDMS-air}$  for a factor of two regarding Fth and Pyr (also listed in Table 4.10). Both higher diffusion and lower partition coefficients lead to faster uptake kinetics into the PDMS coated jars and shorter equilibration times compared to PE sheets. Furthermore, thin polymer layers and thus a high surface area to volume ratio accelerate equilibration (Bruheim *et al.*, 2003). Equilibrium state may be checked by using different thicknesses of PDMS (Reichenberg *et al.*, 2008): in case of equilibrium, equal concentrations are expected independent of the volume of PDMS. Currently, PDMS-coated jars are being used to sample contaminants from sediments, soils, and water (Jahnke *et al.*, 2012, Mäenpää *et al.*, 2011); to our knowledge no study was done so far on atmospheric sampling with coated jars. For that purpose, a comparative survey has been conducted in parallel to one of the regular monitoring campaigns during November 2016. Uptake kinetics of PAHs from the atmosphere into PDMS coated jars are determined for three different PDMS thicknesses, aiming to confirm both advantages of PDMS reported for other sampled media being also valid for sampling the gas phase. This way any uncertainties in atmospheric concentrations based on sampling rates or uptake kinetics could eventually be eliminated. Consequently, the following relations are expected:

- I) Much faster equilibration on PDMS compared to PE passive samplers
- II) Combining different coating thicknesses provides equilibrium concentrations on PDMS
- III) Determination of equal atmospheric concentrations independent of the type of sampler

### 4.4.1 Method

#### Preparation of the jars

For this study, 120 ml brown glass vials (*Wheaton*) of 4.7 cm height and a diameter of 5.4 cm were used with plain walls to allow homogeneous coating of the PDMS layer. Before coating, glasses and lids were thoroughly cleaned to eliminate any potential contamination by particles. A silicone-toluene-dispersion (*Dow Corning*) was diluted in Pentane to the amounts of silicone required for the different thicknesses of the coating with 1, 2 and 4  $\mu\text{m}$ . Subsequently, 4 ml of Silicone-Pentane solution was added into each jar while continuously rolling. After complete evaporation of the solvents, glasses were heated up to 90°C overnight and cleaned 4 x 30 minutes with cyclohexane. Subsequently, PDMS coatings were spiked with Ant-D<sub>10</sub> as *PRC* from a Millipore water:MeOH solution with 80% vol. Millipore-water, targeting at 1.5  $\mu\text{g}$  Ant-D<sub>10</sub> per jar as initial mass.

#### Experimental set up

PDMS jars were sampled in a high resolution, especially in the beginning of the campaign with sampling after 3, 6, 9, 12, 24 and 36 hours to determine exchange kinetics of PAHs between air and PDMS coating as well as equilibration times. Because of the high sampling resolution, the PDMS jars were set up in close vicinity of the lab (back yard of the Centre for Applied Geology in Tübingen) instead of using one of the field locations for the regular monitorings. The jars were secured upside down to a setting with individual holdings for each jar as shown in Figure 4.11. This way, the PDMS as passive sampling medium is protected against direct UV-radiation and rain, simultaneously minimizing accidental sampling of particles. Further samples were taken after 3, 5, 8, 12, 17 and 25 days. In addition to the PDMS jars, a set of 6 PE sheets were set-up as equilibrium samplers right beside the jars to provide an accurate comparison by sampling the same air. PE sheets were sampled in the middle and at the end of the monitoring with PDMS coated jars reflecting two time spans.

For the kinetics of the PE sheets, uptake curves are determined in the same way as for the regular monitoring at the field study sites.

#### Extraction

For the extraction of the PDMS coatings, 3 ml cyclohexane were added into each jar and kept on the roller mixer for 30 minutes. Subsequently, the extracts were transferred into clean vials and the extraction was repeated 3 times. A mixture of deuterated PAHs as internal standard was added into the combined extracts before reducing the volume to 100  $\mu\text{l}$  at the *Vapotherm* and subsequent measurement by GC/MS. Calibration of the samplers and further evaluation of measured concentrations on the PDMS were conducted identical to PE sheets to ensure a realistic comparison of both methods.



Figure 4.11: Set up of the PDMS coated jars (backyard of the Centre for Applied Geosciences in Tübingen)

#### 4.4.2 Results and discussion

##### a) PRC-loss and uptake kinetics

The measured *PRC*-loss for PDMS coated jars with different coating thicknesses is shown in Figure 4.12. Loading an identical amount of Ant-D<sub>10</sub> on varying masses of PDMS generated different starting concentrations of the *PRC*. Loading of the PDMS coatings was apparently not 100 % reproducible with initial masses of the *PRC* varying between 1.2 and 1.7 µg per glass jar. Yet, the respective *PRC*-loss rate constants for the different coating thicknesses were almost identical and in the range of 3.4 – 3.6 day<sup>-1</sup>. The determined loss rates for PDMS were faster than for PE sheets with a rate constant of 0.5 day<sup>-1</sup>. For both types of sampler an exponential *PRC*-loss was observed. Based on this loss, air-side boundary layers were calculated as 0.9 mm, 0.6 mm and 0.3 mm for 1 µm, 2 µm and 4 µm of PDMS coating respectively. Fitted air-side boundary layers for PE sheets of the parallel monitoring campaign at the three study sites were ca. 0.8 mm. As discussed earlier, an inverse correlation of polymer thickness and air-side boundary layer is observed resulting from the almost identical loss rate constants. After loss of ca. 90 % of the initial *PRC* concentration, further decline slows down considerably and finally stops for unclear reasons. Thus, the estimated loss shown in Figure 4.12 was corrected for a residual concentration referring to 10 % of the initial concentration. One potential explanation for this observation might be the inner structure of the polymer. Polymers used as sampling material are defined as one homogeneous phase, which is not 100% true. In general, polymers comprise two different phases; a crystalline and an amor-

phous structure, similar as described by Xing & Pignatello (1997) for natural organic matter with different states of condensation. Diffusion coefficients may be very low and limiting in the crystalline phase leading to an apparent residual concentration of *PRC* within the polymer. Besides, considerable fluctuation of the *PRC*-concentration can be identified subsequent to the linear loss; this is most pronounced for PDMS coatings with 2 and 4  $\mu\text{m}$  thickness.

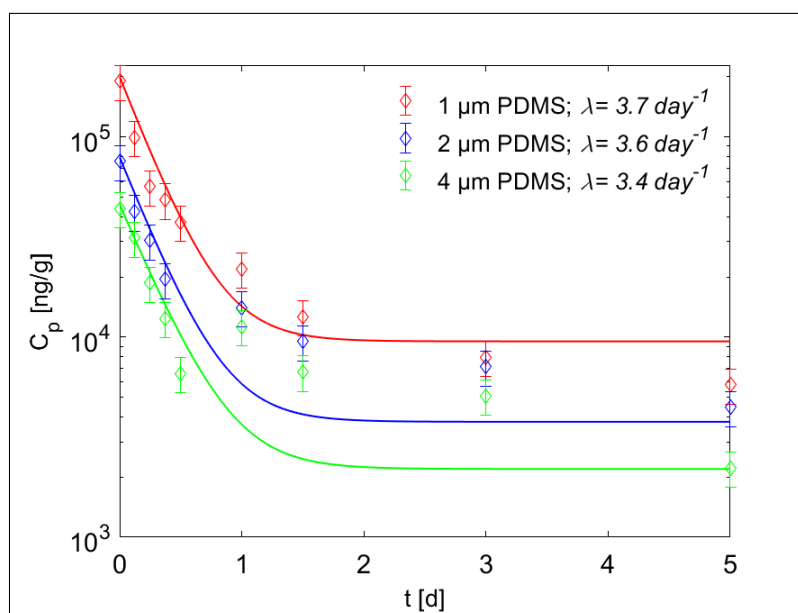


Figure 4.12: *PRC*-loss (*Ant-D*<sub>10</sub>) measured on PDMS coated jars for three thicknesses of PDMS coating, including  $\lambda$ , which is calculated based on the linear loss during the first 9 hours of sampling. The error bars account for 20% standard deviation.

Based on the air-side boundary layer, calibrated according to the *PRC*-loss, uptake rate constants were also calculated for Fl<sub>n</sub>, Phe, Fth and Pyr exemplarily, as listed in Table 4.11. Fluorene with lowest  $K_{PDMS-air}$  is the fastest compound. The determined rate constants are in the same range for the different thicknesses of polymer coating with 11.7 – 15.6, 2.0 – 2.7, 0.5 – 0.6 and 0.3 – 0.4  $\text{day}^{-1}$  for Fl<sub>n</sub>, Phe, Fth and Pyr respectively. The observed uptake rate constants ( $\lambda$ ) of the target compounds onto PDMS exceed the corresponding  $\lambda$  for PE sheets at the parallel monitoring campaign by a factor of 40 for Fl<sub>n</sub> and Phe and a factor of 100 for Fth and Pyr, respectively. This was expected due to the thinner layers and lower partition coefficients for PDMS; differences in the partition coefficients air-polymer are notably higher for Fth and Pyr compared to Fl<sub>n</sub> and Phe. Uncertainties for PDMS coated jars may be caused by variation of PDMS coating thicknesses of about 20%, particularly observed here for 2  $\mu\text{m}$  thick coatings.

**Table 4.10: Partition and diffusion coefficients (in [L/kg] and [m<sup>2</sup>/s]) between polymer and gas phase for PE and PDMS at 25°C and 20°C, resp. With <sup>a</sup>Lohmann (2012), <sup>b</sup>Rusina et al. (2010), <sup>c</sup>K<sub>PDMS-water</sub> taken from <sup>b</sup> and adapted for gas phase**

Compound	<sup>a</sup> Log K <sub>PE-air</sub>	<sup>c</sup> Log K <sub>PDMS-air</sub>	<sup>a</sup> Log D <sub>PE</sub>	<sup>b</sup> Log D <sub>PDMS</sub>
Fln	6.31	6.2	-12.4	-10.3
Phe	7.02	6.9	-12.4	-10.3
Fth	8.10	7.4	-13.0	-10.5
Pyr	8.06	7.5	-12.8	-10.5

**Table 4.11: Calculated uptake rate constants for each coating thickness and characteristic times to reach 90% equilibrium.**

polymer (thickness)	Fln		Phe		Fth		Pyr	
	$\lambda$ [day <sup>-1</sup> ]	t <sub>0.9</sub> [day]	$\lambda$ [day <sup>-1</sup> ]	t <sub>0.9</sub> [day]	$\lambda$ [day <sup>-1</sup> ]	t <sub>0.9</sub> [day]	$\lambda$ [day <sup>-1</sup> ]	t <sub>0.9</sub> [day]
1 $\mu$ m	15.6	0.15	2.7	0.9	0.6	3.8	0.4	5.8
2 $\mu$ m	11.7	0.19	2.0	1.1	0.5	5.1	0.3	7.7
4 $\mu$ m	14.0	0.16	2.4	0.9	0.5	4.2	0.4	6.4
80 $\mu$ m PE	0.38	6	0.06	38	0.004	617	0.004	603

Figure 4.13 shows measured uptake curves on PDMS coated jars for the four PAHs chosen earlier as representatives (regarding PE sheets). Uptake curves from air onto PE are also included for comparison, combining the measured data set and a numerically modelled curve. PE passive sampling was done in triplicates at each of the three locations resulting in 9 replicas. The observed spreading of measured concentrations of PAHs on the PE reflects slight spatial variation of uptake kinetics. However, as demonstrated in *Correlation of PAH concentrations, uptake kinetics and environmental parameters* the study sites reflect the same atmospheric influence with only minor variation within atmospheric concentrations of target compounds. This can be confirmed by the good fit of one modelled uptake curve, describing the measured data at all three locations. Accordingly, uniform atmospheric concentrations at large scale (~ 10 km distance) may be accepted and equivalent values for the sampling site of the PDMS jars are expected, as this location lays within the same radius. Except for the temporal increase of the concentrations measured on the PDMS after 17 days, uptake curves on PDMS and PE converge with time. At the end of the monitoring, concentrations of Fln, Phe and Fth are within the same range for both types of polymer, while concentrations of Pyr are exceedingly higher on PDMS than PE (up to a factor of 4). However, notable differences are observed

#### 4 Development of an appropriate sampling set-up in the field

for the various coatings during the whole monitoring period. This is especially evident and without a clear trend for Fl<sub>n</sub>. Besides, Phe, Fth and Pyr concentrations demonstrate a considerable inverse correlation of concentrations on the sampler to the PDMS thickness.

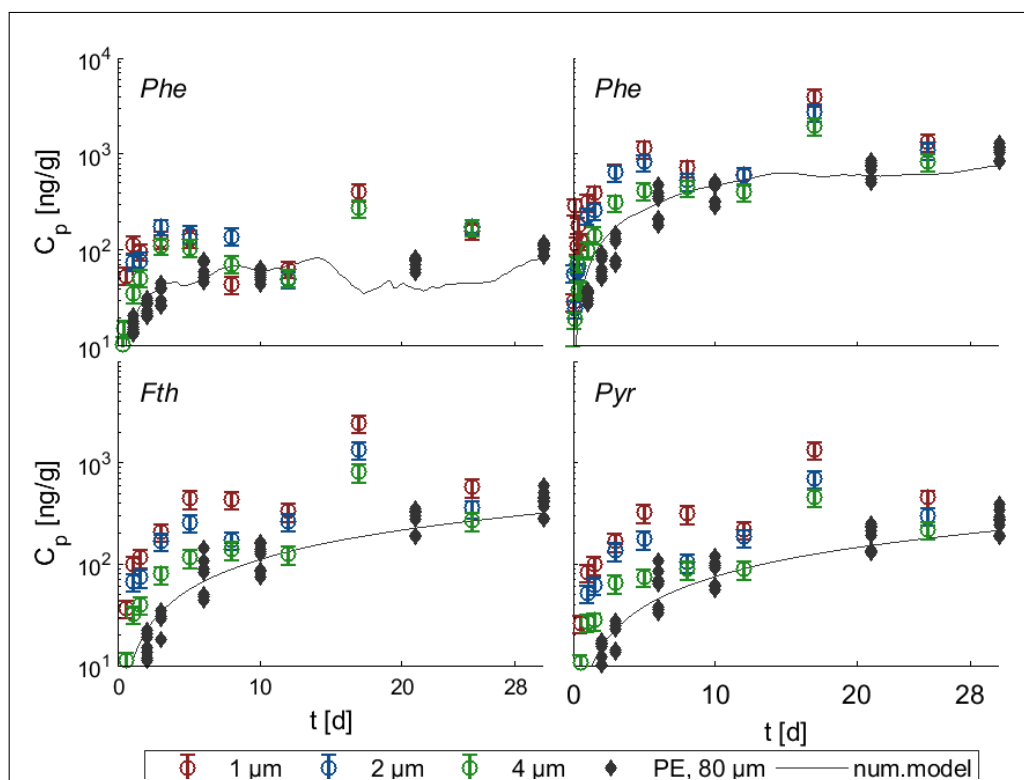


Figure 4.13: Measured uptake curves of four representative PAHs in PDMS coated jars with different thicknesses as well as on PE (with 9 replicates) combined with the numerical model for uptake onto PE sheets (accounting for temperature changes). Error bars for PDMS indicate variation of 20%.

The thin coatings showing highest concentrations would only be expected during the linear uptake mode with same amounts of target compounds within each jar. Accidentally sampled dust particles might lead to an overestimation of concentrations determined for the lowest amounts of PDMS. Another explanation for this observation might be a continuous increase of atmospheric concentrations over the course of the sampling campaign. Since this monitoring was conducted during November, the sampling began simultaneous to the commencement of the regular heating period. Thus, a constant increase of PAH emission might be reflected here. In combination with slightly shorter characteristic times of Fth and Pyr for 1 μm coating compared to 4 μm this could cause the consistently highest concentrations on the thinnest coating. Most of equilibrium (63



%) is obtained after less than 1 day for Fl<sub>n</sub> and Phe which is consistent with the observed loss of the PRC (Ant-D<sub>10</sub>). For Fth and Pyr, the fast uptake period seems to be less than 5 days. Uptake of target compounds onto PDMS coated jars was also calculated analytically and with the numerical model, as shown in Figure 4.14 (exemplarily for 4 μm PDMS coating). For the analytical solution, the last measurement on the PDMS was used as the equilibrium concentration and a mean partition coefficient was applied to integrate over the whole monitoring campaign (Table 4.12). Within the numerical model, the last measurement was fixed as the atmospheric concentration, assuming equilibrium was achieved. The partition coefficients throughout the sampling campaign were adapted to hourly measured ambient temperature (Table 4.12). Both attempts to calculate the uptake onto the PDMS generate a good fit to the measured data.

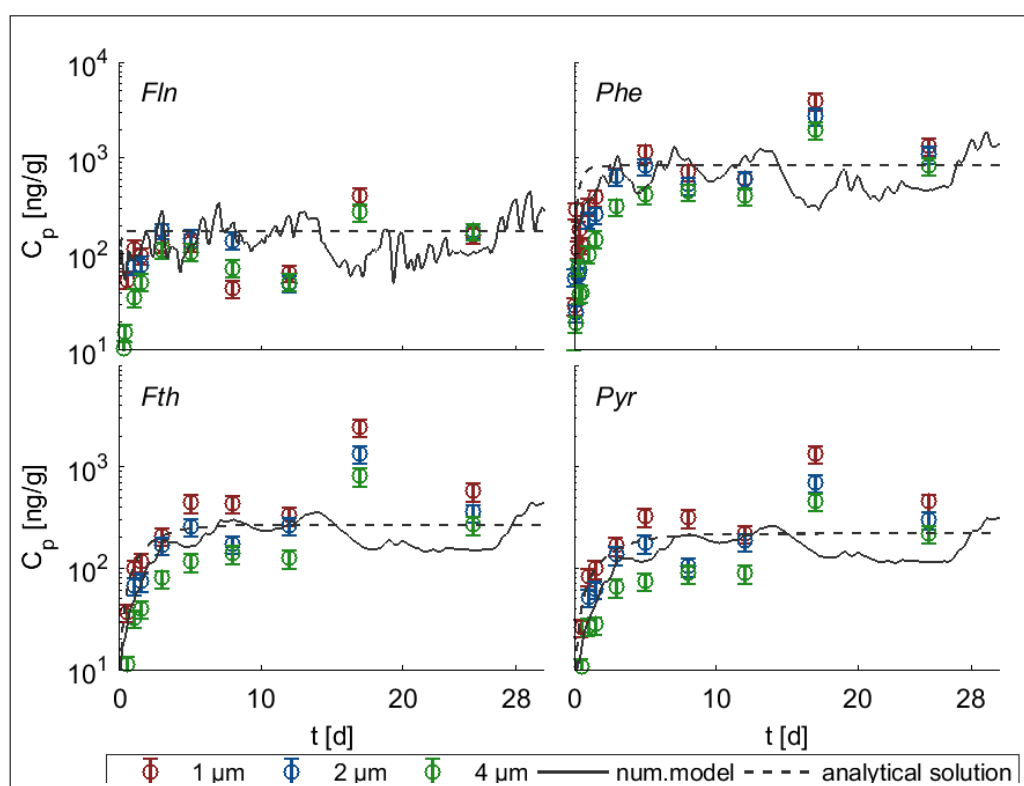


Figure 4.14: Uptake of four representative PAHs in PDMS coated jars with different thicknesses, combined with calculated uptake curves on 4 μm coating (including the analytical solution as well as the numerical model).

This confirms the assumption of the air-side boundary layer as limiting factor also for the PDMS coated jars. The numerically modelled uptake curves onto PDMS demonstrate distinctive short-term variation of the target compounds on the sampler, which are most pronounced for Fl<sub>n</sub> as the most volatile and fastest compound. Consequently, the numerical model illustrates a significantly higher sensitivity of the PDMS jars to changing influences in the atmosphere as observed for the PE sheets (Figure 4.13), even for

less volatile compounds like Fth and Pyr. Differences between measurement and the numerical model indicate varying atmospheric concentrations during the sampling period. In particular, the high concentrations measured on the sampler after 17 days can only be explained by increasing atmospheric concentrations. This would also be in agreement with the constant observation of highest concentrations on the thinnest PDMS coating. Consequently, and as to be expected, PDMS coated jars provide the opportunity to determine atmospheric concentrations of target compounds in significantly higher temporal resolution as PE sheets.

**Table 4.12: Partition coefficients ( $K_{PDMS-air}$  [L/kg]) of Fln, Phe, Fth and Pyr, adapted for different time spans (dependent on the temperature), depending on the approach to determine atmospheric concentrations (numerically, analytically and assuming equilibrium).**

Adapted for data evaluation		Covered time span	Fln	Phe	Fth	Pyr
Numerical model	min	hourly calculated	6.6	7.3	7.9	8.1
	max		7.7	8.5	9.2	9.4
	mean		7.2	7.9	8.6	8.8
Analytical solution		30 days (the whole monitoring)	7.2	7.9	8.6	8.7
Equilibrium assumed		Last 8 days of the monitoring	7.3	8.0	8.7	8.8

#### b) Validation of equilibrium and atmospheric concentrations

One fundamental advantage of the multi-thickness PDMS approach is the validation of equilibrium conditions based on the linear relation between mass of target compound and mass of PDMS, which circumvents the need of calibrating the respective kinetics (Reichenberg *et al.*, 2008). The characteristic times in Table 4.11 suggest equilibration of sampler and atmosphere after less than 8 days for all of the target compounds on PDMS. Therefore, the relation of the four target compounds and mass of the PDMS was examined for the last sampling times at 8, 12, 17 and 25 days. A linear relation was accepted for a coefficient of determination ( $R^2$ ) of at least 0.7, as shown in Figure 4.15. Once equilibrated, the slope of a linear regression for the individual coating thicknesses refers to the equilibrium concentration on the PDMS. PDMS jars were thoroughly cleaned in advance of the monitoring campaign and blanks indicate no detectable background concentration for Fln, Fth and Pyr but low masses of Phe. Thus, an initial concentration of zero was confirmed for the target compounds on the PDMS. Subsequently, the respective regression was forced through the origin leading to a significant non-linearity of Pyr and Fth independent of the sampling time as well as for Phe after 17 and 25 days. A clear linear relation can only be observed for Fln after 12, 17 and 25 days with a coefficient of determination between 0.95 and 0.99. The respective linear regression lines of Phe, Fth

and Pyr, on the other hand, only fit if a significant intercept on the y-axis is accounted for. As already mentioned above, accidental sampling of dust particles might lead to an overestimation of concentrations, particularly for the thin PDMS. Therefore, the observed intercept might indicate the amount of target compound sampled additionally by particle-deposition. As included in Figure 4.15, this intercept relates to masses of target compounds as low as 4-30 ng. This is well below the standard deviation of the PE sheets. At the end of this sampling campaign, around 1800 ng of Phe were detected on the PE with a standard deviation of 300 ng. Hence, small dust particles are more likely to influence the highly sensitive PDMS coated jars, due to the substantially low amount of polymer and much higher surface to volume ratio. Besides, Fl<sub>n</sub> as the most volatile PAH seems the least affected by dust particles. Yet, the considerable variation of the intercept with an increase after 17 days and a subsequent decrease seems contradictory to the assumption of a continuous sampling of artifacts. This observation rather suggests a direct relation of this offset to the respective atmospheric concentration. However, equilibrium concentrations on the PDMS might still be obtained as ascending slope of the respective regression. Consequently, relating the mass of target compounds to the according mass of PDMS within the coated jars provides a convenient method to determine equilibrium concentrations within the passive samplers. The outcome of this approach is listed in Table 4.13 demonstrating an obvious increase of atmospheric concentrations of Fl<sub>n</sub> and Phe after 12 days of sampling. Since PAHs are generally emitted as mixtures rather than individual compounds, a simultaneous increase of Fth and Pyr seems reasonable. This might explain the significant nonlinearity of Fth and Pyr on the different PDMS coatings during the first two weeks of sampling.

**Table 4.13: Atmospheric concentrations [ng/m<sup>3</sup>] of Fl<sub>n</sub>, Phe, Fth and Pyr, determined with PDMS coated jars, based on scatter plots as equilibrium validation, again only including data sets with  $R^2 \geq 0.7$ .**

Sampling after	Fl <sub>n</sub>	Phe	Fth	Pyr
8 days		3.8		
12 days	3.0	3.3		
17 days	17.9	14.7	0.7	0.3
25 days	15.3	8.2	0.4	0.2

#### 4 Development of an appropriate sampling set-up in the field

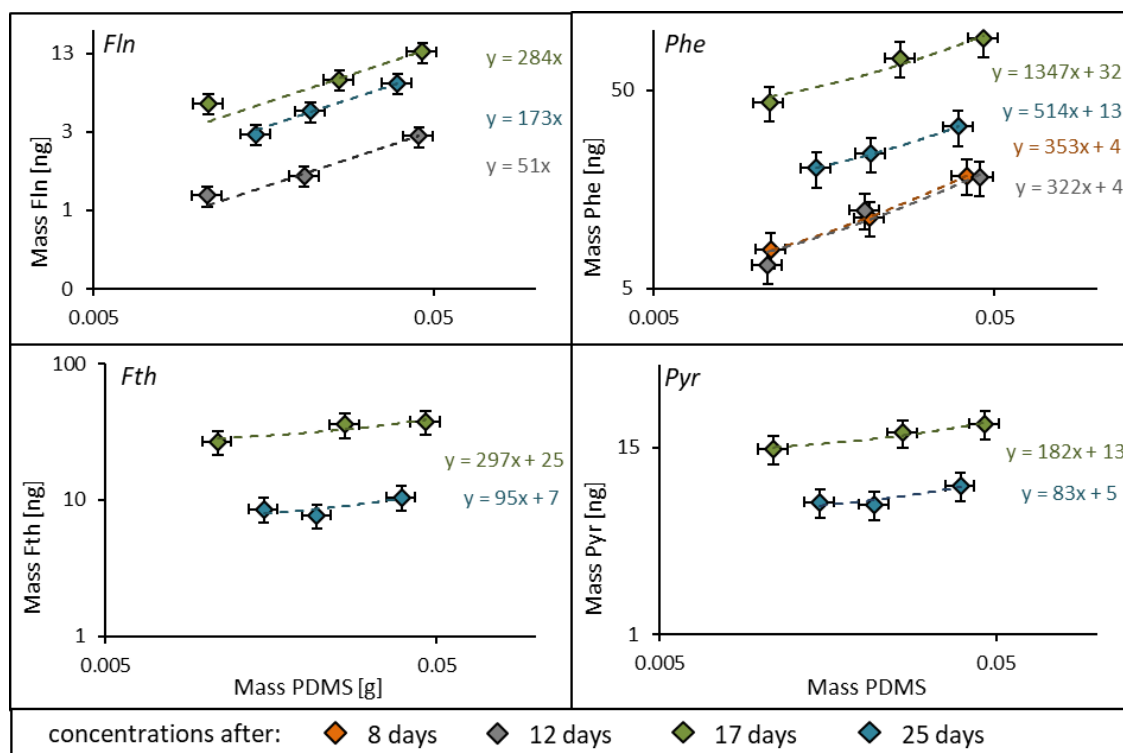


Figure 4.15: Double logarithmic plot of masses of the target compounds (Fluorene, Phenanthrene, Fluoranthene and Pyrene) versus mass of the PDMS for sampling after 8, 12, 17 and 25 days. With a linear regression as equilibrium concentration, only data sets with  $R^2 \geq 0.7$  are included. Error bars illustrate 20% variation.

As demonstrated earlier (see *Validation with active sampling*), PE sheets provide a reliable passive sampling method to determine atmospheric concentrations of PAHs (up to Pyrene). Therefore, atmospheric concentrations determined with PE are used here as a reference for validating the measurements on PDMS. Two sets of PE sheets are used, accounting for temporal variations by reflecting (a) the first and (b) the second half of the monitoring separately. This way, significant fluctuations of target compounds within the atmosphere were determined, indicating an increase of a factor of two during the second half of the sampling campaign. Concentrations of target compounds on the PDMS were transferred into atmospheric concentrations for each coating thickness analytically (Equation 3.5) assuming equilibrium and based on the numerical model as listed in Table 4.14. The analytical solution and equilibrium concentrations both refer to the last measurement, but were assumed to integrate over different time spans. For equilibrium concentrations, the partition coefficients were applied corresponding to the characteristic times and therefore averaged over the last 8 days of sampling. The analytical solution was assumed to integrate over the whole monitoring period and average coefficients for the whole sampling period were used (Table 4.12). The resulting atmospheric concentra-

tions of the analytical solution agree well with equilibrium conditions. Slight variations are caused by minor differences in the applied partition coefficients. This demonstrates the crucial impact of the defined time span covered by the respective coefficients. Both approaches exceed the numerically fitted values by a factor of two independent of the target compound or the PDMS thickness. The numerical model includes every measurement during the monitoring and adapts partition coefficients to temperature for every hour. Thus, this attempt was expected to provide the most accurate results. However, a higher sampling resolution in the beginning of the monitoring leads to a bias of the model towards the earlier time period, including considerable uncertainty with particularly low concentrations in the beginning.

**Table 4.14: Atmospheric concentrations [ng/m<sup>3</sup>] of Fl<sub>n</sub>, Phe, Fth and Pyr, determined with PDMS coated jars fitted from the analytical solution, based on equilibrium conditions at the end of the sampling campaign and fitted from the numerical model for each thickness of the coatings; for comparison concentrations determined with PE sheets are shown sampled a) after the first half of the monitoring and b) at the end of the sampling campaign.**

PDMS thickness	Fl <sub>n</sub>			Phe			Fth			Pyr		
	anal.	eq.	num.	anal.	eq.	num.	anal.	eq.	num.	anal.	eq.	num.
1 μm	9.8	8.7	5.5	14.5	12.8	7.2	1.4	1.2	0.7	0.7	0.6	0.3
2 μm	10.9	9.7	6.3	11.9	10.5	5.8	0.9	0.8	0.4	0.5	0.4	0.2
4 μm	11.9	9.6	4.5	9.6	7.9	3.7	0.7	0.6	0.3	0.4	0.3	0.1
PE (80 μm)	a) 4.9 b) 11.2			a) 10 b) 19			a) 0.1 b) 0.2			a) 0.05 b) 0.1		

Comparing atmospheric concentrations determined with PE and PDMS demonstrates no clear trend. For Fl<sub>n</sub>, the first set of PE agrees with the numerical evaluation of PDMS jars while the second set of PE sheets provides equal concentrations as the analytical solution for the PDMS. For Phe, the first set of PE sheets demonstrates a comparable concentration as the analytical solution or equilibrium conditions on PDMS. Opposed to that, the second set of PE sheets exceeds this value for a factor of two. Considering Fth and Pyr, concentrations based on PDMS coated jars are notably higher than according to the PE, especially for the first set of PE sheets. Furthermore, only Fl<sub>n</sub> shows consistent atmospheric concentrations for the individual PDMS coatings. Figure 4.16 illustrates the temporal variation of atmospheric concentrations for the four PAHs determined with the PDMS coated jars, based on equilibrium conditions for each of the sampling times and each coating thickness. Calculated atmospheric concentrations are supposed to provide identical results independent on the amount of PDMS. Yet, the different thicknesses lead to diverse atmospheric concentrations, especially for the second half of the monitoring. Highest atmospheric concentrations are consistently determined with the thinnest PDMS coating. As discussed above, this might be due to accidentally sampling of dust and

#### 4 Development of an appropriate sampling set-up in the field

particle-associated PAHs or caused by an actual variation of atmospheric concentrations. Yet, such a variation illustrates the uncertainty of passively sampling atmospheric PAHs with PDMS coated jars.

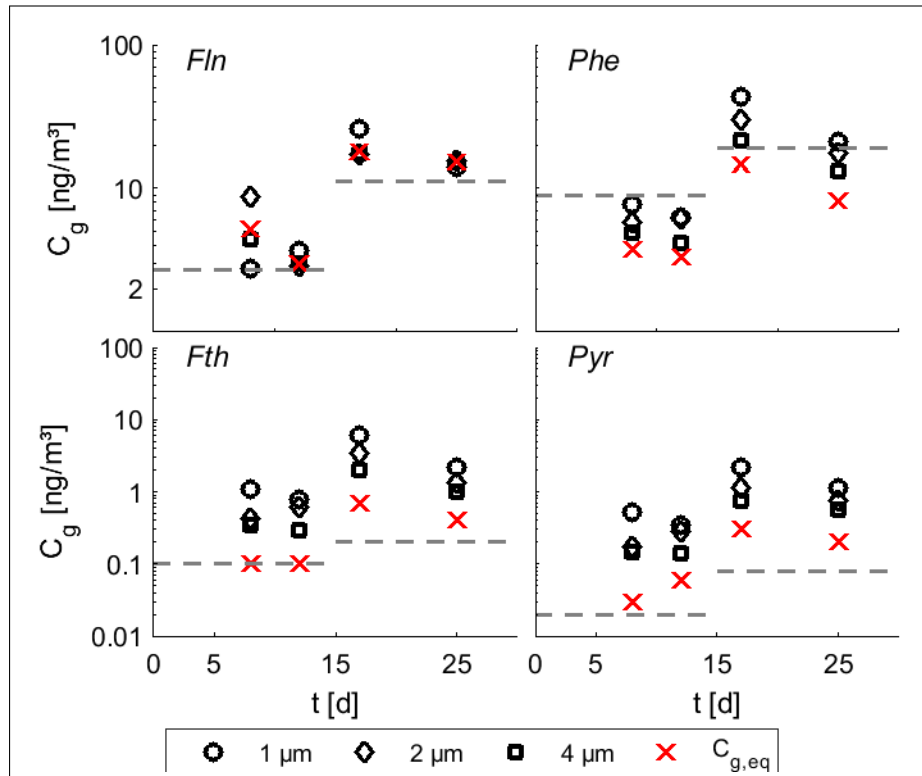


Figure 4.16: Comparison of atmospheric concentrations of Fln, Phe, Fth and Pyr based on different PDMS thicknesses, assuming short equilibration times, including  $C_g$  determined with PE sheets (dashed line).

Additionally, atmospheric concentrations were determined based on the regression slopes from Figure 4.15. This approach provides distinctively lower values for Fln, Fth and Pyr as calculated for the individual jars and therefore leads to a significantly better fit to the reference concentrations monitored with PE sheets. Thus, combining the three thicknesses appears as a simple attempt to correct for a potential overestimation of  $C_g$ . In particular, this accounts for the exclusion of accidentally sampled particles or the integration over a broader period of time for the different coatings. Furthermore, the significant temporal variation of atmospheric concentrations observed here is in contrast to the expectation of stable conditions and concentrations throughout the sampling period. However, this comparative monitoring including PDMS coated jars and PE sheets was conducted under special prerequisites: the samplers were located right beside the parking lot of the Center for Applied Geosciences, a considerable point source of exhaust fumes – especially during the cold period. Besides, this location is close to the city centre of Tübingen and therefore potentially influenced by several point sources, such as

traffic as well as exhaust air produced by the laboratories, the adjacent Mensa kitchen or by heating of the surrounding houses. Hence, the PDMS coated jars do not reflect fairly constant background concentrations of atmospheric PAHs, which are determined by the regular monitoring campaigns.

#### 4.4.3 Conclusion

High sensitivity of fast passive samplers (e.g. thin PDMS coatings) and semi-volatile compounds to temporal variations of atmospheric concentrations hamper the comparison of data if sampling resolution is too high (< few days). Thus, temporal point sources might be overrated compared to average concentrations, complicating the comparison of different locations. Due to the high sensitivity of thin PDMS coatings, slight variations of coating thicknesses and measured masses of target compounds lead to a quick error propagation, increasing uncertainties for data evaluation. This is again especially evident with respect to faster kinetics. The combination of different coating thicknesses is essential to check for equilibrium concentrations in the PDMS and to account for sampling artefacts. Yet, an additional drawback of PDMS coating seems to be the apparent collection of particles loaded especially with low volatile PAHs. In combination with the low amount of the polymer, this generates considerable overestimation of atmospheric concentrations. Within this study, despite the short equilibration times of the target compounds on PDMS, combining the different coating thicknesses led to a range of atmospheric concentrations instead of confirming equilibrium between sampler and air. Since concentrations in the atmosphere show diurnal changes and depend on local emissions, time integrative passive sampling averaging over several days are preferred to examine seasonal variations at separate locations (i.e. using thick coatings or only focussing on low volatile compounds). Therefore, further monitoring campaigns were continued with PE sheets, as they provide more consistent uptake curves generating reliable atmospheric concentrations.

## 5 Correlation of PAH concentrations, uptake kinetics and environmental parameters

Several studies on atmospheric concentrations of PAHs report considerable spatial and temporal variability (Kong *et al.*, 2010, Masih *et al.*, 2012, Liu *et al.*, 2014, Venier *et al.*, 2016). Generally, variations of atmospheric concentrations strongly depend on the different seasons with higher PAH concentrations during autumn and winter compared to spring and summer. This seems very reasonable with respect to the major emission sources like industrial and domestic heating or burning of garden waste after harvest in autumn. In addition, a range of aspects was studied focusing on potential correlations regarding atmospheric deposition rates as well as temperature and air mass trajectories (Wania *et al.*, 1998, Schiffman & Boving, 2015). Pozo *et al.* (2009), however, consider seasonal variation as negligible on a global scale but underline its relevance on a small scale, particularly when comparing regional sites. Albuquerque *et al.* (2016) suggest a lower height of the atmospheric boundary layer and less mixing of air masses for lower temperatures as an additional factor leading to higher atmospheric concentrations during winter. Furthermore, partitioning of PAHs between particles and gas phase shows seasonal differences due to their temperature-dependency (Pankow, 1987, Finizio *et al.*, 1997, Klánová *et al.*, 2008). Naturally, diverse effects generate explicitly varying concentrations on passive samplers, depending on the season. Melymuk *et al.* (2011) criticize the uncertainty of these different aspects in terms of their quantifiable influence on passive sampling rates and the corresponding accuracy within data evaluation. As discussed before, the chosen passive sampling practice in combination with the numerical approach provides a reliable method to determine atmospheric concentrations of target compounds. First, an accurate knowledge of crucial parameters influencing the exchange between sampler and air is essential for the calculation of  $C_g$  from  $C_p$ . Subsequently, a precise characterization of sampling conditions with respect to these parameters is obligatory. Therefore, one objective of this study is to check for potential correlations between concentrations, uptake kinetics and environmental parameters such as temperature and wind. Seasonal monitoring campaigns at three study sites in combination with the numerical modelling approach and simultaneous evaluation of ambient conditions were performed with respect to this objective. Furthermore, the following hypotheses can be set up:

1. A well-mixed atmospheric boundary layer generates spatially homogeneous background concentrations of PAHs in the atmosphere on a regional scale.
2. Temporal variations with notably higher atmospheric concentrations during autumn and winter are expected.
3. Short-term fluctuations of PAH concentrations on passive samplers are mainly caused by temperature variation and corresponding temperature-dependent partitioning.



4. For stable distribution patterns the measurement of one single compound is sufficient to determine the whole range of PAHs.

## 5.1 Sampling set-up and data evaluation

Based on the preliminary test described in *Data analysis*, transparent PE sheets with 80  $\mu\text{m}$  thickness were used as passive samplers. Sheets were deployed under an aluminum cover, shielding samplers from direct sun light and to some extent from wind and particle deposition. This set-up generates rather stable and thus comparable conditions for the individual monitorings. Each cover provided fixations for 21 samplers, corresponding to 7 sampling times with triplicates. Sampling campaigns were performed during May, August, November 2016 and February 2017. Samples were taken after 12, 24, 48 and 72 hours and after 10, 20 and 30 days during the first three monitorings. In the case of potentially changing atmospheric concentrations, a higher sampling resolution was required, which in turn led to additional sampling times after 15 and 25 days during February 2017. Furthermore, a sampling campaign was performed in the course of a Master Thesis (Bettina Rüdiger, 2017) during June and July 2016 targeting the sensitivity of passive samplers by focusing on diurnal concentration variations of Phe. In advance of a high-resolution sampling, PE sheets were deployed for 30 days, thus low and medium molecular weight PAHs are expected to reach equilibrium between air and PE sheets. Subsequently, samples were taken in duplicates every six hours to cover a time span of 24 hours in total. Extraction and measurement of PAHs was performed as described earlier.

In accordance to the preliminary test, four representative PAHs (Fln, Phe, Fth and Pyr) were selected for detailed analysis as they span a range of partition coefficients of almost two log units. Additionally, these compounds are contributing between 50 and 95 % of the sum of gaseous PAHs during each monitoring period (excluding NAP), illustrating their environmental relevance. Compounds with a partition coefficient higher than Pyr are not included since their uptake is very slow and they could only be detected during the winter monitoring. In order to determine uptake curves onto the passive samplers as well as fit the corresponding atmospheric concentrations to these curves, the aforementioned numerical model was applied. Based on this numerical model accounting for temperature dependent partition coefficients, the air-side boundary layer as limiting factor for the uptake of target compounds was determined. Subsequently, using this layer, concentrations in the gas phase were fitted to the measured uptake curves as a constant value throughout the individual monitorings. Concentrations of Fth and Pyr on the sampler were extrapolated to equilibrium using this numerical model. Additionally, atmospheric concentrations were calculated with the analytical solution. The combination of measured and calculated (numerically and analytically) data sets provides the opportunity to differentiate between temperature induced fluctuations on the passive sampler and actual changes of atmospheric concentrations.

## 5.2 Results and discussion

### 5.2.1 Comparison of study sites based on numerical and analytical data evaluation

Figure 5.1 illustrates measured and modelled uptake curves onto the sampler for the four PAHs comparing the numerical and the analytical approach during May 2016 at each of the study sites. The analytical solution is calculated only once for all sites, based on average temperature adapted partition coefficients. Thus, average concentrations were fitted. The numerical model, however, uses a site-specific calibration of the samplers. Standard deviation for the numerically calculated concentrations on the sampler is included exemplarily for the uptake curves in Entringen. This way, the accuracy of the model for an individual location may be read off the figure. In general, a good fit can be determined for the calculated and measured concentrations on the passive samplers. Only for Pyr the modelled uptake curves on the PE sheets show significantly lower concentrations in the beginning of the monitoring in comparison to the measured data set. In particular, the analytical solution generates an uptake curve for Pyr, which fits the measured concentrations not before the end of the monitoring campaign. Comparing uptake curves of the four representative compounds during May 2016 to August 2017 (as shown in Figure 4.7) shows similar trends. Fln indicates equilibrium after 24 hours, followed by explicit diurnal variation. Phe seems to reach equilibrium within a week and illustrates afterwards similar variations as Fln, just to a lesser extent. Fth depicts ongoing uptake onto the passive sampler throughout the whole monitoring, while Pyr surprisingly seems to reach equilibrium towards the end of the sampling campaign. Characteristic times are calculated, as introduced before, with 0.3, 1.8, 25 and 24 days for Fln, Phe, Fth and Pyr to reach 63% equilibrium respectively, as listed in Table 5.1. Mean partition coefficients on which characteristic times are based on are listed in Table 5.2. Characteristic times are again in good agreement with the surveyed uptake data, except for Pyr. The reason for that remains unclear. The whole set of fitted atmospheric concentrations for each of the sampling locations is shown in Table 5.3. Concentrations observed at the different locations are in a narrow range of  $0.8 - 0.9 \text{ ng/m}^3 \pm 0.1 \text{ ng/m}^3$ ,  $1.4 - 1.9 \text{ ng/m}^3 \pm 0.3 \text{ ng/m}^3$ ,  $0.1 - 0.2 \text{ ng/m}^3 \pm 0.02 \text{ ng/m}^3$  and  $0.04 - 0.06 \text{ ng/m}^3 \pm 0.02 \text{ ng/m}^3$  regarding Fln, Phe, Fth and Pyr respectively. Therefore, the different sampling sites demonstrate a very good agreement indicating good reproducibility of the method with respect to the target compounds Fln, Phe and Fth. The chosen sampling sites are in close proximity to each other (max. 12 km distance) and are all located within the Ammer valley, close to Tübingen with agriculture as the main land use. Additionally, the sites were selected on the prerequisite that no major local emission source is sampled. Hence, the observations suggest that the sampled air masses reflect the same influences. Consequently, this passive sampling method indicates either a broad catchment area or relates to homogeneous background concentrations provided by a well-mixed atmospheric boundary layer.

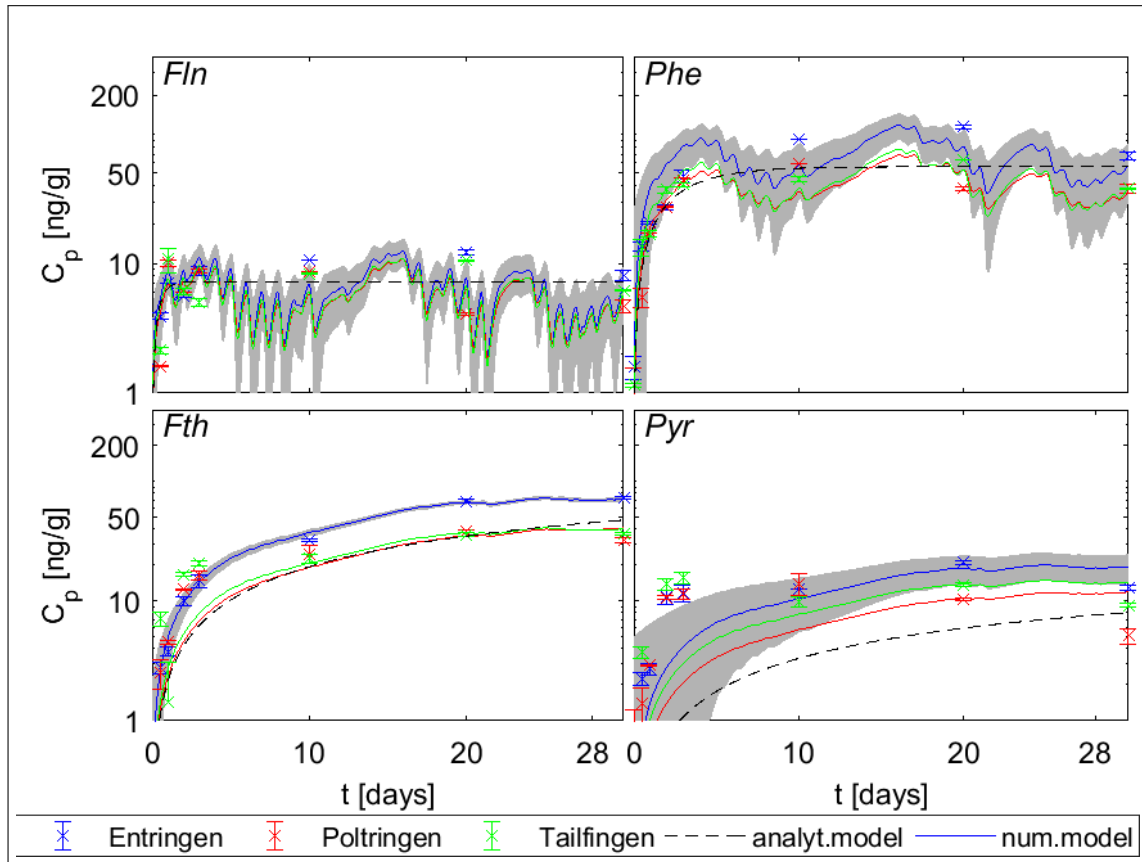


Figure 5.1: Measured uptake of Fln, Phe, Fth and Pyr onto PE at the study sites in May 2016; solid lines: predicted uptake based on the numerical model including the previously fitted air-side boundary layer and the fitted  $C_g$ , black dashed line: predicted uptake based on the analytical solution considering Entringen as exemplary site, error bars indicate standard deviation of triplicates and the grey areas show confidence intervals for the numerical model of Entringen, again exemplarily.

**Table 5.1: Air-side boundary layers [mm] for the seasonal monitorings in May, August and November 2016 and February 2017 and characteristic times [days] to reach 63 % equilibrium on the sampler, calculated for Fln, Phe, Fth and Pyr.**

Monitoring	$\delta_g$ [mm]	Fln	Phe	Fth	Pyr
May 16	0.3	0.3	1.8	25	24
Aug 16	1.1	0.6	3.2	43	40
Nov 16	0.9	2.6	17	272	266
Feb 17	0.8	2.5	16	260	255

**Table 5.2: Mean values for log  $K_p$  [L/kg] of the four representative compounds during seasonal monitorings of the first year of sampling.**

Monitoring	Fln	Phe	Fth	Pyr
May 16	6.8	7.7	8.7	8.7
Aug 16	6.6	7.3	8.4	8.4
Nov 16	7.3	8.0	9.2	9.2
Feb 17	7.3	8.0	9.2	9.2

Table 5.3 additionally includes atmospheric concentrations calculated based on both the analytical solution as well as on the assumption of equilibrium between air and PE, which is valid for Fln and Phe. Identical atmospheric concentrations of Fln are obtained for the numerical and analytical fit as well as for the assumption of equilibrium conditions. This observation suggests stable atmospheric conditions throughout the whole sampling campaign, as Fln equilibrates fast and measured Fln concentrations on the PE reflect only short time periods. For Phe slightly higher concentrations are determined with the numerical fit compared to the analytical solution and equilibrium conditions. Fth and Pyr show the lowest atmospheric concentrations if equilibrium was assumed, which is not valid for those two compounds. Equilibrium concentrations have to be extrapolated and show different values depending on the used fitting approach (numerical vs. analytical). The difference is highest for atmospheric concentrations of Pyr and relatively high standard deviations (5 ng/g) are obtained. This is due to the use of different data sets. Atmospheric concentrations based on the analytical solution are calculated according to the last measurement on PE only. In contrast, the numerical model accounts for all samples within the fitting process of  $C_g$ . Furthermore, the individual ways of data evaluation rely on different partition coefficients. The analytical solution averages over the whole sampling campaign, while the assumption of equilibrium status only refers to the second half of the monitoring (after equilibrium was attained). Hourly calculated values of  $K_{pg}$  are included in the numerical model, providing a high resolution of temperature-adjustment. The corresponding partition coefficients are listed in Table 5.4, including the min and max value of  $K_{pg}$  for the numerical approach. A broad range of  $K_{pg}$  of ca. one log unit for Fln and Phe and even higher spreading for Fth and Pyr is covered within the numerical approach. Therefore, the numerical fitting seems to provide more accurate concentrations while averaging over the chosen time span of several weeks.

**Table 5.3: Atmospheric concentrations [ng/m<sup>3</sup>] and respective standard deviations of the representative PAHs determined with the numerical model, analytical solution and under equilibrium conditions in May 2016.**

Location	Data evaluation	Fln	Phe	Fth	Pyr
Entringen	Numerical model	0.9	1.9	0.2	0.06
	Analytical solution	1.0	1.6	0.2	0.03
	Averages over 14 days	1.0	1.6	0.1	0.02
	+/-	0.1	0.3	0.02	0.01
-----					
Poltringen	Numerically fitted	0.8	1.3	0.2	0.04
	Analytical solution	0.6	0.8	0.1	0.02
	Averages over 14 days	0.6	0.9	0.05	0.01
	+/-	0.1	0.2	0.02	0.02
-----					
Tailfingen	Numerically fitted	0.8	1.3	0.1	0.04
	Analytical solution	0.8	0.8	0.1	0.03
	Averages over 14 days	0.8	0.9	0.05	0.02
	+/-	0.1	0.1	0.01	0.02

**Table 5.4: Partition coefficients (Log K<sub>pg</sub> [L/kg]) of Fln, Phe, Fth and Pyr, adapted for different time spans, depending on the approach to determine atmospheric concentrations (numerically, analytically and assuming equilibrium).**

Adapted for data evaluation		Covered time span	Fln	Phe	Fth	Pyr
Numerical model	min	hourly calculated	6.24	6.95	8.02	7.97
	max		7.28	8.07	9.27	9.26
Analytical solution		30 days	6.86	7.63	8.78	8.76
		(the whole monitoring)				
Averages over 14 days		2 <sup>nd</sup> half of the monitoring	6.84	7.59	8.75	8.73

### 5.2.2 Seasonal variations of passive air sampling kinetics

Figure 5.2 depicts concentrations of the representative PAHs on the PE measured for the last sampling time of each monitoring and each location. This enables explicitly a comparison of the measurements used as basis for the analytical solution. Two distinctive correlations can be observed within this plot. First, a characteristic pattern of the four compounds was determined for all seasons. Phe consistently presents the highest concentrations followed by Fth, while Pyr and Fln contribute the lowest concentrations. Second, almost identical measurements at the different locations can be observed for each of the respective target compounds. This observation was already reflected by the consistent (fitted) values of  $C_g$  for the three study sites, shown in Table 5.3.

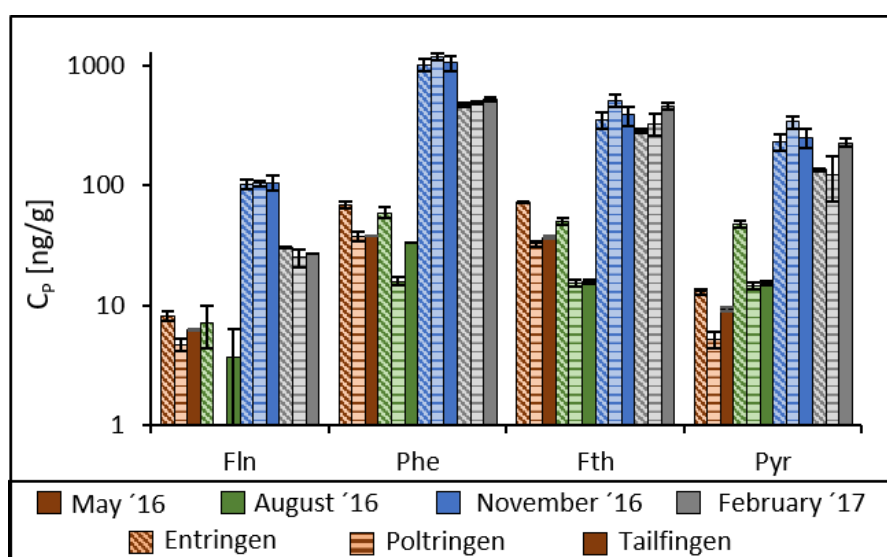


Figure 5.2: Concentrations of four representative PAHs on PE for the last sampling of the seasonal monitorings (May, August and November 2016 and February 2017) in Entringen, Poltringen and Tailfingen. Error bars illustrate the measured standard deviation of triplicate samplers.

Thus a good reproducibility of the measured data can be confirmed, independent of the monitored season. Based on this stable distribution pattern of the PAHs on the sampler throughout the seasons, it is sufficient to focus on one compound for further and more detailed data analysis. Phe seems most appropriate as the compound of choice, due to highest and therefore most robust concentrations. Consequently, Figure 5.3 shows seasonal uptake curves of Phe during the first year of monitoring. Measured concentrations at the separate study sites are combined with modelled uptake curves based on individually calibrated  $\delta_g$  and fitted  $C_g$ . The uptake curves displaying Fln, Fth and Pyr can be found in the appendix Figure A.3 – Figure A.7. Both measured and calculated uptake curves are rather comparable for the individual locations during each sampling campaign, as already observed for the four target compounds in May 2016 (Figure 5.1). Minor variations are determined during May and August with slightly higher Phe concentrations

measured in Entringen, compared to Poltringen and Tailfingen. This observation may be caused by a small railway as local emission source (run with a Diesel engine) in close vicinity of the sampling site Entringen.

During May and August, diurnally varying concentrations on the passive sampler are fitted by the numerical model. A shift of the temperature during day and night is expected to cause such a fluctuation of the more volatile PAHs on PE. For Phe, this effect can only be observed during the spring and summer monitoring, due to fast equilibration at higher temperatures, as demonstrated by correspondingly short characteristic times (Table 5.1).

Equilibrium concentrations on the passive samplers at the end of the monitoring campaigns in May and August 2016 are in the range of 20 - 70 ng/g, depending on the location. November 2016 and February 2017, however, show much higher concentrations with 1014 - 1194 ng/g and 470 - 520 ng/g, respectively. During November 2016 a variable accumulation of Phe on the passive sampler was detected. In particular, increasing concentrations were measured on the sampler after equilibrium conditions were attained indicating variations in atmospheric concentrations. Additionally, in February 2017 decreasing concentrations on the PE was observed towards the end of the monitoring. Table 5.5 shows average temperatures and wind speeds in combination with calibrated air-side boundary layers. Furthermore, Phe concentrations on the PE as well as in the atmosphere are provided. This may be used as a proxy for the distribution of PAHs between particles and gas phase demonstrating the corresponding PAH distribution between particles and gas phase exemplarily. The air-side boundary layers demonstrate almost identical values around 1 mm regardless of the study site and the surveyed season. One exception was determined for May 2016, with thinner boundary layers of 0.3 - 0.4 mm, again regardless of the location. Photodegradation can be excluded as a relevant loss-process for the conducted sampling method, as shown before. Since temperature-dependent diffusion and partition coefficients are used, wind is the only parameter influencing the uptake kinetics onto the passive sampler. The measured wind speeds during May are the highest of all seasonal monitorings. The sensitivity analysis considering calculated air-side boundary layers based on Sherwood numbers confirms a strong correlation of thinner layers for higher wind speeds, as illustrated earlier (see *Background theory of passive sampling*). However, to generate boundary layers of the determined thicknesses in May, the corresponding wind speeds need to be a factor of two higher than observed. Thus, no unambiguous explanation for this distinctively thinner boundary layer during May 2016 can be given.

Characteristic times (of max. 17 days during November) suggest equilibrium of Phe between PE and air towards the end of each monitoring. A comparison of ongoing exchange between sampler and air to hourly data of temperature, wind speed and precipitation (illustrated in the appendix; Figure A.4) reveals a more accurate insight into potential influences on equilibrium conditions. These data sets reflect each monitoring in a high

resolution and illustrate a rather broad scattering of the wind speed. However, no correlation of concentrations on the sampler to the respective wind speeds was observed, once equilibrium is reached. Opposed to that, a significant correlation of characteristic times to ambient temperature with faster equilibration for higher temperatures was determined for each target compound. This is expected due to the temperature-dependent partition coefficients (Lohmann & Lammel, 2004, Lohmann, 2012) and continues for equilibrium conditions during each monitoring, indicating only a slight temporal delay. This can be observed explicitly during May with a mean temperature of 13.6 °C compared to August with 19.4 °C. Phe concentrations on the PE during May exceed concentrations in August by a factor of two, whereas fitted atmospheric concentrations are in the same range.

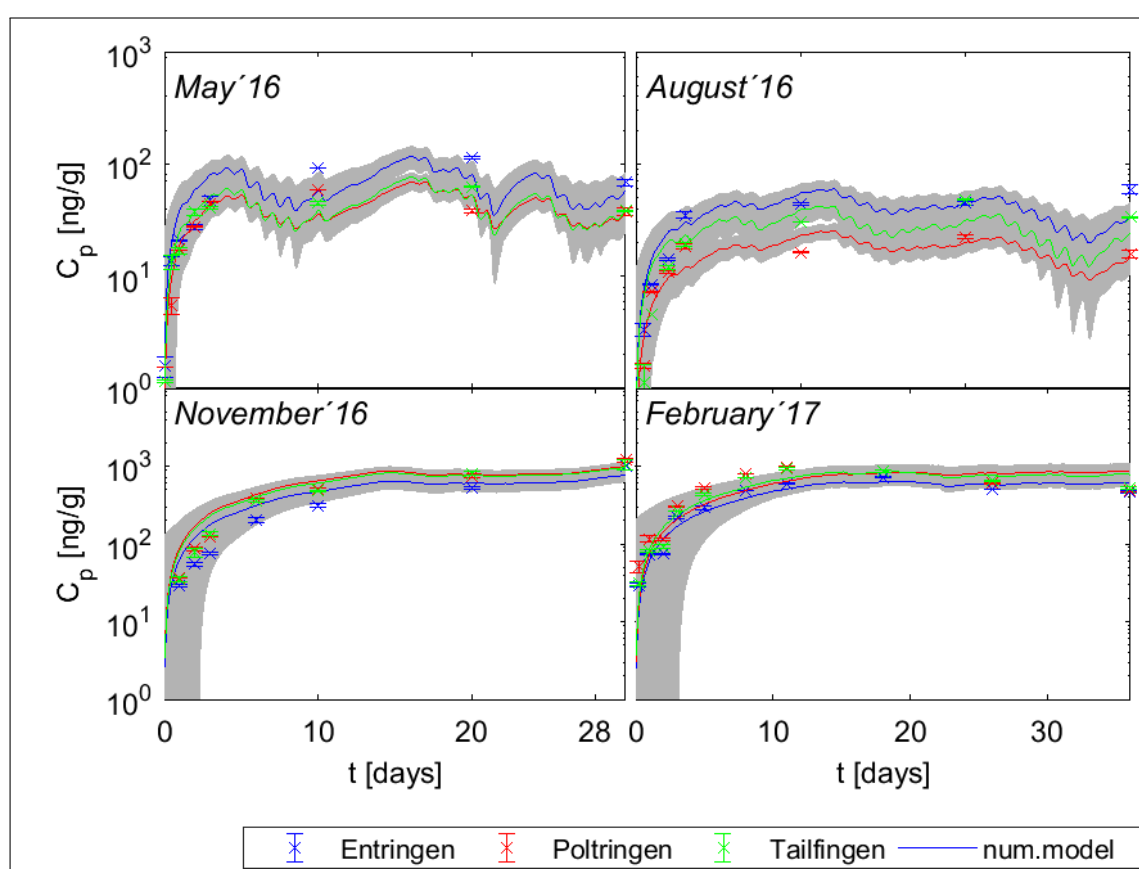


Figure 5.3: Measured and numerically fitted uptake curves of Phe for each of the seasonal monitorings, considering the three locations individually. The grey area indicates the standard deviation of the numerical model.

The observed delay reflects the reaction time of Phe to changes of environmental conditions. Therefore, the main environmental influence on this passive air sampling method varies with the equilibrium state and uptake mode of the sampler. Hence, wind speed may be defined as the main influence for the uptake kinetics and temperature for equilibrium



conditions. Additionally, considerable variation during rain events can be observed in parallel to changes of Phe concentrations on the passive sampler, again after reaching equilibrium. This is explicitly evident at the end of November 2016 with increasing concentrations on the passive sampler determined in parallel to a decrease of precipitation. Towards the end of February 2017 a decline of concentrations of Phe on the sampler simultaneous to increasing precipitation was observed. Therefore, precipitation might lead to a wash-out effect of PAHs in the atmosphere, generating a temporal decrease of atmospheric concentrations. This effect has been reported by Yan *et al.* (2012), Škrdlíková *et al.* (2011), Wang *et al.* (2015), Li *et al.* (2016) and Offenbergl and Baker (2002) amongst others.

**Table 5.5: Average environmental parameters (Temp in °C, wind speed in m/s) during the different monitorings, air-side boundary layers [mm] determined from PRC-loss, concentration ranges of Phe on the sampler [ng/g] and in the atmosphere [ng/m<sup>3</sup>], numbers in brackets are average values covering the time period used for calibrating  $\delta_g$ .**

Monitoring	Temp	Wind speed	Location	$\delta_g$	Phe $C_p$	Phe $C_g$
May '16	13.6	2.7	Entringen	0.3	68 – 114	1.9 ± 0.3
	(10.5)	(3.1)	Poltringen	0.4	38 – 59	1.3 ± 0.2
			Tailfingen	0.3	38 – 45	1.3 ± 0.08
August '16	19.4	2.1	Entringen	1.1	44 – 60	2.4 ± 0.3
	(19.2)	(2.1)	Poltringen	1.3	16 – 22	1.1 ± 0.1
			Tailfingen	0.8	30 – 48	1.6 ± 0.2
November '16	4.5	2.2	Entringen	0.9	310 – 1014	8.3 ± 0.9
	(5.4)	(1.6)	Poltringen	0.8	500 – 1194	10.4 ± 0.8
			Tailfingen	0.8	480 – 1056	10.2 ± 0.6
February '17	4.8	2.7	Entringen	0.8	468 – 720	7.6 ± 0.5
	(4.2)	(1.3)	Poltringen	1.0	492 – 978	10.8 ± 1.4
			Tailfingen	0.7	529 – 925	9.6 ± 0.8

### 5.2.3 Variability of PAH concentrations in the atmosphere and on PE considering smaller scales

A general assumption underlying each method to calculate  $C_g$  includes stable atmospheric concentrations of the target compounds throughout the entire monitoring. This introduces an additional uncertainty into the calculated uptake curves and the fitted atmospheric concentrations or induces a loss of information in terms of resolution. Two time

spans were defined in the numerical model to address this problem. Thus, atmospheric concentrations were fitted for two intervals. The first interval (a) covers the uptake onto the sampler considering day 1 to 10 and the second interval (b) accounts for day 10 to 30. This was done exemplarily for Entringen during the monitoring in May 2016. The correspondingly calculated uptake curves of target compounds onto the passive samplers are therefore based on two explicit values for  $C_g$ . Figure 5.4 shows measured uptake curves of Fl<sub>n</sub>, Phe, Fth and Pyr in combination with the numerical model implementing the two individual  $C_g$ s with respect to the predefined time spans. No significant difference can be identified for the variable  $C_g$  compared to the uptake curves based on a constant  $C_g$  (shown in Figure 5.1). Yet, differences can be observed for the standard deviation of the numerical model at the beginning of the monitoring regarding Fth and Pyr. Calculated uptake curves for those two compounds do not fit the measured uptake very well for constant  $C_g$ . Particularly, in the beginning of the monitoring lower concentrations were calculated than measured. Implementing a second  $C_g$  as an additional variable to describe the first time interval of the uptake naturally improves the calculated standard deviation for this time span. On the other end, the standard deviation slightly increases within the second interval, independent of the compound. This is due to the lower resolution of measured concentrations during the second half of the monitoring period.

Fitted atmospheric concentrations of each target compound for the two distinctive time-spans are depicted in Figure 5.5 for each season. During May and August 2016 as well as February 2017 almost identical values for  $C_g$  are obtained for each target compound in both time spans. Thus, the assumption of generally stable conditions and constant background concentrations over the course of several weeks is confirmed. Stable concentrations within the atmosphere are most likely generated by well-mixed air masses. Opposed to that, the sampling campaign in November 2016 demonstrates considerably higher  $C_g$ s during the second time interval. This is most pronounced for Phe with an increase of 5.2 ng/m<sup>3</sup> to 10.7 ng/m<sup>3</sup>. The determined concentrations during the second interval in November 2016 are in good agreement with the concentrations measured during February 2017 (around 9 ng/m<sup>3</sup>). Therefore, the detected increase of PAHs within the atmosphere during November 2016 most likely reflects the beginning of the heating period leading to increasing emission rates. Furthermore, a decreasing height of the atmospheric boundary layer, in parallel to a decrease of ambient temperature (Figure A.4) might induce a concentrating effect on pollutants in a low layer of air (Albuquerque *et al.*, 2016, Bao *et al.*, 2016). Other local emission sources are not likely since the characteristic distribution pattern remains stable.

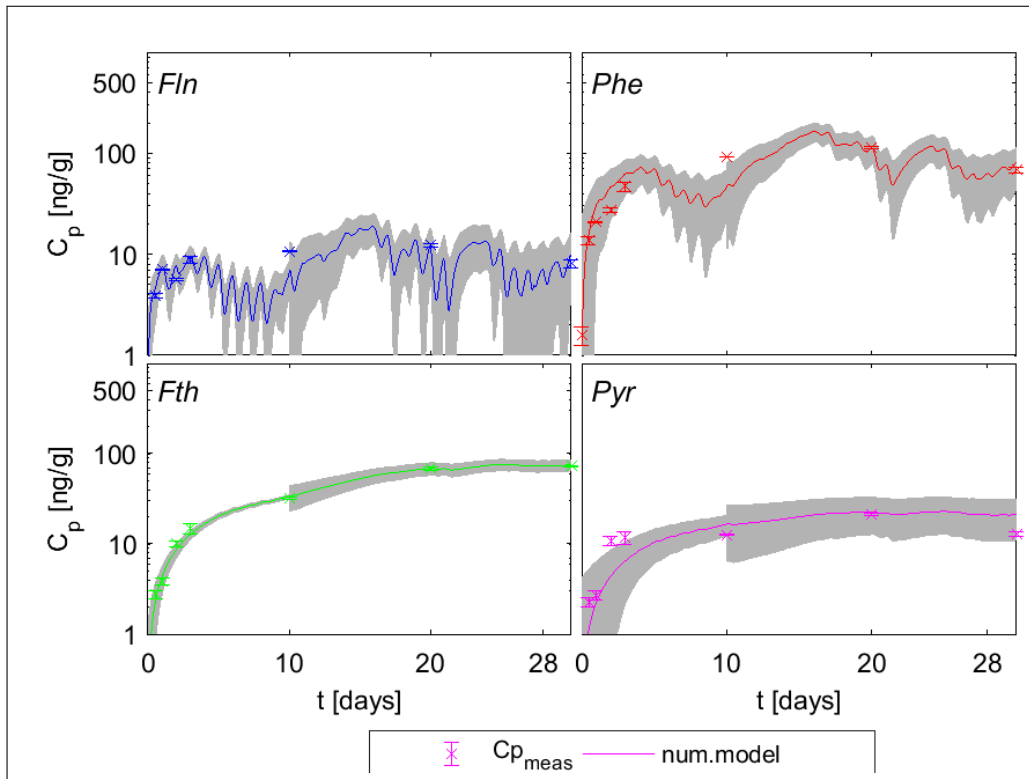


Figure 5.4: Uptake of representative PAHs onto the PE sheets during May 2016 in Entringen; measured data: symbols; numerical model with variable  $C_g$  in two time-intervals (0-10 and 10-30 days). The grey area illustrates the standard deviation of the numerical model.

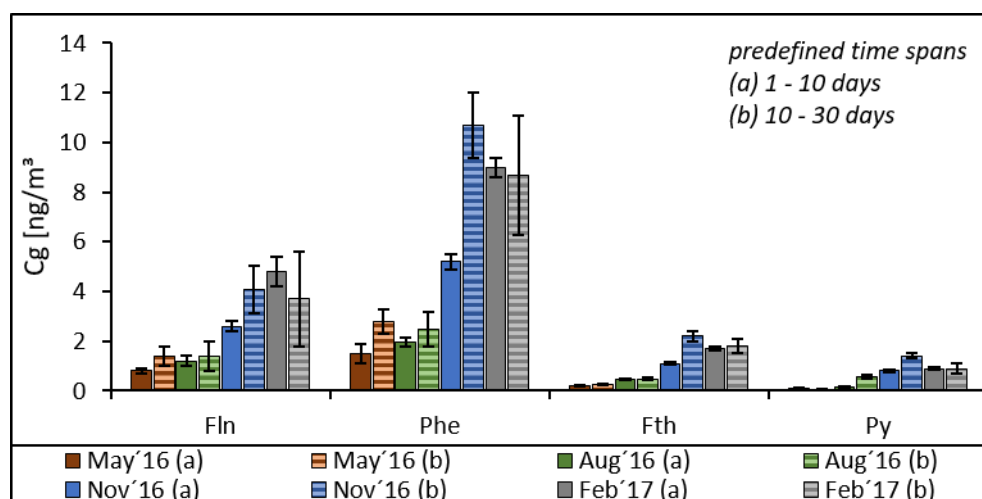


Figure 5.5: Atmospheric concentrations of the representative target compounds in Entringen, fitted with the numerical model during two predefined time spans (filled: 0-10 days, lined: 10-30 days). Errorbars indicate standard deviation calculated with the numerical model, as aforementioned standard deviation increases for the second time span due to fewer data.

#### 5.2.4 Diurnal fluctuation of Phe on the passive air sampler

Calculated characteristic times demonstrate the potential of determining high-resolution concentrations of Phe on PE at high temperatures. Accordingly, an additional sampling campaign was performed during June and July 2016. As described above, warmer temperatures result in faster exchange kinetics, inducing the potential to reflect short-term fluctuations of Phe on the sampler. This may not be surveyed for colder temperatures. Therefore, low and moderately volatile PAHs were equilibrated on the passive sampler in advance of a sampling resolution of 6 hours, covering 24 hours in total as shown in Figure 5.6. With characteristic times of 3-5 days for Phe to reach equilibrium between PE and air, such a high resolution cannot provide equilibrium concentrations for the individual sampling times. Yet, measured concentrations of Phe on the sampler varied between 64 ng/g during the night and 80 ng/g corresponding with lowest temperature in the morning. The numerical model confirms this diurnal variation just by accounting for the measured temperatures, while referring to a constant  $C_g$  of 6 ng/m<sup>3</sup>. Lowest Phe concentrations on the sampler occur in the evening, demonstrating a clear amplitude with a shift of 12 hours regarding minimum and maximum concentrations on the sampler. Therefore, fluctuations on the passive sampler are mostly due to temperature with highest values of 31 °C at 6 PM and lowest values of 18 °C in the morning, around 4

AM. This is in good agreement with Wania *et al.* (1998), who report the distribution of semi-volatile compounds between surfaces and gas phase as mainly temperature dependent. However, the measured and the calculated fluctuation on the sampler illustrate a slight delay with respect to changes in temperature. This temporal delay was already observed for the seasonal monitorings and reveals the time required by Phe on the passive sampler to react on changes of environmental conditions. This observation is in fact in good agreement to the day vs. night sampling campaign described earlier (also discussed in “*development of accurate passive sampling methods*”). During that test, higher concentrations of LMW PAHs were determined after sampling at lower temperatures during the night in comparison to sampling during the day. Both sampling campaigns support the hypothesis of temperature-dependent partitioning as the main factor for short-term fluctuations of PAHs on PE passive air samplers. These results align with the findings of Liu *et al.* (2013), who determined diurnal variation of PAHs in the gaseous phase as well as bound to particles; lower concentrations in the gas phase were observed in parallel to higher concentrations on the particles at night and vice versa during the day. This diurnal cycling was explained by correlating temperature variation ( $>10\text{ }^{\circ}\text{C}$ ) and according gas-particle partitioning. The same effect has been observed by Wu *et al.* (2010) for particle-bound PAHs at a traffic site in China. Here, additionally thermal inversion during colder months is discussed as concurrent pressure for partitioning processes. Furthermore, a comparative study on short-term variations for urban versus coastal sites has been conducted by Dachs *et al.* (2002). The authors relate diurnal variation at the urban site directly to changes of the emission rates. Yet, with increasing distance from the emission sources, temperature and wind direction were identified as drivers for such fluctuations.

### 5.2.5 Seasonal variations of $C_g$ and the use of representative compounds

The atmospheric concentrations of all target compounds at each study site and for each monitoring phase are fitted individually and illustrated in Table A 1. Equivalent to the concentrations on the PE (Figure 5.2), a consistent pattern of the monitored PAHs in the atmosphere was detected independent of season and sampling site, shown in Figure 5.7. This pattern is dominated by Phe as well, but otherwise depicts minor deviations. Thus, Fl<sub>n</sub> provides the second highest and Pyr the lowest concentrations in the atmosphere, which is in perfect agreement with their respective partition coefficients. Hence, besides the explicit spatial continuity for the determined distribution pattern of the respective compounds, also a temporal consistency can be observed for PAHs in the atmosphere. Since distribution patterns of PAHs directly reflect the influences on sampled air masses, constant patterns indicate stable atmospheric conditions. Stable atmospheric conditions are in turn most likely provided by well-mixed air masses within the atmospheric boundary layer. Numerically fitted concentrations during May and August 2016 are in a range of 0.5 - 1.3 ng/m<sup>3</sup>, 1.1 - 2.4 ng/m<sup>3</sup>, 0.1 - 0.4 ng/m<sup>3</sup> and 0.05 - 0.3 ng/m<sup>3</sup> for Fl<sub>n</sub>, Phe, F<sub>th</sub> and Pyr, respectively (Table A.3). Significantly higher values were determined during

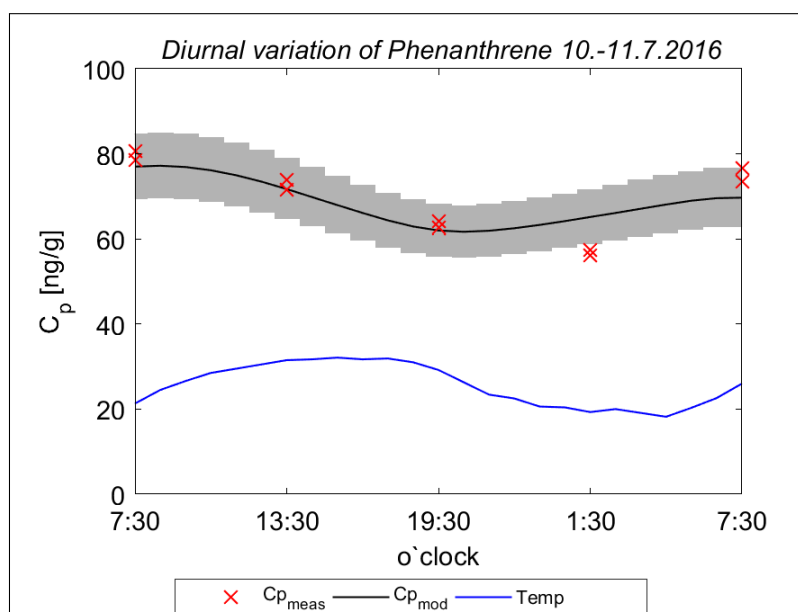


Figure 5.6: Diurnal variation of Phe on PE sheets covering 24 hours on 10.-11.7.16 (unpubl. data, provided by Bettina Rüdiger). Comparison of measured concentrations to a numerical solution based on a constant  $C_g$  of 6 ng/m<sup>3</sup> and varying temperature. The grey area illustrates the standard deviation of the numerical model.

November 2016 and February 2017 with ranges of 3.4 - 4.9 ng/m<sup>3</sup>, 7.6 - 10.8 ng/m<sup>3</sup>, 1.4 - 2.4 ng/m<sup>3</sup> and 0.7 - 1.5 ng/m<sup>3</sup> (Flu, Phe, Fth and Pyr, respectively). Hence, seasonal variations are observed according to the expectation of higher concentrations for colder months. During May and August 2016, a minor variation for the generally consistent atmospheric concentrations can be observed for Entringen with slightly higher values compared to Poltringen and Tailfingen. For example, Phe concentrations in August 2016 vary between  $2.4 \pm 0.3$  ng/m<sup>3</sup> in Entringen and  $1.1 - 1.6 \pm 0.3$  ng/m<sup>3</sup> in Poltringen and Tailfingen, respectively. In contrast, for the colder periods the lowest concentrations were obtained in Entringen with  $7.6 \pm 0.5$  ng/m<sup>3</sup> compared to  $10.8 \pm 1.4$  ng/m<sup>3</sup> and  $9.6 \pm 0.8$  ng/m<sup>3</sup> in Poltringen and Tailfingen, respectively during February 2017. Thus, Poltringen and Tailfingen demonstrate more distinct seasonal variations. This observation may be explained by the closer surrounding of the individual locations. The sampling site in Entringen is in close vicinity to diesel fuelled trains, running regularly (2 x per hour) throughout the whole year. Therefore, a small local emission source may exist in Entringen, slightly increasing the background concentrations compared to Poltringen and Tailfingen. Study sites in Poltringen and Tailfingen, on the other hand, are in closer vicinity to villages. Hence, higher emission rates during winter (caused by domestic heating) are likely to be more pronounced at those two sides. Besides, during summer no additional emission source was observed here. Consequently, lower background concentrations during summer and higher emission rates during winter generate the stronger seasonal

variations, observed in Poltringen and Tailfingen. Altogether, passive air sampling in the Ammer valley is capable to determine homogeneous background concentrations as well as to examine minor local variations. This finding is well in line with a study published by Peng *et al.* (2016). The authors report PAH concentrations in rural areas as reflecting the diffusive influx after long range transport from urban sites in combination with local point sources.

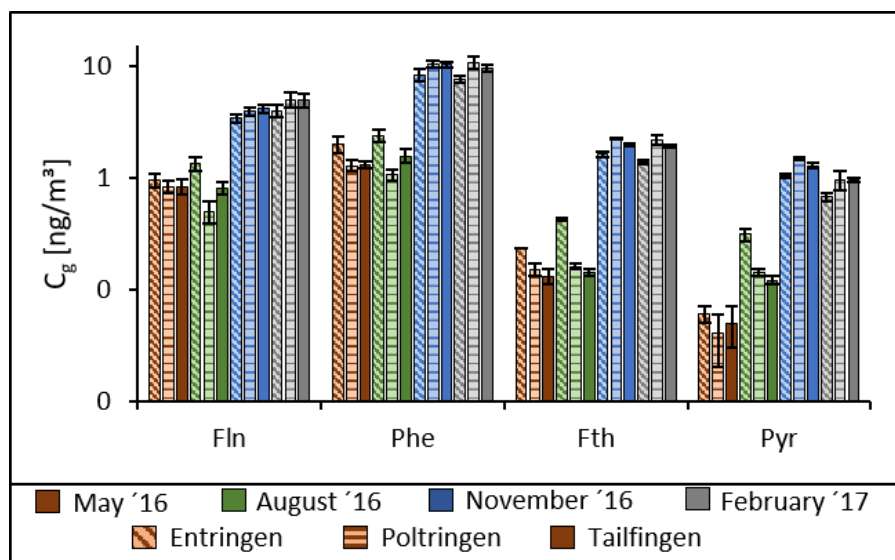


Figure 5.7: Fitted atmospheric concentrations of the four representative PAHs during seasonal monitorings (May, August, November and February) at each study site. Error bars demonstrate the standard deviation measured for triplicate samplers

Stable characteristic distribution patterns allow the calculation of atmospheric concentrations of several compounds based on just a few or one reference compound, e.g. Phe. This holds true in the case of stable concentration ratios (of e.g. Flu/Phe, Fth/Phe and Pyr/Phe) for consistent patterns over the seasons. Such ratios were estimated based on atmospheric concentrations determined during the summer monitoring in 2016. Subsequently, these ratios were used in combination with atmospheric concentrations of Phe during the other monitorings to calculate concentrations for each of the representative compounds. The outcome of this approach is illustrated in Figure 5.8 comparing measured and estimated  $C_g$ s of Flu, Fth and Pyr for all monitoring periods. A reasonable agreement is obtained for the estimated values to measured atmospheric concentrations (fitted with the numerical model). Estimated concentrations of Pyr during May 2016 are distinctively higher than those fitted with the numerical model. For unknown reasons, the numerical model does not provide a good fit for the measured uptake of Pyr during May 2016 (as shown in Figure 5.1). Therefore, those three data points may be defined as outliers. The generally good agreement of estimated and fitted concentrations can be accepted to confirm the reliability of this approach to use one reference compound and

stable ratios to determine the whole range of atmospheric concentrations.

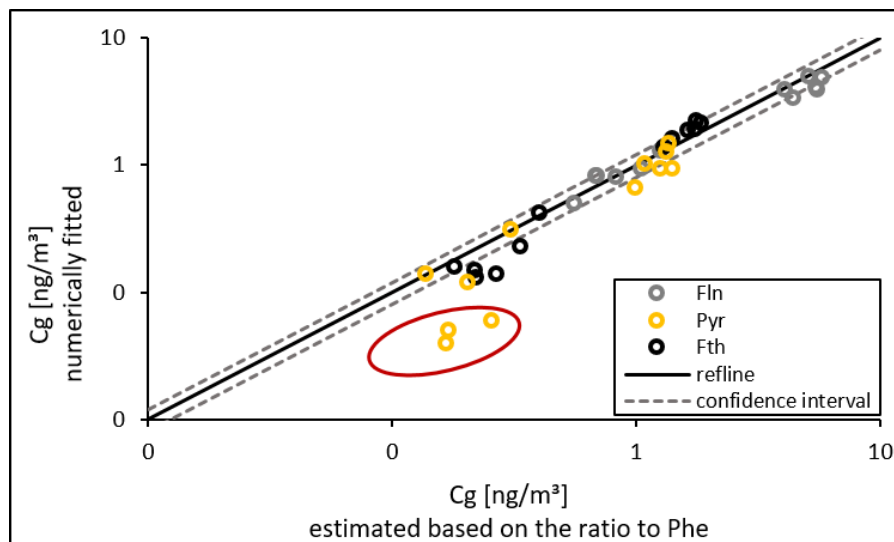


Figure 5.8: Atmospheric concentrations of Fln, Fth and Pyr for all seasons and all locations calculated from Phe and the average distribution patterns during August 2016. The red circle denotes outliers during May 2016.

### 5.3 Conclusions

Atmospheric concentrations of target PAHs are quite stable and reproducible on a regional scale, confirming the assumption of sampling well-mixed air masses within the atmospheric boundary layer. In summary, two periods can be differentiated according to the seasonal sampling performed within this study. During colder seasons higher atmospheric concentrations of PAHs occur compared to lower concentrations during warmer seasons. The numerical model accounts for short-term fluctuations of fast equilibrating PAHs on the PE, which reflect rapid changes of atmospheric influences. Diurnal variations of low molecular weight PAHs on the PE mainly depend on temperature (temperature-dependent partitioning). Both the analytical and the numerical solution for atmospheric concentrations provide rather constant atmospheric concentrations within a season. Furthermore, the characteristic distribution patterns observed remain identical throughout the seasons, supporting the hypothesis of similar sources for PAHs in this area. Those stable distribution patterns allow to confirm the use of one reference target compound to predict the atmospheric concentrations of other PAHs. Phe was suggested here as the most reliable compound, providing an average value over a few days (time integrated passive sampling). Consequently, atmospheric concentrations for the whole range of monitored PAHs can be calculated based on the measurement of Phe only.



---

## 6 Concentration gradients of PAHs within the atmosphere

The overall objective of this study is the determination of the current flux direction of PAHs across the soil-atmosphere interface. Gaseous fluxes are primarily driven by diffusion and depend on concentration gradients across both compartments. Regarding air masses in general, two distinctive layers may be differentiated within the atmosphere. The upper part or atmospheric boundary layer (ABL) is essentially influenced by temperature driven eddy diffusion generating a thick homogeneous layer of up to several hundreds of meters depending on daytime and season (Farrar *et al.*, 2005, Bao *et al.*, 2016). In contrast, right above ground a thin layer (< 0.1 m) with laminar flow develops (low-energy regime), potentially preventing a thorough mixing of air masses at the soil surface with the homogeneous ABL. Thus, the air right above the soil surface may strongly be influenced by the underlying soil, whereas air masses in upper heights are potentially transported over long range distances. Accordingly, clear concentration gradients of contaminants in the atmosphere may evolve, as observed e.g. by Wang *et al.* (2017) and Kurt-Karakus *et al.* (2006). Sampling semi-volatile pollutants in air close to the soil surface may reflect to some extent concentrations within the soil (Zhang *et al.*, 2011, Donald & Anderson, 2017). Several studies report the use of flux chambers and fugacity samplers, aiming to reflect air in equilibrium with the soil (Cabrerizo *et al.*, 2009, Meijer *et al.*, 2003, Wang *et al.*, 1997, Biache *et al.*, 2014). Consequently, the flux direction of target compounds across the soil-atmosphere interface may be obtained by sampling air in various heights with adequate proximity to the ground.

Based on the observations made during the first year of atmospheric sampling, the following hypotheses are formulated:

1. Stable distribution patterns of atmospheric PAHs determined during the first year of monitoring apply also for the subsequent sampling campaigns.
2. Variations within these distribution patterns for the individual heights may reflect the different influences on air masses depending on the proximity to the ground.
3. Atmospheric sampling in two heights may be used as a first indication on the flux direction of PAHs at the soil-atmosphere interface.
4. For higher emission rates during the heating period (winter), the concentration gradient from the atmosphere to the soil is steeper.

## 6.1 Sampling and data evaluation

Atmospheric monitoring campaigns were conducted seasonally during May, August and November 2017 and February 2018, equivalent to the first year of passive sampling in the atmosphere. To this end, PE sheets were deployed in 1.2 m height under an aluminum cover but sampled in a slightly higher resolution with measurements after 12, 24, 48 and 72 hours as well as after 5, 10, 15, 25 and 30 days. For the second year of sampling an additional sampling height was implemented at 0.1 m above ground to check on potential concentration gradients in the atmosphere. Passive samplers at this height were also deployed within an aluminum box, which was exclusively opened at the bottom and hovered only 2-3 cm above the soil surface. Sampling, extraction, and measurements of the target compounds were performed as described earlier. Again, the numerical model was applied to fit first  $\delta_g$  and then  $C_g$  (based on temperature-adapted  $K_{pg}$  before predicting the uptake of PAHs onto the PE samplers.

## 6.2 Results and discussion

### 6.2.1 Uptake kinetics at the two sampling heights

Measured and modelled uptake curves for the four representative PAHs are shown exemplarily for May 2017 for samplers at 0.1 m and 1.2 m height in Figure 6.1. The observed trends are equivalent to previously determined uptake onto passive samplers, illustrating a good agreement of the numerical model with the measurements in general. Fln equilibrates within 48 hours and Phe reaches equilibrium after ten days independent of the sampling height. Explicit differences can be observed for Fth and Pyr with respect to the upper sampling height despite similar partition coefficients. In this set up both compounds seem to equilibrate with the sampler after ten to fifteen days. Subsequently, Fth shows stable and Pyr even decreasing concentrations until the end of the monitoring. At 0.1 m height, modelled curves of these compounds indicate ongoing uptake throughout the whole monitoring and approximate equilibrium towards the end of the sampling campaign. The two sampling heights thus show different uptake kinetics. Additionally, the modelled diurnal fluctuation of Fln and Phe on the passive samplers at 1.2 m height seems negligible right above ground. Therefore, exchange kinetics between sampler and air are considerably slower for sampling at 0.1 m providing an integration over longer periods compared to 1.2 m. This is also reflected in the correspondingly calibrated air side boundary layers, as listed in Table 6.1.

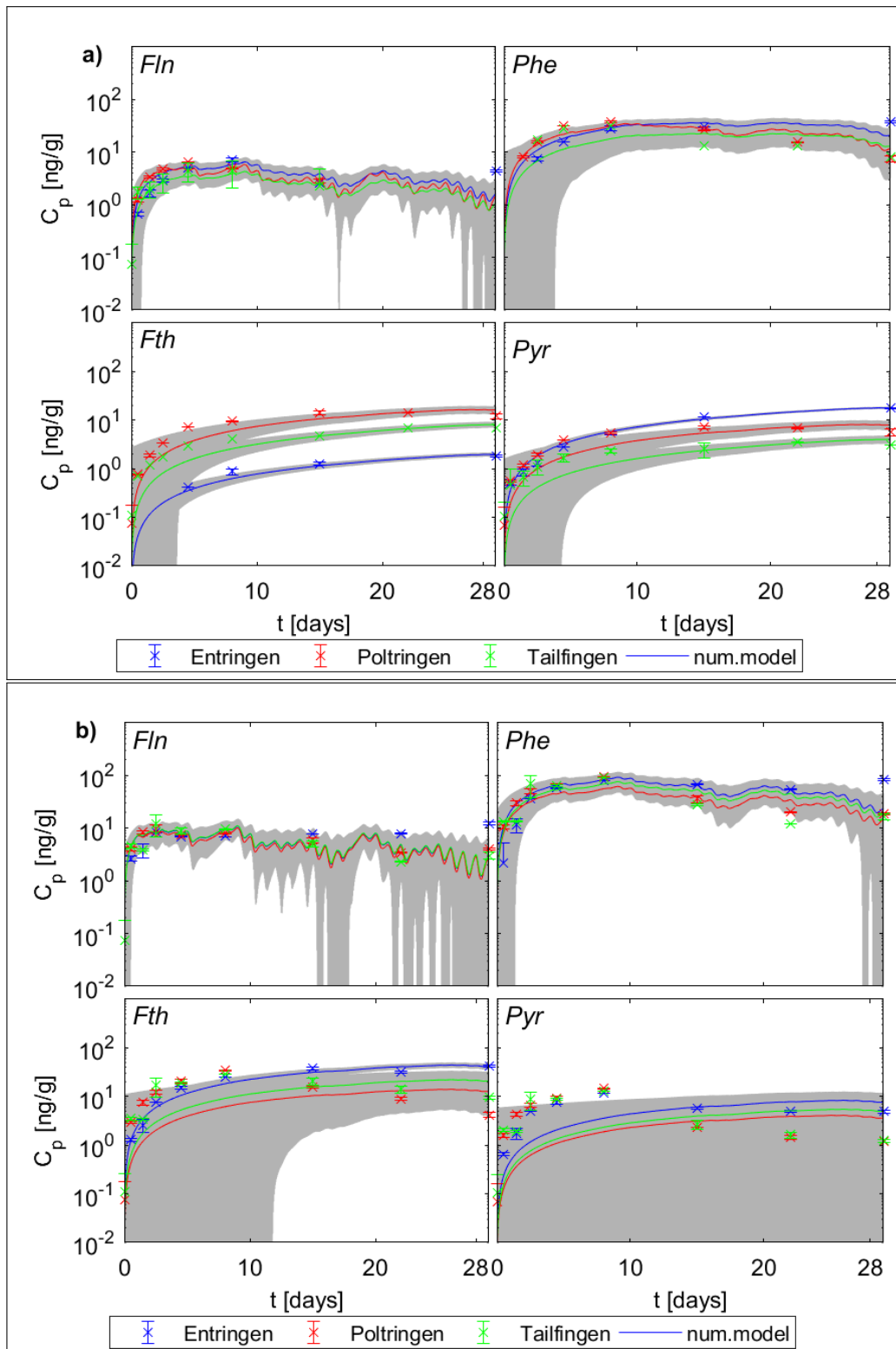


Figure 6.1: Measured and modelled uptake curves of Fln, Phe, Fth and Pyr onto the passive sampler at a) 0.1 m and b) 1.2 m height during May 2017, considering the three locations individually. The grey area illustrates the standard deviation of the numerical model. Calibrated boundary layers for the regular sampling height of 1.2 m in May 2017 are

quite comparable to the values determined during the first year of sampling and vary between 0.5 and 1.3 mm, depending on season and study site. In contrast, boundary layers right above ground result in values in the range of 1.7 to 5.1 mm, with one exception during February in Tailfingen, where a  $\delta_g$  of 0.8 mm was determined. Wind speed is the main influencing factor on uptake kinetics generating thinner layers at higher wind velocities. Therefore, higher values for  $\delta_g$  regarding the lower sampling height are caused by the low wind velocities. This in turn explains the thin boundary layer in Tailfingen for February, where the box was slightly tilted to one side during the first few days, which allowed a complete circulation of air around the samplers. Besides, the soil acts as a buffer for diurnal and temperature-driven fluctuations of semi-volatile compounds in the air: lower concentrations during the day are counterbalanced by a release from soil and vice versa during the night.

**Table 6.1: Atmospheric boundary layers during the second year of sampling, calibrated for both sampling heights at each of the study sites individually (except for May 2017: PRC-loss for MAY 2017 was derived from measurements in August 2017).**

Monitoring Location\sampling height	May and August 2017		November 2017		February 2018	
	$\delta_g$ [mm]		$\delta_g$ [mm]		$\delta_g$ [mm]	
	0.1 m	1.2 m	0.1 m	1.2 m	0.1 m	1.2 m
Entringen	2.0	0.6	3.9	1.3	1.7	0.5
Poltringen	1.9	0.5	5.1	1.1	2.8	1.0
Tailfingen	2.0	0.6	2.6	1.2	0.8	1.0

### 6.2.2 Temporal variations of atmospheric PAH concentrations

In order to investigate spatial and seasonal variations of atmospheric PAHs in more detail, the numerical approach was combined with the observed Phe uptake for each monitoring. Results for 0.1 m and for 1.2 m height are shown in Figure 6.2. Measured and calculated uptake curves are illustrated for each of the study sites individually. In general, the uptake curves during the second year are well comparable to the respective seasons within the first year. Yet, modelled diurnal variations are significantly attenuated for the samplers right above ground. Differences with respect to the sampling sites are a little more pronounced during the second year of monitoring. This is particularly evident in Entringen during August with considerably higher concentrations on the PE sheets at both heights compared to Poltringen and Tailfingen. Additionally, during November and February higher concentrations can be observed for the sampler at 0.1 m above ground in Tailfingen. Higher concentrations in Entringen during the summer monitoring can be

explained by construction works involving diesel engines on the sampling site, generating a temporal local point source for PAHs. Similar construction work has also been conducted during November at the study site in Tailfingen. As discussed before, concentrations of target compounds on the passive sampler after equilibration depend to a major extent on the ambient temperature. The observed decline of target compounds on the PE at 1.2 m height during May 2017 illustrates a strong correlation to an increase of the ambient temperature by a factor of 2 (Figure A.4). Another aspect of the data evaluation concerns the temporal variability of PAHs in the atmosphere and therefore the sensitivity of the chosen method. Based on the good agreement of the measured data to the numerical model, a reliable average concentration throughout the seasonal monitoring campaigns was obtained during this second year.

Figure 6.3 shows fitted atmospheric concentrations, comparing the seasonal monitorings for both years and each location. A stable characteristic pattern was observed for all sampling campaigns during both years, independent of location or sampling height. Yet, atmospheric concentrations during the first year of sampling exceed the concentrations during each monitoring of the second year slightly but not significantly (+ 5%). Since spatial variation was observed to be negligible during the first year of monitoring, the different locations are accepted to reflect the same atmospheric influence. The second year of monitoring, however, shows minor site-specific variations probably due to small, local influences. Furthermore, atmospheric concentrations obtained at 0.1 m height illustrate slightly higher site-specific variability compared to concentrations determined for 1.2 m height. In particular, the samplers right above ground indicate slightly lower concentrations (compared to 1.2 m height) in Tailfingen during May. The same pattern was observed in Poltringen during August and November. Such variations for the samplers right above ground may be caused by the set-up. Since the cover was intended to hover right above ground, small variations of the soil surface elevations and surrounding vegetation (as to be expected on agricultural used land) affects the air flow into the shielding and around the samplers. Thus, the conditions for the uptake of target compounds from air may vary between the individual sampling sites at the lower height. Still, Phe is the dominating compound, followed by Fl<sub>n</sub> and considerably lower concentrations of F<sub>th</sub> and Pyr, regardless of the sampling campaign, height and location. Seasonal variations can also be observed as expected with higher concentrations during colder months. At 1.2 m height almost identical concentrations are observed during May and August as well as for November and February, respectively. Thus, confirming the definition of two distinctive time spans with lower atmospheric concentrations during spring and summer and higher values during autumn and winter (as heating period).

## 6 Concentration gradients of PAHs within the atmosphere

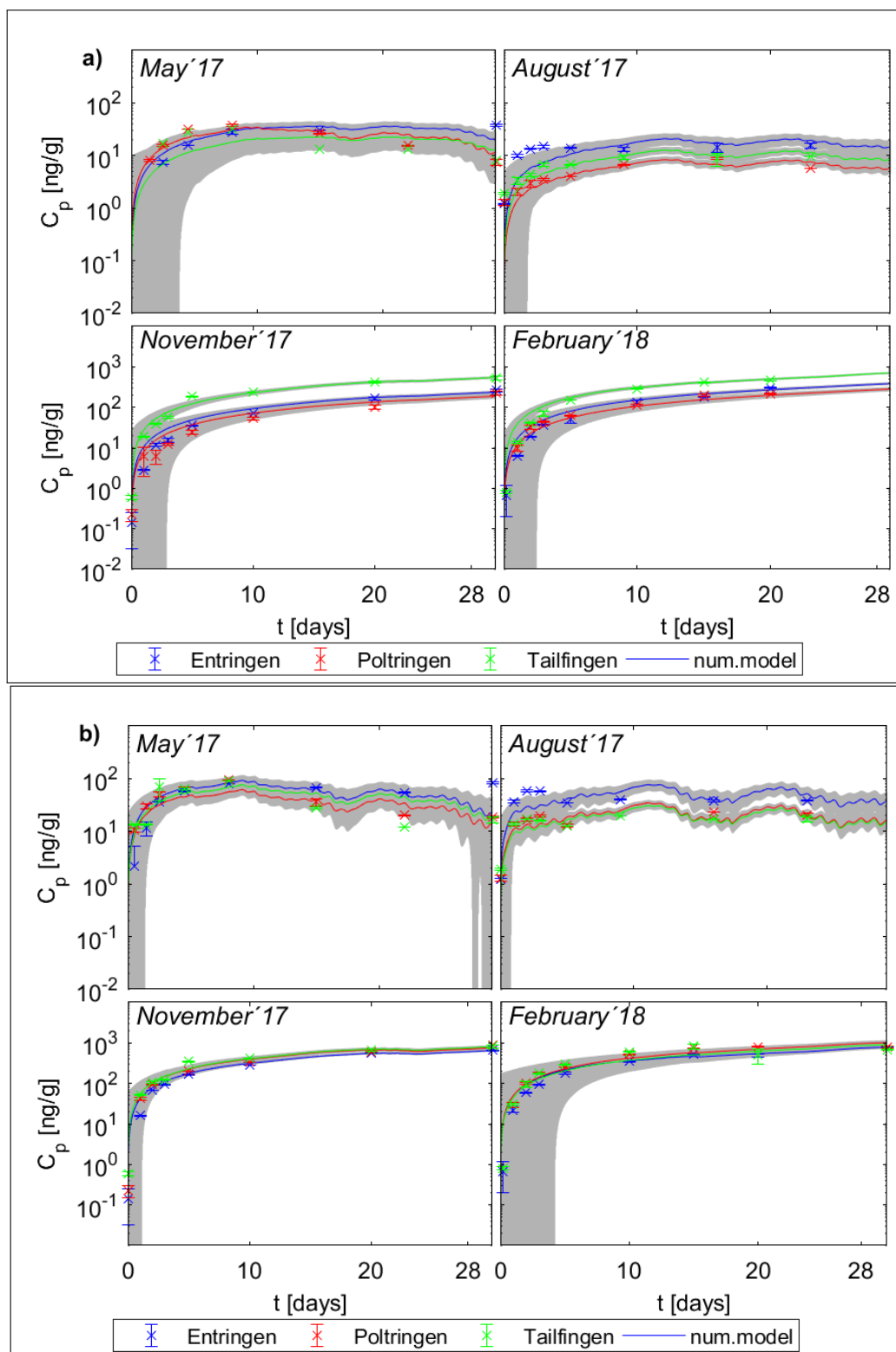


Figure 6.2: Measured and modelled uptake curves of Phe onto the passive sampler at a) 0.1 m and b) 1.2 m height for each of the seasonal monitorings during the second year of sampling, considering the three locations individually. The grey area illustrates the standard deviation of the modelled uptake.

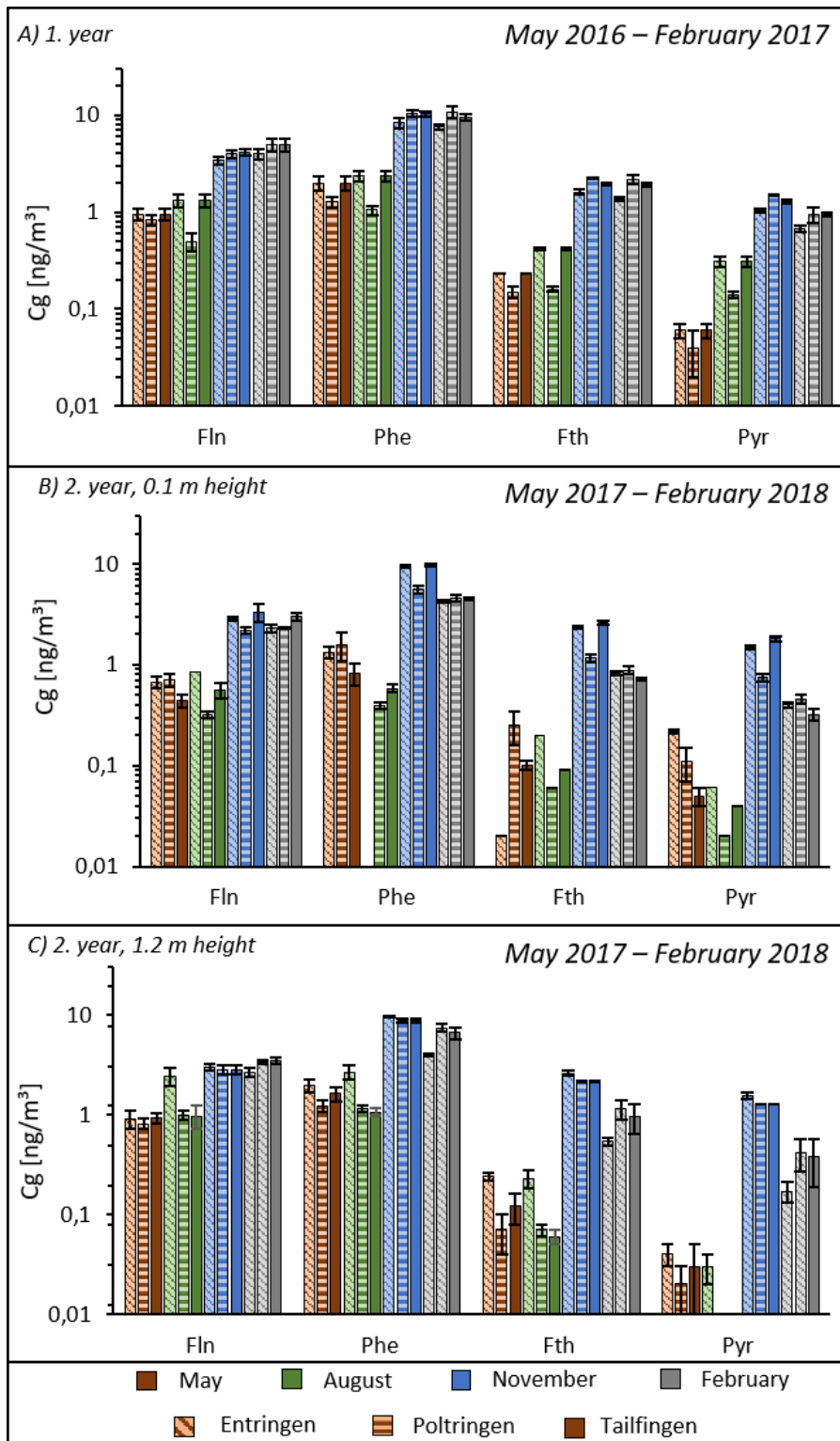


Figure 6.3: Atmospheric concentrations of the four representative PAHs fitted to measured uptake and therefore averaging over each seasonal monitoring, respectively. Error bars indicate standard deviation of triplicate samples.

Numerous studies discuss the influence of plants as a considerable factor on temporal variations of semi-volatile organic contaminants (SVOCs) in the atmosphere (e.g. PAHs, Polychlorinated Biphenyls (PCBs), Polybrominated Diphenyl Ethers (PBDEs)). Thomas *et al.* (1998) as well as Gouin *et al.* (2002) relate decreasing atmospheric concentrations of PCBs to vegetation growths, providing a buffering effect for the atmosphere. Furthermore, Barber *et al.* (2004) report in great detail the storage capacity and the scavenging effect of plants on POPs and Bao *et al.* (2016) report short-term variations of SVOCs in the atmosphere as a result of plants as a fast-reacting storage compartment (fast reacting surface absorption). Thus, site-specific variations may be compared by taking the respective canopy, and particularly canopy densities, into account. In Entringen the sampler box is deployed in a meadow with grass around the cover reaching a height of around 1m (during summer) and a canopy density of ca. 50 %. The study site in Poltringen was fallow (during both years) and therefore covered in a low density of clover not higher than 5-10 cm. On the agricultural field in Tailfingen, comparably big plants of sugar-beets were evolving during the growing season developing leaves of up to 30 cm length. However, the small area below and around the individual sampling stations in Poltringen and Tailfingen was attempted to remain cleared of plants. The influence of plants on the sampler and sampler-air exchange might be most pronounced in Entringen potentially leading to an overestimation of sampled air (sampling rates) and thus an underestimation of atmospheric concentrations. Besides, an explicit increase of vegetation was observed in Tailfingen with the upgrowth of beets. According to Thomas *et al.* (1998) and Gouin *et al.* (2002), this should generate simultaneously decreasing concentrations in the atmosphere. Yet, no indication of such a scavenging effect could be identified within this study. Instead, stable atmospheric concentrations were determined during the growing season despite the notable differences of plant coverage at the individual sites. Consequently, seasonal varying concentrations of PAHs in the atmosphere may be mostly explained by changing primary emission rather than plants as a buffering compartment.

### 6.2.3 Evaluation of potential concentration gradients in the atmosphere

The direct comparison of air concentrations at 0.1 m and 1.2 m height may provide a first insight into atmospheric concentration gradients. Figure 6.4 shows atmospheric concentrations of the four representative compounds determined at both heights for each monitoring period and each location (the respective concentrations are listed in Table A.4). A reference line with the ratio 1:1 and a confidence interval of 20 % are included within this comparison as a measure for the conformity of determined concentrations. In general, a good agreement for the different heights may be observed during November 2017 and February 2018, independent of the compound and the sampling location. Thus, no gradient in the atmosphere was determined. In contrast, for May and August 2017 for Fl<sub>n</sub> and Phe higher concentrations were obtained at 1.2 m height, while Pyr showed higher values at 0.1 m height. For the semi-volatile compounds (Fl<sub>n</sub> and Phe) this can



be explained by higher temperatures below the cover right above the soil surface (i.e. a sampling artefact). The temperature within this cover is influenced by solar radiation as well as thermic radiation from the underlying soil. During May and August the temperature within the topsoils reaches maximum values of up to 30-40 °C. Additionally, the temperature of the ambient air reaches a maximum value of 30 °C during both seasons. Moreover, the exchange of air masses below the cover and the ambient atmosphere was restricted to a minimum. Consequently, air temperatures were substantially higher within the lower cover opposed to the sampling height at 1.2 m. Hence, higher temperatures within the lower cover generate lower partition coefficients for the PAHs between polymer and air, compared to the sampling height at 1.2 m. Thus, atmospheric concentrations of Fl<sub>n</sub> and Phe calculated for 0.1 m height most likely underestimate the actual values when identical partition coefficients are applied for both heights.

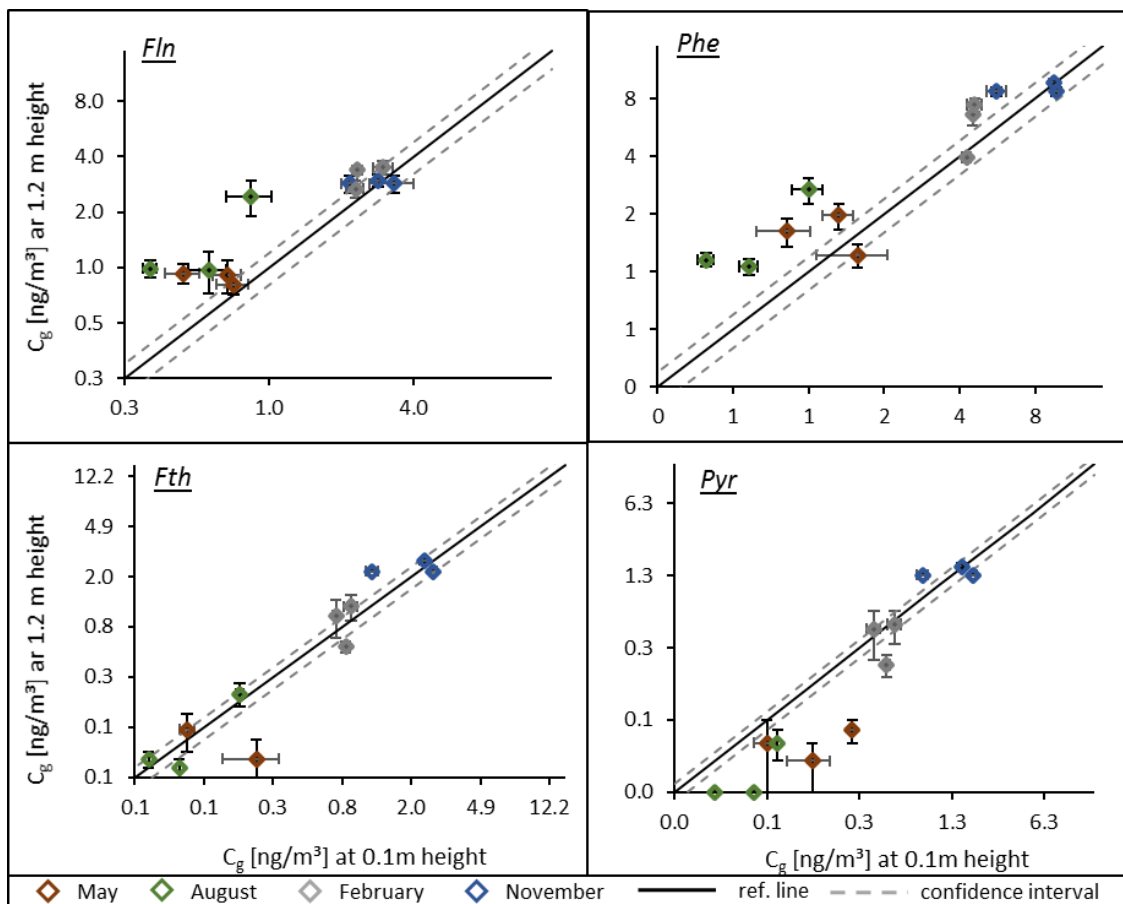


Figure 6.4: Double logarithmic scatter plot comparing concentrations of a) Fl<sub>n</sub>, b) Phe, c) Fth and d) Pyr at 1.2 m height to concentrations right above ground at each station for seasonal sampling campaigns. Error bars indicate the standard deviation of triplicate samplers, the solid line demonstrates a reference line with a ratio of 1:1 and the dashed lines define a confidence interval of 20%.

To address this issue, temperatures for the lower sampling height were increased for ten degrees within the numerical model. Based on measured temperatures for ambient air and topsoil, a raise of ten degrees seemed reasonable. This correction for heating-effects within the shielding of the samplers right above ground provides atmospheric concentrations, which are in the same range or higher as measured at 1.2 m, as shown in Figure 6.5. Hence, a concentration gradient within the atmosphere may be observed, indicating volatilization of Fln and Phe during warm periods. Adjusting the according partition coefficients of Fth and Pyr to higher temperatures showed no significant influence on the atmospheric concentrations, respectively. This may be due to the general offset to equilibrium conditions of both compounds on passive samplers in the atmosphere. Fth shows rather stable concentrations in the atmosphere, independent of the sampling height or the monitoring campaign. Pyr, on the other hand, also indicates volatilization during May and August, which is against the expectation. Fth and Pyr are characterized by almost the same strong partitioning behaviour and illustrate comparably low concentrations in the gas phase. Additionally, the concentration of Fth in soils exceeds concentrations of Pyr. Consequently, equal concentration gradients were expected for those two compounds, indicating net deposition throughout the year. Thus, the observed offset for Pyr remains unclear. Bao *et al.* (2016) suggest even a maximum temperature within the uppermost mm of the soil as high as 50-60 °C. Thus, despite the adjusted partition coefficients for the samplers right above the soil surface, atmospheric PAH concentrations at 0.1 m height may still be underestimated.

Nevertheless, seasonal sampling in the atmosphere at the two heights mostly confirms the hypothesis of varying concentration gradients for semi-volatile compounds (Fln and Phe) by indicating the potential for volatilization during summer. This is in good agreement to a study of Zhang *et al.* (2011), who demonstrate a concentration gradient of PAHs in air as only detectable at smaller scales up to 30 cm height. Above that height, atmospheric PAH concentrations illustrate homogeneous values. Consequently, the influence of soil air gets counterbalanced with distance to the soil surface, generating homogeneous air masses. Therefore, potential revolatilization from soils should not influence the samplers at 1.2 m height. This was observed by Zhang and Tao (2009) as well, who determined clear concentration gradients for Fln and Phe during late summer at three locations close to Beijing. The authors deployed passive samplers in different heights above ground, yet with a distinctively higher spatial resolution (14 samplers between 5 and 500 mm above ground).

Table 6.2 summarizes measured atmospheric PAH concentrations from a selection of studies in Europe, the USA and Asia, therefore covering a broad spatial range. Most studies provide average concentrations accounting for different seasons (or years). Considering Fln, the concentrations determined within the Ammer valley (0.5- 4.9 ng/m<sup>3</sup>) are within the same range as observed in literature. The measured concentrations of Phe span a narrow range of 1.1- 10.8 ng/m<sup>3</sup> ( $\pm$  0.1-1 ng/m<sup>3</sup>) for the different seasons and

with that indicate comparably low values. Phe values in background and rural areas are reported to reach up to 25 and 26 ng/m<sup>3</sup> in the US as well as averaging for 22 European countries, respectively (Liu *et al.*, 2017, Jaward *et al.*, 2004). For suburban and urban regions, Phe concentrations are reported with values of 80 ng/m<sup>3</sup> close to Shanghai, and up to 300 ng/m<sup>3</sup> in an industrialized region in Turkey (Wang *et al.*, 2015, Kaya *et al.*, 2012). Thus, background concentrations were sampled at the chosen study sites. Besides, a good agreement may be observed with concentrations determined in 30-360 m height in Toronto (0.4-11.4 ng/m<sup>3</sup>), reported by Farrar *et al.* (2005). Pyr and Fth indicate a similar relation with notably lower concentrations (0.01- 2.6 ng/m<sup>3</sup>) measured in the presented study compared to literature data on rural locations in the US (2.0- 6.9 ng/m<sup>3</sup>). Mandalakis *et al.* (2002) and Lohmann *et al.* (2011) determined concentrations within the same range (0.04- 1.0 ng/m<sup>3</sup> in Narrangset Bay and Athens) as observed here.

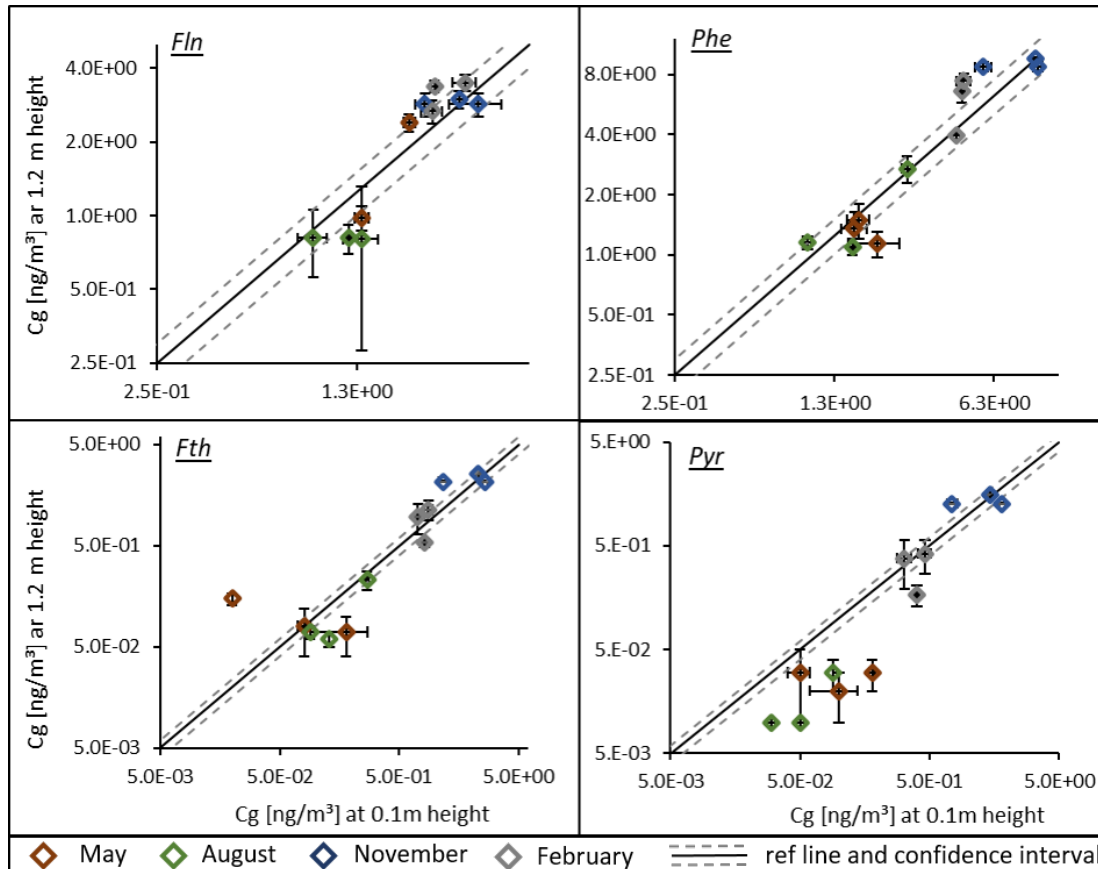


Figure 6.5: Double logarithmic scatter plot comparing concentrations of a) Fln, b) Phe, c) Fth and d) Pyr at 1.2 m height to temperature-corrected concentrations right above ground at each station for seasonal sampling campaigns. Error bars indicate the standard deviation of triplicate samplers, the solid line demonstrates a reference line with a ratio of 1:1 and the dashed lines define a confidence interval of 20%.

## 6 Concentration gradients of PAHs within the atmosphere

**Table 6.2: Comparison of  $C_g$  [ng/m<sup>3</sup>] of Fln, Phe, Fth and Pyr in the atmosphere.**

Author/ study	Fln	Phe	Fth	Pyr	$\Sigma$ PAHs	Study set-up
Albuquerque <i>et al.</i> (2016)	0.05 – 12 3.7	0.02- 23.3 8.0	0.02- 6.04 2.04	0.02- 4.36 1.6	8.0- 89.0 30.5	Av. an. conc. outskirts of Porto, Portugal
Carratalá <i>et al.</i> (2017)	0.25 (±0.5)	0.81 (±1.5)	0.21 (±0.3)	0.07 (±0.1)		Mean annual conc. urban sites, Mar Menor, Spain (2010)
Chen <i>et al.</i> (2011)	8.4 ± 5.8 ( <i>gas+part.</i> )	79.5 ± 37.2 ( <i>gas+part.</i> )	36.8 ± 27.5 ( <i>gas+part.</i> )	23.6 ± 16.2 ( <i>gas+part.</i> )	216 ± 86.5 ( <i>gas+part.</i> )	Suburban of Shanghai, China
	0.23-11.8 (4.03)	1.26-29.7 (12.5)	0.59-14.8 (3.43)	0.48-9-26 (2.14)	5.54-131 (39.4)	July 1997, Baltimore Harbour
Dachs <i>et al.</i> (2002)	0.43-8.21 (2.09)	1.3-12.2 (3.61)	0.24-1.03 (0.58)	0.14-1.21 (0.42)	4.26-73.2 (17.98)	Feb. Chesapeake Bay, 1997
	0.05-10.4 2.65)	1.5-18.5 (5.57)	0.23-1.71 (0.85)	0.12-1.78 (0.55)	4.13-105 (20.2)	July
Farrar <i>et al.</i> (2005)	1.3 – 10.1 3.3	0.4 - 11.4 2.7	0.01 - 5 1.5	0.01 - 2.2 0.66	~ 20	Av. conc. 3 weeks, Toronto, Canada
	14.79	23.03	11.19	35.68		February mean. Conc. urban+ rural locations Birmingham, UK
Harrison <i>et al.</i> (1996)	6.79	3.59	1.76	2.78		August
Jaward <i>et al.</i> (2004)	0.1 - 7.3	0.23 - 26	0.01 - 13.2	0.12 - 7.2	0.5 - 61.2 (12 PAHs)	Av. Conc. 6 weeks, 22 European countries
Kaya <i>et al.</i> (2012)	0.07 - 44.3 (6.9)	0.1 - 302 (38.7)	0.09 - 144 (17.4)	0.01 - 210 (13.3)	1.62 - 838 (89.1)	Av. conc., Turkey Industrial region
Liu <i>et al.</i> (2017)	6.5 (±14.8)	12.9 (±25)	3.3 (±6.9)	2.0 (±4.2)	38.1 - 72.1 (15 PAHs)	28-31 rural sites, US, av. Long-term conc.
Liu <i>et al.</i> (2013)	10 - 23 (17)	52 - 180 (110)	2.1 - 20 (9.0)	1.1 - 7.7 (4.0)	79 - 230 (150)	Av. conc. 1 week suburban area, Lhasa City, Tibet
Lohmann <i>et al.</i> (2011)	0.2 - 2.2	0.6 - 5.6	0.17 - 1.0	0.04 - 0.5		Narragansett Bay, USA
Mandalakis <i>et al.</i> (2002)	0.14	1.03	0.58	0.4	3.5	background conc. 1 week, Athens, Greece
Nguyen <i>et al.</i> (2018)	0-3.09	0.47-5.96	0.11-1.48	0.08-1.48	1.04-10.9	Mean values (1 year), South Korea
Prevedouros <i>et al.</i> (2004)	3 - 9 4 - 20	20 - 22 20 - 50	4 - 6 5 - 10	2.5 - 5 3.5 - 8		London Manchester
Comparative study, 1991-2000	0.5 - 2 - -	70 - 160 0.8 - 3 0.2 - 0.7	5 - 10 0.3- 1.7 0.1- 0.3	5 - 10 0.1- 1 0.05- 0.2		Hazelrigg Rörvik Pallas
Wang <i>et al.</i> (2015)	220 - 1100	310 - 1200	150 - 480	180 - 520		Large power plants, China

### 6.3 Conclusion

Seasonal atmospheric monitorings during two subsequent years illustrate the observed PAHs to be distributed homogeneously within the studied area. Concentrations, distribution patterns and temporal trends have been shown to be consistent for the different locations. Consequently, the three study sites apparently reflect the same mix of PAHs. Besides, both years of monitoring can be divided into two periods, according to a correlation of higher atmospheric concentrations for lower air temperatures. Slight variations within the distribution patterns occur simultaneously to changes in concentrations. Additionally, sampling the atmosphere in two heights indicates seasonally varying concentration profiles for the semi-volatile compounds (after temperature-correction). Hence, during spring and summer higher concentrations right above the ground compared to sampling at 1.2 m height indicate revolatilization of Fl<sub>n</sub> and Phe from the soil. For the cold seasons, however, stable concentrations were observed, independent of the sampling height.

## 7 Characteristic ratios and source appointment

### 7.1 Background and objectives

A variety of diagnostic ratios of certain PAHs is published in literature to differentiate between characteristic emission sources, as described in detail by Tobiszewski and Namieśnik (2012), amongst others. A more elaborate approach for source identification refers to principal component analysis or the definition of emission factors. These attempts account for a wide range of compounds simultaneously, assigning characteristic patterns to distinctive PAH groups for individual emission sources (Singh *et al.*, 2008, Jang *et al.*, 2013, Khalili *et al.*, 1995, Larsen & Baker, 2003, Lee *et al.*, 2005b, Zou *et al.*, 2015). Particularly, for urban air, which is influenced by a broad range of sources, this attempt was found to be more reliable than the use of simple ratios. In general, it should be noted that the application of such relations is most appropriate to differentiate between specifically known emission sources instead of conducting a new source-inventory. The chosen locations within this study are all in rural areas and significant influence of industry was excluded. As expected, wood and coal combustion have been determined as main emission sources within this area (*Characterization of study sites - land use and soil properties*). Only in Poltringen the soil indicates a considerable influence of traffic emission. Consequently, diagnostic ratios were calculated within this study for three clear purposes: (i) to identify potential differences of the sampled catchment areas regarding passive sampling in the atmosphere, (ii) to determine seasonal variations of respective influences in the atmosphere and (iii) to differentiate between domestic heating and traffic as major emission sources.

### 7.2 Data evaluation

Diagnostic ratios are determined, providing a measure for the source identification, as introduced for the soil within *Characterization of study sites - land use and soil properties*. Only two of the suggested ratios may be used here, since sampling of PAHs in the atmosphere is mainly restricted to smaller compounds with faster kinetics. Accordingly, ratios of Fth/Pyr and Ant/Phe were applied to each of the atmospheric monitoring campaigns. These ratios relate individual compounds with almost identical physicochemical characteristics to each other (see Table 1.1). Hence, potential errors based on different partitioning behaviour can be excluded and the respective ratios may be applied for the different phases (gas and particles). Relations of those four compounds are used by Yunker *et al.* (2002) and Biache *et al.* (2014) to differ between petrogenic and pyrogenic combustion. In particular, fossil fuel, and wood/coal combustion may be identified. The respective ratios were calculated for atmospheric concentrations of each sampling campaign during the two years of monitoring.

### 7.3 Results and discussion

Figure 7.1 shows the ratios of Fth/Fth+Pyr and Ant/Ant+Phe for each location and each seasonal monitoring (including both heights for the second year), providing almost identical values for the three locations (see Table A.5). For all samples, the ratio of Fth/Fth+Pyr is above 0.5 and Ant/Ant+Phe is below 0.1 indicating mainly combustion, especially combustion of coal and wood as the predominant emission source. This observation is in perfect agreement to the investigation of the soil profiles at the respective study sites. Furthermore, a slight trend can be observed for the atmosphere with sampling campaigns in November providing the highest values for the relation of Ant/Ant+Phe regarding both years and both heights (as encircled in the plot). This may be due to two reasons. On the one hand, an increase of traffic (less bicycles) was observed with the beginning of the cold season, which could potentially cause a shift within the mixture of atmospheric PAHs. Additionally, the photolytic behaviour of Ant and Phe illustrates half-lives of Phe exceeding Ant by several orders of magnitude, potentially posing a bias (Behymer & Hites, 1985). Photodegradation can be excluded as a significant influence for PAHs on passive samplers due to the respective set-up with protection to incident light. Still, photolytic degradation of Ant in the atmosphere may be expected as less relevant during winter and for lower solar radiation, generating a particular bias of the ratio Ant/Phe for different seasons. Therefore, global radiation as well as diffuse solar radiation obtained from the *German Weather Survey* were examined for the seasonal monitorings (Figure A.5). Comparing the obtained data sets for November and February to May and August show considerably higher incoming radiation during May and August but similar radiation for November and February. Consequently, the same (low) ratios of Ant/(Ant+Phe) were expected during autumn and winter. However, the monitoring during November illustrates notably higher ratios than observed during February (around 0.06 compared to 0.01 – 0.02), as highlighted within Figure 7.1. This observation suggests the determined increase of Ant/(Ant+Phe) as valid indication for a slight shift of emission sources. Therefore, the higher ratio of Ant/Ant+Phe reflects the increase of traffic within the studied region during November.

In addition to different emission patterns, also transport, deposition and degradation processes vary considerably, which introduces a potential change of specific ratios over time. HMW PAHs may be deposited close to the emission source, whereas LMW PAHs provide the potential for long range transport. De La Torre-Roche *et al.* (2009) relate LMW PAH to petrogenic emission and HMW PAHs to pyrogenic emission. Hence, the two ratios used here may reflect different air masses coming from different sources. However, the ratios indicate consistent emission sources in the Ammer valley (with slightly varying contributions), excluding this option to differentiate between air masses. However, Biache *et al.* (2014) and Dvorská *et al.* (2011) criticise the use of diagnostic ratios, as diverse alterations of PAH mixtures may occur during the atmospheric transport. The authors discuss the difficulties of a clear identification of emission sources due to pho-

## 7 Characteristic ratios and source appointment

todegradation, deposition and revolatilization of individual compounds interfering with the original ratios of PAHs at the emission source.

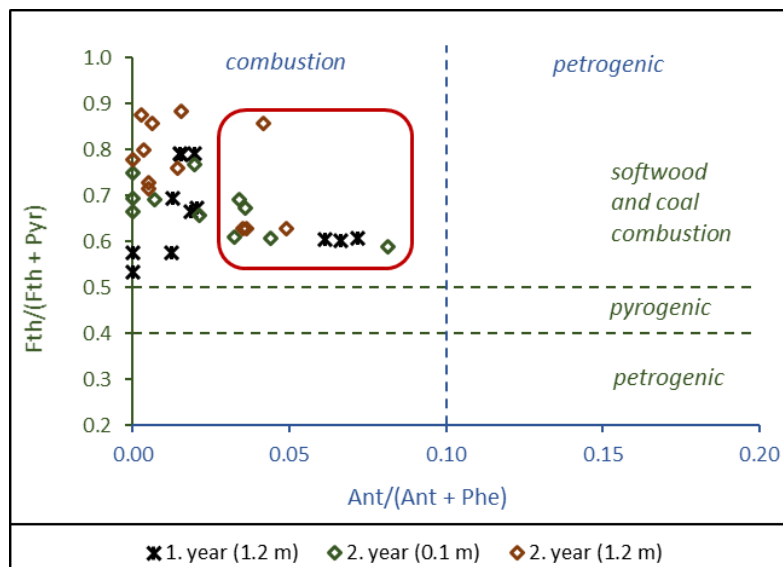


Figure 7.1: Scatter plot of diagnostic ratios for atmospheric concentrations for each location and seasonal monitoring, based on Ant, Phe, Fth and Pyr. Encircled data points illustrate ratios observed during November monitorings of both years.

To account for these uncertainties of single diagnostic ratios, distribution patterns of a broad range of target compounds are considered additionally in this study. Figure 7.2 shows distribution pattern for eight PAHs on the passive sampler at the end of each sampling campaign during both years of monitoring. With respect to homogeneous concentrations in the atmosphere, samplers at 1.2 m height are considered exclusively. Any, Ace, Fln, Phe, Ant, Fth, Pyr and BaA are included as compounds which could be detected for each monitoring. Variations of the respective concentrations at the individual locations are more pronounced during spring and summer. This may be due to the overall low concentrations for warm periods, which are generally more sensitive to slight changes. Despite that, the regular patterns remain very comparable for the three locations with Phe as dominating compound, followed by Fth, Pyr and Fln. This is in good agreement with several studies found in literature (Farrar *et al.*, 2005, Terzaghi *et al.*, 2015, Ribes *et al.*, 2003, Cetin *et al.*, 2017, Degrendele *et al.*, 2016, Aydin *et al.*, 2014). The proportion of Ace seems relatively higher during May and August compared to November and February during the two years. Larsen and Baker (2003) and Khalili *et al.* (1995) independently define Ace as part of characteristic fingerprints corresponding to vehicular emission. Thus, traffic as emission source within the Ammer valley apparently loses some relevance during the cold period. Furthermore, the observed patterns for November 2016 and February 2017 illustrate substantial differences with lower contribution of smaller compounds like Any, Fln, Phe and Ant during February 2017.



Khalili *et al.* (1995) define all of these compounds as part of the characteristic pattern for coke oven combustion. Additionally, Lee *et al.* (2005a) report a relative enrichment of Ant compared to Fth and Pyr due to coal combustion. Therefore, the distribution pattern determined during November 2016 apparently indicates domestic heating as major emission source for atmospheric PAHs. Comparable relations can be observed for November 2017 and February 2018, which are all expected to reflect the heating period. Thus, the sampling in February 2017 provides an exception. However, the concentrations included in Figure 7.2 refer to the last measurement of the separate sampling campaigns. Considering February 2017, this pattern changes over the course of the monitoring respectively. Thus, concentrations measured after two weeks of sampling in February 2017 generate the same distribution pattern as observed for November 2016 (see Figure A.8). The temperatures increase during February 2017 towards the end of the monitoring period (Figure A.4), potentially indicating the end of the heating season. These relations suggest domestic heating as prevalent emission source for November 2016, as beginning of the heating period. This is in good agreement with other studies found in literature: Motelay-Massei *et al.* (2007) as well as Nguyen *et al.* (2018) characterize domestic heating as major emission source for PAHs at urban sites during winter. Liu *et al.* (2017) determine a general increase of heating-related PAHs in the atmosphere correlating to lower air temperatures, studying 169 sites in the US. Subsequently, with increasing ambient temperature towards the end of February 2017, PAH emission by domestic heating gets less relevant. Additionally, a decrease of atmospheric PAH concentrations has been observed during this monitoring period in parallel to the increase of temperature. Consequently, a shift within the emission rates as well as emission source seems valid. However, the use of Ant/Ant+Phe as diagnostic ratio indicated a contrasting relation with an increasing influence of traffic emission for November. Combining both findings suggests a parallel increase of domestic heating as well as traffic during cold periods. Thus, accounting for a broader range of compounds and respective ratios in parallel provides a more robust interpretation of varying emission sources.

## 7 Characteristic ratios and source appointment

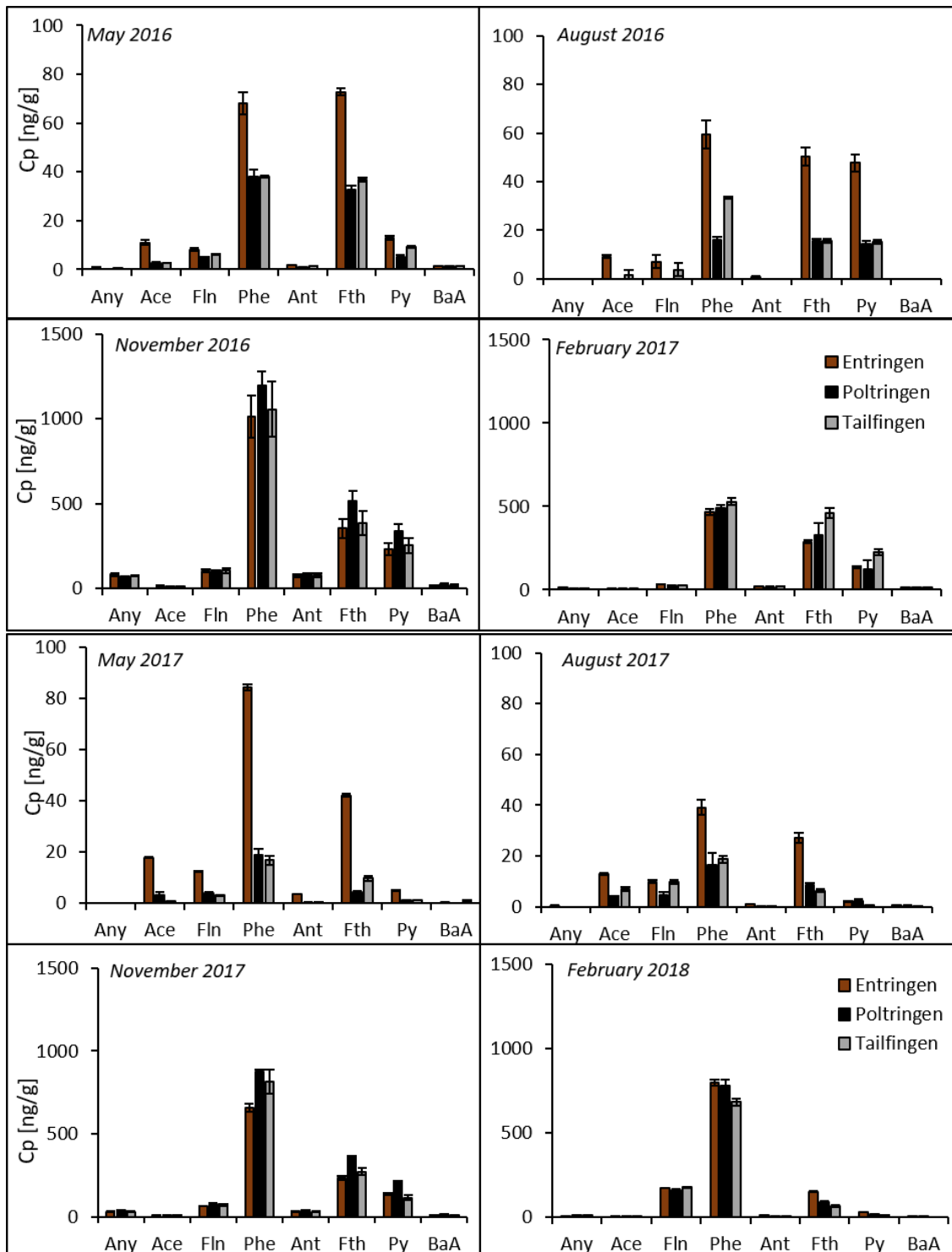


Figure 7.2: Distribution pattern of eight PAHs (Any, Ace, Fln, Phe, Ant, Fth, Pyr and BaA) on PE, measured for the last sampling of each seasonal monitoring during both years of sampling campaigns; covering May 2016 - March 2018. Error bars indicate the standard deviation determined for triplicate samplers.

## 7.4 Conclusion

Domestic heating and traffic were determined as the major emission sources for all study sites throughout the two years. During November the ratio of Ant/Ant+Phe and distribution patterns of eight PAHs (covering a considerably broad range of the U.S. EPA Priority PAHs) indicate an increase of both traffic and domestic heating as emission source. These findings agree well with the considerable increase of PAH concentrations in the atmosphere during autumn and winter. Yet, during the heating season the respective increase of PAH emission caused by domestic heating exceeds the increase of traffic. Consequently, domestic heating was determined as the prevalent emission source during autumn and winter, while traffic seems relatively more relevant during spring and summer.

## 8 Passive sampling in soils

### 8.1 Concept and Objectives

The basic concept of passive sampling in soil is identical to sampling in the atmosphere with implementing a synthetic polymer as sink for hydrophobic compounds. Passive sampling in soil is driven by a complex exchange of target compounds as pores in an undisturbed soil are filled with both air and water to varying extends (Cousins *et al.*, 1999). This leads to complicated mass transfer processes: compounds desorb from soil into the water, potentially volatilize from water into the air, and finally they are sorbed from air or water onto the passive sampler. Different and unknown amounts of air and water within pores as well as potential local depletion of the sampled matrices are likely to complicate estimations regarding time scales to reach equilibrium (Adams, 2007, Cornelissen *et al.*, 2008). Several studies describe the advantages of using passive samplers in *ex situ* laboratory tests to determine freely available concentrations of target compounds in sediments and soils (Gschwend *et al.*, 2011, Hawthorne *et al.*, 2011, Niehus *et al.*, 2018, Ghosh *et al.*, 2014, Arp *et al.*, 2015, Cornelissen *et al.*, 2008). Constant mixing within *ex situ* batch tests minimizes local depletion and enhances the accessibility of target compounds leading to faster uptake kinetics (Arp *et al.*, 2015). Ghosh *et al.* (2014) report the use of *ex situ* passive samplers as equilibrium samplers as the most convenient approach. This characterizes a relevant distinction compared to sampling within the atmosphere where passive samplers can be used as kinetic samplers and concentrations may be corrected for equilibrium (Khairy & Lohmann, 2012, 2014). One major prerequisite to determine equilibrium concentrations of PAHs in soils is the negligible depletion of target compounds within the bulk soil during equilibration (Porschmann *et al.*, 1997, Reichenberg *et al.*, 2008). This was defined as uptake of target compounds of up to 10 % of the total amount in the system (DiFilippo & Eganhouse, 2010). Moreover, a well-mixed (and therefore homogeneous) suspension is required. A comparison of two different types of passive samplers, namely Polyethylene (PE) sheets and Polydimethylsiloxane (PDMS) coated jars, was performed equivalent to the atmosphere. PDMS coated jars aim for short equilibration times by using explicitly thin polymers generating a large surface area to volume ratio of the polymer. The application of different thicknesses of polymer coating can be used to validate equilibrium (Jahnke *et al.*, 2012, Reichenberg *et al.*, 2008) and overcome the need of a time series (Mäenpää *et al.*, 2011).

Within this study, four representative PAHs are chosen for a more detailed analysis with respect to the atmospheric monitorings: Fluorene, Phenanthrene, Fluoranthene and Pyrene (Fln, Phe, Fth and Pyr). Partition coefficients between water and the individual polymers (PE, PDMS) are listed in Table 8.1; PE and PDMS have similar values, especially for Fln and Phe as low molecular weight (LMW) PAHs. A good agreement of these coefficients leads to the assumption of equal concentrations of the target com-

pounds on both polymers in soil batches at equilibrium (regarding the same soil). First estimates of expected characteristic times yield equilibration of Phe within seconds to hours for batches comprising PDMS and PE respectively. This is in contrast to observations of previous batch tests in the lab as well as comparable studies found in literature, which suggest 14 or 28 days as sufficient equilibration times for passive sampling of hydrophobic organic compounds within sediments (Endo *et al.*, 2017, Mayer *et al.*, 2014, Cornelissen *et al.*, 2008). Therefore, preliminary tests were performed on both types of passive samplers to determine respective equilibration times and check on the reproducibility of measured concentrations.

Accordingly, the main objectives of this study are:

1. The development of an accurate method for passive sampling of PAHs in soils.
2. The determination of freely available aqueous PAH concentrations ( $C_{w,eq}$ ) within the soil profiles of each study site.

With respect to the development of an appropriate *ex situ* sampling method for freely available PAHs in soils, three hypotheses were set up:

- a) Sorption of target compounds and desorption of the performance reference compound (*PRC*) in batch tests are characterized by the same kinetics (regardless of the flux direction, and thus isotropic).
- b) PDMS coated jars show significantly shorter equilibration times compared to PE sheets due to thinner coatings.
- c) Equilibrium concentrations on the passive sampler ultimately mirror concentrations on natural organic matter.

Subsequent to the evaluation of an appropriate passive sampling method for PAHs in soils, batch tests were conducted for the three study sites. Considering the application of the chosen passive sampling method, additional hypotheses can be formulated as:

- d) Identical concentrations of PAHs in the aqueous phase are expected to be obtained with passive samplers and measured sorption isotherms.
- e) Stable distribution patterns allow to use one (or few) representative compounds to calculate the sum of PAHs.

**Table 8.1: Log  $K_p$  [L/kg] for the representative compounds between water and the two polymers PE and PDMS (at 20°C).**

PAH	PE-water	PDMS-water
Flu	3,9	3,6
Phe	4,3	3,9
Fth	5,0	4,2
Pyr	5,0	4,2

## 8.2 Theoretical Background

### 8.2.1 Redistribution of contaminants in multiple phases

Equilibrium concentrations on the passive sampler are directly related to the respective distribution and partition coefficients between soil, water and polymer. A significant non-linear relation was determined for the sorption of target compounds to the surveyed soils. Freundlich sorption isotherms of Phe were determined for each soil sample to obtain an accurate measure regarding the distribution of Phe between soil and water for the concentration ranges of interest. Based on the subcooled liquid solubility ( $S$ , in [kg/L]) Freundlich coefficients were normalized obtaining an unit-equivalent coefficient ( $K_{Fr}^*$ ), which may be applied to all target compounds (see *Characterization of study sites - land use and soil properties; Equation 2.10 and Equation 2.11*). Subsequently, mass balances provide an approach for estimating equilibrium concentrations, which is straightforward by referring to the sum of target compounds in each phase at equilibrium, coupled to the general relations of:

$$C_{w,eq} = \frac{C_{p,eq}}{K_p} \quad \text{and} \quad C_{s,eq} = K_{Fr}^* \left[ \frac{C_{w,eq}}{S} \right]^{1/n} \quad (8.1)$$

with  $C_{w,eq}$ ,  $C_{p,eq}$  and  $C_{s,eq}$  as equilibrium concentrations of the target compound in water [ $\mu\text{g/L}$ ], polymer [ $\mu\text{g/kg}$ ] and soil solids [ $\mu\text{g/kg}$ ], respectively and  $K_{Fr}^*$  as (solubility-normalized) Freundlich coefficient regarding distribution between soil and water and  $n$  as respective Freundlich exponent.  $K_p$  depicts the partition coefficient between water and polymer.  $K_p$  values for PDMS coated jars were calculated following Rusina *et al.* (2007) while  $K_p$ s for PE sheets are taken from Lohmann (2012). The total amount of the considered compound (here Phe exemplary) in the system ( $X_{\text{tot}}$  [ $\mu\text{g}$ ]) can be described by the previously determined concentration in the bulk soil ( $C_{\text{bulksoil}}$  [ $\mu\text{g/kg}$ ]) and the mass

of bulk soil in each batch ( $m_{bulksoil}$  [kg]):

$$X_{tot} = C_{bulksoil}m_{bulksoil} \quad (8.2)$$

After equilibration in a batch system containing soil, water and passive sampler, the target compound redistributes over all phases:

$$X_{tot} = C_{soilsolids,eq}m_{soil} + C_{w,eq}V_w + C_{p,eq}m_p \quad (8.3)$$

with  $V_w$ ,  $m_{soil}$  and  $m_p$  accounting for the volume of water [L], mass of solids [kg] and mass of polymer [kg] within the batches, while  $C_{soilsolids,eq}$  describes the equilibrium concentration of the target compound on the soil solids. Including the respective distribution (here  $K_{Fr}$ ) and partition coefficients ( $K_p$ ), while relating the mass balance explicitly to concentrations on the passive sampler leads to:

$$X_{tot} = C_{p,eq}m_p + \frac{C_{p,eq}}{K_p} V_w + K_{Fr} \left( \frac{C_{p,eq}}{K_p} \right)^n m_{soil} \quad (8.4)$$

Subsequently, equilibrium concentrations on the passive sampler were estimated by solving Equation 8.4 for the three phases numerically in Matlab. Since passive sampler in soil-batches are defined to be used as equilibrium sampler (and not kinetic sampler), accurate characterization of the sampling set-up with respect to equilibration of soil and sampler is required. Therefore, a preliminary batch test has been conducted to study the kinetics of redistribution and the respective characteristic times to reach equilibrium. Redistribution in the lab happens in a closed 3-phase system consisting of soil solids, passive sampler and water, permanently shaken at a constant temperature. Concentrations in the gas phase were neglected within this set-up, due to the low Henry's law constant of Phe (9.43E-4 [-], *New Jersey Department of environmental protection*). Within such a batch experiment, aqueous phase and solids form a well-mixed suspension which enhances the accessibility of target compounds for the passive samplers. Two processes occur in parallel within the batches, which are interconnected by the aqueous phase; i) desorption of compounds from soil particles and ii) sorption onto passive samplers. Those processes may be characterized by different kinetics.

- (i) Desorption from soils may be differentiated even further considering film diffusion as well as intraparticle diffusion as potential processes:

Defining soil particles as spheres, film diffusion in a finite bath (batch vial) can be described as:

$$\frac{C_{w,t}}{C_{w,eq}} = 1 - e \left[ -\frac{D_{aq}6}{\delta_{aq}d\rho_s} \left( \frac{1}{K_d^*} + \frac{m_s}{V_w} \right) t \right] \quad (8.5)$$

with  $C_{w,t}$  and  $C_{w,eq}$  as concentration [ $\mu\text{g}/\text{kg}$ ] in the aqueous phase at time  $t$  [s] and in equilibrium,  $D_{aq}$  denoting the aqueous diffusion coefficient [ $\text{m}^2/\text{s}$ ],  $\delta_{aq}$  the aqueous boundary

layer [m],  $d_s$  refers to the diameter [m] and  $\rho_s$  to the density of the soil grains [kg/L].  $\frac{m_s}{V_w}$  describes the solid to liquid ratio [kg/L] and  $K_d^*$  the distribution coefficient [L/kg] between soil and water, adjusted to the low concentrations of the target compounds measured in the bulk soil. The last term in brackets  $\left(\frac{1}{K_d^*} + \frac{m_s}{V_w}\right)$  arises from the finite batch boundary conditions (here 0.54 for Phe). Such a factor may be applied with respect to exchange processes between soil solids and water as well as for passive sampler and water. Accordingly, this approach relies on desorption from soils and sorption onto samplers as separate processes, which is not 100 % valid.

Basic assumptions for film diffusion are steady state diffusion in an aqueous boundary layer with homogeneous concentrations in the solid phase and well-mixed conditions in the aqueous phase. Regarding high values of  $K_d^*$  (here around 2000 L/kg for Phe) or high  $\frac{m_s}{V_w}$  (here, 0.54 kg/L) and thus  $\frac{m_s}{V_w} \gg \frac{1}{K_d^*}$  kinetics become independent of sorption. This applies always if the concentration of the compound in soil solids does not decrease significantly during desorption, which is one of the prerequisites mentioned above. Furthermore, desorption from soils may be governed by slow intraparticle diffusion. If sorption is strong, then diffusion of compounds within the soil pores gets strongly retarded. The respective relation to describe desorption from soils by considering single grains refers to Fick's second law (Wu & Gschwend, 1986):

$$\frac{\partial C_{w,intra}}{\partial t} (\varepsilon + (1 - \varepsilon) \rho_s K_d^*) = D_e \left[ \frac{\partial^2 C_{w,intra}}{\partial r^2} + \frac{2}{r} \frac{\partial C_{w,intra}}{\partial r} \right] \quad (8.6)$$

with  $\varepsilon$  [-] as intraparticle porosity,  $C_{w,intra}$  [ $\mu\text{g/L}$ ] describes the concentration of the solute within the pore volume of the grain,  $\rho_s$  [kg/L] is the dry solid density,  $D_e$  [ $\frac{\text{m}^2}{\text{s}}$ ] the effective diffusion coefficient and  $r$  [m] the radial coordinate. The effective diffusion coefficient relates the aqueous diffusion coefficient to the properties of the porous media (porosity and, if possible, tortuosity) and can be estimated based on the empirical relation:

$$D_e = D_{aq} \varepsilon^2 \quad (8.7)$$

An apparent diffusion coefficient ( $D_a$ ) may be defined accounting for the sorption capacity of the soil particles:

$$D_a = \frac{D_e}{\varepsilon + (1 - \varepsilon) \rho_s K_d^*} \quad (8.8)$$

Intraparticle diffusion may also be solved approximately, similar to Equation 8.5 (Liu,



2019, personal communication):

$$\frac{M_t}{M_{eq}} = e^{\left[-6\left(1+K_d^* \frac{m_s}{V_w}\right) \sqrt{\frac{D_a t}{\pi r^2}}\right]} \quad (8.9)$$

with  $M_t$  and  $M_{eq}$  denoting the mass [kg] of the compound sorbed or desorbed at time  $t$  [s] and in equilibrium.  $\frac{D_a t}{r^2}$  is also known as Fourier number and relates the apparent distribution coefficient  $D_a$  [ $m^2/s$ ] to the time  $t$  and the radius of the sphere. Here kinetics get accelerated with the square root of  $K_d^*$  at high values of  $K_d^* \frac{m_s}{V_w}$ .

(ii) Sorption onto passive samplers

The chemical properties of PDMS and PE as synthetic polymers are well understood and described in detail by Seethapathy and Górecki (2012) and Lohmann (2012). Additionally, Lohmann (2012) states the exchange of hydrophobic compounds between PE (<100  $\mu m$  thick) and water as mainly being limited by an aqueous boundary layer. Similarly, film diffusion through the aqueous boundary layer was demonstrated as the governing process for Phe exchange between water and PE by Seidensticker *et al.* (2017). Due to faster diffusion of Phe in PDMS than PE, instead of the aqueous boundary layer the limitation for film diffusion can be transferred to the uptake onto PDMS (Allan *et al.*, 2010, Allan *et al.*, 2013). If soil solids are a much stronger source than PE sheets are sinks, the uptake onto the polymer does not change the mass balance significantly. Thus, at a constant concentration in water the uptake can be calculated based on Fick's first law, corresponding to sampling the atmosphere leading to:

$$\frac{C_{p,t}}{C_{p,eq}} = 1 - e^{\left[-\frac{A_p D_{aq}}{V_p \delta_{aq} \rho_p K_{pw}} t\right]} \quad (8.10)$$

with  $C_{p,t}$  and  $C_{p,eq}$  [ $\mu g/kg$ ] as concentrations in the polymer at time  $t$  and in equilibrium,  $K_{pw}$  [ $L/kg$ ] denoting the respective polymer-water partition coefficient, while  $A_p$ ,  $V_p$  refer to the geometry of the sampler with surface area [ $m^2$ ] and volume [ $m^3$ ] of the polymer (=  $2/d$  for plane sheets). These relations (Equation 8.5, Equation 8.9 and Equation 8.10) already indicate a clear correlation of mass transfer within the batches to the ratios of solid to liquid phases as well as surface area to volume of the passive sampler. Additionally, in the case of varying concentrations in the aqueous phase, finite bath boundary conditions apply for the batches and the relation of  $m_p/V_w$  needs to be taken into account, the same way as for the desorption from soils. Hence, *ex situ* batches provide the possibility to influence time scales until equilibrium by varying the set-up within the batches. Mass transfer processes between soil solids, water and passive sampler may be calculated analytically if sorption is linear. Therefore, concentration changes in each time step may be coupled to the aqueous phase as linkage between soil and sampler. Consequently, aqueous concentrations are of crucial influence on the kinetics and redistribution of target compounds within the considered 3 phase-system. Redistribution processes also occur on a small scale for all particles within the batches. This generates a very complex system

with an unknown mixture of compounds with various characteristics affecting each other as well as the aqueous phase. This leads to a high uncertainty in the interplay of desorption from soil and sorption onto the passive sampler. Exchange rate constants might be determined as an effective parameter to overcome the issue of accounting for each distribution process occurring within the batches individually (Booij, 2003, Huckins *et al.*, 1993, Huckins *et al.*, 1999). Subsequently, characteristic times to estimate specific proportions of equilibrium can be calculated based on the rate constant.

### 8.2.2 Rate constants and characteristic times

(i) Mass transfer between soil and water

Film diffusion for the desorption of target compounds from soil into water leads to the following rate constant  $\lambda_{des}$  [day<sup>-1</sup>]:

$$\lambda_{des} = \frac{D_{aq} \delta}{\delta_{aq} d_s \rho_s} \left( \frac{m_s}{V_w} + \frac{1}{K_d^*} \right) \quad (8.11)$$

As already introduced for the atmospheric monitoring, characteristic times to reach 63 % of the equilibrium in water are defined as the inverse of the respective rate constants  $\lambda$  (loss or uptake rate constant) and adapting this relation to 90 % equilibrium yields  $t_{0.9}$  according to:

$$t_{0.9} = \frac{2.3}{\lambda} \quad (8.12)$$

For intraparticle pore diffusion, the use of Fourier numbers  $\left( \frac{D_a t}{a^2} [-] \right)$  provides a qualitative measure of mass transfer processes and equilibration times. They refer solely to the geometry of the considered particle and the boundary conditions (infinite vs. finite bath). One important measure within this relation is the ratio of the masses of the target compounds in the aqueous and the solid phase at equilibrium. Regarding the soil used within the first kinetic batch experiment, this relation demonstrates a considerably low value of 9.9E-4 (indicating already the substantial influence of the soil). Grathwohl (2012) illustrates the correlation between equilibrium status and Fourier number in the finite bath for different properties of batch tests  $\left( \frac{V_w}{K_d^* m_d} \right)$  (see Figure A.9). Accordingly, the Fourier number was obtained graphically as approximately 0.1 for 90 % equilibrium within the batch systems and this simple relation may be applied:

$$0.1 = \frac{D_a t_{0.9}}{r^2} \quad (8.13)$$

Referring to the combination of Equation 8.8 to Equation 8.13 the characteristic time to

reach 90 % equilibrium based on intraparticle diffusion can then be estimated by:

$$t_{0.9} = \frac{0.1r^2 (\varepsilon + (1 - \varepsilon)K_d^* \rho_s)}{D_{aq} \varepsilon^2} \quad (8.14)$$

(ii) Mass transfer between water and passive sampler

Characteristic times were also calculated for the exchange between passive sampler and water. This was done individually for the loss of Ant-D<sub>10</sub> as *PRC* from PE sheets and for the uptake of Phe from soil slurries onto the passive sampler. Ant and Phe are characterized by almost the same physicochemical properties (see Table 1.1) providing an optimal comparison for uptake and loss processes for PE sheets in soil slurries. Expected exchange rate constants ( $\lambda_{exp}$ ) for film diffusion can be calculated according to:

$$\lambda_{exp} = \frac{A_p D_{aq}}{V_p \delta_{aq} K_{pw}} \quad (8.15)$$

with  $\delta_{aq}$  as aqueous boundary layer determined on the basis of the dimensionless Sherwood number (*Sh*). Seidensticker *et al.* (2017) determined *Sh* for a comparable set-up of ~ 37. Adjusting this value for the sampler thickness (*d*) of 30  $\mu\text{m}$  yields a Sherwood number of 5, which was used in the following relation:

$$\delta_{aq} = \frac{d}{Sh} \quad (8.16)$$

Additionally, loss rates constants ( $\lambda_{obs}$  [ $\text{day}^{-1}$ ]) were estimated based on the measured decline of the *PRC* (here Ant-D<sub>10</sub>):

$$\lambda_{obs} = \frac{\left( \ln \frac{C_{PRC,0}}{C_{PRC,t}} \right)}{t} \quad (8.17)$$

with  $C_{PRC,0}$  and  $C_{PRC,t}$  as initial concentration of the *PRC* and at the sampling time *t*. Subsequently, the loss of the *PRC* was modelled to compare the different curves based on the expected and the observed loss rate constant. Due to the finite bath boundary condition a redistribution of the *PRC* occurs between all three phases (its mass is conserved). This leads to a final non-zero equilibrium concentration of Ant-D<sub>10</sub> within the PE and the need for a slight correction of the simple first order loss taking this residue into account:

$$C_{PRC,t} = \left( C_{PRC,0} e^{[-\lambda t]} \right) + C_{PRC,eq} \quad (8.18)$$

Following Tomaszewski (2008) the same approach with first order kinetics was applied to fit an uptake rate constant ( $\lambda_{up}$  [ $\text{day}^{-1}$ ]) to the measured concentrations of Phe on PE

sheets:

$$\lambda_{up} = \left(-\frac{1}{t}\right) \ln \left[1 - \frac{C_{p,t}}{C_{p,eq}}\right] \quad (8.19)$$

Finally, the uptake of Phe was modelled based on the fitted  $\lambda_{up}$ :

$$C_{p,t} = C_{p,eq} \left(1 - e^{(-\lambda_{up}t)}\right) \quad (8.20)$$

All attempts for characteristic times to reach 90 % equilibrium between the considered phases in the soil batches are summarized in Table 8.2.

**Table 8.2: Characteristic times of Ant-D<sub>10</sub> and Phe to reach 90 % equilibrium in batches comprising PE and PDMS respectively, considered mass transports are film and intraparticle diffusion (<sup>1</sup>parameters for intraparticle diffusion were defined as  $\varepsilon = 0.7$  and  $r_s = 0.05$  mm).**

Mass transport process	Batches with PE	Batches with PDMS
Desorption of Phe from soil; film diffusion	128 min	85 min
Desorption of Phe from soil; intraparticle diffusion <sup>1</sup>	22 min	22 min
Desorption of Ant-D <sub>10</sub> from passive sampler; film diffusion	89 min	Within seconds
Sorption of Phe to sampler; film diffusion	92 min	Within seconds

### 8.3 Set-up Batch tests (soil slurries)

#### Soil batches including PE sheets

In a preliminary experiment with just one soil sample, characteristic time scales to reach equilibrium were determined. 15 batches were set up identically and kept shaking for predefined time spans of 1, 2, 3, 4 and 12 weeks. At each time, three batches were separated providing triplicate PE samples and respective extracts. The solid – liquid composition of the batches was 80 g soil and 150 mL Millipore water, using a low liquid to solid ratio to allow short equilibration times between soil solids and water. 1 g of PE with 30  $\mu\text{m}$  thickness was cut into strips of ca. 10 cm length and 1 cm width before adding to each batch to ensure a complete mixing of the passive samplers into the soil slurries. In advance of the batch test, passive samplers were cleaned and spiked with Ant-d<sub>10</sub> as *PRC* identical as for the atmospheric sampling. To avoid biodegradation of target compounds, 0.5 mg of sodium azide was added to each batch as cell toxin, inhibiting enzymatic activity. Batches were kept on a horizontal shaker (ca. 150 rpm) at a constant temperature of 20 °C, aiming to reach equilibrium between PE, water and soil. Following the shaking, batches were separated manually into the different phases (soil, water, PE). Prior to the extraction (following the protocol described earlier), PE sheets were thoroughly rinsed with Millipore water and wiped dry with lint-free tissue.

This procedure was slightly adapted for the regular batch experiments performed on the whole soil profiles: In contrast to the theoretical considerations, time to reach equilibrium between soil and samplers in the preliminary test exceeded 12 weeks. Therefore, equilibration time was extended to 4.5 months for the regular *ex situ* batch tests. An increase in the amount of soil to 100 g yielding a lower liquid-to-solid ratio additionally was used, aiming for shorter equilibration times.

#### PDMS coated jars

In addition, a kinetic test was performed with one soil sample on coated jars to determine characteristic time scales for equilibration between soil and PDMS. Ahead of the kinetic test, a soil suspension was prepared with 220 g of soil and 2 g of sodium azide on 580 mL Millipore water to ensure proper replicates for the individual jars (solid to liquid ratio = 0.38 kg/l). Jars with PDMS coatings of 1, 2 and 4  $\mu\text{m}$  were filled with 80 g of this suspension, kept on a roller mixer (*Mercateo*) and sampled after 2, 4 and 6 weeks. At each point in time, one jar of each PDMS thickness was opened in parallel. Adjacent to opening the jars, the suspension was discarded and PDMS coatings were cleaned cautiously to remove any soil particle from the surface by rinsing several times with Millipore water. After drying with lint free tissues the jars were extracted as described before.

## 8.4 Results and discussion: Accurate passive sampling of PAHs in soils

### 8.4.1 Loss and uptake rate constants for batches with PE

Ant-D<sub>10</sub> was used as *PRC* to determine loss rates from the PE sheets over the course of the preliminary batch kinetic test as shown in Figure 8.1. The measured concentrations are combined with the analytic solution of simple first order kinetics (Equation 8.18). Standard deviation of Ant-D<sub>10</sub> is very low with ca. 6 % variation for measured triplicates for each sampling time, illustrating a very good reproducibility of the observed loss. Two modelled curves are shown to compare the expected loss rate constant for the *PRC* of 16 day<sup>-1</sup> (film diffusion, Equation 8.15) to an observed loss rate constant of 0.07 day<sup>-1</sup> (first order kinetics, Equation 8.17). For this modelling approach,  $C_{PRC,eq}$  was calculated based on mass balances (Equation 8.4), applying the measured  $K_{Fr}$  of Phe also for Ant-D<sub>10</sub> (which seems valid, based on their almost identical characteristics, shown in Table 1.1). The direct comparison of the different rate constants generates significantly different curves for the observed and the expected loss of Ant-D<sub>10</sub> from PE sheets. Naturally, the fitted curve fits the data set very well. Only slightly higher concentrations were estimated than measured due to the correction for the residual or equilibrium concentration. The observed loss rate constant leads to an equilibrium status of 90 % for the *PRC* within the batches after ca. 32 days. Explicitly fast declining concentrations, and equilibration within 3.5 hours would be expected for film diffusion as limiting process for the desorption of Ant-D<sub>10</sub> from PE. Consequently, for this specific set-up, desorption of PAHs from PE is not limited by film diffusion. This is due to a slow exchange process between soil and water compared to PE and water. Hence, the difference of the actual rate constant ( $\lambda_{obs}$ ) to the expected rate constant ( $\lambda_{exp}$ ), which accounts merely for film diffusion, might be interpreted as a measure for the effect of the soil on exchange processes between the soil slurry and the passive sampler. In general, exchange processes between water and PE are independent of the flux direction (Huckins *et al.*, 2002, Booij *et al.*, 1998, Vrana & Schüürmann, 2002). Furthermore, for compounds with the same solubility, these rate constants are expected to be equal (here fitted as 0.072 day<sup>-1</sup> for both Ant-D<sub>10</sub> and Phe). This expectation seemed reasonable considering  $\lambda$  as an overall rate constant, controlled by soil - water exchange kinetics and not by water - PE. Moreover,  $K_{Fr}^*$  (of Phe) is stable for the non-depletive sampling set-up of the soil and partitioning to the polymer is generally independent of concentrations. Accordingly, Booij (2003) determined a good agreement for the loss of *PRCs* and the uptake of PCBs as target compounds from sediment slurries onto PE strips. Therefore, redistribution of PAHs within the considered three phase system should be independent of the flux direction leading to an identical  $\lambda$  for Ant-D<sub>10</sub> and Phe.

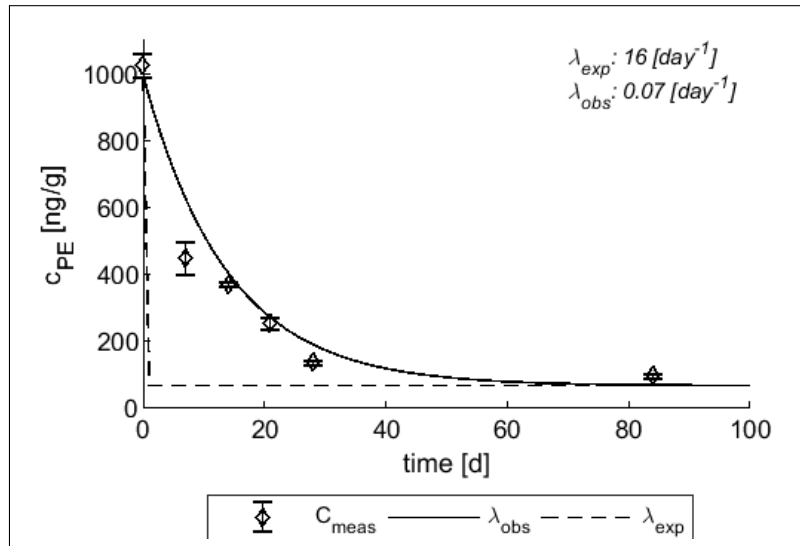


Figure 8.1: Measured loss of Ant-d<sub>10</sub> during three months of equilibration combined with the calculated loss, following the first order kinetic model and for desorption from PE alone; slow uptake in soil limits kinetics.

In contrast to this expectation, Figure 8.2 illustrates a notably faster loss of Ant-D<sub>10</sub> compared to the uptake of Phe within the first batch test. Equilibrium concentration of Phe on the sampler was calculated based on the mass balances introduced above (Equation 8.4), using the measured  $K_{Fr}$  (based on sorption isotherms). The first order model of Equation 8.20 (based on the fitted  $\lambda_{up}$ ) generates a perfect fit to measured concentrations. However, the desorption of Ant-D<sub>10</sub> is notably faster with a characteristic time of 32 days to reach 90 % of equilibrium compared to 81 days for the sorption of Phe onto PE. Accordingly, the loss rate constant determined for Ant-D<sub>10</sub> does not describe the uptake of Phe onto the PE very well, as shown in Figure 8.3. This figure illustrates two attempts to model the uptake of Phe implementing the observed  $\lambda_{loss}$  for Ant-D<sub>10</sub> ( $0.072 \text{ day}^{-1}$ ) in comparison to the fitted  $\lambda_{up}$  of Phe ( $0.028 \text{ day}^{-1}$ ). The calibrated rate constant based on Ant-D<sub>10</sub> generates a distinctively faster uptake curve for Phe than measured. As stated by Booij (2003), Equation 8.10 can only be applied to determine uptake kinetics onto passive samplers when exchange processes are not limited by the soil. In this study, however, soil solids limit the respective exchange kinetics. As shown in 'Characterization of study sites - land use and soil properties' sorption of Phe within all studied soils is best described by nonlinear Freundlich isotherms. Therefore, sorption and desorption within the batches are concentration-dependent generating specific  $K_d^*$  with stronger sorption at low concentrations. For concentration-dependent sorption, the loss of PRCs on passive samplers in soil cannot be applied to correct measured concentrations of target compounds for equilibrium, as reported by Ghosh *et al.* (2014). Therefore, the concentration-dependency of the exchange processes occurring in the chosen set-up was analysed. For Phe a stable distribution coefficient of  $10^{3.4} [L/kg]$  may be

used, since depletion in the bulk soil was determined to be negligible (see Figure A.10). Oppositely, a decrease of the apparent distribution coefficient of Ant-D<sub>10</sub> occurs with increasing concentrations in the bulk soil during the batch test. This way, the exchange kinetics of Ant-D<sub>10</sub> get faster with increasing concentration in the soil. At equilibrium a  $K_d^*$  of  $10^{3.6}$  [L/kg] was estimated for Ant-D<sub>10</sub> based on the regular mass balance (Equation 8.4). Therefore, at equilibrium in the batches the distribution coefficient of Ant-D<sub>10</sub> still exceeds the one of Phe and cannot explain the observed faster kinetics of Ant-D<sub>10</sub>. Consequently, for the different processes affecting redistribution in finite baths their respective sequence needs to be considered, presumably: i) fast desorption of Ant-D<sub>10</sub> from PE occurs in advance of rather slow sorption to soil solids leading to high initial concentrations in water and slow sorption to soils and ii) slow desorption from soil solids of target compounds is followed by fast sorption to PE.

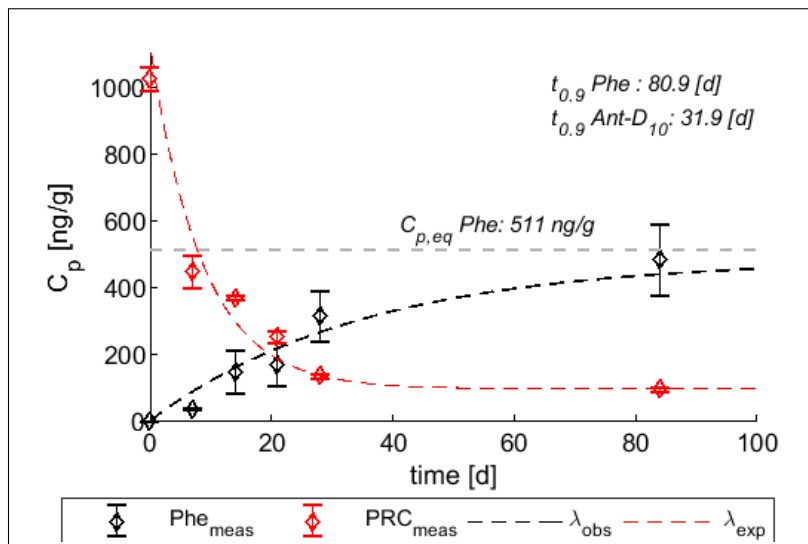


Figure 8.2: Comparison of measured and calculated uptake of Phenanthrene from soil slurries onto the passive samplers to the observed loss of Ant-D<sub>10</sub> and the respective characteristic times to reach 90 % equilibrium. Error bars indicate the determined standard deviation of triplicate samples.

Kan *et al.* (1994) describe differences in adsorption and desorption isotherms for hydrocarbon pollutants as a widespread observed hysteresis effect related to nonlinear sorptive behaviour of soils. This hysteresis effect provides generally faster sorption compared to desorption, which describes exactly what has been observed here. However, the experimental work of Kleineidam *et al.* (2004) and Wang *et al.* (2007) illustrates no hysteresis effect for sorption & desorption of Phe to various materials. Additionally, Huang *et al.* (1998) demonstrate the substantial effect of experimental set-ups and the potential for artificially produced hysteresis effects. Accordingly, the longer equilibration times of both Ant-D<sub>10</sub> and Phe, as expected for PE, might be explained by the slow sorption kinetics of soil samples.



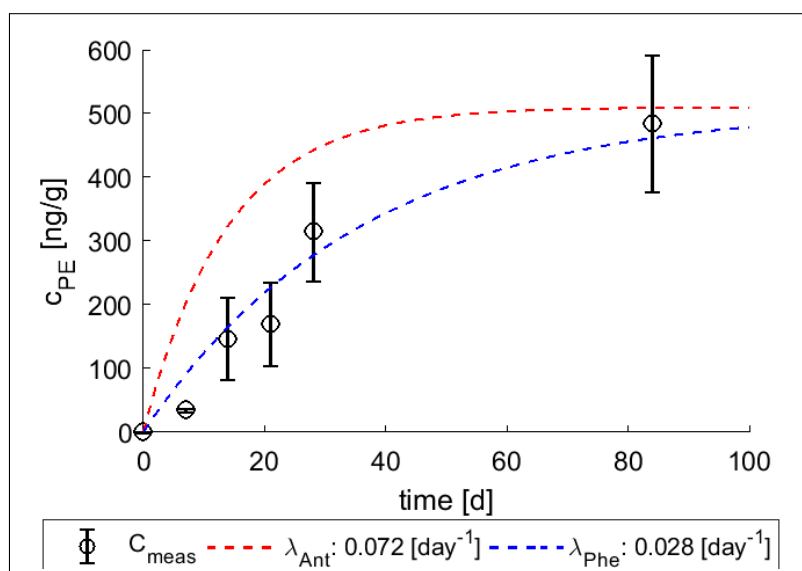


Figure 8.3: Uptake of Phe onto PE in soil slurries comparing the two fitted rate constants  $\lambda$  for Ant and Phe.

In addition to nonlinear sorption isotherms, grain size, quantity and quality of organic material may influence sorption kinetics in soils (Schlebaum *et al.*, 1998, Weber & Huang, 1996, Lu & Pignatello, 2002, Pan *et al.*, 2007). Wu and Gschwend (1986) describe intraparticle diffusion in soil agglomerates as a process retarding the complete equilibration up to months. They observe a significant increase of rate constants after sonification and therefore disaggregation of the sediment samples. For example, assuming aggregates with a size of 2 mm in diameter and a porosity of 40 % would already yield a characteristic time of 37 days for Phe. The same approach without considering agglomerates leads to  $t_{0.9}$  of 22 minutes, which illustrates the sensitivity of exchange kinetics for the characteristics of the soil suspension. Consequently, equilibration times for sorption in natural bulk soils are very difficult to predict, unless a very precise characterization of the soil and the respective batches has been conducted.

In this work, sorption isotherms were measured with freeze dried and ground soil, following Kleineidam *et al.* (1999). This procedure was chosen to ensure homogeneity on very small scale to maintain reproducible data and rapid equilibration times (< 10 days). Batch tests (with PE) involved bulk soils, which were homogenized manually in the field and the lab. Thus, they include bigger grain sizes as well as small agglomerates which limits the prediction of exchange kinetics between passive sampler and soil solids (Witt *et al.*, 2013). High solid to liquid ratios were employed to allow for short equilibration times, with respect to Equation 8.11. This however may have hampered thorough mixing of the soil slurry and led to additional agglomeration of soil particles in form of lumps around the PE strips. Such clusters were observed around tangled PE strips during the

separation of the three phases following equilibration. Agglomerates and lumps generate distinctively longer diffusive pathways and therefore lead to significantly slower exchange kinetics between soil solids and water. Additionally, the direct contact of polymer to the water phase, which was intended to enhance the overall exchange processes, was reduced by the observed soil clusters. (Thus, the chosen set-up apparently did not fulfill the requirements of a well-mixed suspension and dis-aggregation of soil solids.) Heterogeneous concentrations within the soil slurry may support additional interaction of single particles leading to local depletion (Witt *et al.*, 2013). Cho *et al.* (2012) modelled substantially longer time scales for the mass transfer of PCBs in sediments amended with activated carbon (AC) if AC distribution was heterogeneous on mm scale. Therefore, within a heterogeneous soil slurry, equilibration of the different phases may take exceedingly long. Furthermore, if single particles were taken into account instead of assuming the soil solids as one homogeneous phase, equilibration of Ant-D<sub>10</sub> within the whole system might indicate identical time scales as observed for Phe. However, the exchange of Ant-D<sub>10</sub> between individual soil particles cannot be reflected by the passive sampler, once the *PRC* is desorbed. With respect to that, the formation of aggregates and lumps within the suspension may also explain the differences of the observed rate constants for the loss of Ant-D<sub>10</sub> and the uptake of Phe from/to the sampler. Phe-uptake is directly limited by slow desorption from soil, whereas the *PRC*-loss from PE is fast causing high concentrations in the water, followed by the slow sorption of Ant-D<sub>10</sub> to soil solids.

However, the observed rate constants and equilibrium states of Ant-D<sub>10</sub> and Phe within the batches apparently reflect different equilibration and thus exchange kinetics. Therefore, the first hypothesis of identical kinetics for both flux directions cannot be confirmed for this explicit set-up. This may be explained, as discussed above; if presumably relevant requirements for passive sampling in soil-slurries are not fulfilled here, like a homogeneous suspension. The exceedingly fast equilibration of pulverized (and thus homogeneous) soil samples in water underlines the relevant influence of heterogeneity in suspensions and the formation of clusters generating distinctively slow kinetics within batch tests including passive samplers. Additionally, the soil has been characterized by considerably high  $K_d^*$  values, exceeding the linear approaches of  $K_d = K_{oc}f_{oc}$  (see *Characterization of study sites - land use and soil properties*). This indicates strongly sorbing particles (e.g. coal particles like soot) within the soil samples. Consequently, a heterogeneous distribution of such particles within the batches would result in remarkably long equilibration times, similar to observations reported by Kleineidam *et al.* (2004) and Cho *et al.* (2012).

### 8.4.2 Uptake of target compounds onto PE sheets

Figure 8.4 compares the uptake of Phe from soil slurries onto PE sheets to Fl<sub>n</sub>, F<sub>th</sub> and Pyr over the course of the preliminary batch test. Again, the measured concentrations are

combined with modelled uptake curves, based on fitted rate constants (Equation 8.17). The trend of the uptake curves is quite comparable for all compounds, independent of the respective distribution coefficient. This was to be expected, based on the high solid to liquid ratio of 0.5, constant concentrations in the soil, and high distribution coefficients ( $K_d^*$ ) of  $10^{3.4}$  to  $10^{3.9}$ . As stated earlier, under such prerequisites (particularly with  $\frac{m_s}{V_w} \gg \frac{1}{K_d^*}$ ) kinetics get independent of sorption (see Equation 8.11).

Each curve illustrates a linear increase in the concentration on PE during the first four weeks, followed by flattening of the curve, potentially approaching a plateau. Significant spreading of triplicates can be observed for every compound at each time point. At equilibrium, PE-triplicates are expected to reflect the same concentrations in water regardless of slight variation in the composition of the batches. Constraints in the mixing and presumably small scale heterogeneity of the individual batches might have produced significant variances during the uptake process of target compounds. Accordingly, the standard deviation of triplicate batches can be interpreted as an indicator for the equilibrium status. For example, Fl<sub>n</sub> shows a standard deviation of 60 % after 2 weeks of shaking which improves to 16 % after 3 months. In contrast, Pyr demonstrates a rather constant relative standard deviation of about 24 %.

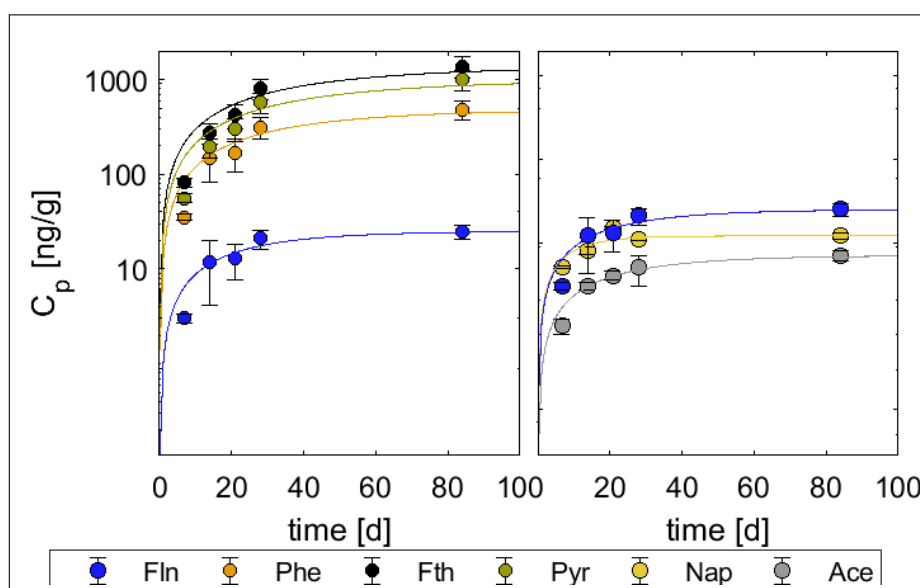


Figure 8.4: Uptake of target compounds onto PE sheets out of soil slurry comparing Fl<sub>n</sub>, Phe, Fth, and Pyr (left plot) and LMWC Nap, Any to Fl<sub>n</sub> (right plot). Error bars indicate the observed standard deviation of triplicate batches.

With respect to ongoing uptake processes versus equilibrium conditions, a comparison of explicit values after 4 weeks and after 3 months of shaking may provide a more accurate insight. For that explicit time span, Fl<sub>n</sub> and Pyr demonstrate notably different

trends on the sampler. FlN shows apparently stable concentrations of  $21 \pm 4.8$  ng/g and  $25 \pm 4.2$  ng/g after 4 weeks and 3 months, respectively. Pyr shows a notable increase during the last two months with  $570 \pm 134$  ng/g after 4 weeks and  $993 \pm 232$  ng/g after 3 months of shaking, indicating continuous uptake onto the sampler. For a further insight into compound specific behaviour, the uptake of FlN on PE was compared to uptake of Naphthalene and Acenaphthylene (Nap and Any). Nap and Any are characterized by low partition coefficients. This comparison is also included in Figure 8.4, where particularly Nap shows a fast uptake onto the sampler and apparently reaches equilibrium during the first half of this kinetic test. Hence, equilibration of passive samplers in *ex situ* batch experiments seems to depend to a minor extend on the respective partition coefficients of target compounds. However, this relation of equilibration time to solubility indicates no proportionality as only slight variation can be observed for the different compounds.

**Table 8.3: Comparison of the fitted rate constants, polymer-water partition coefficients, concentration dependent distribution coefficients and equilibrium concentrations in the bulk soil as relevant parameters for the uptake of LMW PAHs (Nap, Any and FlN), compared to the regular representative PAHs onto PE passive samplers within the batches.**

Compound	fitted $\lambda$ [day <sup>-1</sup> ]	Log $K_{pw}$ <sup>a</sup> [L/Kg]	Log $K_d^*$ [L/Kg]	$C_{s,eq}$ [ng/g] (OC normalized)
NAP	0.108	2.83	2.5	100 ( $\pm$ 3)
ANY	0.039	3.53	3.1	467 ( $\pm$ 47)
FLN	0.043	3.94	3.4	406 ( $\pm$ 22)
PHE	0.028	4.29	3.3	2769 ( $\pm$ 161)
FTH	0.024	5.01	3.8	6793 ( $\pm$ 254)
PYR	0.024	5.01	3.9	4676 ( $\pm$ 176)
ANT-D <sub>10</sub>	0.072	4.3	3.3	1000 ( $\pm$ 200)

For further details, the fitted rate constants ( $\lambda_{up}$ ),  $K_{pw}$ ,  $K_d^*$  and  $C_{s,eq}$  are compared for the six compounds and the *PRC* and listed in Table 8.3. In case of nonlinear sorption, the equilibrium concentration on the soil solids would affect  $\lambda$  by inducing faster exchange rates for lower  $C_{s,eq}$ . Therefore, the higher distribution coefficient of FlN compared to Any might be counterbalanced by slightly lower concentrations of FlN, leading to similar rate constants. In contrast to that, Fth and Pyr are characterized by almost the same  $K_d^*$  and demonstrate identical values for  $\lambda$  despite their difference in  $C_{s,eq}$ . Consequently, a compound specific uptake behaviour was only determined with respect to the smallest

(and therefore fastest) compound, Nap. In case of intraparticle diffusion within a heterogeneous suspension, exchange kinetics and characteristic times to reach equilibrium are predominantly influenced by the particle size (Equation 8.14). Therefore, uptake onto the sampler does not correspond to the distribution coefficient of the individual compounds.

### 8.4.3 Uptake onto PDMS coated jars

Figure 8.5 shows the outcome of the kinetic test performed with PDMS coated jars after 4 and 6 weeks of equilibration with soil slurries. Here, only Phe, Fth and Pyr provide reliable data for evaluating the uptake kinetics in PDMS for each of the coating thicknesses. At equilibrium a linear relation exists for the masses of target compound collected and the mass of the polymer. After 4 weeks Phe, Fth and Pyr are not in equilibrium for the 4  $\mu\text{m}$  PDMS coating. After 6 weeks however, uptake correlates linearly with thickness obtaining coefficients of determination between 0.94 (Pyr) and 0.99 (Phe). These observations support equilibrium conditions between soil slurry and passive sampler after six weeks. Compared to the equilibration with PE sheets, the PDMS illustrates significantly faster uptake kinetics. With the soil as limiting factor within the batches, faster uptake onto PDMS coating is most likely due to the respectively lower solid to liquid ratio (0.38), better mixing and contact of PDMS coating with the soil suspension. Other studies report equilibration times for PDMS coated jars with soil or sediment slurries of less than two weeks (Jahnke *et al.*, 2012, Mäenpää *et al.*, 2011, Reichenberg *et al.*, 2008). Here, however, the dataset for 2 weeks of rolling is excluded, since the measured concentrations are too close or below the limit of detection. The observed slow kinetics are most likely also due to agglomeration of solid particles as well as potentially strong sorbing particles within the soil suspensions. Thus, the slope of the linear regression at sampling after 6 weeks provides the respective equilibrium concentrations on the sampler with 170 ng/g Phe, 265 ng/g Fth and 164 ng/g Pyr. Additionally, the expected equilibrium concentration of Phe on PDMS was estimated based on mass balances (Equation 8.4) taking account of the corresponding  $K_{PDMS}$  and  $K_{Fr}$  yielding 230 ng/g. Hence, measured concentrations on the PDMS are notably lower than expected. In case of equilibrium, concentrations on the different coating thicknesses are supposed to serve as replicates, illustrating the same value (Mäenpää *et al.*, 2011, Jahnke *et al.*, 2008). Opposed to that, slight differences were measured within this study with 171, 158 and 218 ng/g of Phe for 1, 2 and 4  $\mu\text{m}$ , respectively. Therefore, the different methods for data analysis lead to varying equilibrium concentrations within the batches. The most precise results are expected to be obtained by combining the different thicknesses (as observed for the atmosphere).

However, the expected advantages of PDMS coated jars with rapid equilibration and simultaneous validation of equilibrium state were not observed within this study. The combination of low contaminant concentrations within the studied soils and very low amounts of PDMS generate an issue regarding limits of quantification for several of

the target compounds. A robust data set on the whole range of measured PAHs would be obtained by sampling higher masses of the target compounds. This could easily be maintained by increasing the mass of PDMS within each jar (Bruheim *et al.*, 2003). Higher masses lead to thicker coatings and consequently to proportional longer equilibration time, due to lower surface to volume ratios, as indicated in Equation 8.15 and Equation 8.17 for characteristic times. In theory, with desorption from soil as main limitation on exchange rates, a retarding influence of thicker coatings should be insignificant. Yet, Figure 8.5 demonstrates a considerably slower uptake of target compounds onto 4  $\mu\text{m}$  coatings opposed to 1 and 2  $\mu\text{m}$  PDMS coating, which remains unclear.

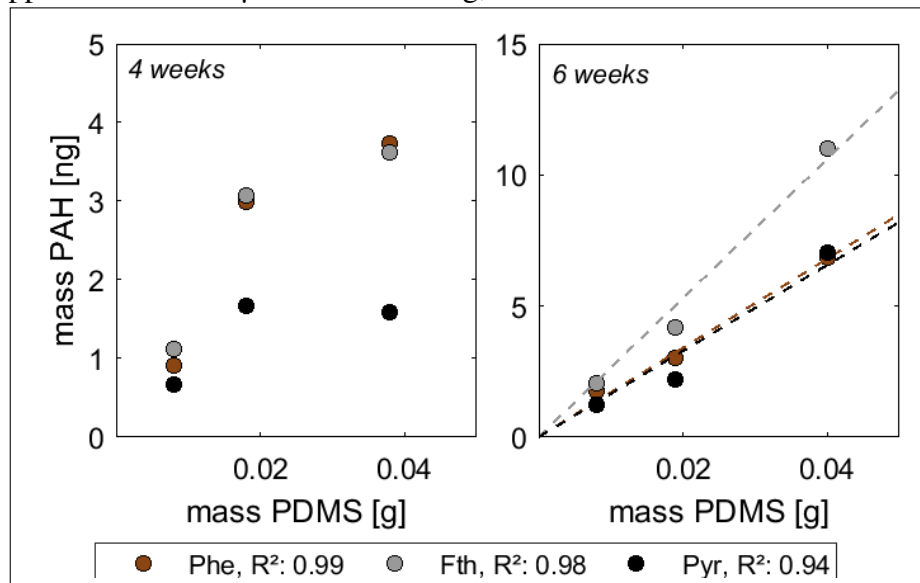


Figure 8.5: Masses of Phe, Fth, and Pyr plotted against mass of PDMS in the respective jars after a) 4 weeks (4  $\mu\text{m}$  coating not yet in equilibrium) and b) 6 weeks of equilibration.

#### 8.4.4 Passive samplers as mirror for natural organic carbon

The partitioning of target compounds between soil and water is mainly driven by soil organic carbon (OC) (Karickhoff *et al.*, 1979, Brändli *et al.*, 2008, Yang, Zhang, *et al.*, 2010, Yang, Tao, *et al.*, 2010). Consequently, the distribution of contaminants within the 3 phase system (soil solids – water – polymer) can directly be considered as distribution between natural organic carbon and the polymer. At equilibrium, concentrations on the polymer reflect the concentrations on natural organic carbon depending on the ratio of the respective partition coefficients:

$$\frac{C_{oc}}{C_p} = \frac{K_{oc}^*}{K_p} \quad (8.21)$$

with  $K_{oc}^*$  adapted for measured concentrations of the target compounds. In particular, for the preliminary tests organic carbon normalized equilibrium concentrations of Phe

#### 8.4 Results and discussion: Accurate passive sampling of PAHs in soils

were expected to exceed concentrations on the sampler by a factor of 6 for PE and a factor of 15 for PDMS. The characteristic distribution pattern of the U.S. EPA Priority PAHs in soil samples theoretically should be reflected by the passive sampler, provided that equilibrium conditions were reached. Figure 8.6 compares distribution patterns of PAHs determined in the bulk soil normalized to OC as well as for the PE passive samplers extracted at the different equilibration times. The characteristic distribution pattern observed for the 16 U.S. EPA Priority PAHs within the soil samples is almost identical to the PE sheets in the batch test at each time of sampling. This pattern is characterized by highest concentrations for Fth and Bbf-BkF, followed by the rest of the 4-ring PAHs. Phe and the 5-ring PAHs show comparable concentrations about half the value of Fth while DahA and LMW PAHs contribute only up to 10 % of the concentration of Fth. Thus, the distribution pattern of the 16 U.S. EPA Priority PAHs in soils can be determined with PE passive samplers at any time throughout the batch test.

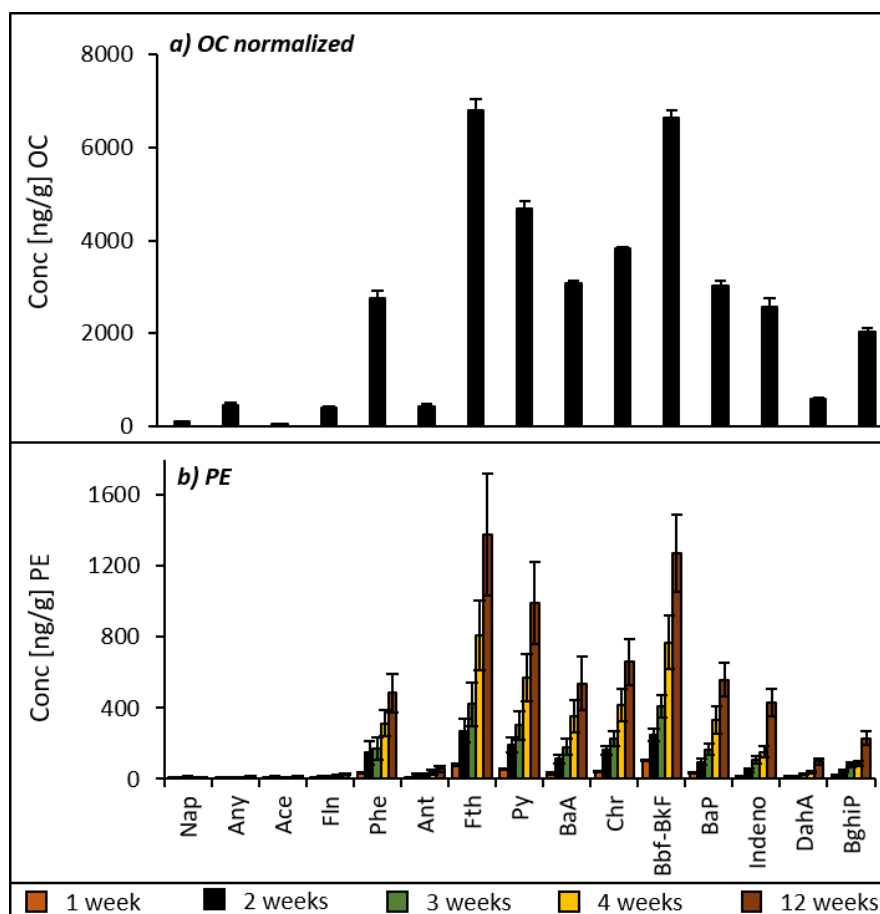


Figure 8.6: Distribution patterns of the 16 U.S. EPA Priority PAHs comparing a) OC-normalized concentrations in the bulk soil and b) PE in soil batches (error bars reflecting triplicates) after 1,2,3,4 and 12 weeks.

As a result, these stable distribution patterns confirm the previous observation of almost identical uptake rates for the whole range of examined target compounds. Consequently, the investigation of distribution patterns cannot not be used on its own to confirm equilibrium status. Measured concentrations on PE increase at each time step and for each target compound, indicating ongoing desorption from the soil sample (except for Nap). OC-normalized concentrations of the bulk soil still exceed concentrations on the PE samplers even after 3 months of equilibration by a factor of 5-8 for most compounds (Figure A.11), which is in perfect agreement with the above mentioned expectation. Therefore, the ratio of measured concentrations on the organic carbon and on the PE apparently illustrate equilibrium status within the batches after 3 months of shaking.

Figure 8.7 compares distribution patterns in soil normalized to OC and on the 4  $\mu\text{m}$  thick PDMS coating after 6 weeks of equilibration. The distribution patterns on PDMS reflect corresponding patterns in soil not as well as observed on PE samplers. Nap, for example, shows an unexpectedly high concentration, whereas Chr, BaP, Indeno and BghiP are considerably lower compared to the OC-normalized values of the bulk soil. No consistent ratio was observed for concentrations on OC and PDMS ranging from 5.6 for Nap to 1850 for DahA, yet without a notable compound-specific trend. Since most of the compounds were below the limit of detection on PDMS coatings with 1 and 2  $\mu\text{m}$  thickness, no replicates are available for proper data evaluation. Even with respect to the 4  $\mu\text{m}$  coated jar, the PDMS passive sampler seems less reproducible and less accurate compared to PE. Overall, none of the expected advantages considering PDMS coated jars as a fast and self-validating method to sample PAHs from soil suspension could be observed. The PE sheets, however, mirror the characteristic distribution patterns of contaminants within the observed soil samples and reflect almost the expected ratio of PE/OC concentrations also confirming equilibrium conditions. Consequently, PE sheets were chosen as appropriate passive sampling method for PAHs within batch tests. This is in accordance to the method of choice regarding the atmospheric sampling. Based on the results shown in Figure 8.2, the equilibration time was extended from 12 to 18 weeks for the following batch tests.



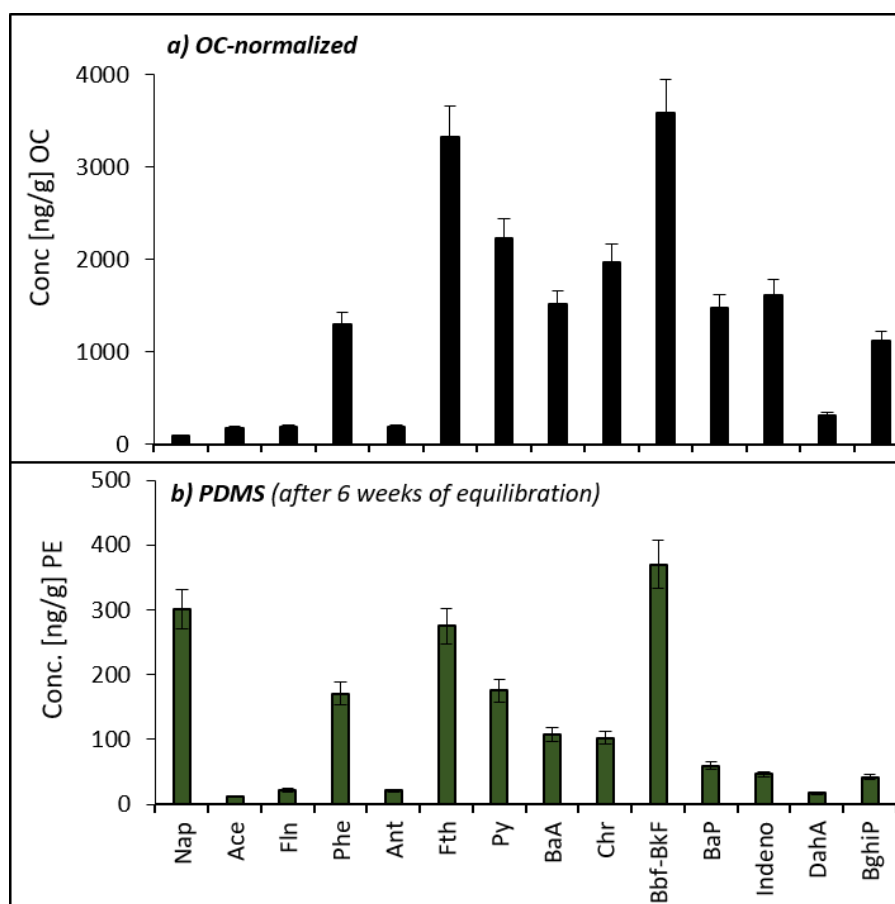


Figure 8.7: Distribution pattern of the 15 U.S. EPA Priority PAHs in soil, comparing a) the bulk soil with OC-normalized concentrations and b) PDMS batches, extracted after 6 weeks of equilibration.

## 8.5 Results and discussion: $C_{w,eq}$ within the three soil profiles

As described for the batch kinetic test, the loss of Ant-D<sub>10</sub> from the passive sampler was measured and related to the expected loss to determine the equilibrium state of the individual batches. The respective equilibrium status in percent is listed in Table 8.4, indicating notable differences for the three study sites. Apparently, Ant-D<sub>10</sub> reached equilibrium in each soil sample of the profiles in Poltringen and Tailfingen illustrating 94 - 112 % of the expected loss. The observed *PRC*-loss for the soil profile in Entringen varies between 69 and 89 % of the calculated loss, indicating a correlation for samples with a high  $f_{oc}$  attaining the highest degree of equilibrium. This relation is in contrast to the general observation; batch tests with soil samples from Poltringen and Tailfingen are characterized by low values of  $f_{oc}$  and yet the loss of Ant-D<sub>10</sub> from PE indicates equilibration. However, Table 8.3 illustrates no correlation of sorption kinetics and equilibration times to corresponding distribution coefficients. Thus, the varying degrees of

equilibrium for the different study sites underlines the complexity of ongoing processes and the need of further characterization of the examined soils and their respective influences on relevant time scales for PAHs to reach equilibrium.

**Table 8.4: Percentage equilibrium status determined for each batch based on the loss of Ant-D<sub>10</sub> from PE as PRC, after 4.5 months of equilibration and a liquid to solid ratio of 1.5.**

Location	Entringen	Poltringen	Tailfingen
Topsoil	89 %	101 %	94 %
Root horizon 1	86 %	100 %	97 %
Root horizon 2	86 %	103 %	96 %
Root horizon 3		107 %	97 %
Subsoil 1	77 %	103 %	97 %
Subsoil 2	69 %	112 %	98 %

Equivalent to the preliminary test, mass balances were used to estimate equilibrium concentrations of Phe on the sampler. Again, total concentrations of Phe in the bulk soil were used together with measured values of  $K_{Fr}$  (sorption isotherms) for each soil, applying Equation 8.4. Figure 8.8 compares the measured concentration of Phe on PE to the expected equilibrium concentration for the soil profiles at each site respectively. The concentrations observed in Poltringen demonstrate a good agreement with the estimated values, except for the lowest soil sample (which is characterized by the lowest concentration and highest uncertainty). For Tailfingen and Entringen, considerably higher concentrations were estimated than measured indicating non-equilibrium. As discussed above for the preliminary kinetic batch test, the loss of Ant-D<sub>10</sub> from passive samplers should only be used as a qualitative measure to compare different batches. Thus, an additional control on the equilibrium status of target compounds on the passive sampler in the individual batches is demonstrated in Figure 8.9, according to Equation 8.21. Here, the ratio of Phe concentrations on OC in soils to the concentration measured on the PE is related to the ratio of the respective partition coefficients  $K_{oc}^*/K_{pw}$ . At equilibrium both ratios are expected to be identical. In contrast to this expectation, the concentration ratio provides higher values compared to the ratio of the partition coefficients for most of the soil samples. Hence, for those samples Phe did not reach equilibrium on the passive sampler during the conducted batch tests. The set-up of these batch tests was slightly changed with the intention to reach equilibrium of target compounds on the passive sampler. The time on the horizontal shaker got extended to 4.5 months and the solid to liquid ratio was increased. Higher solid to liquid ratios, however, increases the potential of soil cluster formation and less mixing with the passive sampler. Therefore, longer diffusion path-

ways and less direct exchange between aqueous phase and passive sampler (as discussed in detail for the preliminary test) lead to slower kinetics.

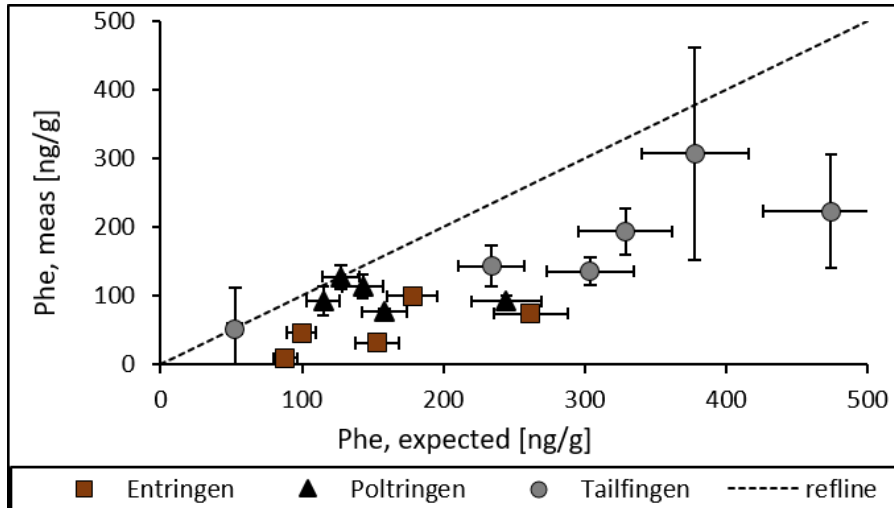


Figure 8.8: Measured versus estimated concentrations on the passive sampler of Phe after 4.5 months of equilibration, comparing Entringen, Poltringen, and Tailfingen. Error bars show the measured standard deviation of triplicate samples.

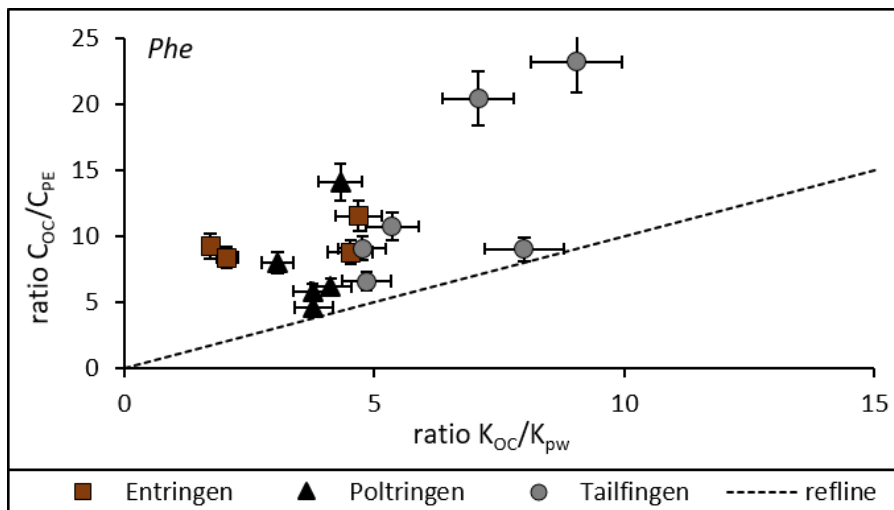


Figure 8.9: Scatter plot of concentration ratios of Phe in the bulk soil, normalized to OC and PE plotted against the ratio of the expected  $K_{oc}$  values and  $K_{pw}$  of Phe, shown for the soil profiles of Entringen, Poltringen, and Tailfingen. Error bars are set as 10 % assumed standard deviation.

If achieved, equilibrium concentrations on passive samplers allow to determine the freely dissolved concentrations in water ( $C_{w,eq}$ ). Complementary,  $C_{w,eq}$  can be estimated from concentrations in the bulk soil and Freundlich sorption isotherm parameters (Equation 8.1). Figure 8.10 shows the comparison of equilibrium concentrations of Phe determined with both approaches. Estimations based on Freundlich coefficients serve as an additional control on equilibrium conditions for the performed *ex situ* passive sampling. The encircled data points indicate concentrations determined with the different passive samplers for the same soil sample. For this sample, PE and PDMS passive sampler provide almost identical values with  $15.7 \pm 7.9$  ng/L and  $14 \pm 1.5$  ng/L. The different approaches to determine equilibrium concentrations in the water are in good agreement for some of the soil samples, indicating an average difference of about a factor of 2 (max at very low concentrations with a factor of 7). No correlation was observed with soil characteristics like grain size or  $f_{oc}$  values (data not shown here). In general, higher aqueous concentrations were calculated from the sorption isotherm than from partitioning between passive sampler and water. High water content during sampling in the field complicated the homogenization of the soil samples in Tailfingen. Therefore, considerably heterogeneous sub samples were produced, which can be observed by the broad spreading of measured concentrations for the profile in Tailfingen. In this case, soil clusters were observed right from the beginning. However, although the target compounds did not reach equilibrium between soil and water (and thus passive sampler), both PE sheets and PDMS coated jars provide a good estimate for Phe concentrations within the water.

Based on the unit-equivalent  $K_{Fr^*}$ , equilibrium concentrations in the aqueous phase were calculated for the whole range of U.S. EPA Priority PAHs and for all soil samples. Figure 8.11 shows the result of this approach in comparison to  $C_{w,eq}$  determined with PE passive samplers in *ex situ* batches including all horizons of the soil profile in Entringen. The respective results for Poltringen and Tailfingen are shown in the appendix (Figure A.12 and Figure A.13). For all three profiles a slight but systematic offset was determined with lower concentrations in the water measured than expected. Only in Tailfingen some of the 2-3 ring PAHs (particularly, Nap- Ace) illustrate identical concentrations in the water for both approaches. However, the measurement of generally lower concentrations than calculated confirms that 4.5 months is not sufficient to completely equilibrate PAHs in the chosen set-up.

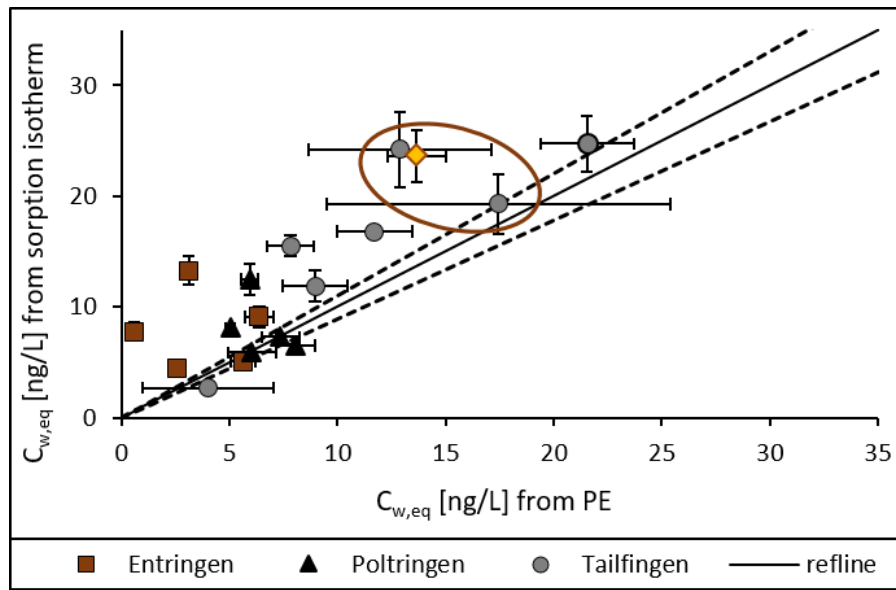


Figure 8.10:  $C_{w,eq}$  of Phe calculated according to the measured Freundlich sorption isotherm as well as based on the batch tests with PE for each soil sample in Entringen, Poltringen, and Tailfingen; the yellow diamond was calculated from PDMS. The solid line illustrates a ratio of 1:1 as reference, and dashed lines indicate  $\pm 10\%$  as confidence interval.

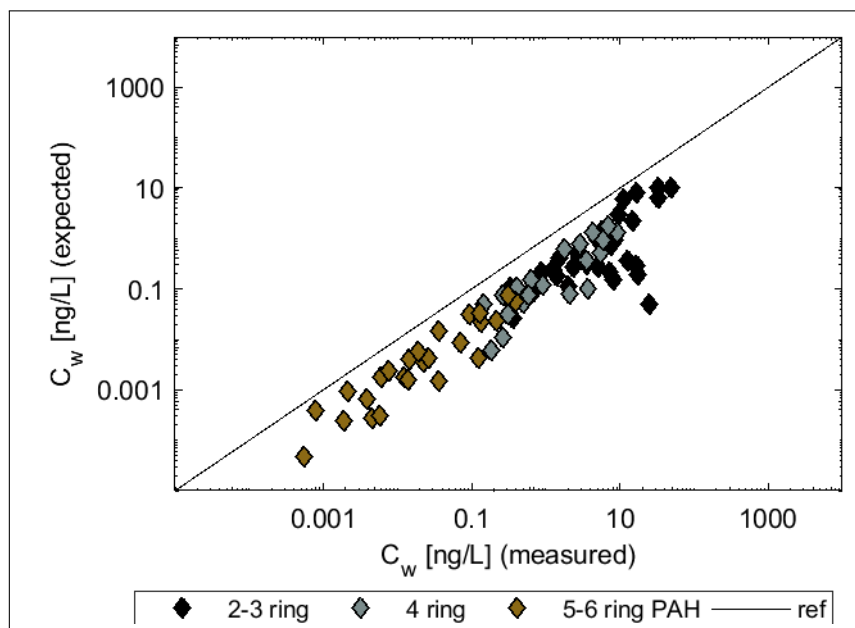


Figure 8.11: Comparison of  $C_{w,eq}$ , determined for the 16 U.S. EPA Priority PAHs with PE passive samplers in soil batches and calculated according to measured  $K_{Fr}$ , exemplarily for Entringen.

### 8.5.1 Vertical concentration profiles of PAHs determined with PE passive samplers

Concentration profiles of Phe, Fth and Pyr on the PE passive samplers are shown in Figure 8.12 for each of the study sites individually. The observed profiles of the representative PAHs on PE are in very good agreement with the previously determined profiles in the bulk soil normalized to OC shown in *Characterization of study sites - land use and soil properties*. Poltringen depicts the most homogeneous trend with almost constant concentrations throughout the whole profile. Tailfingen indicates homogeneous concentrations until 30 cm depth, followed by a significant decrease of concentrations, which relates to the depth of the plough horizon. In Entringen, an increase of concentrations was determined within the root horizons, up to 15 cm depth, followed by a slow decline. Measured concentrations are highest for Tailfingen and lowest for Entringen for all target compounds and each soil horizon, respectively. Again, this reflects the same observation as for the OC-normalized profiles. Consequently, the described *ex situ* batch tests with PE passive samplers provide a robust method to determine PAH soil profiles. Furthermore, the individual compounds illustrate an identical trend with depth, already relating to a stable distribution pattern of the PAHs throughout each whole profile. This can be interpreted as a first indicator that only one compound may be sufficient to describe the sum of the PAHs in the soil profiles and calculate the whole range of target compounds.

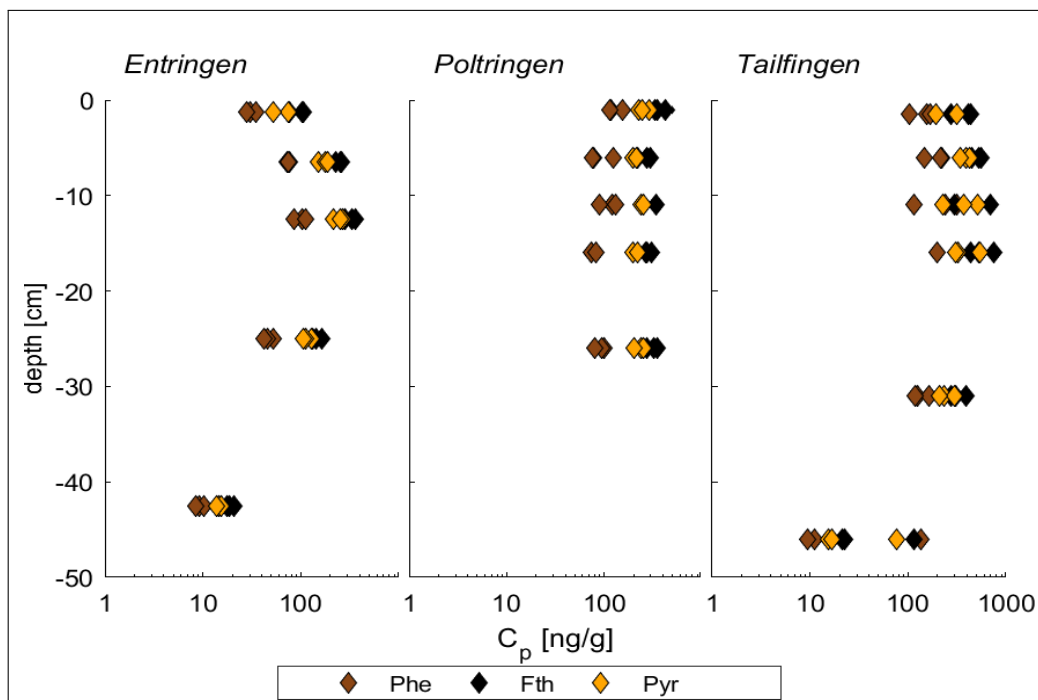


Figure 8.12: Concentration profiles of Phe, Pyr, and Fth at the three locations, measured on PE-sheets after the *ex situ* batch tests.

### 8.5.2 Distribution pattern and specific relations of individual compounds

As already indicated in Figure 8.12, the proportions of the individual PAHs are stable throughout the depth of the soil profile at each study site. As shown earlier, Freundlich sorption isotherms determined for Phe may be adopted for other target compounds, referring to their respective subcooled liquid solubility. Accordingly, equilibrium concentrations in the aqueous phase were estimated for the 16 U.S. EPA Priority PAHs and transferred into equilibrium concentrations on the passive samplers. Aiming for a good comparability, distribution patterns of the 16 U.S. EPA Priority PAHs were determined in percentage for the calculated equilibrium concentrations on the samplers. Figure 8.13 depicts a comparison of these distribution patterns in percentage for the different phases for Entringen exemplary. Concentrations measured in the bulk soil and on the passive sampler are compared to predicted concentrations on the sampler, according to the respective distribution and partition coefficients. See appendix for corresponding comparisons in Poltringen and Tailfingen (Figure A.4 and Figure A.14). The results illustrate distribution patterns that are well in line for the individual phases (bulk soil and PE), as well as for measured and calculated relations (with respect to PE) for all soil horizons.

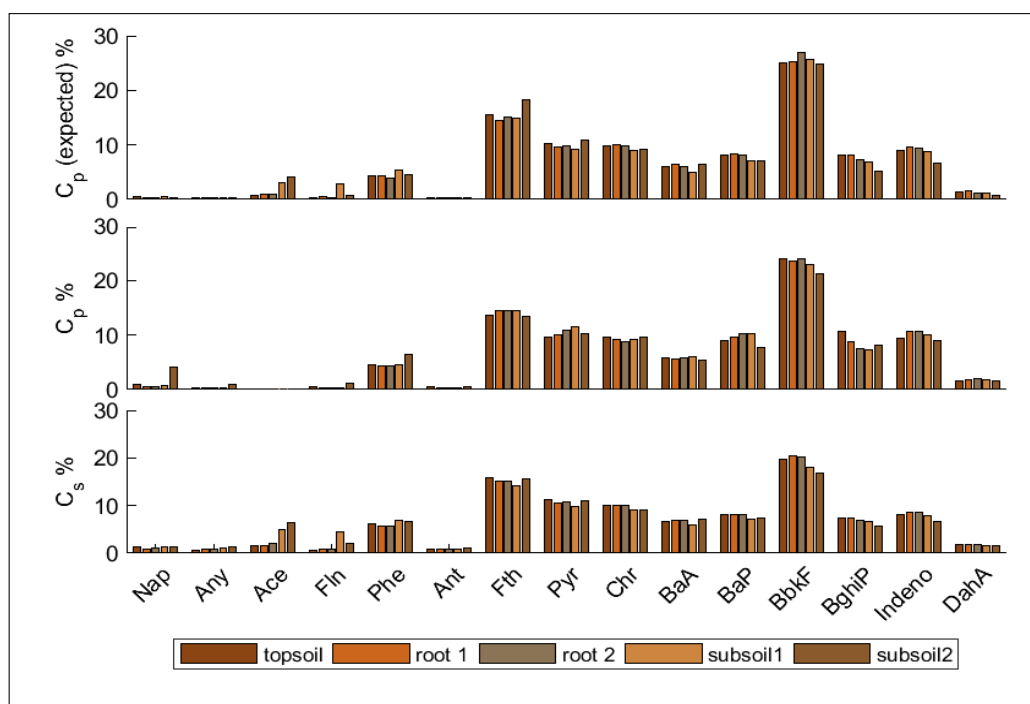


Figure 8.13: Distribution patterns of the 16 U.S. EPA Priority PAHs in each soil horizon in Entringen, determined for the bulk soil and comparing expected to observed patterns on PE passive samplers.

Therefore, it seems sufficient to focus on the distribution pattern of the 16 U.S. EPA Priority PAHs within the top soil when comparing the different locations. The respective

## 8 Passive sampling in soils

patterns are shown in Figure 8.14 regarding the bulk soil as well as the PE passive sampler subsequent to the *ex situ* batch tests. The same pattern is determined for each study site, illustrating the comparability of the three locations. Only minor variations can be observed for Entringen with a slightly higher amount of BghiP and slightly lower proportion determined for Fth compared to Poltringen and Tailfingen. Furthermore, higher contribution of Ant was observed in Tailfingen opposed to Entringen and Poltringen. In general, distribution patterns at the three study sites are in good agreement with literature (Wilcke, 2000).

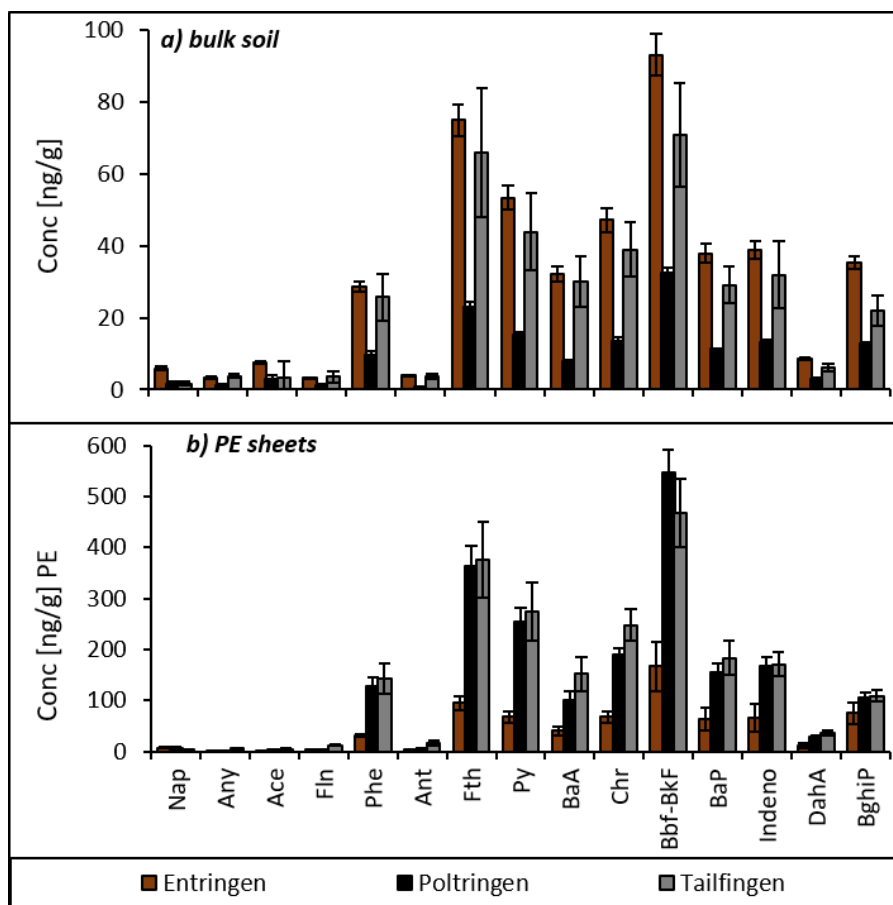


Figure 8.14: Distribution patterns of 16 U.S. EPA Priority PAHs determined for the top soils of Entringen, Poltringen, and Tailfingen regarding a) the bulk soil and b) the PE-sheets after shaking for 4.5 months.

Stable distribution patterns observed for each soil sample, independent of sampling the bulk soil or using PE sheets, supports the potential to determine equilibrium concentrations for the whole range of target compounds based on the measurement of only one compound. A corresponding approach has been introduced by Wilcke (2000), who determined a linear relation of BaP to  $\Sigma_{16}$  U.S. EPA Priority PAHs concentrations by



combining data sets of several studies on topsoils in temperate areas. This evaluation was also tested for the monitored study sites by relating measured concentrations of BaP and Phe to  $\Sigma_{16}$ U.S. EPA Priority PAHs as shown in Figure 8.15. Accordingly, clear linear relations can be determined for both compounds with coefficients of determination of 0.99 and 0.96 for BaP and Phe, respectively. Phe was chosen as reference compound as it is best characterized by sorption tests and provides robust measurements independent of the method and the sampled medium. Therefore, concentrations of all target compounds in one soil horizon for each location were also related to Phe.

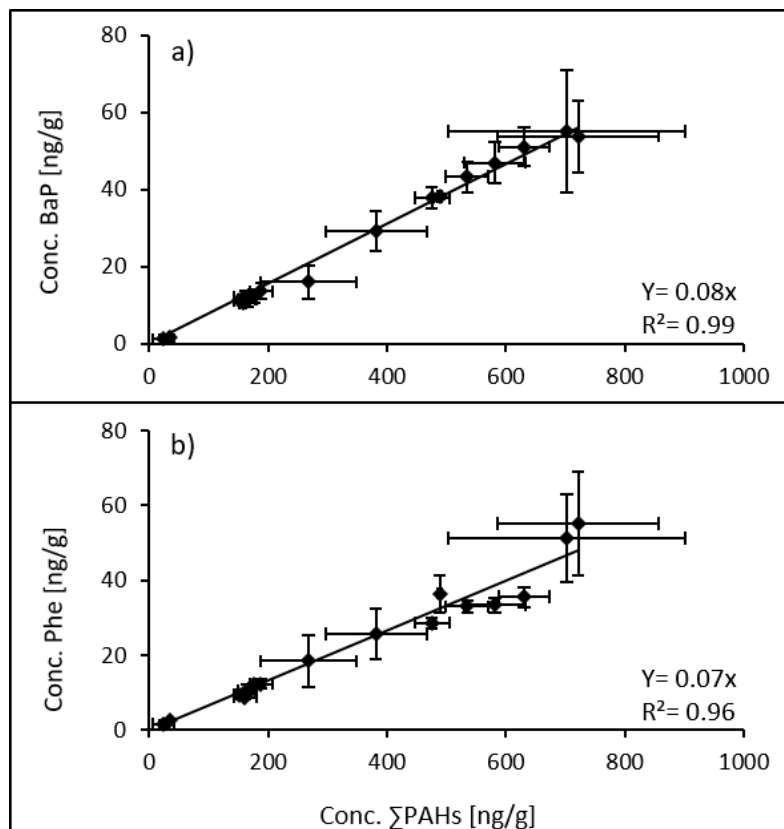


Figure 8.15: Linear relation determined for a) BaP and b) Phe to the sum of the measured U.S. EPA Priority PAHs considering all soil samples of Entringen, Poltringen and Tailfingen with error bars indicating the standard deviation of measurements in triplicates.

Subsequently, the specific ratios were applied to the rest of the soil horizons. Based on these ratios and measurements of Phe, the concentrations of the other 15 U.S. EPA Priority PAHs were estimated. This was done for the bulk soil as well as for the PE passive samplers individually. Results are shown in Figure 8.16 together with the 1:1 reference line as well as an offset of  $\pm 10\%$ . For the bulk soil, almost all data points plot within this confidence interval, while spreading of data on the PE is considerably more pronounced. The majority of the spreading can be related to the soil profile in Tailfingen, which rep-

represents the most heterogeneous samples. Yet, in general, the concentrations of the target compounds predicted based on Phe agree very well with measured concentrations in the bulk soil as well as the PE sheets. Thus, calculating concentrations of target compounds based on the measurement of Phe alone seems feasible.

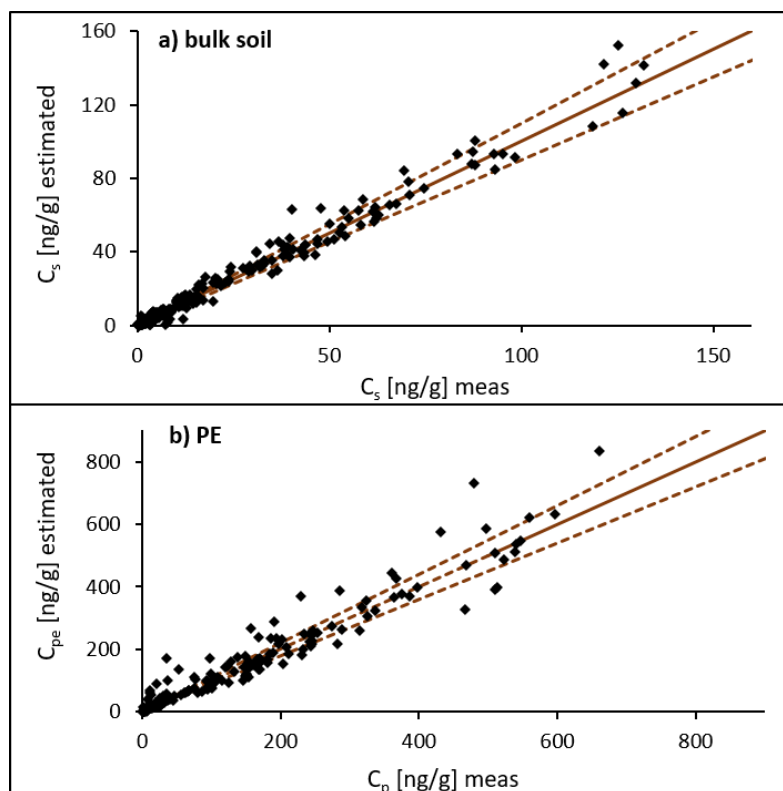


Figure 8.16: Comparison of measured concentrations of the 16 U.S. EPA Priority PAHs in bulk soil a) and PE b) to values predicted based on Phe and the distribution patterns.

The percentage contribution of the four representative PAHs to the sum of the 16 EPA PAHs was calculated, averaging for each soil profile as well as over all soil samples, as listed in Table 8.5. Relating individual compounds to  $\Sigma_{16}$  U.S. EPA Priority PAHs yields rather consistent contributions of 1-5 %, 6-7 %, 14-15 % and 9-11 % for Fl<sub>n</sub>, Phe, Fth and Pyr, respectively. This calculation was done for each soil horizon individually as well, including the respective standard deviation, as listed in Table A.6. Standard deviation depends strongly on the heterogeneity of sub samples and increases significantly for low concentrations, especially for values close to the limit of quantification. The contribution of the individual compounds to the sum of the PAHs, however, remains considerably stable over a wide range of soil samples and concentrations. This observation supports the advantage of using Phe as reference compound to minimize uncertainties of measurements. Additionally, PAH concentrations determined on 23 topsoils in Switzerland reported by Bucheli *et al.* (2004) were compared. The respective mean contribution of

Fln, Phe, Fth and Pyr to  $\Sigma_{16}$ U.S. EPA Priority PAHs within their work were 0.6, 8.4, 15.1 and 11.6 % which is in very good agreement to the observation of this study.

**Table 8.5: Contribution [%] of the four representative compounds Fln, Phe, Fth and Pyr to  $\Sigma_{16}$ U.S. EPA Priority PAHs, averaging for the individual soil horizons.**

Contribution [%] to $\Sigma_{16}$ EPA PAHs				
PAH	FLN	PHE	FTH	PYR
Entringen	2	6	15	11
Poltringen	5	6	14	9
Tailfingen	1	7	15	10
<b>overall</b>	<b>2</b>	<b>7</b>	<b>15</b>	<b>10</b>

### 8.5.3 Diagnostic ratios for PAHs on PE

Finally, diagnostic ratios of specific compounds were used as indicator for emission sources, as introduced in *Characterization of study sites - land use and soil properties*. Figure 8.17 shows the respective diagnostic ratios of (a) Fth/(Fth+Pyr) to Ant/(Ant+Phe) and (b) Indeno/BghiP to BaA/Chr for each soil profile considering the bulk soil, while Figure 8.18 shows the same ratios for the PE passive sampler. This comparison illustrates a distinctive differentiation for the bulk soil in comparison to the passive sampler. For instance, the relation of Ant to Phe within the bulk soil indicates traffic emission while the same compounds on PE sheets refer to combustion of organic material as main emission source. Considering the heavier compounds, differences of the individual ratios get more diverse. In Poltringen, the ratio of BaA/Chr is apparently stable but the ratio of Indeno/BghiP shifts from wood and vehicular to coal combustion for the soil and sampler, respectively. For Tailfingen, a rather constant relation of Indeno/BghiP was observed indicating coal combustion as the major emission source for the bulk soil as well as in the batch experiment. The relation of BaA/Chr shifts from coal and wood combustion for the bulk soil to mainly wood combustion observed on the PE. The soil profile in Entringen illustrates wood and coal as emission sources with respect to the bulk soil and a mixture of wood, coal and vehicular emission on the passive samplers. Regardless of these variations, the ratios based on heavier compounds indicate mainly on wood and coal combustion.

Although the stable distribution patterns and linear relationships between Phe, BaP and the sum of the U.S. EPA Priority PAHs suggest otherwise, PE passive sampler appar-

ently discriminate individual compounds during equilibration. Consequently, relating single (non-equilibrated) compounds to each other increases the uncertainty of data evaluation. This uncertainty gets less pronounced when taking account of a whole range of compounds instead of single PAHs. Following Hwang et al. (2003) the ratio of  $\Sigma$ HMW PAHs (Fth-BghiP) to  $\Sigma_{16}$ U.S. EPA Priority PAHs was determined for the bulk soil and PE sheets, respectively. This comparison provides a stable ratio of 0.8-0.9 for both the bulk soil and the passive sampler indicating combustion processes (presumably of wood and coal) as main emission sources of PAHs for the studied soils. Such a relation was expected for rural sites without explicit industrial areas in closer vicinity.

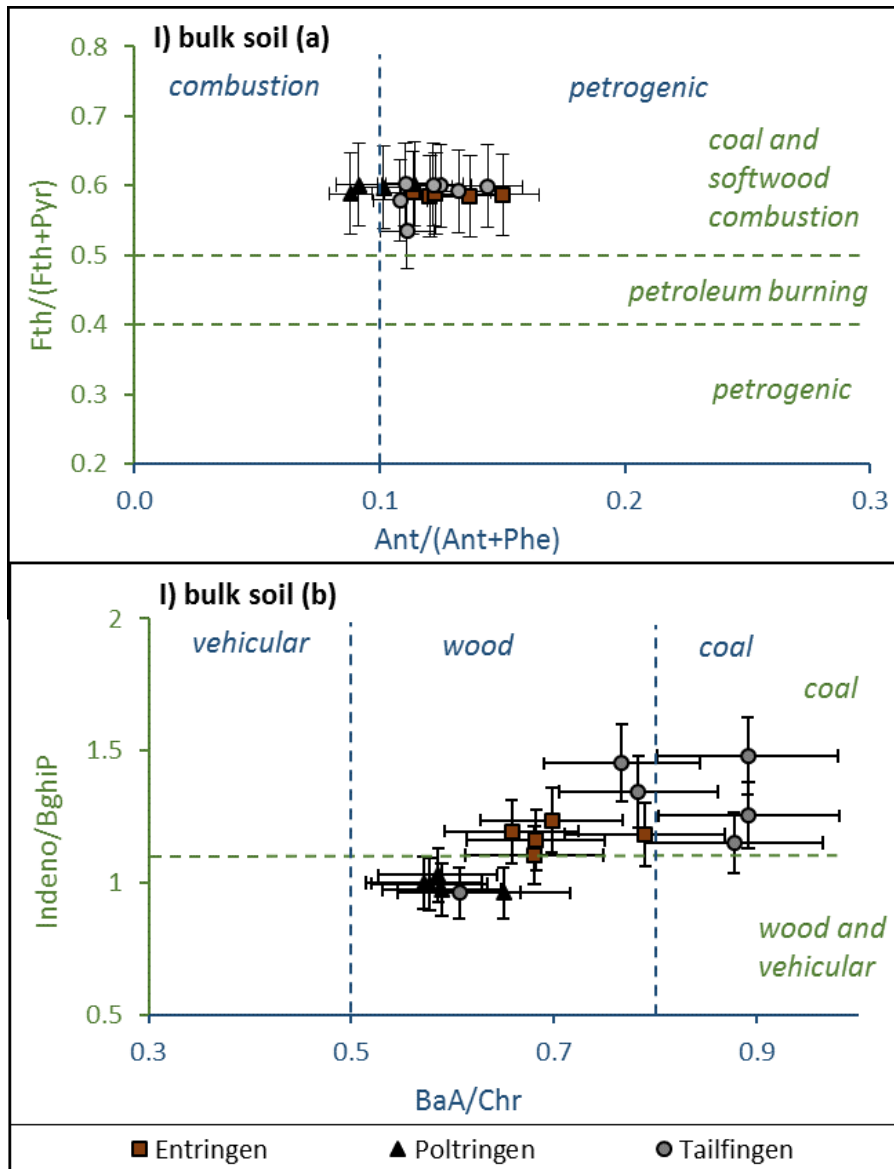


Figure 8.17: Diagnostic ratios relating a) Ant, Phe, Fth and Pyr and b) Indeno, BghiP, BaA and Chr to each other; determined for bulk soil samples (I), considering Entringen, Poltringen, and Tailfingen. Error bars indicate the measured standard deviation for triplicate samples.

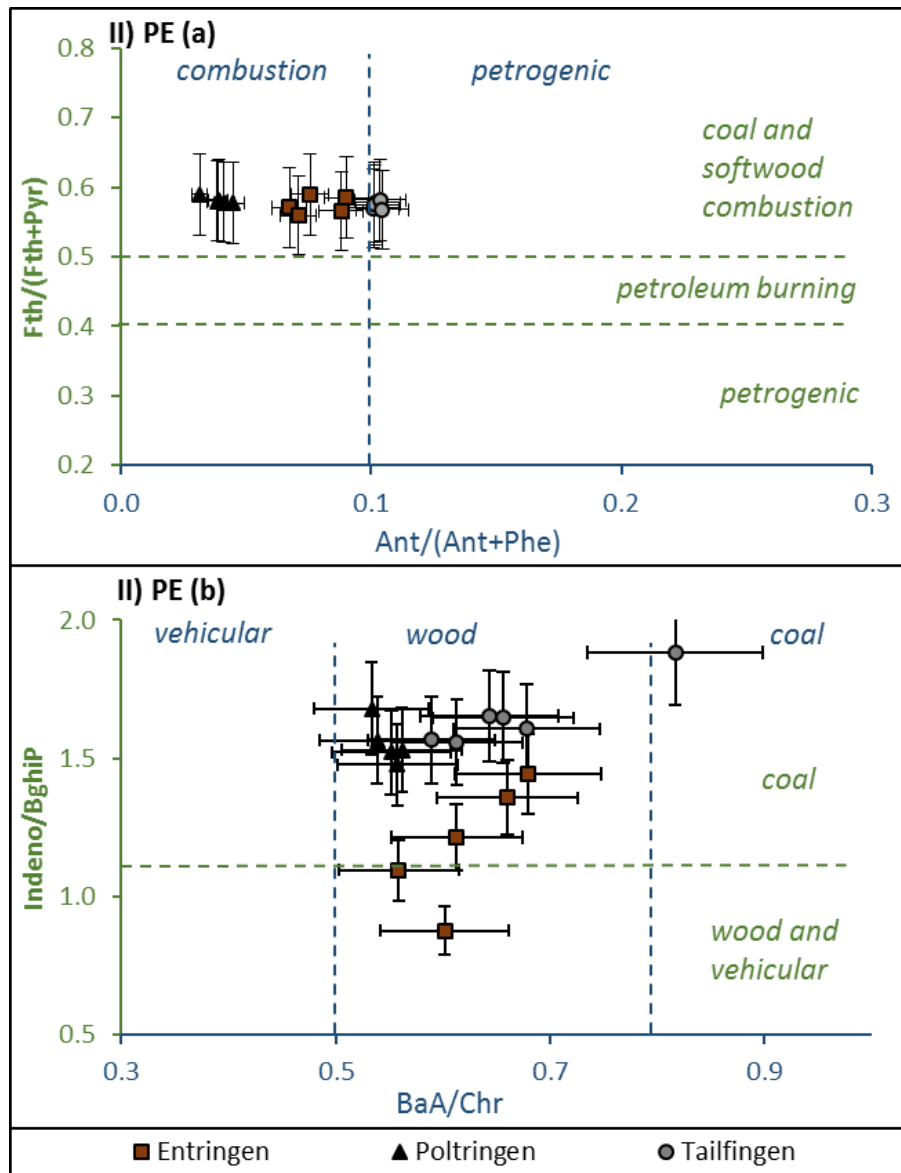


Figure 8.18: Diagnostic ratios relating a) Ant, Phe, Fth and Pyr and b) Indeno, BghiP, BaA and Chr to each other; determined for PE sheets from batch tests (II), considering Entringen, Poltringen, and Tailfingen. Error bars indicate the measured standard deviation for triplicate samples.

## 8.6 Conclusion

Exchange processes between soil and passive sampler are distinctively influenced by the soil properties and the set-up of the batch experiments, especially the homogeneity of the soil suspension. Uptake and release to and from passive samplers were observed to be limited by the soil sorption/desorption kinetics. A major issue of unexpectedly long equilibration times were observed, presumably due to small-scale features like agglomerates and lumps within the soil samples causing slow kinetics. Despite this issue, PE sheets provide reproducible and reliable concentrations of PAHs in soils and can be used to obtain freely-available aqueous concentrations. Furthermore, stable distribution patterns of the PAHs support the use of Phe as reference compound to estimate the concentrations of the 16 U.S. EPA Priority PAHs. However, slow equilibration led to slightly different distribution patterns on PE compared to soil solids which for source apportionment generates different specific ratios of the monitored PAHs. Finally, combustion of organic matter was determined as a general major emission source of PAHs in all soil samples.

## 9 Soil-atmosphere exchange

### 9.1 Theoretical background

PAHs are emitted into the atmosphere as gaseous matter and bound to particles during incineration of organic material (Marino *et al.*, 2000, Mantis *et al.*, 2005). Once in the atmosphere, PAHs are affected by numerous processes like sorption and volatilization to/from particles (including water droplets) as well as oxidation by atmospheric radicals and uptake by plants (Hippelein & McLachlan, 1998). Sorption to organic material in soils is a major process with respect to the fate of PAHs in the environment (Wilcke, 2000). Atmospheric deposition, as one of the main input pathways into soils (Garban *et al.*, 2002, Bozlaker *et al.*, 2008, Liu *et al.*, 2013), can be differentiated into gaseous, wet and particle-associated deposition. Transport of PAHs into subsoil layers may involve seepage water flow (including potentially particle facilitated transport), gas diffusion, bioturbation and agricultural activities (Harner *et al.*, 2001, Kuppusamy *et al.*, 2017). Soils have been reported as sinks for hydrophobic contaminants providing a major reservoir of PAHs in the terrestrial environment (Cabrerizo *et al.*, 2011a, b, Zhang *et al.*, 2011b, Bao *et al.*, 2015). In regions where environmental regulations lead to a reduction of concentrations in the atmosphere, semi-volatile legacy compounds may revolatilize and therefore soils may serve as a secondary source (Bao *et al.*, 2015, Bao *et al.*, 2016). Exchange processes between soil and the atmosphere concern mostly PAHs in the gas phase. Regarding the bulk soil, the availability of PAHs depends on the sorption capacity of soils, which is closely related to the quantity and quality of soil organic carbon (Cetin *et al.*, 2017b). Semi-volatile PAHs such as Nap, Ace, Any, Fl<sub>n</sub> and Phe may be released back into the atmosphere (Cabrerizo *et al.*, 2011b, Bao *et al.*, 2015, Cetin *et al.*, 2017a). Therefore, these interactions between soil and atmosphere are driven by two dominant aspects: the concentration gradient across the soil-atmosphere-interface and diffusion in gas phase in soils, which again depend on sorption of the respective compounds within soils. In order to assess fate and transport of pollutants within the environment, it is of relevance to characterize the source/sink relation of the atmosphere and soils as the compartments reflecting ongoing emission and main accumulation of PAHs. Several methods exist to determine the exchange of pollutants between soil and atmosphere and which are used to characterize the flux direction across the interface of those compartments: i) concentration gradients measured directly in the gas phase, ii) concentrations or pressures in gas phase calculated from concentrations in bulk soil and iii) concentration gradients measured indirectly using passive samplers as chemometers, which relate to the following points:

- i) Direct measurement of the gas phase is impractical because large volumes of soil-air have to be sampled, which is difficult in shallow soil profiles.
- ii) Calculations based on the bulk soil rely on uncertain empirical relationships to estimate distribution coefficients from organic content of soils.



- iii) Passive samplers mimick soil organic carbon by partitioning to a well-defined synthetic polymer, which accumulates hydrophobic compounds according to well-known partition coefficients.

Studying gaseous PAHs explicitly excludes the particle bound fraction within the atmosphere, which accounts for a substantial contribution of high molecular weight PAHs input into the soil (Garban *et al.*, 2002, Gocht *et al.*, 2007, Motelay-Massei *et al.*, 2007, Zhang *et al.*, 2011a). Consequently, for a coherent data set regarding the relation of PAHs in soil and atmosphere, the bulk input into the soil needs to be included. Hence, wet and dry deposition samplers were established at each location during the second year of sampling (May 2017-May 2018) to complete the information on the input of PAHs into the soil. The major objective of this study was to determine concentration gradients of PAHs across the soil-atmosphere interface. Prerequisites for reliable results include:

1. Reproducible concentration profiles of PAHs across the soil-atmosphere interface, independent of the chosen approach.
2. Seasonal variations with higher net deposition during colder months caused by high  $C_g$ s, and potential revolatilization during warmer months have to be captured.
3. Compound-specific differences of the flux direction, corresponding to their respective partition coefficients ( $K_{OC-air}$ ) have to be considered.
4. Dry deposition as major pathway of atmospheric PAHs into the soil has to be monitored in addition to the diffusive input to determine total accumulation of PAHs in soils.

### 9.1.1 Theoretical background for the mathematics of the different approaches

- i) Concentration gradients within the vapour phase calculated from concentrations in the bulk soil

Concentrations analysed in the bulk soil can be transferred into concentrations in the soil air. This holds if local equilibrium between soil solids, pore water and soil air exists and concentrations within the bulk soil are constant. The equilibrium distribution between the different phases can be calculated, provided that respective distribution coefficients are known;  $K_d^*$  for soil solids and pore water,  $H$  for pore water and soil air, and  $K_{soil-air}$  for soil solids and soil air, respectively. Since sorption of PAHs in soils is expected to depend solely on the organic carbon in soils, the accordingly normalized distribution coefficient  $K_{OC-air}$  is often employed (Harner *et al.*, 2000, Shoeib & Harner, 2002). However, most of them apply to linear partitioning and are not reliable if nonlinear sorption occurs and concentrations of interest are very low. In that case, sorption isotherms have

to be determined to obtain reliable distribution coefficients, (like the Freundlich coefficient in this study). Based on these coefficients, aqueous concentrations are obtained and subsequently, gaseous concentrations may be calculated based on Henry's law constant:

$$C_{soilair} = HC_{porewater} \quad (9.1)$$

Henry's law constants also exhibit considerable uncertainty (Harner & Bidleman, 1998, Booij & van Drooge, 2001).

ii) Concentration gradients on passive samplers

Booij and van Drooge (2001) combine uptake models of target compounds on passive samplers in air and water as a measure for the equilibrium status between both compartments:

$$\frac{N_{air}(t)}{N_{water}(t)} = \frac{C_{air}}{C_{water}K_{air-water}} \frac{1 - e^{(-k_{air} t)}}{1 - e^{(-k_{water} t)}} \quad (9.2)$$

$N$  denotes the amount of the target compound within the sampler at the sampling time  $t$  [s] and  $k_i$  refer to rate constants [ $s^{-1}$ ] for the samplers in air and water respectively. In case of equilibrium between air and water, the ratio of equilibrated passive samplers becomes one. As a result, measured concentrations on passive sampler in different media may be combined: The ratio of target compounds on both samplers (in equilibrium or at the same state of equilibrium) serves as direct indicator on the equilibrium status between the studied compartments. Morgan and Lohmann (2008) describe the same approach by referring to the dimensionless activity ( $a$ ) of target compounds. Activities can be used as a measure for the potential of a chemical to remain within the surveyed medium. Relating measured concentrations of a compound within a specific phase to its respective solubility ( $S$ ) provides its activity within this phase:

$$a_{PAH} = \frac{C_{PE}}{S_{PE}} = \frac{K_{PE} C_w}{K_{PE} S_w} = \frac{C_w}{S_w} \quad (9.3)$$

At a constant temperature, the solubility of the compound within the observed phase is constant and the equilibrium concentration behaves proportional to its activity. Hence, equilibrium concentrations on passive samplers deployed in different media can be used as a proxy for activity of the target compounds within different compartments (Reichenberg & Mayer, 2006, Cornelissen *et al.*, 2008). Therefore, concentration gradients measured on passive samplers indicate directly the flux direction of the target compound across phases (Morgan & Lohmann, 2008, Lohmann *et al.*, 2011). Relevant requirements for the application of this attempt are: equilibrium concentrations on the sampler (or correction for equilibrium), stable samplers (e.g. no swelling or shrinking) and passive sampling without depletion of the sampled medium.

## 9.2 Sampling and extraction

### Deposition sampler

Dry and wet deposition sampling was performed according to the sampling set-up and procedure developed by Grathwohl (2001) (DIN 19736). The respective field set-up comprises of a glass funnel with 25 cm opening at the top, 25 cm height of straight walls and a conical part with a degree of 50° ending in an outlet with 1 cm in diameter. Accordingly, the atmospheric deposition was monitored on an area of 0.049 m<sup>2</sup>. At the outlet of this funnel, a glass cartridge containing sorbing material (*Amberlite IRA-743*) was connected. This sorbing phase consists of macroporous polystyrene particles of 0.5-0.7 cm in diameter with N-methylglucosamine as a functional group which improves wettability of the material. Within the cartridges, the IRA material was fixed between two layers of quartz wool. The cartridge opened at the bottom with 0.5 cm in diameter providing an outlet for water sampled during precipitation events. As protection against potential photodegradation, the whole set-up was protected with a custom made aluminium cover.

### Preparation of the sorbing material (IRA)

Before use, the IRA material underwent several cleaning steps. First, it was rinsed several times with Millipore water and once with acetone (technical grade). Until pre-extraction at the Soxhlet, the material was stored within acetone. Subsequently, IRA was rinsed again with acetone of 99.9% purity (GC-Grade) and extracted at the Soxhlet for 3 days and 3 nights. While removing from the Soxhlet, the IRA material was kept moistened with acetone and direct contact to air was minimized. Several rinsing steps were performed with Millipore water to remove any remains of acetone. Finally, the cartridges were filled with wet IRA material and quartz wool, covered with Millipore water until installing at the field sites to avoid contact to air within the lab or during transport.

### Sampling and extraction

Sampling of the cartridges was generally performed as an exchange with a new cartridge, filled with clean IRA material. After taking the cartridges off the glass funnel, they were thoroughly sealed with parafilm at the bottom and Teflon-lined silicone caps at the top. Glass funnels were rinsed with approximately 250 ml of acetone to wash off any particles deposited to the glass wall before connecting the new cartridge to the outlet. For the extraction, IRA material was transferred into a 100 ml glass syringe and extracted 4 times for 10 minutes with 50 ml acetone. The combined extracts were spiked with 5 µl of internal standard (*PAH mix 31*) before reducing the volume at the rotary evaporator to about 100 ml. Subsequently, the PAHs in acetone were transferred into cyclohexane by adding 1700 ml millipore water and 30 ml cyclohexane and shaking the mixture for 30 minutes. After 12 hours and a clear separation, the cyclohexane phase was then transferred into round flasks and reduced to 1 ml at the rotary evaporator before measurement by GC/MS.

### 9.3 Data analysis

In accordance to the previous chapter, data evaluation is mainly focussed on Phe, since accurate distribution coefficients are known for this compound. Thus, the uncertainty of estimating equilibrium concentrations for separate phases was minimized. Three different methods to obtain concentration gradients in the vapour phase were used including the measurement of: i) the concentration in the bulk soil extracted with ASE, ii) concentrations on the PE subsequent to the ex-situ batch equilibration in a soil slurry, and iii) aqueous equilibrium concentrations based on the hot water extraction. Concentrations in the vapour phase were calculated as follows:

- i) First, concentrations of the bulk soil were transferred into concentrations of the aqueous phase based on measured Freundlich coefficients. Subsequently, multiplication with Henry's law constants (taken from the *New Jersey Department of Environmental Protection*) yields the corresponding concentration in the gas phase:

$$C_{soilair,Phe} = \left( \left( \frac{C_{bulksoil,Phe}}{K_{Fr,Phe}} \right)^{1/\frac{1}{n}} \right) H_{Phe} \quad (9.4)$$

As introduced in *Characterization of study sites - land use and soil properties*, solubility normalized Freundlich coefficients ( $K_{Fr}^*$ ) in combination with the compound specific subcooled liquid solubility ( $S$ ) provides the opportunity to estimate  $C_{porewater}$  for each compound  $i$  of the whole range of PAHs. This approach may also be applied for the calculation of  $C_{soilair}$ :

$$C_{soilair,i} = \left( \left( \frac{C_{bulksoil,i}}{K_{Fr}^*} \right)^{1/\frac{1}{n}} S_i \right) H_i \quad (9.5)$$

- ii) For the passive sampler  $K_{pg}$  values (taken from Lohmann *et al.* (2011), which are in perfect agreement with other studies (Adams, 2007, Smedes *et al.*, 2009)) were used to calculate respective equilibrium concentrations in the gas phase:

$$C_{soilair} = \frac{C_{PE}}{K_{pg}} \quad (9.6)$$

- iii) Aqueous concentrations based on the hot-water extraction were extrapolated according to the van't Hoff relation for ambient temperatures within the soil (10-20 °C). Concentrations in the soil air were calculated by multiplying the concentration of the pore water with Henry's law constant (Equation 9.1).

Since partitioning and sorption is strongly temperature dependent, the applied partition coefficients as well as Henry's law constant were adapted to the temperature within the soils (based on the general van't Hoff relation, introduced in *Background theory of passive sampling*). Consequently, transferring measured concentrations on the passive samplers as well as in the bulk soil into gaseous concentrations provides the opportunity to take this temperature dependency into account. Atmospheric monitoring results obtained with PE passive samplers were transferred into gaseous PAH concentrations using the same  $K_{pg}$  values as above. If needed, measured concentrations were extrapolated to equilibrium state based on the numerical model. Concentrations in the batch test with soil slurries did not reach equilibrium state to 100 % (as discussed in *Passive sampling in soils*). However, the resulting aqueous concentrations were in good agreement with mass balances and expected concentrations. Therefore, it seems sufficient to use the concentrations measured on the passive samplers for a direct comparison of both sampled compartments. The temperature effect on partition coefficients within the soil equally applies for both partitioning between soil solids and pore water (or soil air) and for partitioning between PE and pore water (or soil air) respectively. Consequently, this effect is balanced out for passive sampling in soils and stable concentrations on PE are obtained after equilibration.

## 9.4 Results and discussion

As shown before (*Correlation of PAH concentrations, uptake kinetics and environmental parameters* and *Concentration gradients of PAHs within the atmosphere*), the distribution patterns of PAHs in the atmosphere are rather stable throughout the seasons and very similar for the different study sites. They mostly vary between the different phases; particles, water and gas. Heavier compounds dominate the solid phase and lighter compounds are the main contributors within the gas phase. This is consistent with literature studies (Akyüz & Çabuk, 2010, Masih *et al.*, 2012, Verma *et al.*, 2017) and corresponds to expectations based on their respective partition coefficients (Pankow, 1987). Since Phe has relatively high concentrations in all three phases it may be used as a reference compound, as shown earlier.

### 9.4.1 Phe concentrations in soil air

Figure 9.1 illustrates a comparison of Phe concentrations within the soil air determined with concentrations of the bulk soil and measured sorption isotherms (Equation 9.4) versus concentrations determined with passive samplers from soil slurries (Equation 9.6). The concentrations included here refer to 20 ° C as field temperature within the soil during spring and summer. The respective comparison for concentrations adapted to 5° C as soil temperature during autumn and winter produces an identical trend and can be found in the appendix Figure 9.1. In general, both approaches provide Phe concentrations of the soil air within the same range, with highest variation up to a factor of four at low con-

centrations. The best agreement of both approaches can be observed for the soil profile in Poltringen. This profile is characterized by the most homogeneous soil samples on the one hand and additionally reaches the highest state of equilibrium between passive sampler and soil slurry on the other hand. Thus, transferring concentrations measured on the PE into  $C_{soilair}$  may provide the most reliable values for Poltringen compared to Entringen and Tailfingen. Besides, an overall trend was determined with slightly higher concentrations according to sorption isotherms compared to the passive samplers. This is most likely caused by the passive samplers, which do not equilibrate completely with the soil slurries during the batch test. Hence, concentrations in the soil air are underestimated according to the passive samplers.

Figure 9.2 shows a comparison of Phe in the soil air based on the hot-water extraction, which was performed exemplarily for Entringen, and concentrations determined with the respective sorption isotherms. Originally, the hot-water extraction was performed as an attempt to determine  $C_{soilair}$  with high resolution for the topsoil. Thus, concentrations are obtained for 4 soil layers within the uppermost 10 cm. For the up-most centimetre Phe concentrations are in very good agreement for both attempts. Yet, for the underlying soil samples  $C_{soilair}$  based on the hot-water extraction is much lower than determined with the sorption isotherm (up to a factor of 20). This may be due to extrapolating equilibrium concentrations from fairly high to low field temperatures which potentially underestimates the concentrations in the soil water. However, since several methodical issues occurred during this extraction (as discussed in *Characterization of study sites - land use and soil properties* the result of this approach is of limited reliability and won't be used for further data evaluation or discussion.

Overall, the measured sorption isotherms ( $K_{Fr}$ ) provide an accurate basis to obtain reliable  $C_{soilair}$  for each soil sample. Consequently, concentration gradients for the gas phase across the soil-atmosphere interface are based on this approach.

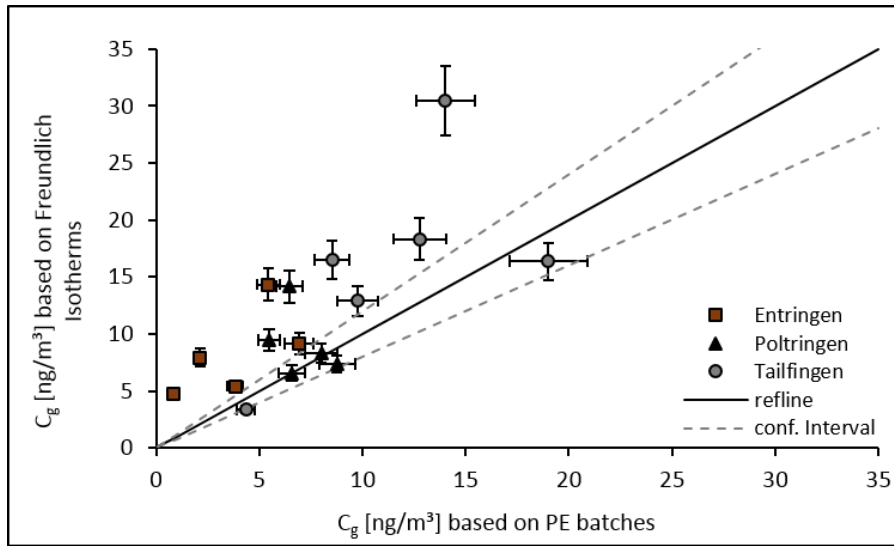


Figure 9.1: Comparison of Phe concentrations in the soil air (for 20°C) based on measured Freundlich coefficients versus PE equilibrated with soil slurries, determined for Entringen, Poltringen and Tailfingen individually.

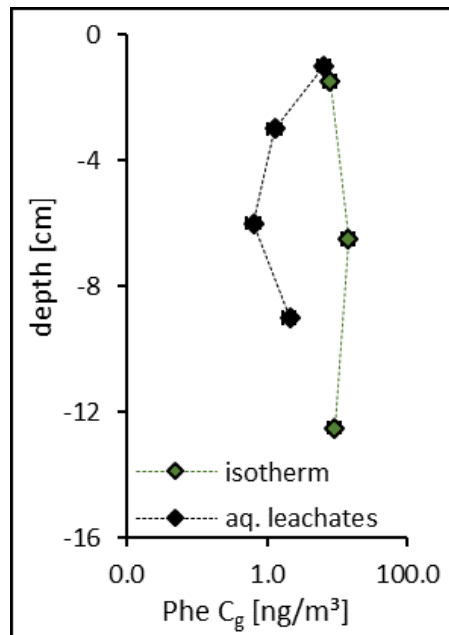


Figure 9.2: Comparison of Phe in the soil air based on the hot-water extraction and measured sorption isotherms, both referring to 20° C as soil temperature during summer. Error bars indicate 20% standard deviation..

#### 9.4.2 Seasonally varying concentrations gradients across the soil-atmosphere interface

Seasonal concentrations of Phe in the atmosphere are well comparable for both years during spring and summer on the one hand and autumn and winter on the other hand (as listed in Table A.7 and Table A.8). Additionally, to account for seasonal varying temperatures within the soil, temperature data were obtained by the *German Weather Survey*, referring to the same station as for the ambient air temperature measurements. This data set reflects stable temperatures for four horizons (5, 10, 20 and 50 cm depth), as listed in Table 9.4. Therefore, temperature-adaption for concentrations of the soil air refers to one temperature during August (20 °C) and November (5 °C) for all depths, respectively. Hence, the examination of seasonal variations for the soil-atmosphere exchange simply refers to winter vs. summer concentrations in both compartments. Figure 9.3 illustrates Phe profiles in the gas phase across the soil-atmosphere interface with  $C_{soilair}$  based on the bulk concentration of Phe within the soil samples and applying the determined  $K_{Fr}$  values. Shown here is the second year of monitoring campaigns, including the two sampling heights in the atmosphere. (The first year of sampling is shown in the appendix, in Figure A.16.) Concentrations based on the sampler at 0.1 m above ground were adjusted for higher temperatures estimated below the cover, as discussed in *Concentration gradients of PAHs within the atmosphere*. Thus, the samplers right above ground should be considered qualitatively rather than quantitatively. As expected, higher concentrations in the soil air during summer compared to winter were observed due to the higher volatility of Phe at higher temperatures. Correspondingly, seasonal variations of concentration profiles across the soil-atmosphere interface occurred. During winter the concentrations within the soil air are notably lower than in the atmosphere, which leads to atmospheric deposition as ongoing process. Conversely during summer, the atmospheric concentrations are considerably lower than concentrations within the soil air. Accordingly, the profiles indicate revolatilization of Phe for the summer monitorings. The described relation and seasonal variation of Phe in soil air and atmosphere was determined for each of the study sites. Only minor variations can be observed in terms of concentrations within the soil air of 7.9, 7.4 and 12.9 ng/m<sup>3</sup> in the topsoil of Entringen, Poltringen and Tailfingen during summer and 1.4, 1.3 and 2.3 ng/m<sup>3</sup> during winter, respectively. Thus, highest Phe concentrations within the soil air were determined in Tailfingen, corresponding to highest concentrations of PAHs in the bulk soil.



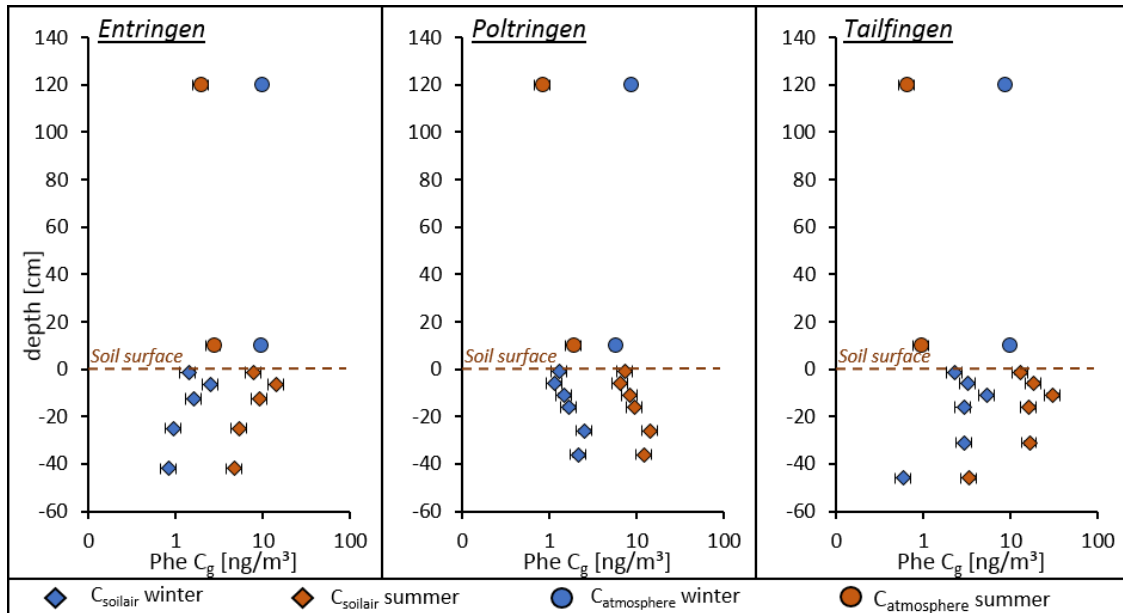


Figure 9.3: Phe concentration profiles in gas phase, in the atmosphere measured by passive sampling and in the soil calculated from the bulk soil concentration and measured Freundlich coefficients comparing summer (with 20 °C) and winter (5 °C) at the different locations.

Figure 9.4 illustrates the initial idea of this study by directly comparing Phe concentrations measured on the passive samplers in both compartments during the second year of monitoring. (See Figure A.17 for the first year of sampling.) As introduced above, the concentrations on the sampler from the soil batches are independent of temperature variation, because both coefficients ( $K_d$  and  $K_{pw}$ ) depend to the same extent on the temperature. With increasing temperature  $K_d$  decreases, leading to higher concentrations in water, while simultaneously  $K_{pw}$  decreases and thus  $C_{PE}$  remains stable. Phe concentrations on PE sampled in the atmosphere are included for each seasonal monitoring campaign individually, as equal concentrations in the gas phase may result in different concentrations on the sampler. In general, seasonal variation of concentration gradients can be observed by referring directly to the samplers, similarly to the gas phase shown in Figure 9.3. Net deposition is indicated by higher concentrations in the atmosphere in Poltringen and Tailfingen during autumn and winter. Higher concentrations within the soils during spring and summer, however, indicate revolatilization. Except for Entringen, where during August 2017 the passive samplers have equal concentrations in the atmosphere and the soil, which illustrates equilibrium for the two compartments. Additionally, during May 2017 higher concentrations were determined on the sampler in the atmosphere than for samplers from soil batches. Thus, for Entringen this approach indicates a continuous net deposition of Phe, with temporal equilibrium between soil and atmosphere, but no revolatilization. Since the batch test with soil samples from Entringen was furthest away from equilibrium, this observation may be due to underestimated

## 9 Soil-atmosphere exchange

Phe concentrations for the soil profile using PE. On the other hand, the soil samples in Entringen are characterized by the highest content of organic carbon, with  $f_{oc}$  being up to 10 fold higher compared to (top-) soils in Poltringen and Tailfingen. Thus, PAHs accumulated in the soil in Entringen are less likely to be released again.

However, using concentrations measured on the passive samplers directly without transferring them into another phase illustrates a reliable trend of Phe across the soil-atmosphere interface and captures seasonal variations of the respective flux.

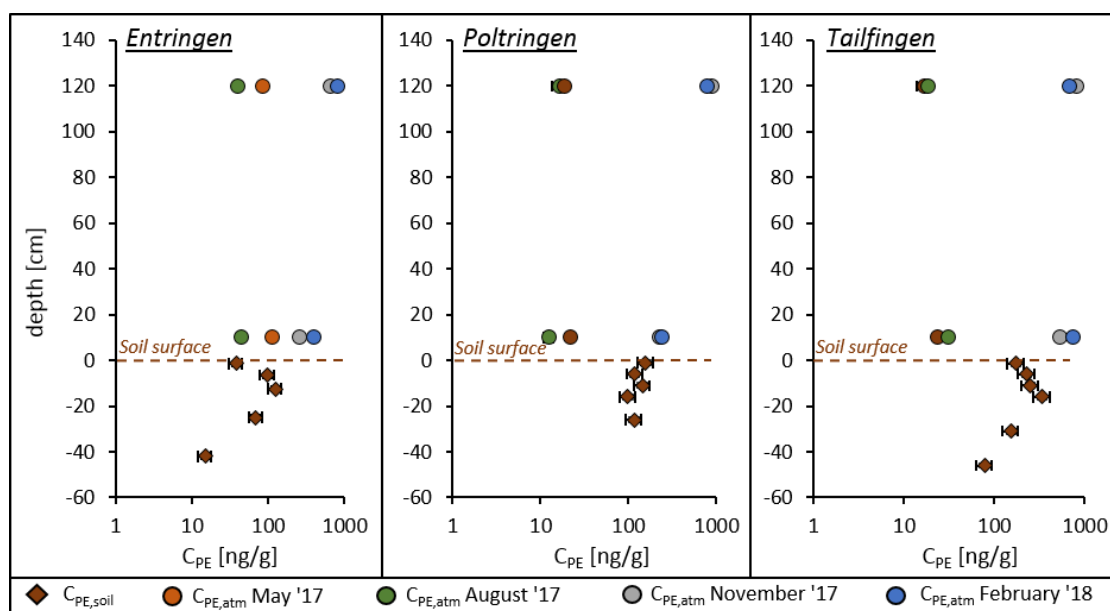


Figure 9.4: Seasonal concentration gradients of Phe across the soil-atmosphere interface, directly comparing passive samplers deployed in both compartments at each of the study sites during the second year of monitoring campaigns.

A more detailed insight considering the flux direction is given by concentration ratios of Phe in the atmosphere versus the soil, listed in Table 9.1 and Table 9.2 referring to concentrations in the gas phase and on the samplers (at 1.2 m height), respectively. As an indicator for the activity of target compounds within the sampled medium, passive samplers provide additional information beyond the mere concentration within the respective phase (here gas). In general, those concentration ratios are very consistent for both years of sampling as well as for both phases (gas and PE). Slight differences for  $C_g$  ratios may be induced by the uncertainty of Henry's law constant. Furthermore, in Entringen  $C_{PE}$  ratios during November and February exceed the respective ratios in Poltringen and Tailfingen considerably by a factor of 3 - 4. Average temperatures in air and soil for each monitoring are listed in Table 9.3 and Table 9.4.

**Table 9.1: Concentration ratios of Phenanthrene in the gas phase (atmosphere/soil) determined with respect to sampling at 1.2 m height for each atmospheric monitoring at each location individually for both years of sampling.**

1.2 m height	1 <sup>st</sup> year C <sub>g</sub> ratios (atm/soil) (May 2016 – February 2017)			2 <sup>nd</sup> year C <sub>g</sub> ratios (atm/soil) (May 2017 – February 2018)		
	Entringen	Poltringen	Tailfingen	Entringen	Poltringen	Tailfingen
Monitoring						
May	0.2	0.2	0.1	0.2	0.1	0.1
August	0.3	0.1	0.1	0.2	0.1	0.1
November	5.9	8.0	4.5	2.8	6.7	3.8
February	5.4	8.3	4.2	6.2	3.5	2.0

**Table 9.2: Concentration ratios of Phenanthrene on PE passive samplers (atmosphere/soil) at 1.2 m sampling height for each atmospheric monitoring at each location individually for both years of monitoring.**

1.2 m height	1 <sup>st</sup> year C <sub>PE</sub> ratios (atm/soil) (May 2016 – February 2017)			2 <sup>nd</sup> year C <sub>PE</sub> ratios (atm/soil) (May 2017 – February 2018)		
	Entringen	Poltringen	Tailfingen	Entringen	Poltringen	Tailfingen
Monitoring						
May	1.5	0.2	0.2	2.2	0.1	0.1
August	0.9	0.1	0.1	1.0	0.1	0.1
November	20.1	6.3	5.5	17.2	5.6	4.6
February	16.0	5.4	4.4	20.9	5.0	3.9

**Table 9.3: Average ambient temperatures [°C] during the seasonal atmospheric monitorings, covering both years of sampling, data taken from *German Weather Survey*.**

Monitoring	1 <sup>st</sup> year (May 2016 – February 2017)	2 <sup>nd</sup> year (May 2017 – February 2018)
	May	15.6
August	21.7	20.6
November	4.5	5.1
February	4.8	-1.2

**Table 9.4: Average soil temperatures [°C] in different depths during each of the seasonal monitorings, data taken from *German Weather Survey*.**

Monitoring	5 cm	10 cm	20 cm	50 cm
May 16/ 17	15/ 15.5	14.4/ 15	13.8/ 14.3	12.6/ 13
August 16/ 17	20.8/ 21.3	20.4/ 20.8	20.1/ 20.7	19.2/ 19.7
November 16/ 17	5.5/ 5.8	5.7/ 5.9	6.8/ 7	8/ 8.2
February 17/ 18	2.8/ 1	2.7/ 1.2	2.6/ 2.2	2.7/ 3.2

### 9.4.3 Compound specific relations between soil and atmosphere

Due to sorption to organic matter as one of the major influences on exchange processes between soil and atmosphere (Ribes *et al.*, 2003, Bozlaker *et al.*, 2008, Degrendele *et al.*, 2016, Cetin *et al.*, 2017b), the flux direction of the respective target compounds may vary in relation to their solubility. Amongst others, Cousins and Jones (1998) and Demircioglu *et al.* (2011) demonstrate a temperature-dependent flux direction across the soil-air interface for Fl<sub>n</sub> and Phe, but net deposition of Fth and Pyr. Figure 9.5 compares concentrations of the four representative PAHs for summer and winter sampling campaigns in the atmosphere during the two years of monitoring to the topsoil at the three study sites. Extrapolation of Fth and Pyr for equilibrium concentrations on passive samplers induces considerable uncertainties due to exceedingly long characteristic times (shown in Figure A.5 – Figure A.19). Therefore, concentrations in the gas phase are considered here for both the atmosphere and the soil. Atmospheric concentrations refer to the samplers at 1.2 m height only, aiming to exclude the discussed uncertainty of temperature-induced underestimation for concentrations measured on the samplers right above ground. Generally, a clear seasonally alternating flux direction is observed independent of the study site, the year of sampling or the examined compound. During November and February, all compounds show higher concentrations in the atmosphere and therefore net deposition occurs. Conversely, during spring and summer the surveyed compounds indicate net volatilization from soil. Considering concentrations on the sampler instead of the gas phase generates the same overall trend (Figure A.20). Only slight variations can be observed for Entringen with Fl<sub>n</sub> and Phe on the PE indicating equilibrium between atmosphere and soil during warm sampling periods.

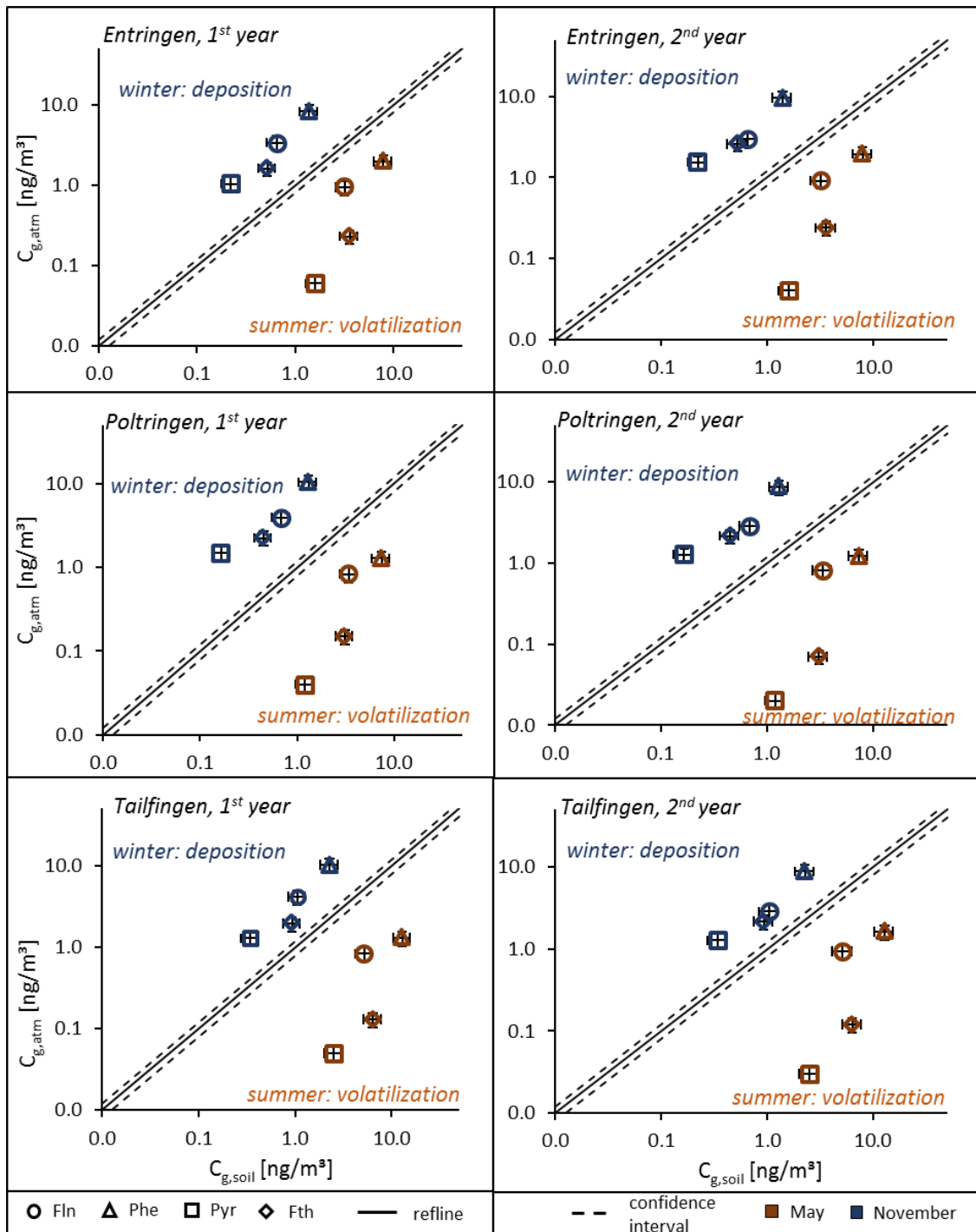


Figure 9.5: Double logarithmic scatter plots of seasonal atmospheric concentrations of Fln, Phe, Fth and Pyr to estimated concentrations of the soil air in the topsoil, both based on passive samplers. Concentrations on the sampler within the atmosphere were extrapolated during November and February (of both years) to obtain equilibrium conditions. Error bars indicate the measured standard deviation for triplicate samples, the reference line depicts a ratio of 1:1 and the confidence interval includes 20 % deviation.

With respect to the studied compounds, the examined relation between soil and atmosphere (when referring exclusively to the gas phase) appears only to a minor extent to be compound-specific. In contrast, the observed variation in Entringen underlines soil properties as the main influence on the soil-atmosphere exchange of semi-volatile compounds. Similarly, Wang *et al.* (2014) and Luo *et al.* (2015) identify the direct gaseous PAH exchange across the soil-atmosphere interface as mainly site- and not compound-specific. Although calculated vertical profiles of  $C_g$  provide correct concentration gradients across the soil-atmosphere interface for the gas phase, the determination of the total fluxes also requires the particulate input into soils. Essentially, for compounds with higher molecular weight the particle bound deposition potentially exceeds the gaseous flux (Wong *et al.*, 2004, Demircioglu *et al.*, 2011).

### 9.4.4 Atmospheric bulk deposition

Particle deposition is expected to contribute a significant fraction of PAHs to the overall input into soils (Leister & Baker, 1994, Garban, 2002, Gocht *et al.*, 2007, Peng *et al.*, 2016). Seasonal atmospheric bulk deposition of the representative PAHs is shown as aerial deposition flux per day in Figure 9.6, while Figure 9.7 shows the respective distribution patterns for the three study sites (as percentages). The observed deposition rates as well as the distribution patterns of the representative PAHs are in very good agreement for the different locations. Between May and August, only Tailfingen showed significantly lower values of Fl<sub>n</sub> and Phe compared to Entringen and Poltringen. Besides that, Phe and Fth each contribute 40 and 35 % to the sum deposition of the four representative U.S. EPA Priority PAHs. Pyr contributes around 22%, also independent of the monitoring period, while Fl<sub>n</sub> only accounts for ca. 5%. Highest deposition rates were measured between November and February with 10, 70, 60 and 35 ng/m<sup>2</sup>/day for Fl<sub>n</sub>, Phe, Fth and Pyr, respectively. Lowest values were detected during August-November with 0.3, 2.5, 2.7 and 1.8 ng/m<sup>2</sup>/day. The seasonally varying deposition rates with highest deposition during autumn and winter coincide with higher gaseous concentrations during colder months indicating higher atmospheric emission rates during autumn and winter. Additionally, the consistency of distribution patterns for the deposition throughout the year is in good accordance to rather stable distribution patterns determined for the seasonal atmospheric monitorings. Consequently, both the concentration of PAHs in the gas phase and their atmospheric bulk deposition suggest consistent sources throughout the year, mainly varying in the overall emission rate. A fourth sampling location in Tübingen was included for Figure 9.7 (unpublished data provided by Stephanie Müller, 2018). This enables the comparison of the rural study sites to a sampling location close to the city center of Tübingen. Yet, despite the vicinity to a broader range of emission sources, the same distribution pattern was determined for the atmospheric deposition of Fl<sub>n</sub>, Phe, Fth and Pyr as for the rural sites. This confirms a well-mixed ABL as a main reason for the homogeneous concentrations observed at the individual locations.

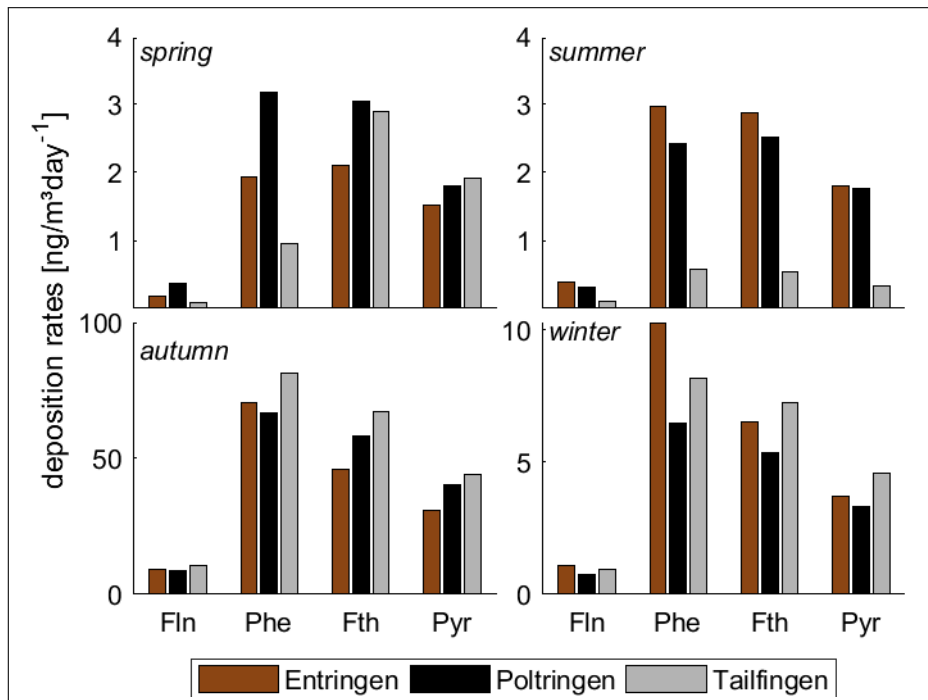


Figure 9.6: Seasonal deposition rates [ng/m²/day] of the four representatives, sampled at the three study sites during the second year of monitoring (May 2017- May 2018).

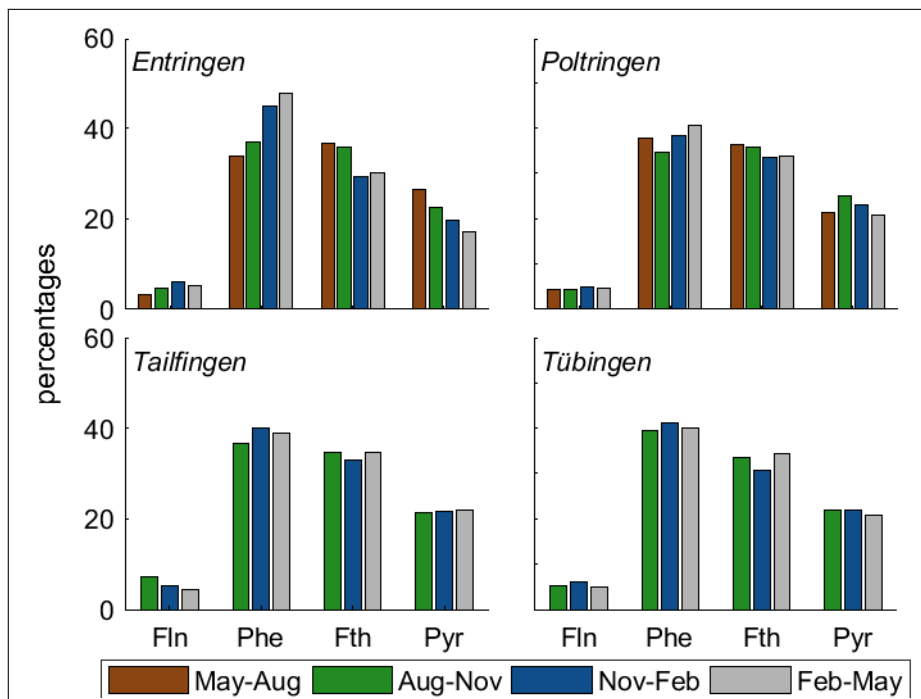


Figure 9.7: Seasonal distribution patterns (in %) of the atmospheric deposition for Fln, Phe, Fth and Pyr comparing the three study sites to an additional location, close to the city centre of Tübingen.

The sum of deposition rates for 12 PAHs (excluding Nap, Ace, Any and Fl<sub>n</sub> as LMW PAHs) was calculated (in  $\mu\text{g}/\text{m}^2/\text{year}$ ) for comparison to literature results (Table 9.5). Relatively low deposition rates were determined within this work. Kiss *et al.* (2001) reported PAH deposition exceeding the measured values by a factor of twelve, although sampling was also executed at a rural site; at Lake Balaton in Hungary. The authors' explanation for distinctively high concentrations and PAH deposition refers to the influence of westerly winds carrying substantial loads of pollutants from highly industrialized countries. Significantly higher deposition rates are reported by several studies in China with  $43 \pm 58 \text{ mg}/\text{m}^2/\text{year}$  as average deposition in Shanghai (Liang *et al.*, 2016). Furthermore, Feng *et al.* (2017) define a sum depositon of PAHs in Shanghai as 2.5-10 tons per year and describe a range of global deposition fluxes of  $1.4 - 170\,000 \text{ ng}/\text{m}^2/\text{day}$ . This comparison indicates clear background emission determined within the presented study. The measured deposition also differs from previous studies in South-Western Germany; Gocht *et al.* (2007) report higher rates of up to a factor of 6, while Schwarz *et al.* (2011) determined twofold higher deposition rates than observed here. Their studies are conducted at comparable rural sites, which are situated with a maximum distance of ca. 300 km. Additionally, both sampling campaigns covering two subsequent years provide rather stable deposition rates with time. Schwarz *et al.* (2011) emphasize the clear influence of local emission sources, which becomes particularly evident when comparing seasonal variations of deposition rates. Those are substantially less pronounced at rural sites with fewer emission sources compared to fluctuating deposition in villages. Particularly close sites were investigated by Martin (2000), who measured high deposition rates, exceeding the values determined within this study up to a factor of 11 for the City Center of Tübingen and a factor of six for more rural sites. Combining the results of Gocht *et al.* (2007), Martin (2000) and Schwarz *et al.* (2011) with this study might be interpreted either as an indicator for an overall decrease of PAH deposition rates in rural areas of South-Western Germany due to progression within the prevention of air pollution or confirming the strong local influence observed by Schwarz *et al.* (2011). Besides, Golomb *et al.* (2001) describe considerably varying deposition rates as well as respective distribution patterns of examined PAHs for two sites in Maine and Massachusetts, approximately 230 km apart. The authors explain the observed variation by the influence of different air masses carrying diverse loads of pollutants to the separate locations. However, the best agreement can be observed for rural study sites in France with deposition rates of  $52\text{-}68 \text{ }\mu\text{g}/\text{m}^2/\text{year}$  (Garban, 2002). Besides, the determined seasonal variation with higher deposition rates during cold periods is a widespread observation (Kiss *et al.*, 2001, Garban, 2002, Gigliotti *et al.*, 2005, Gocht *et al.*, 2007, Tian *et al.*, 2009, Birgül *et al.*, 2011, Wang *et al.*, 2016, Feng *et al.*, 2017).



**Table 9.5: Comparison of measured PAH deposition rates for  $\Sigma_{12}$ PAHs (excluding LMW PAHs) with literature studies.**

Author/ study	Sampling method	$\Sigma_{12}$ PAHs [ $\mu\text{g}/\text{m}^2/\text{year}$ ]	Study area
Birgöl <i>et al.</i> (2011)	Wet + dry deposition	12	Butal, Turkey
			Rural sites in France
Garban (2002)	Wet + dry deposition	68	Abreschviller
		59	Eclaron
		52	Pleumeur-Bodou
Gigliotti <i>et al.</i> (2005)	Wet + dry deposition	186	10 sites around New Jersey, USA
Gocht <i>et al.</i> (2007)	Funnel -adsorber cartridge (dry and wet deposition)		Rural forest sites in <u>South-Western Germany</u>
	Sampling in two consecutive years (2001; 2002)	221; 181	Seebach
		122; 165	Schönbuch
		228; 216	Waldstein
Leister and Baker (1994)	Funnel-adsorber cartridge	184	Chesapeake Bay, USA
Kiss <i>et al.</i> (2001)	Funnel-bottle (wet deposition)	412	Rural site at Lake Balaton, Hungary
Schwarz <i>et al.</i> (2011)	Funnel-bottle (dry + wet deposition)		Rural site at Swabian Alb, Germany
	Sampling in two consecutive years (2004 - 2006)	70	
Martin (2000)	Funnel-bottle (dry + wet deposition)	426.7	Tübingen, City Centre
		130.5	Tübingen, Western City
	Sampling various consecutive periods	120.1	Reutlingen
		157.9	Bad Urach ,Swabian Alb
<i>This study</i>	<i>Funnel -adsorber cartridge 2017-2018</i>	30-35	<i>3 rural sites in South-Western Germany</i>

#### 9.4.5 Distribution patterns of PAHs comparing gas phase, passive sampler, bulk deposition and bulk soil

Characteristic distribution patterns, including the percentages of the representative PAHs to the  $\Sigma_4\text{PAHs}$ , may be used to differentiate the atmospheric influence onto the soils into gas phase and particles (Wang *et al.*, 2016). Figure 9.8 depicts the respective patterns for Fl<sub>n</sub>, Phe, Fth and Pyr in the atmosphere and the soil. In particular, for the atmosphere the gas phase (active sampler), particles (passive sampler) and the bulk deposition (deposition sampler) are compared, while for the soil the bulk soil as well as passive samplers are included. August and November 2017 are compared to account for warm versus cold periods. Only the composition within the bulk soil is accepted as stable throughout the year. For an adequate comparison of the different phases, Fth and Pyr on PE were extrapolated for equilibrium based on the numerical model up to 300 days, accounting for average parameters ( $T$ ,  $C_g$ ,  $\delta_g$ ) as a robust integration (Figure A.5-Figure A.19). Comparing gas phase, bulk deposition, and bulk soil illustrates a gradual decrease of the relative contribution of the low molecular weight compounds (Fl<sub>n</sub> and Phe), which correlates well to their respective distribution coefficients. The distribution pattern within the bulk deposition reflects a combination of gaseous and particle bound PAHs to the total atmospheric deposition. High molecular weight compounds do not reach equilibrium in the extraction cartridges and are therefore underrepresented. Distribution patterns in the bulk soil and equilibrated PE show the importance of equilibrium status for such a comparison. The latter observation confirms the relevance of particle-bound PAHs for the atmospheric deposition and the overall input into the soils. Since extrapolation of Fth and Pyr to equilibrium concentrations on the particles is necessary, the same holds true for masses on the adsorbing phase of the deposition samplers (IRA). Otherwise, the sampled bulk deposition clearly introduces a bias towards the gaseous phase (mainly Phe), due to faster enrichment of lighter compounds on IRA, as observed here.

As a result, passive samplers in equilibrium with the atmosphere illustrate an appropriate measure for the atmospheric concentrations of PAHs. Higher proportions of e.g. Pyr in bulk deposition and soil indicate particle bound PAHs as the major input pathway into soils for heavy compounds. Soils can be described as continuous sinks for PAHs, similarly to the flux reported by Wang *et al.* (2014). Furthermore, Bao *et al.* (2015), modelled the exchange of Phe between soil and atmosphere, accounting for several influencing processes like revolatilization, photodegradation and biodegradation. The authors identified sorption and diffusion as most important process for the redistribution of Phe in the environment, also leading to ongoing uptake of Phe from the atmosphere. With revolatilization and biodegradation as relevant processes, LMW PAHs would have been depleted over time due to their higher volatility and bioavailability compared to HMW PAHs. In contrast, stable ratios of BaP and Phe were determined for each soil sample, regardless of the soil depth or sampling site (Figure A.21). This may be seen as additional proof supporting the conclusion of continuous PAH accumulation in the studied soils.

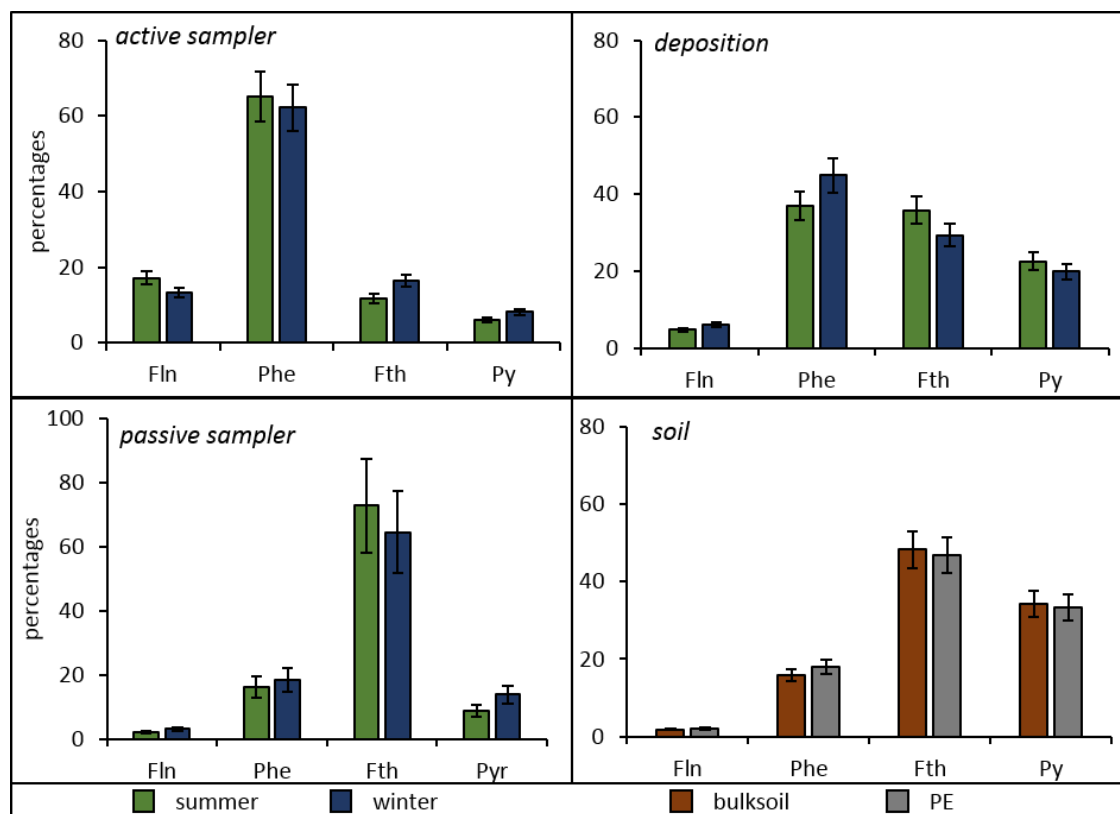


Figure 9.8: Percentage contribution of Fln, Phe, Fth and Pyr, comparing the gas phase (active sampler) and particles (passive sampler) in the atmosphere, bulk atmospheric deposition and soil exemplarily for Entringen.

#### 9.4.6 Sources of PAHs – diagnostic ratios

In order to obtain a more detailed view on the potential sources of PAHs, diagnostic ratios were calculated for each phase individually. Diagnostic ratios observed within the atmosphere as well as for the bulk soil have been shown and discussed earlier (*Characterization of study sites - land use and soil properties* and *Characteristic ratios and source appointment*). Therefore, Figure 9.9 illustrates the ratio of Fth/(Fth+Pyr) against the ratio of Ant/(Ant+Phe) complementary for the bulk atmospheric deposition. Low concentrations of Ant may introduce considerable uncertainty into the respective ratios. Therefore, concentrations close to or below the limit of quantification were not taken into account for this evaluation; resulting in an exclusion of sampling during May-August at each location as well as August-November in Tailfingen. Data sets considered show high reproducibility and indicate combustion as major source of PAHs, independent of the sampling site or the examined season. In particular, the ratio of Fth/(Fth+Pyr) identifies coal (e.g. briquets) and softwood combustion as main source, which is related to domestic heating (Tobiszewski & Namieśnik, 2012). This is in very good agreement with

diagnostic ratios determined for the atmospheric monitorings with PE passive samplers (*Characteristic ratios and source appointment*). The diagnostic ratios within the bulk soil show substantially higher values for Ant/(Ant+Phe), indicating a more pronounced input of traffic related PAH emission, particularly evident in Tailfingen and Entringen.

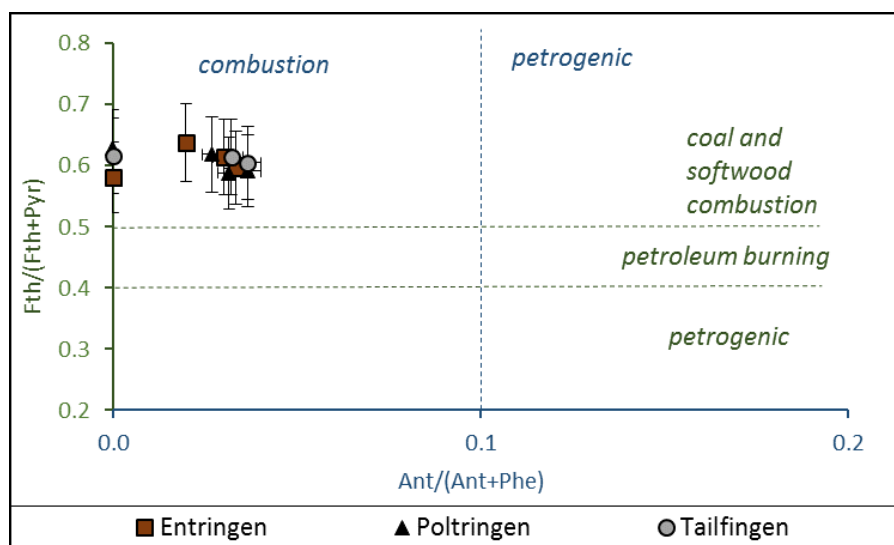


Figure 9.9: Diagnostic ratios for atmospheric bulk deposition comparing Entringen, Poltringen and Tailfingen during the individual seasons.

As aforementioned, Dickhut *et al.* (2000) report source-related diagnostic ratios for particle bound and thus HMW PAHs to differentiate between coal, wood and vehicular combustion. Figure 9.10 and Figure 9.11 show the ratio of Indeno/BghiP versus the ratio BaA/Chr comparing the atmospheric bulk deposition and the bulk soil, respectively. Therefore, the recent input into soils by atmospheric deposition may be linked directly to the accumulated HMW PAHs within the soil. For the bulk deposition, more or less the same ratios were determined for each monitoring and each location with ratios below 0.5 and below 1.1 for BaA/Chr and Indeno/BghiP, respectively. Only small spreading can be observed with Tailfingen demonstrating the lowest and Entringen depicting highest values for both ratios, during each season. For all locations the highest ratio of Indeno/BghiP in the bulk deposition (around 1.1) was determined during the sampling period November 2017 – February 2018. This respective ratio refers rather to coal combustion than traffic emission, which can be explained by the cold season and thus an increase of residential heating. Similar findings are reported by Motelay-Massei *et al.* (2007), who determined traffic as a major emission source for an urban site in Rouen (France) which loses relevance during cold periods due to an increase of coal combustion by domestic heating. In general, the observed spreading of the ratios for HMW PAHs in bulk deposition might indicate minor variances of emission sources on the local scale. Thus, the bulk deposition in Tailfingen indicates a more pronounced influence of traffic emission compared to Poltringen and Entringen. And bulk deposition in Entringen seems to re-

flect a larger influence of coal combustion than observed for Poltringen and Tailfingen. This observation contradicts the suggested explanation for slightly higher atmospheric concentrations in Entringen caused by a small railway train run by a Diesel Engine close to the study site.

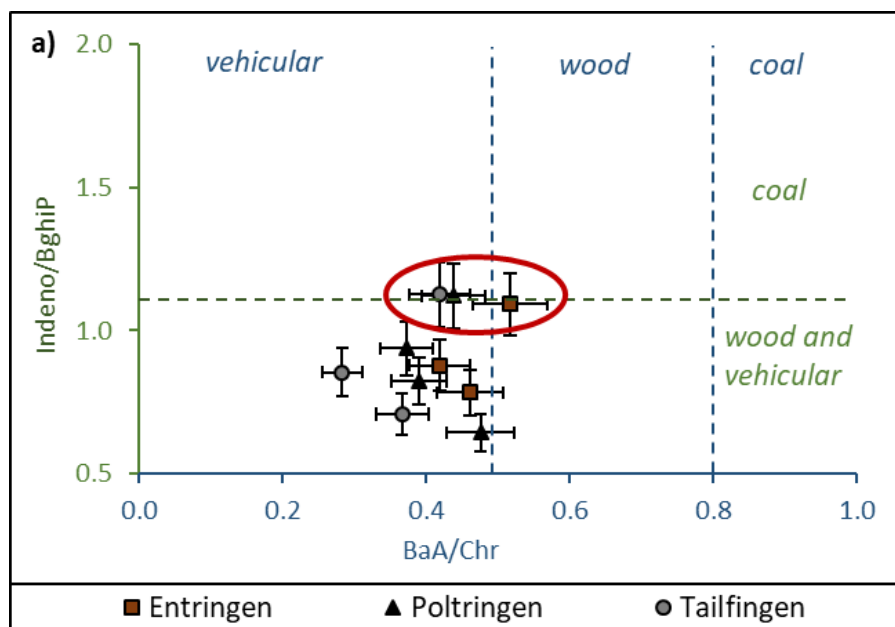


Figure 9.10: Diagnostic ratios of HMW PAHs calculated for the atmospheric bulk (wet and dry) deposition (May 2017 - May 2018). The encircled data points reflect the atmospheric deposition during November 2017- February 2018.

For the bulk soil, characteristic ratios of the HMW PAHs are clearly distinguishable for the different locations. In Poltringen, both ratios indicate vehicular emission and wood burning as major source, while the soil profile in Entringen demonstrates a slight influence by coal combustion. The largest variance is observed at the soil profile in Tailfingen. Here, the lowest horizon plots equal to Poltringen clearly within the range of vehicular emission. The rest of the soil samples in Tailfingen depicts, however, higher ratios of Indeno/BghiP indicating coal combustion as well as for BaA/Chr referring to wood combustion. This can be seen as a mixed signal, combining recent and historical input. However, the deposition samplers reflect the recent input into the soils as they sample the actual atmospheric deposition. The combined use of several ratios enables the identification of various emission sources simultaneously. Thus, the atmospheric bulk deposition reflects a mixture of coal and wood combustion as well as a substantial influence of traffic emission. The soils reflect mainly the accumulation of PAHs during the last decades including vehicular emission as well as wood and coal combustion as relevant PAH sources. This fits quite well to the formerly prevalent heating systems and industrial use of wood and charcoal (Cousins & Jones, 1998). Numerous studies on PAH emission sources report similar findings of heating as major pathway into the

atmosphere (Peng *et al.*, 2016, Dumanoglu *et al.*, 2017). At urbanized sites, on the other hand, traffic exhausts were identified as a major contribution to the overall PAH emission (Golomb *et al.*, 2001, Mantis *et al.*, 2005, Liang *et al.*, 2016). Due to the annual mixing (ploughing) of the sampling sites at Poltringen and Tailfingen, recent and historical signals of emission sources are mixed within the soil and therefore independent of sampling depth and thus provide no information on changes in historical input, which is usually expected in soil profiles.

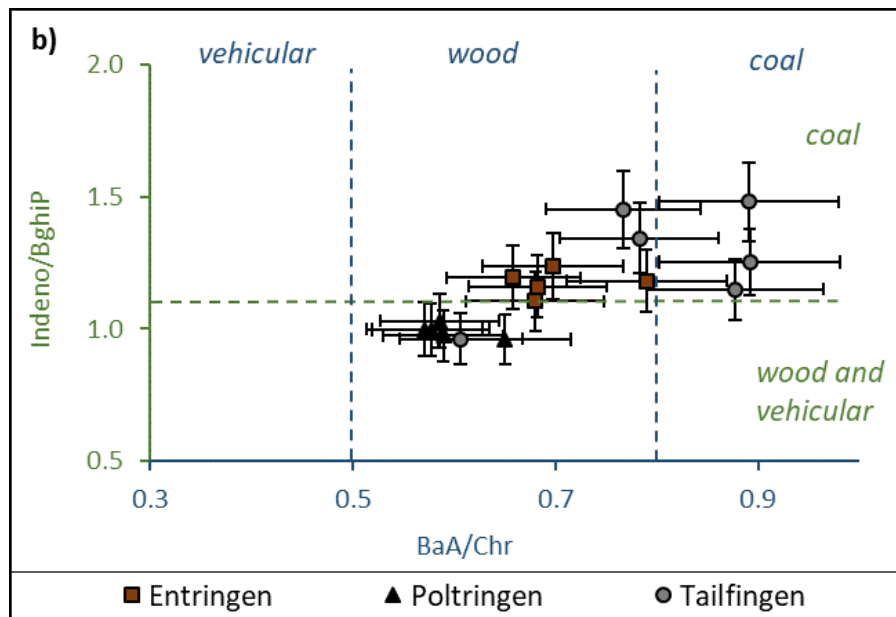


Figure 9.11: Diagnostic ratios of HMW PAHs calculated in the bulk soil of the different study sites.

In contrast, Entringen has the most undisturbed soil profile, as no mixing was allowed for the last 50 years, which is reflected by a clear profile of the organic carbon content as well as a concentration gradient of PAHs with depth. Therefore, soil samples in Entringen are equivalent to an archive, reflecting changes of the input signal. Figure 9.12 depicts the ratios of Ant/(Ant+Phe) as well as Indeno/BghiP over the depth of the soil profile in Entringen to distinguish traffic emission from heating-related combustion. Only for the uppermost 10 cm an obvious change occurs towards a higher ratio of Ant/(Ant+Phe) and a lower value for Indeno/BghiP, both indicating an increase of the contribution from traffic. This fits the approximately 2.5 fold increase of traffic in Germany during the last 50 years (Federal Road Research Institute, see Figure A.22).

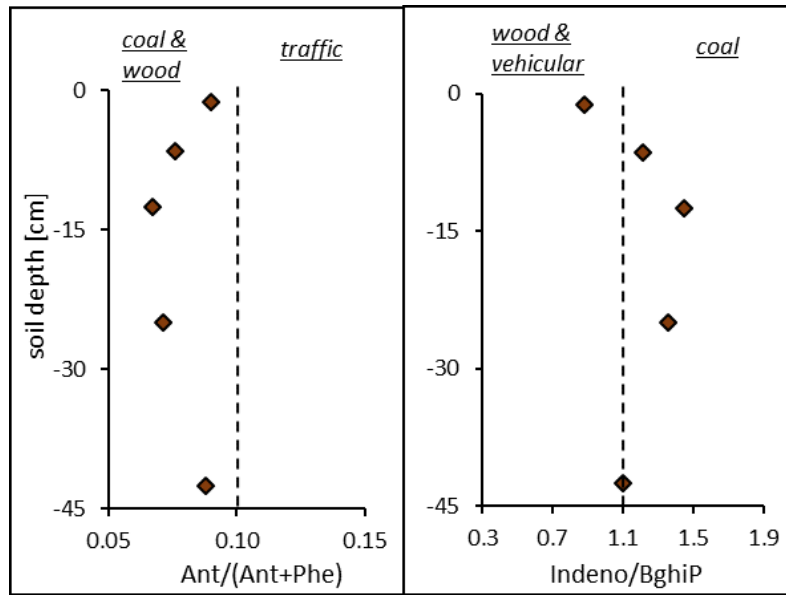


Figure 9.12: Diagnostic ratios of a)  $Ant/(Ant+Phe)$  and b)  $Indeno/BghiP$  in the rather undisturbed soil profile in Entringen, indicating a temporal evolution of these ratios.

Summarizing these findings for the different media suggests the combustion of wood and coal as well as traffic as the main emission sources for PAHs within the studied area. Both the gas phase and the bulk deposition clearly indicate an increase of traffic during November – February. Historical as well as recent input of PAHs into soils is observed simultaneously in Poltringen and Tailfingen, due to the regular mixing. Only Entringen provides a rather undisturbed soil profile and indicates an increase of traffic emission during the last 50 years.

## 9.5 Summary and Conclusion

In summary, the simultaneous deployment of passive and depositional samplers provides comprehensive information on the airborne PAH input into soils. However, the comparison of PAH distribution patterns in PE and the atmospheric bulk deposition is difficult, due to insufficient equilibration of HMW PAHs between particles (here, PE and IRA as adsorbing material) and gas phase. For PE passive samplers this issue may be overcome by extrapolation of sampled concentrations to equilibrium state using numerical or analytical solutions for accumulation of PAHs. Therefore, distribution patterns on equilibrated passive samplers agree well with respective patterns in the bulk soil. Distribution patterns in bulk deposition are similar to bulk soil, while the latter show varying input of PAH mixtures over time. This is indicated by the mainly undisturbed soil profile in Entringen with changing Ant/Phe and Indeno/BghiP ratios differentiating between traffic and heating as main emission sources. Thus, continuous uptake of PAHs into soils seems likely and revolatilization plays only a minor role during warm periods. Taking account of seasonal ratios of  $C_g$  calculated for soil gas and the atmosphere supports the ongoing accumulation of PAHs in soils even for the gaseous phase. Although temporal revolatilization was observed during warm periods, all target compounds illustrate exceedingly stronger deposition during autumn and winter than revolatilization during summer. These findings are in good agreement with the modelling work of Bao *et al.* (2015).



---

## 10 Summary and outlook

Overall, the investigated sites may be summarized as very comparable rural locations. Despite slight differences in the formation of the respective soils (alluvial soils, gley, luvisols) investigated parameters (grain size,  $f_{oc}$ , PAH concentrations, distribution coefficients) are considerably uniform. Regarding the low amount of organic carbon within these agricultural soils (around 1 – 2 %), remarkably high distribution coefficients as well as nonlinear sorption behaviour were obtained by sorption tests with Phe. This is presumably due to the generally low PAH concentrations combined with strongly sorbing particles in soils. Differences among the soil profiles are mainly due to the varying land use with agricultural soils being mixed regularly (at least once a year), which hinders the evolution of gradients. Hence, Entringen was identified as an exception indicating an almost undisturbed soil profile and clearly distinguishable top soil and root horizons. This is reflected by coarser grains, higher  $f_{oc}$  combined with lower maturity and therefore high distribution coefficients  $K_d^*$  (bulk soil – water) but lower sorption coefficients  $K_{oc}^*$  (organic carbon – water). OC-normalized PAH concentrations in the bulk soil were determined within a narrow range of  $\Sigma_{16}$ PAH between 4-24  $\mu\text{g/g}$  for Entringen and Poltringen and slightly higher values in Tailfingen with concentrations up to 60  $\mu\text{g/g}$ . Additionally, stable distribution patterns of all U.S. EPA Priority PAHs were observed for the different sites and soil horizons. Thus, concentrations of all target compounds may be estimated based on consistent relations to Phe as reference compound.

Passive sampling in soils includes some uncertainties, particularly with respect to equilibration times exceeding the predefined timescales, following mathematical approaches. Accordingly, it was difficult to predict the state of equilibrium for PAHs on the PE. Uptake kinetics of target compounds from soil slurries onto PE passive samplers were equal for the different compounds, providing stable distribution patterns on the sampler independent of the time of sampling. Presumably, the formation of clusters around PE strips and heterogeneous soil suspensions increase the complexity of soil batches and interactions between individual grains and the aqueous phase. As a result, the diffusion pathway from soil particles to the sampler increases as well leading to exceedingly long equilibration times. After five months of equilibration, measured concentrations on PE sheets provide equilibrium concentrations in water close to estimations based on measured Freundlich coefficients. For further studies on passive sampling in soils, a more detailed characterization of soil samples as well as homogeneous suspensions are needed. Therefore, a comparative study with freeze dried, pulverized soils and batch tests including only a narrow range of soil particles instead of the bulk soil should provide comprehensive information for the limiting factors of the conducted ex-situ batch tests. However, a precise measurement of sorption coefficients in soil profiles is a fast method to determine the respective aqueous concentration at equilibrium and can be used as the appropriate method of choice for further studies.

On the other end, the quantitative use of passive samplers for atmospheric PAHs was verified by an extensive method-validation combining active and passive sampling as well as different approaches for calibration. Uptake kinetics and equilibrium concentrations were determined to be identical for each of the study sites suggesting stable conditions within a broad catchment area over several months. Uptake kinetics were mainly influenced by wind speed while equilibrium concentrations relate directly to ambient temperatures and corresponding temperature-dependent coefficients (and precipitation to some extent). Therefore, uptake kinetics right above ground were considerably slower, since the cover minimizes the influence of air flow around the samplers. For further monitoring, the temperature under the individual covers should also be measured to minimize uncertainties in the data evaluation. Seasonal variations were identified to apply for two time spans in general, differentiating between warm and cold periods (summer versus winter). Such a classification holds for environmental conditions as well as for variations within PAH emissions and respective concentrations in the atmosphere. During cold periods, substantially higher concentrations of PAHs were determined compared to measurements during spring and summer (a factor of five). Moreover, at high temperatures and accordingly lower partition coefficients, the sensitivity of the samplers increases and allows to reflect short-term fluctuation within the atmosphere.

A combination of numerical and analytical solutions for the uptake kinetics and corresponding PAH concentrations in air (additionally including equilibrium approaches) finally verified the determined atmospheric concentrations. Besides, the numerical model allowed for differentiation of temperature induced fluctuation versus actual variation of atmospheric concentrations. Stable distribution patterns of representative PAHs for the different study sites were determined not only within soil samples but also for the atmosphere. Consequently, concentrations of all target compounds may again be related to Phe as reference. This observation of stable patterns confirmed the assumption of sampling a well-mixed atmospheric boundary layer and therefore referring to the same atmospheric influence or the same catchment area at the different locations within the Ammer valley. Yet, slight variations could be determined for atmospheric concentrations, directly linked to small local point sources like a railroad train or construction works on the study sites. An open question remains with respect to an apparent residual concentration of the *PRC* on PE passive samplers in the atmosphere. With Ant-D<sub>10</sub> as artificial compound and therefore not occurring in the atmosphere, a complete release from PE was calculated. In contrast, a residual concentration of 5-10 % of the initial loading remains within the sampler for several weeks. This behaviour was observed during each monitoring as well as for several types of polymer. Yet, no theoretical approach, besides a simple correction factor, could account for this observation.

Furthermore, a direct comparison of PE sheets and PDMS coated jars illustrated considerable uncertainty for the use of the latter. This might be induced by their explicitly high temporal sensitivity due to thin coatings (1 – 4 µm) and accordingly fast reaction

---

to short-term variation within the atmosphere. The chosen set-up for ex-situ batch tests with PDMS and soil slurries simply lacked the potential of sampling a sufficient mass of the target compounds from soil with considerably low concentrations. An increase of coating thickness would overcome sampling issues within both compartments to some extent, but therefore eliminate one of the main advantages of exceedingly fast equilibration in this case.

Ultimately, concentration gradients of PAHs in the gas phase and across the soil-atmosphere interface confirm continuous uptake of PAHs into soils. During summer, temporal re-volatilization from soil was determined for semi-volatile PAHs (up to Pyr) at all stations and for both years. However, particle bound deposition was determined as the main input pathway of PAHs from the atmosphere into the soils. Therefore, the overall flux direction remains constant throughout the year, illustrating net deposition.

For the identification of PAH emission sources influencing the study sites, diagnostic ratios were applied for the different phases, according to literature. Consequently, combustion of wood and coal as well as traffic exhaust were identified as the main recent emission sources of PAHs within the catchment area. However, the undisturbed soil profile in Entringen might be used as an archive for historical input as well as for changes during the last 50 years. Based on the bulk soil examined within this profile, a considerable shift towards an increasing input of vehicular emissions can be observed for the last years. Such a trend reflects the development of increasing traffic abundance observed in Germany during the same time span.

## A Appendix

### A.1 Characterization of study sites

**Table A.1: Partition coefficients and solubilities of the 16 U.S. EPA Priority PAHs at 25°C:  $\log K_{ow}$  (EPI Suite),  $\log S_{sub}$  (Chiou et al., 2005),  $\log K_{pw}$  (Smedes et al, 2009) as well as calculated  $\log K_{oc}$  (<sup>1</sup> following Karickhoff (1981), and <sup>2</sup> according to Razzaque & Grathwohl (2008)), all in [L/kg], except  $\log S_{sub}$  with [kg/L].**

PAH	$\log K_{ow}$	$\log K_{oc}^1$	$\log S_{sub}$	$\log K_{oc}^2$	$\log K_{pe-w}$
Nap	3.17	2.79	-3.98	2.94	2.8
Any	3.94	3.55			3.2
Ace	4.15	3.76	-4.75	3.65	3.6
Flu	4.18	3.79	-4.93	3.82	2.8
Phe	4.35	3.96	-5.34	4.19	4.2
Ant	4.35	3.96	-5.35	4.2	4.3
Fth	4.93	4.53	-5.91	4.72	4.9
Py	4.93	4.53	-5.98	4.78	5.1
BaA	5.52	5.11	-6.46	5.22	5.7
Chr	5.52	5.11			5.8
BbfBkf	6.11	5.70			6.7
BaP	6.11	5.70	-7.39	6.08	6.8
Indeno	6.99	6.57			7.4
DahA	6.70	6.28			7.3
BghiP	6.70	6.28			7.3

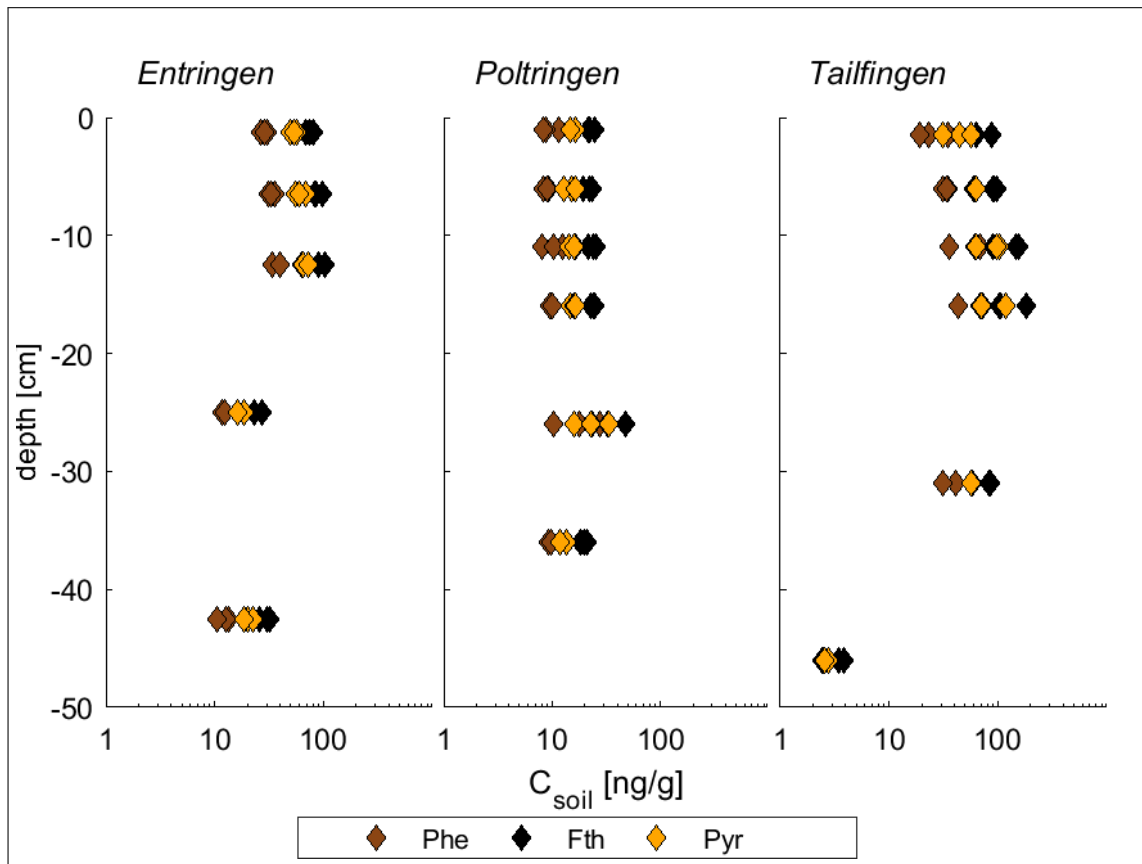


Figure A.1: Concentration profiles of Phe, Pyr and Fth in the bulksoil at the three locations Entringen, Poltringen and Tailfingen (not normalized to OC).

## A.2 Passive sampling

Table A.2: Partition and diffusion coefficients of the 16 EPA-PAHs at 25°C: Log  $K_{pe-air}$  (Lohmann, 2011),  $D_{pe}$  (Lohmann, 2012),  $D_g$  and  $D_w$  (New Jersey Department of environmental protection).

PAH	log $K_{pe-air}$ [L/kg]	log $D_g$ [m <sup>2</sup> /sec]	log $D_{pe}$ [m <sup>2</sup> /sec]	log $D_{aq}$ [m <sup>2</sup> /sec]
Nap	4.8	-5.2	-11.9	-9.12
Any	6.0	-5.2	-12.13	-9.12
Ace	6.0	-5.2	-12.17	-9.11
Fln	6.3	-5.3	-12.36	-9.10
Phe	7.	-5.2	-12.44	-9.12
Ant	7.1	-5.2	-12.42	-9.11
Fth	8.1	-5.3	-12.96	-9.19
Py	8.1	-5.3	-12.76	-9.14
BaA	9.4	-5.3	-12.94	-9.05
Chr	9.4	-5.3	-12.96	-9.21
BbfBkf	10.3	-5.3	-13.45	-9.25
BaP	10.4	-5.3	-13.28	-9.05
Indeno	11.3	-5.3	-13.66	-9.28
DahA	11.5	-5.3	-13.8	-9.25
BghiP	11.4	-5.3	-13.62	-9.28



### A.3 Passive sampling in the atmosphere

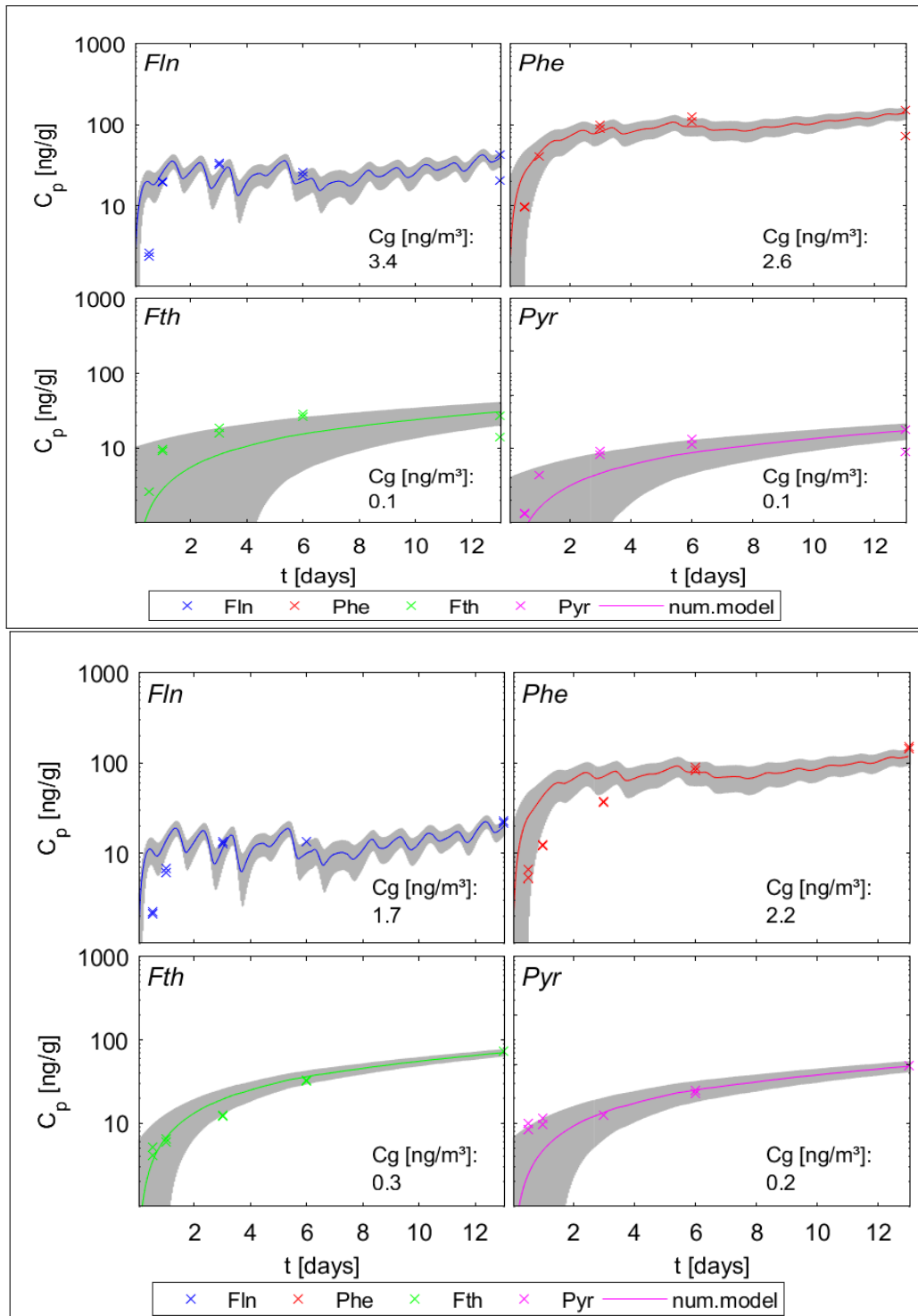


Figure A.2: Measured uptake of the four representative PAHs (Flu, Phe, Fth and Pyr) onto transparent, uncovered PE sheets (upper plot) and onto black, covered PE sheets (lower plot) in combination with the fitted numerical model; the grey area illustrates the standard deviation for the model.



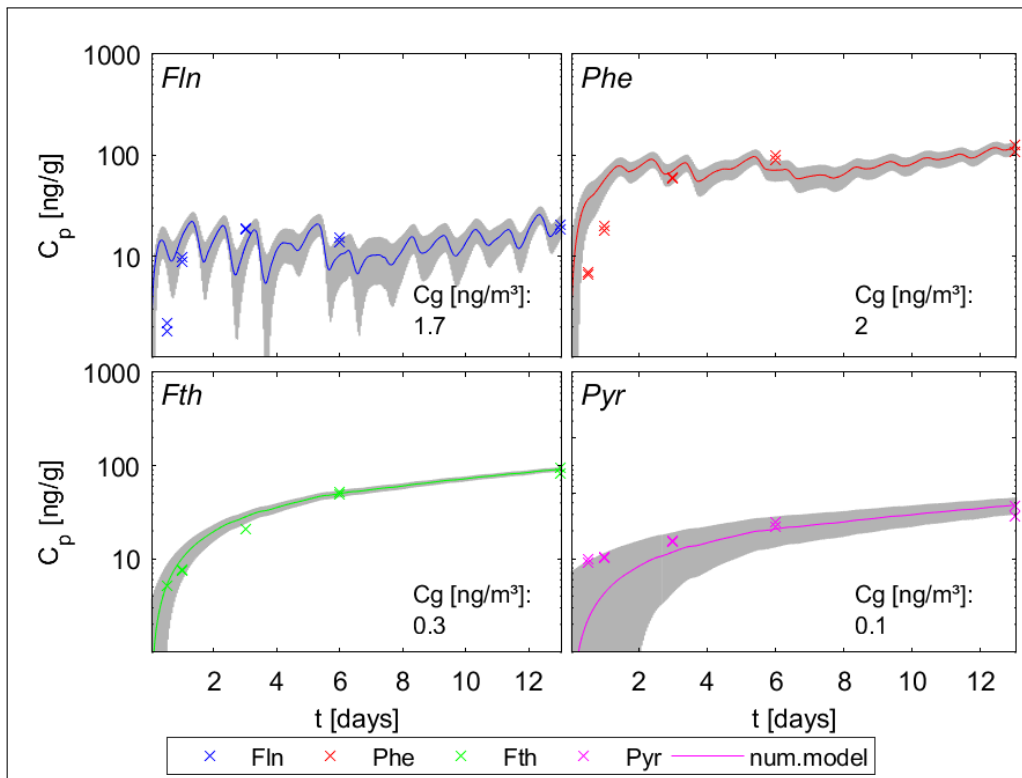


Figure A.3: Measured uptake of the four representative PAHs (Flu, Phe, Fth and Pyr) onto black, uncovered PE sheets in combination with the fitted numerical model; the grey area illustrates the standard deviation for the model.



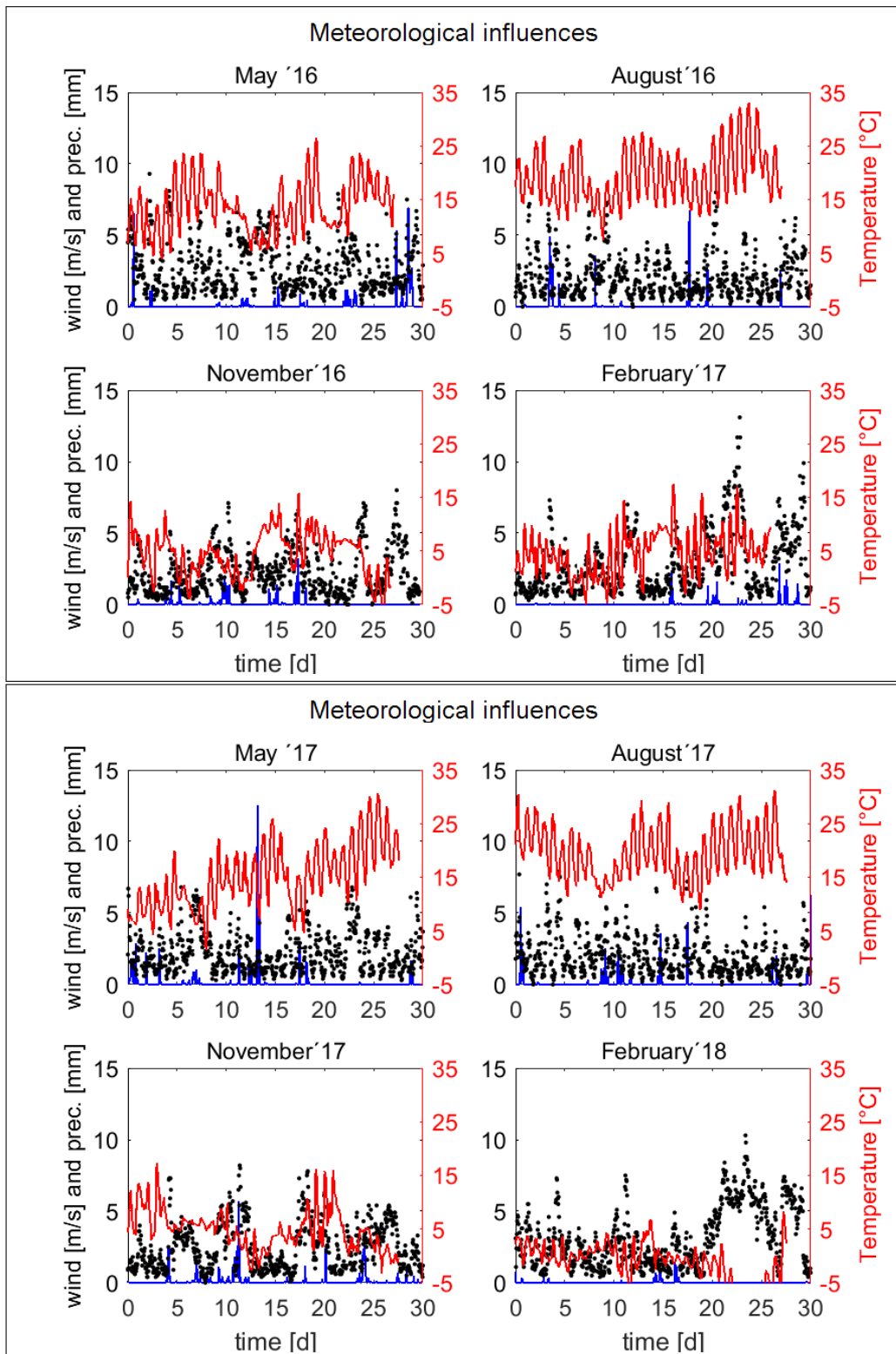


Figure A.4: Meteorological influences, including hourly measurements of wind speed (black), precipitation (blue) and temperature (red) during all seasonal sampling campaigns. Data are obtained from the German Weather Survey (measured in Stuttgart, Echterdingen).

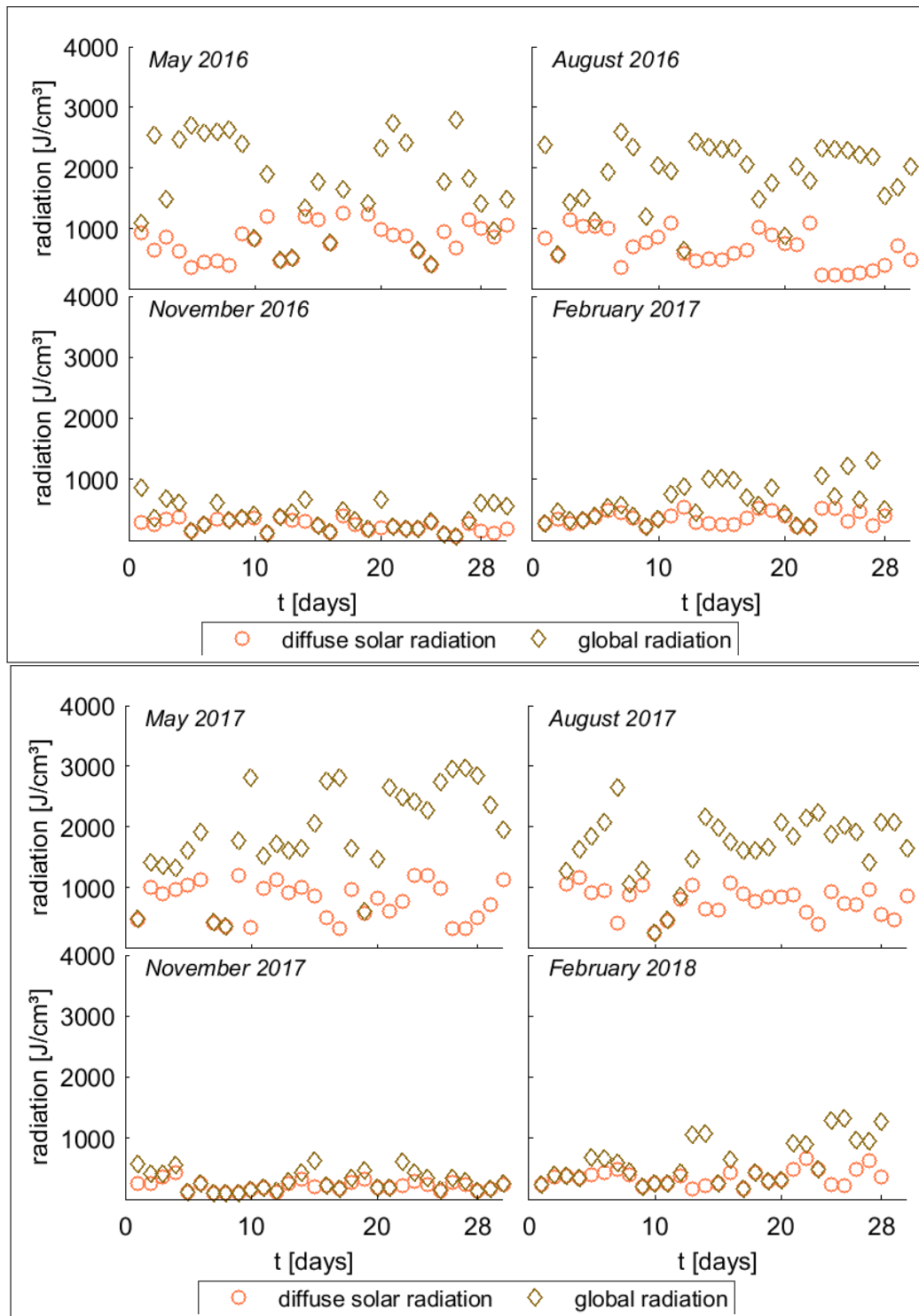


Figure A.5: Diffuse solar and global radiation [ $\text{J}/\text{cm}^3$ ] for seasonal monitorings during the first year. Data are obtained from the German Weather Survey (measured in Stuttgart, Echterdingen).

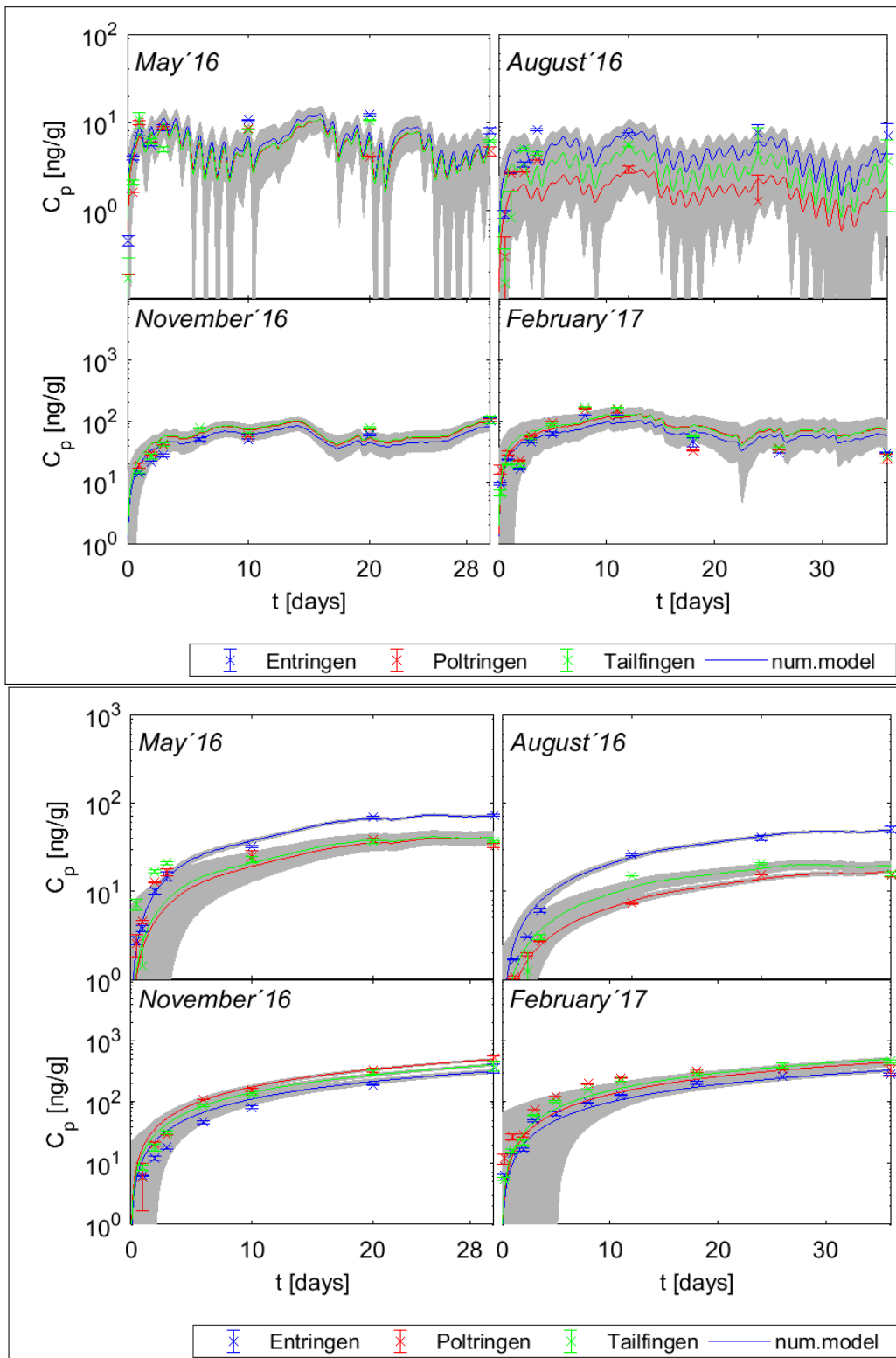


Figure A.6: Measured and numerically fitted uptake curves of  $Flh$  (upper plots) and  $Fth$  (lower plots) for each of the seasonal monitorings, considering the three locations individually. The grey area depicts the standard deviation of the numerical model.

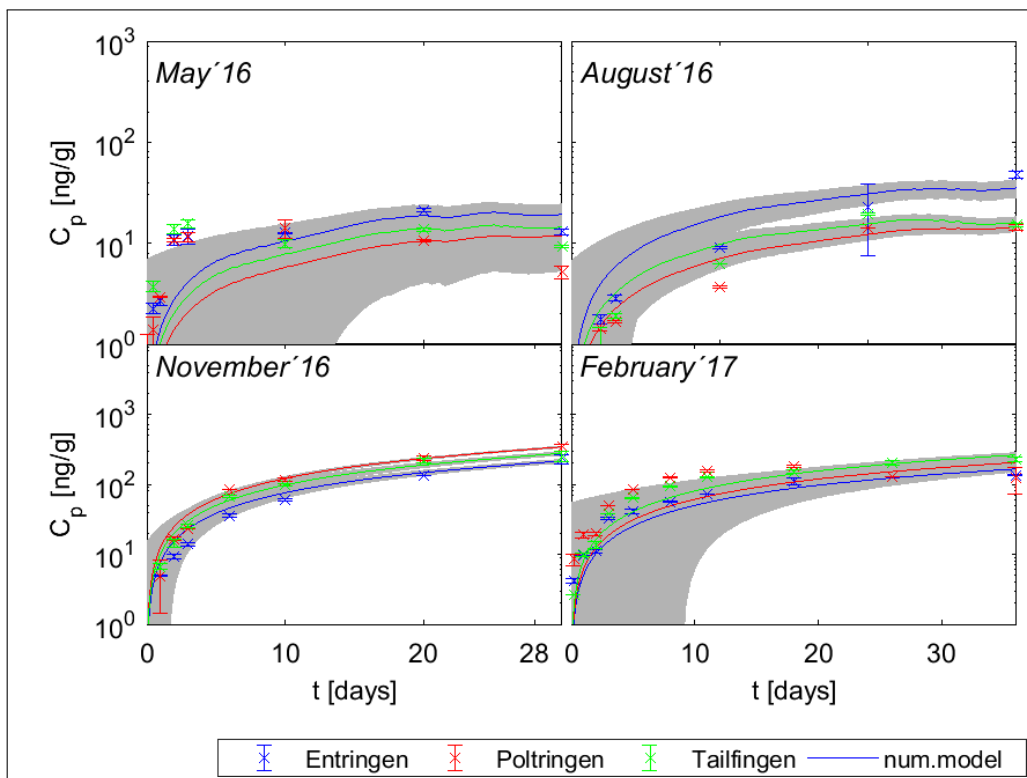


Figure A.7: Measured and numerically fitted uptake curves of Pyr for each of the seasonal monitorings, considering the three locations individually. The grey area depicts the standard deviation of the numerical model.

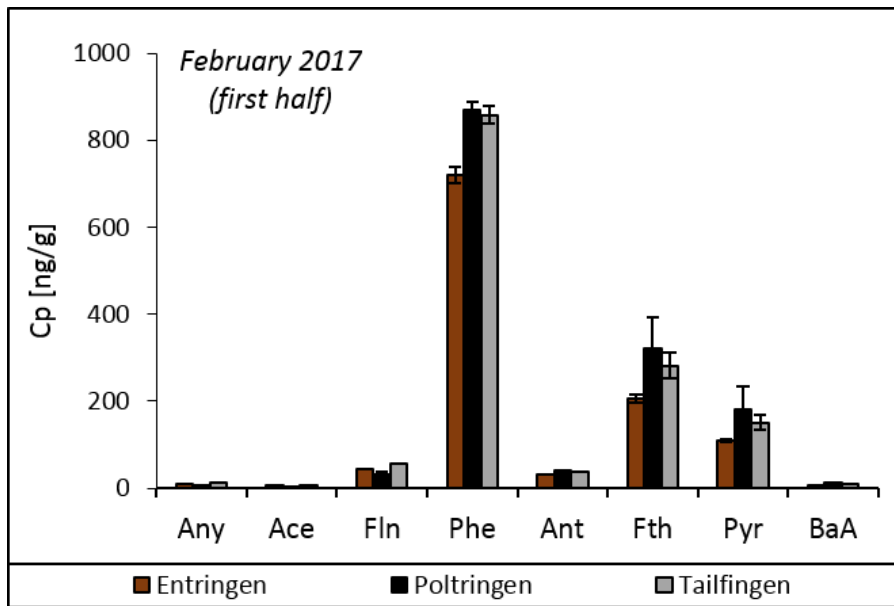


Figure A.8: Distribution pattern of eight PAHs (Any, Ace, Fln, Phe, Ant, Fth, Pyr and BaA) on PE, comparing Entringen, Poltringen and Tailfingen for the first half of the monitoring during February 2017. Error bars indicate the standard deviation determined for triplicate samplers.

**Table A.3: Seasonal atmospheric concentrations [ng/m<sup>3</sup>] of the representative compounds during the first year of sampling campaigns, numerically fitted for each location including respective standard deviations.**

Monitoring	location	Fln	Phe	Fth	Pyr
May 16	Entringen	0.9 ± 0.1	1.9 ± 0.3	0.2 ± 0.01	0.06 ± 0.01
	Poltringen	0.8 ± 0.1	1.3 ± 0.2	0.2 ± 0.002	0.05 ± 0.002
	Tailfingen	0.8 ± 0.1	1.3 ± 0.08	0.1 ± 0.002	0.05 ± 0.002
Aug 16	Entringen	1.3 ± 0.2	2.4 ± 0.3	0.4 ± 0.01	0.3 ± 0.04
	Poltringen	0.5 ± 0.1	1.1 ± 0.1	0.2 ± 0.006	0.1 ± 0.01
	Tailfingen	0.8 ± 0.1	1.6 ± 0.2	0.1 ± 0.01	0.1 ± 0.01
Nov 16	Entringen	3.4 ± 0.3	8.3 ± 0.9	1.6 ± 0.09	1.1 ± 0.05
	Poltringen	3.9 ± 0.3	10.4 ± 0.8	2.4 ± 0.05	1.5 ± 0.03
	Tailfingen	4.1 ± 0.3	10.2 ± 0.6	1.9 ± 0.06	1.3 ± 0.06
Feb 17	Entringen	3.9 ± 0.5	7.6 ± 0.5	1.4 ± 0.06	0.7 ± 0.05
	Poltringen	4.9 ± 0.8	10.8 ± 1.4	2.2 ± 0.2	0.9 ± 0.2
	Tailfingen	4.9 ± 0.8	9.6 ± 0.8	1.9 ± 0.07	0.9 ± 0.05



**Table A.4: Seasonal atmospheric concentrations [ng/m<sup>3</sup>] of the representative compounds during the second year of sampling campaigns, numerically fitted for each location and both sampling heights (0.1 m and 1.2 m) including respective standard deviations.**

0.1 m height	location	Fln	Phe	Fth	Pyr
May 2017	Entringen	0.7 ± 0.1	1.3 ± 0.2	0.02 ± 0	0.2 ± 0.01
	Poltringen	0.7 ± 0.1	1.6 ± 0.5	0.3 ± 0.1	0.1 ± 0.04
	Tailfingen	0.4 ± 0.1	0.8 ± 0.2	0.1 ± 0.01	0.1 ± 0.01
Aug 2017	Entringen	0.8 ± 0.2	1 ± 0.1	0.2 ± 0.01	0.1 ± 0
	Poltringen	0.3 ± 0.02	0.4 ± 0.03	0.1 ± 0	0.02 ± 0
	Tailfingen	0.6 ± 0.1	0.6 ± 0.1	0.1 ± 0	0.04 ± 0
Nov 2017	Entringen	2.8 ± 0.1	9.5 ± 0.3	2.3 ± 0.1	1.5 ± 0.1
	Poltringen	2.2 ± 0.2	5.6 ± 0.5	1.2 ± 0.1	0.8 ± 0.1
	Tailfingen	3.3 ± 0.7	9.7 ± 0.4	2.6 ± 0.1	1.8 ± 0.1
Feb 2018	Entringen	2.3 ± 0.2	4.3 ± 0.2	0.8 ± 0.03	0.4 ± 0.02
	Poltringen	2.3 ± 0.1	4.6 ± 0.3	0.9 ± 0.1	0.5 ± 0.1
	Tailfingen	2.9 ± 0.3	4.5 ± 0.1	0.7 ± 0.03	0.3 ± 0.04
1.2 m height	location	Fln	Phe	Fth	Pyr
May 2017	Entringen	0.9 ± 0.2	2 ± 0.3	0.2 ± 0.02	0.04 ± 0.01
	Poltringen	0.8 ± 0.1	1.2 ± 0.2	0.1 ± 0.03	0.02 ± 0.01
	Tailfingen	0.9 ± 0.1	1.6 ± 0.3	0.1 ± 0.04	0.03 ± 0.02
Aug 2017	Entringen	2.4 ± 0.5	2.7 ± 0.4	0.2 ± 0.1	0.03 ± 0.01
	Poltringen	1 ± 0.1	1.2 ± 0.1	0.1 ± 0.01	0.01 ± 0
	Tailfingen	1 ± 0.3	1.1 ± 0.1	0.1 ± 0.01	0.01 ± 0
Nov 2017	Entringen	3 ± 0.2	9.6 ± 0.2	2.6 ± 0.1	1.5 ± 0.1
	Poltringen	2.9 ± 0.3	8.7 ± 0.5	2.2 ± 0.03	1.3 ± 0.01
	Tailfingen	2.9 ± 0.3	8.7 ± 0.5	2.2 ± 0.03	1.3 ± 0.01
Feb 2018	Entringen	2.7 ± 0.3	4 ± 0.1	0.5 ± 0.1	0.2 ± 0.04
	Poltringen	3.4 ± 0.2	7.4 ± 0.6	1.1 ± 0.3	0.4 ± 0.2
	Tailfingen	3.5 ± 0.3	6.6 ± 0.9	1 ± 0.3	0.4 ± 0.2

**Table A.5: diagnostic ratios, considering Ant, Phe, Fth and Pyr, including both years of sampling campaigns and determined for each season and each study site individually.**

Monitoring		1 <sup>st</sup> year		2 <sup>nd</sup> year, 0.1 m		2 <sup>nd</sup> year 1.2m	
Season	location	Ant/(Ant + Phe)	Fth/(Fth + Pyr)	Ant/(Ant + Phe)	Fth/(Fth + Pyr)	Ant/(Ant + Phe)	Fth/(Fth + Pyr)
spring	Entringen	0,02	0,79	0,04	0,08	0,04	0,86
	Poltringen	0,02	0,79	0,00	0,69	0,00	0,78
	Tailfingen	0,02	0,79	0,00	0,67	0,00	0,80
summer	Entringen	0,01	0,58	0,02	0,77	0,02	0,88
	Poltringen	0,00	0,53	0,00	0,75	0,00	0,88
	Tailfingen	0,00	0,58	0,01	0,69	0,01	0,86
autumn	Entringen	0,07	0,61	0,03	0,61	0,04	0,63
	Poltringen	0,07	0,60	0,04	0,61	0,05	0,63
	Tailfingen	0,06	0,60	0,08	0,59	0,04	0,63
winter	Entringen	0,02	0,67	0,04	0,67	0,01	0,76
	Poltringen	0,01	0,70	0,02	0,66	0,01	0,73
	Tailfingen	0,02	0,67	0,03	0,69	0,01	0,72

## A.4 Passive sampling within soils

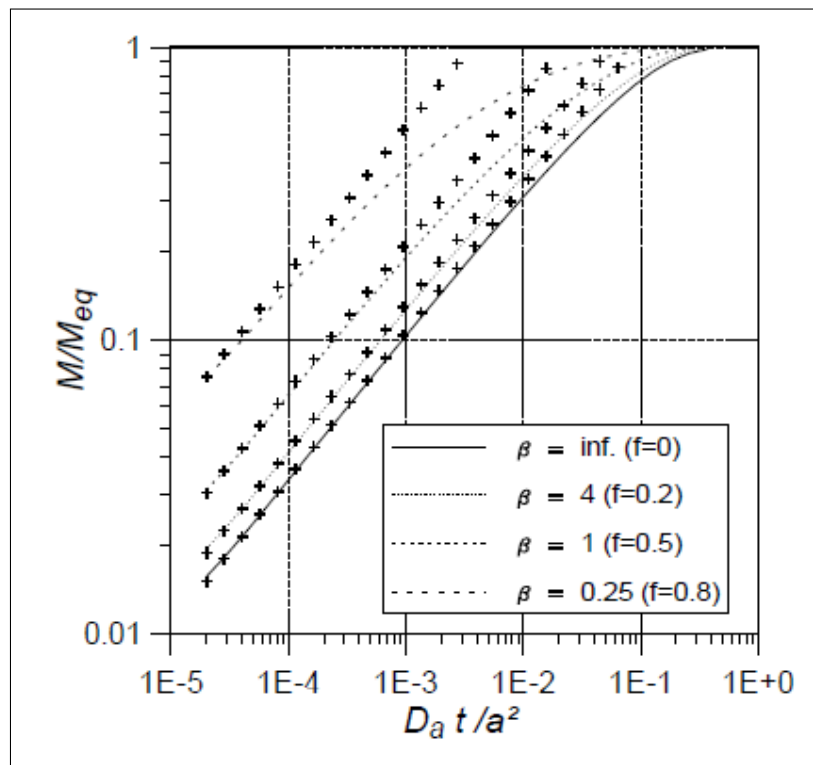


Figure A.9: Relations of  $M/M_{eq}$  to Fourier numbers ( $D_a t/a^2$ ) within a finite bath for different values of  $\beta$  (figure taken from Grathwohl (2012)).

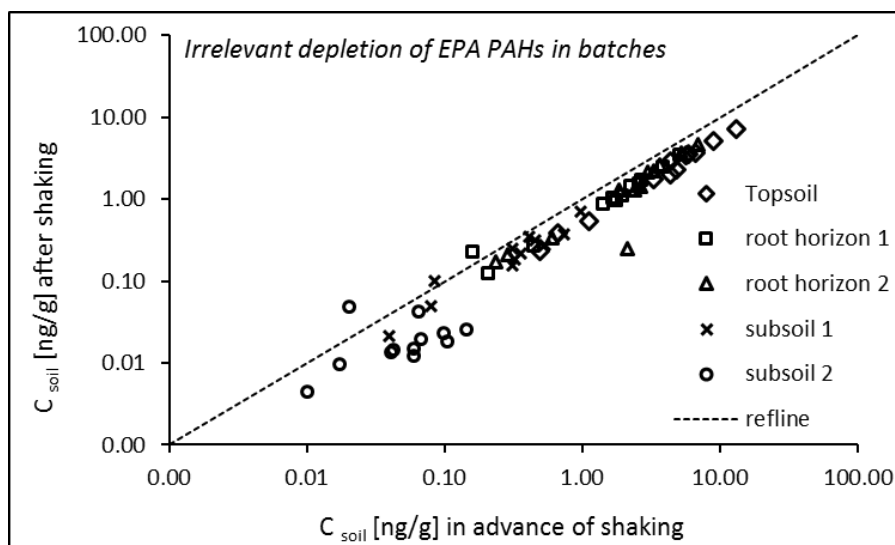


Figure A.10: Measured concentrations of the 16 U.S. EPA Priority PAHs within the bulk soil before and after the batch experiment, shown here exemplarily for Entringen.

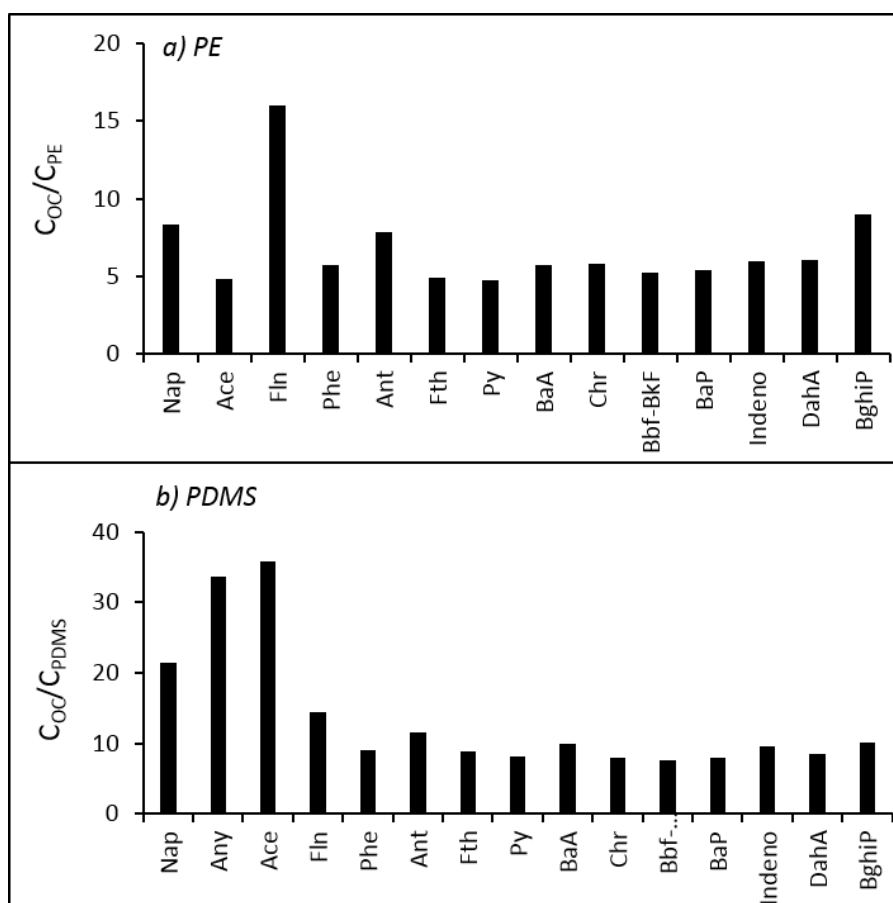


Figure A.11: Ratio of PAH concentration normalized to the organic carbon content within the soil to the measured concentration on the polymer comparing a) PE and b) PDMS, illustrates no correlation to the size of the compound.

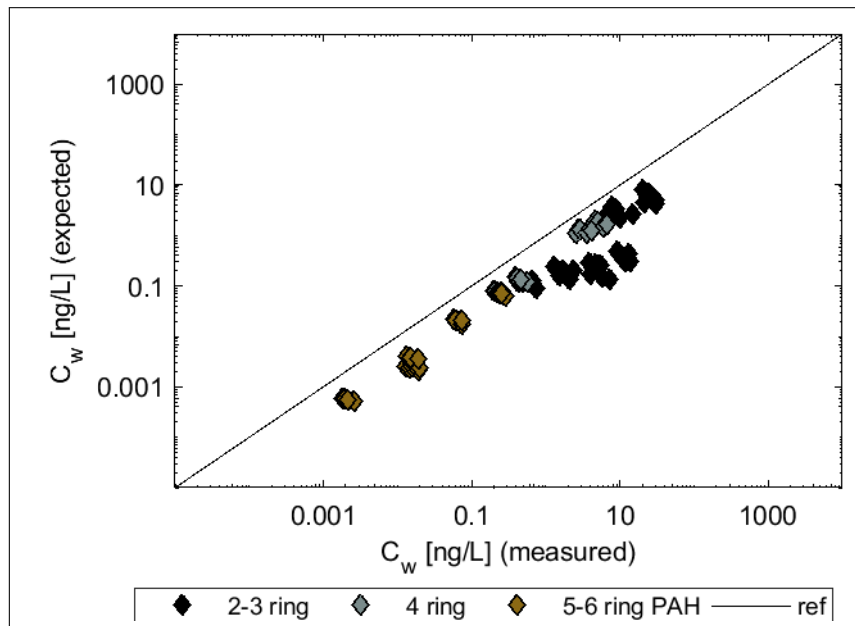


Figure A.12: Comparison of  $C_{w,eq}$ , determined for the 16 EPA PAHs with PE passive samplers in soil batches and calculated according to measured  $K_{Fr}$  for Poltringen.

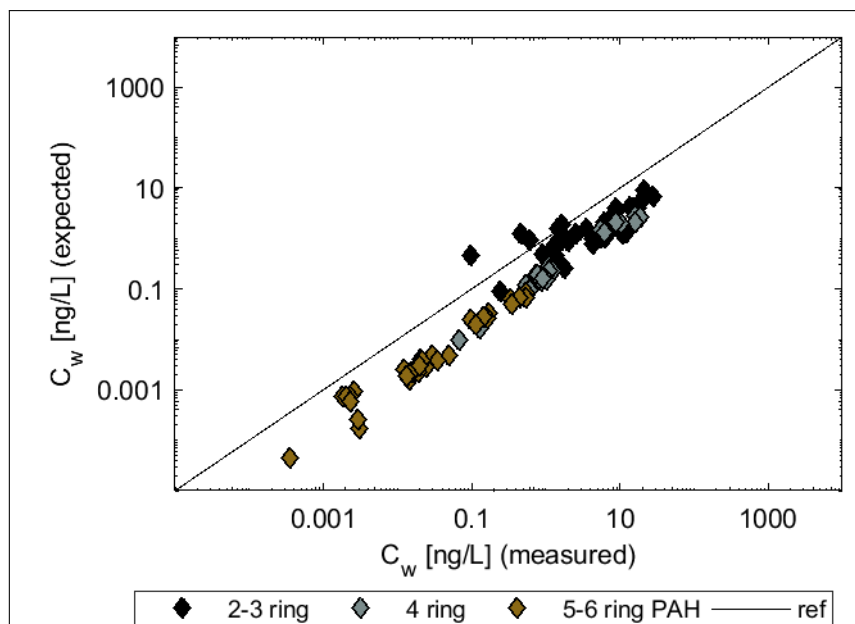


Figure A.13: Comparison of  $C_{w,eq}$ , determined for the 16 EPA PAHs with PE passive samplers in soil batches and calculated according to measured  $K_{Fr}$  for Tailfingen.

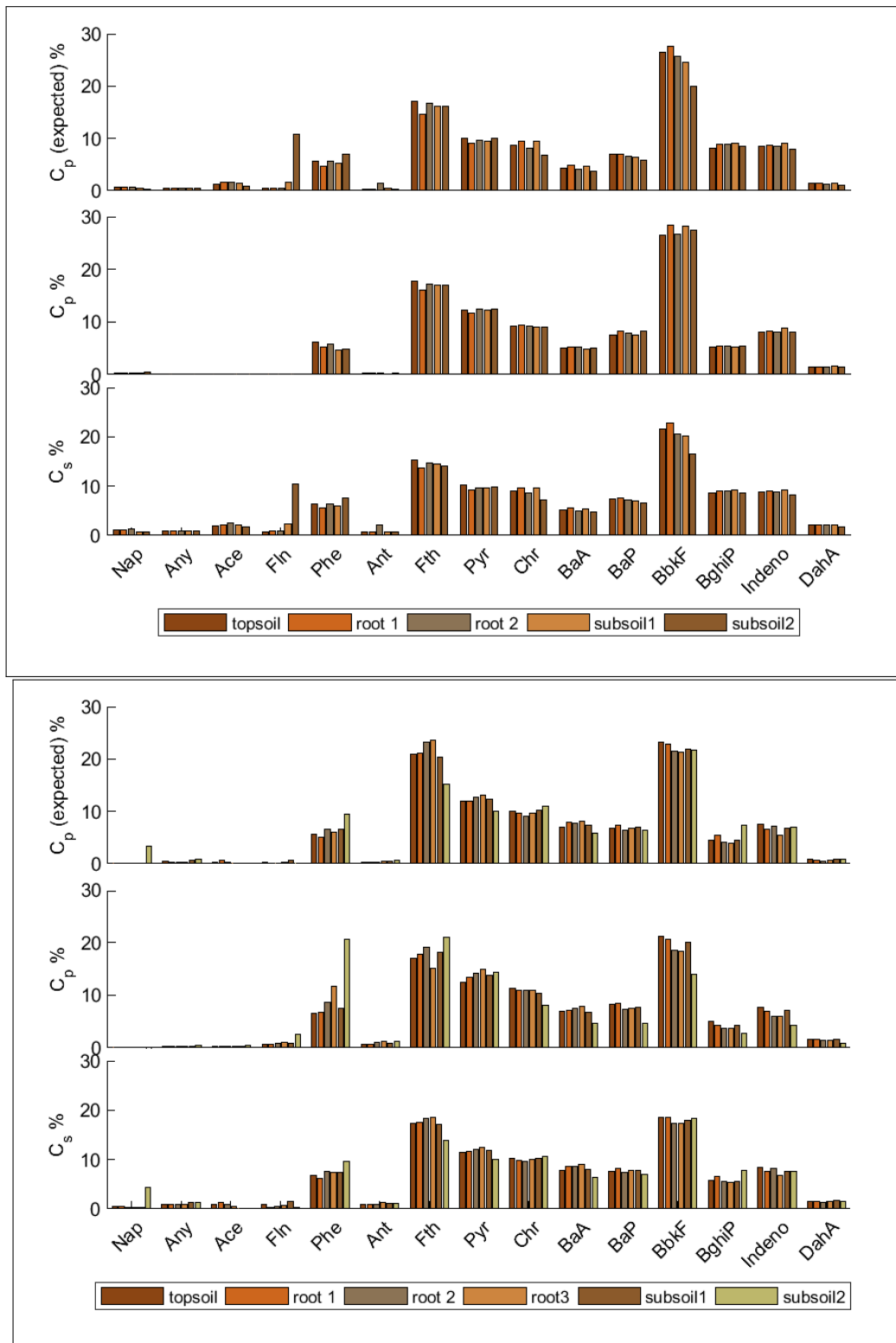


Figure A.14: Distribution patterns of the 16 EPA PAHs in each soil horizon in Poltringen (upper plot) and Tailfingen (lower plot), determined for the bulk soil and comparing expected to observed patterns on PE passive samplers.

**Table A.6: Contribution [%] of the four representative compounds Fln, Phe, Fth and Pyr to the sum of the 16 EPA PAHs and the according standard deviation [%] of their concentrations from triplicate analysis.**

Soil horizon	Contribution to $\Sigma$ PAHs [%]				Standard deviation [%]			
	Fln	Phe	Fth	Py	Fln	Phe	Fth	Py
<b>A) Entringen</b>								
Topsoil	1	6	16	11	3	5	6	6
Root horizon 1	1	6	15	11	5	6	7	9
Root horizon 2	1	6	15	11	2	7	6	5
Subsoil 1	5	7	14	10	32	2	8	6
Subsoil 2	2	7	16	11	7	10	9	8
<b>B) Poltringen</b>								
Topsoil	1	6	15	10	37	14	6	5
Root horizon 1	1	5	14	9	7	5	8	10
Root horizon 2	1	6	15	10	32	17	7	6
Root horizon 3	2	6	15	10	78	2	4	6
Subsoil 1	18	7	13	9	74	38	28	29
Subsoil 2	1	6	13	8	11	2	6	6
<b>C) Tailfingen</b>								
Topsoil	1	7	17	12	46	26	27	24
Root horizon 1	0	6	18	12	7	5	3	3
Root horizon 2	1	8	18	12	34	25	22	20
Root horizon 3	1	7	19	12	28	23	28	25
Subsoil 1	1	7	17	12	18	14	2	2
Subsoil 2	0	7	11	8	3	1	5	4
Subsoil 3	3	7	8	7	129	64	98	102

### A.5 Soil-Atmosphere Exchange of PAHs

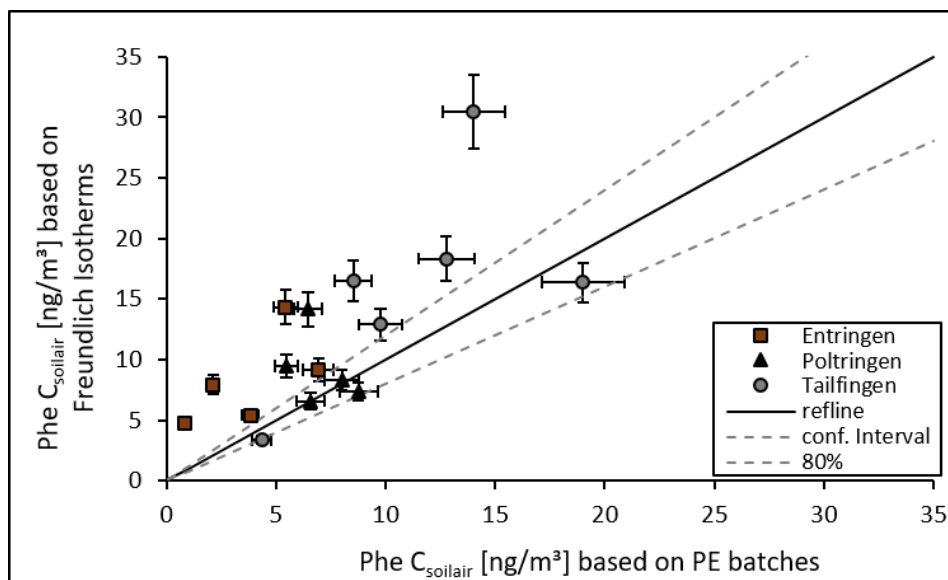


Figure A.15: Comparison of Phe concentrations in the soil air based on measured Freundlich coefficients versus PE equilibrated with soil slurries, determined for Entringen, Poltringen and Tailfingen individually and adapted to a temperature of 5° C.

**Table A.7: Phe concentrations in the atmosphere [ng/m<sup>3</sup>] determined for each location during seasonal monitorings in 2016/2017.**

Monitoring	Entringen	Poltringen	Tailfingen
May '16	2	1	1
August '16	2	1	2
November '16	8	10	10
February '17	8	11	10

**Table A.8: Phe concentrations in the atmosphere [ng/m<sup>3</sup>] determined for each location during seasonal monitorings in 2017/2018, including both sampling heights (0.1 m and 1.2 m).**

Monitoring	0.1 m			1.2 m		
	Entringen	Poltringen	Tailfingen	Entringen	Poltringen	Tailfingen
May `17	3	2	1	2	1	1
August `17	2	1	1	2	1	1
November `17	10	6	10	10	9	9
February `18	4	5	5	4	5	5



## A.5 Soil-Atmosphere Exchange of PAHs

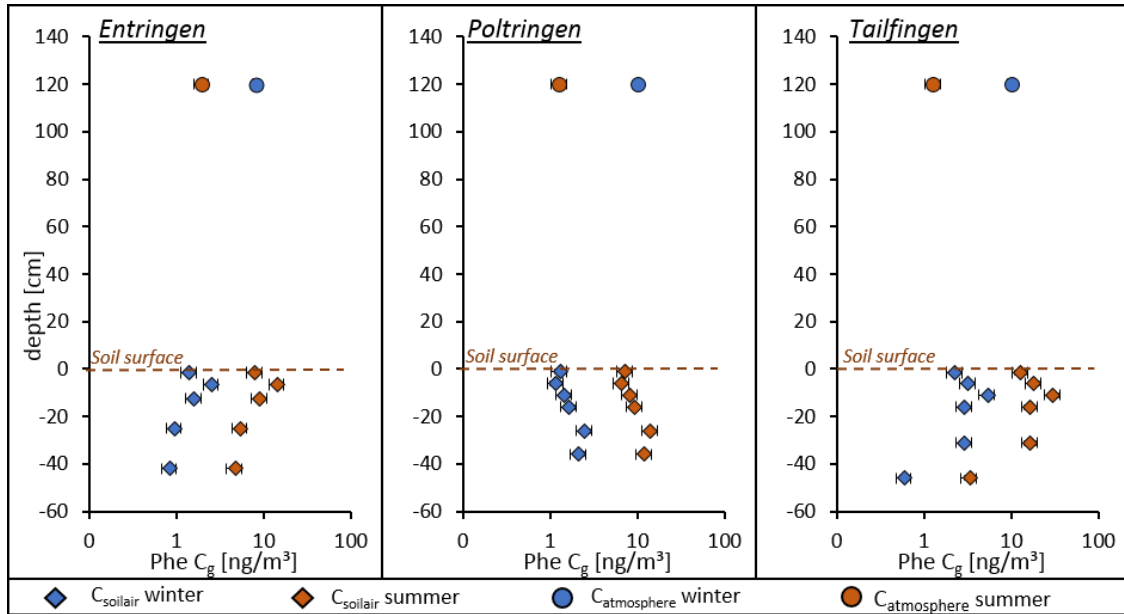


Figure A.16: Phe concentration profiles in gas phase, in the atmosphere measured by passive sampling and in the soil calculated from the bulk soil concentration and measured Freundlich coefficients comparing summer (with 20 °C) and winter (5 °C) at the different locations.

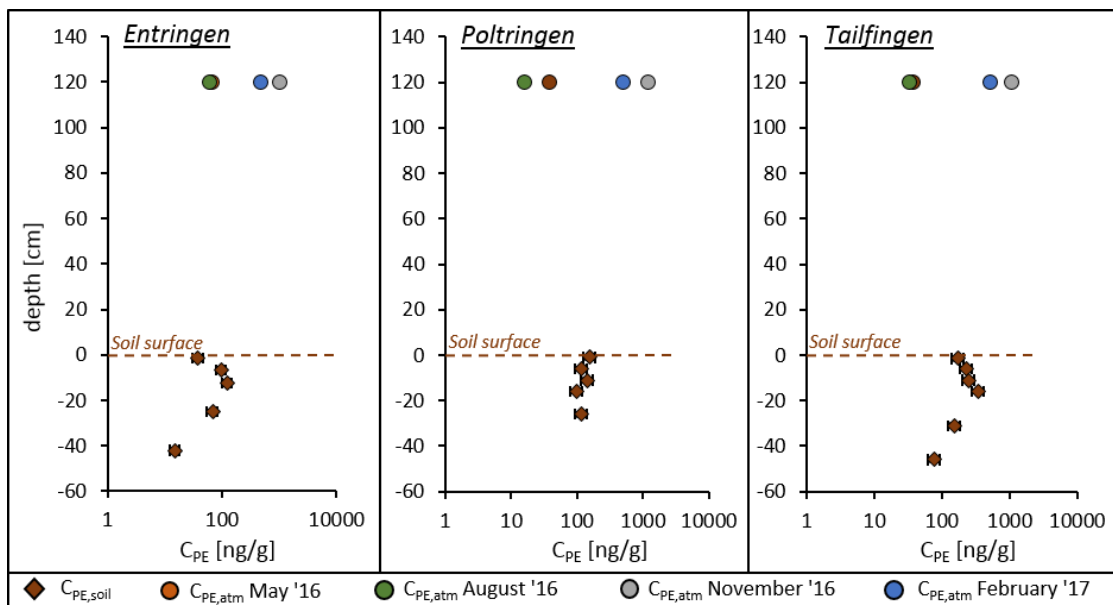


Figure A.17: Seasonal concentration gradients of Phe across the soil-atmosphere interface, directly comparing passive samplers deployed in both compartments at each of the study sites during the first year of monitoring campaigns.

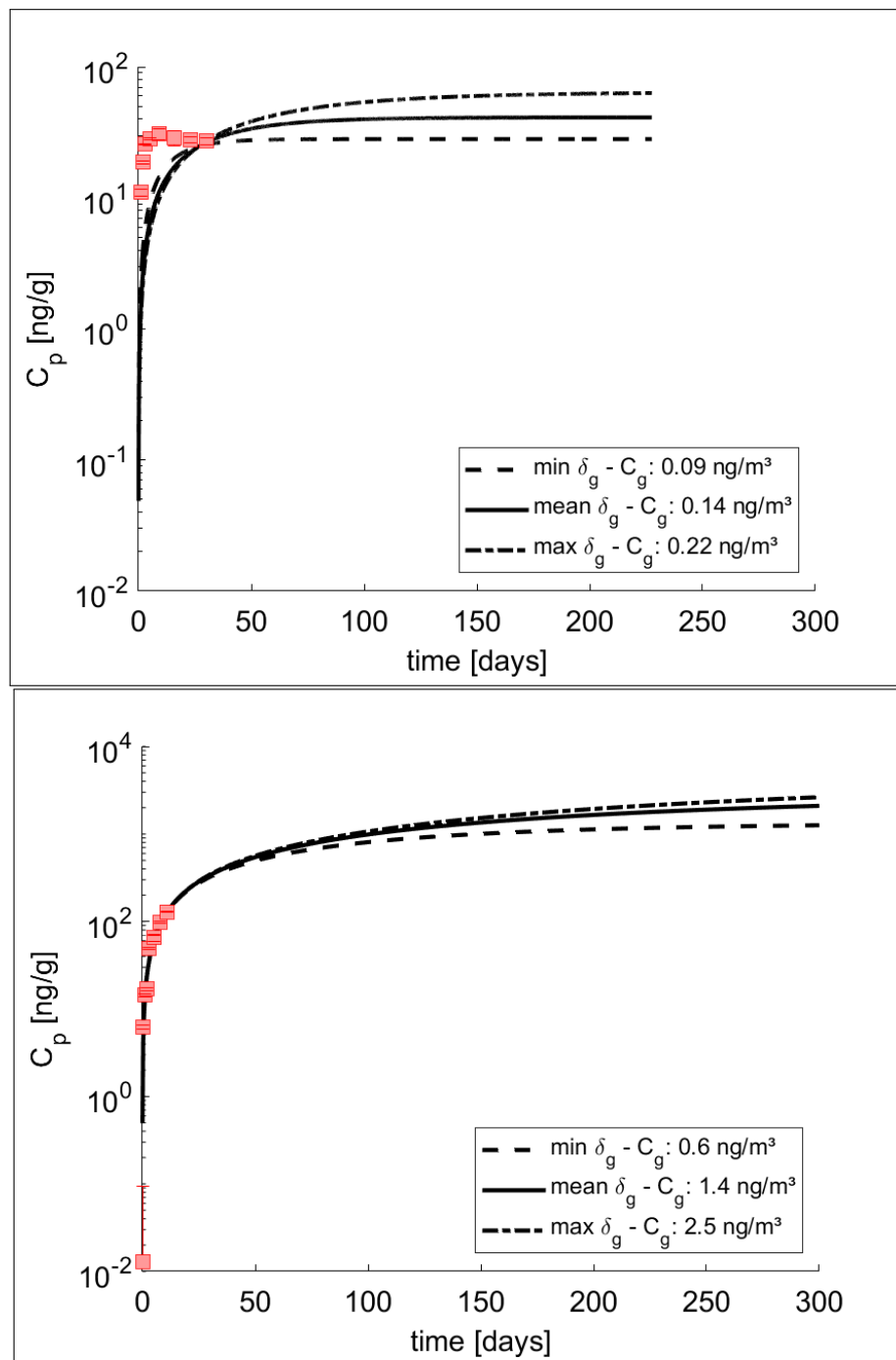


Figure A.18: Extrapolation of  $F_{th}$  on PE passive sampler in the atmosphere during August 2017 (upper plot) and November 2017 (lower plot), based on three different  $\delta_g$  and resulting  $C_g$  values, leading to explicitly different equilibrium concentrations on PE.

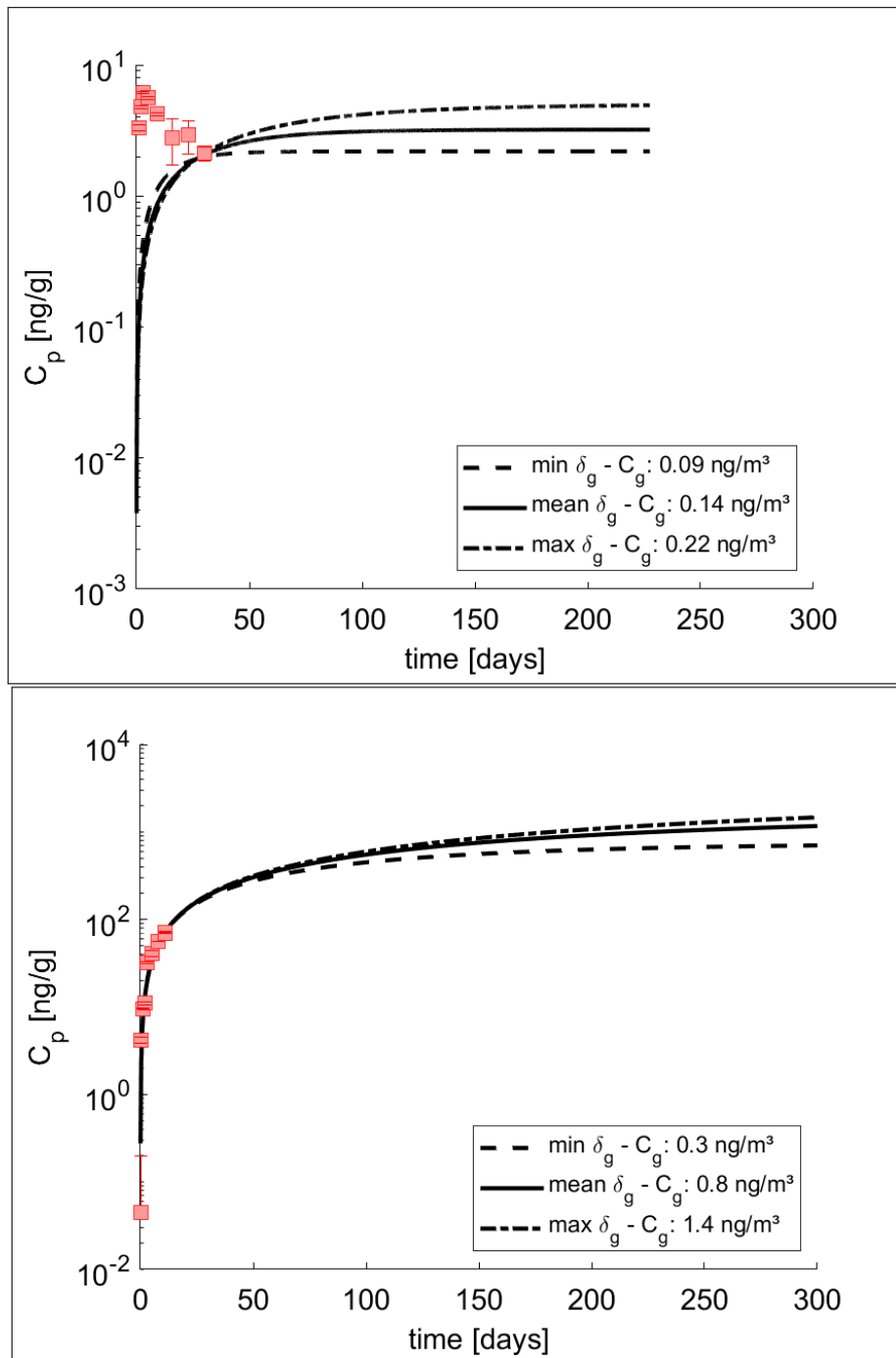


Figure A.19: Extrapolation of Pyr on PE passive sampler in the atmosphere during August 2017 (upper plot) and November 2017 (lower plot), based on three different  $\delta_g$  and resulting  $C_g$  values, leading to explicitly different equilibrium concentrations on PE.

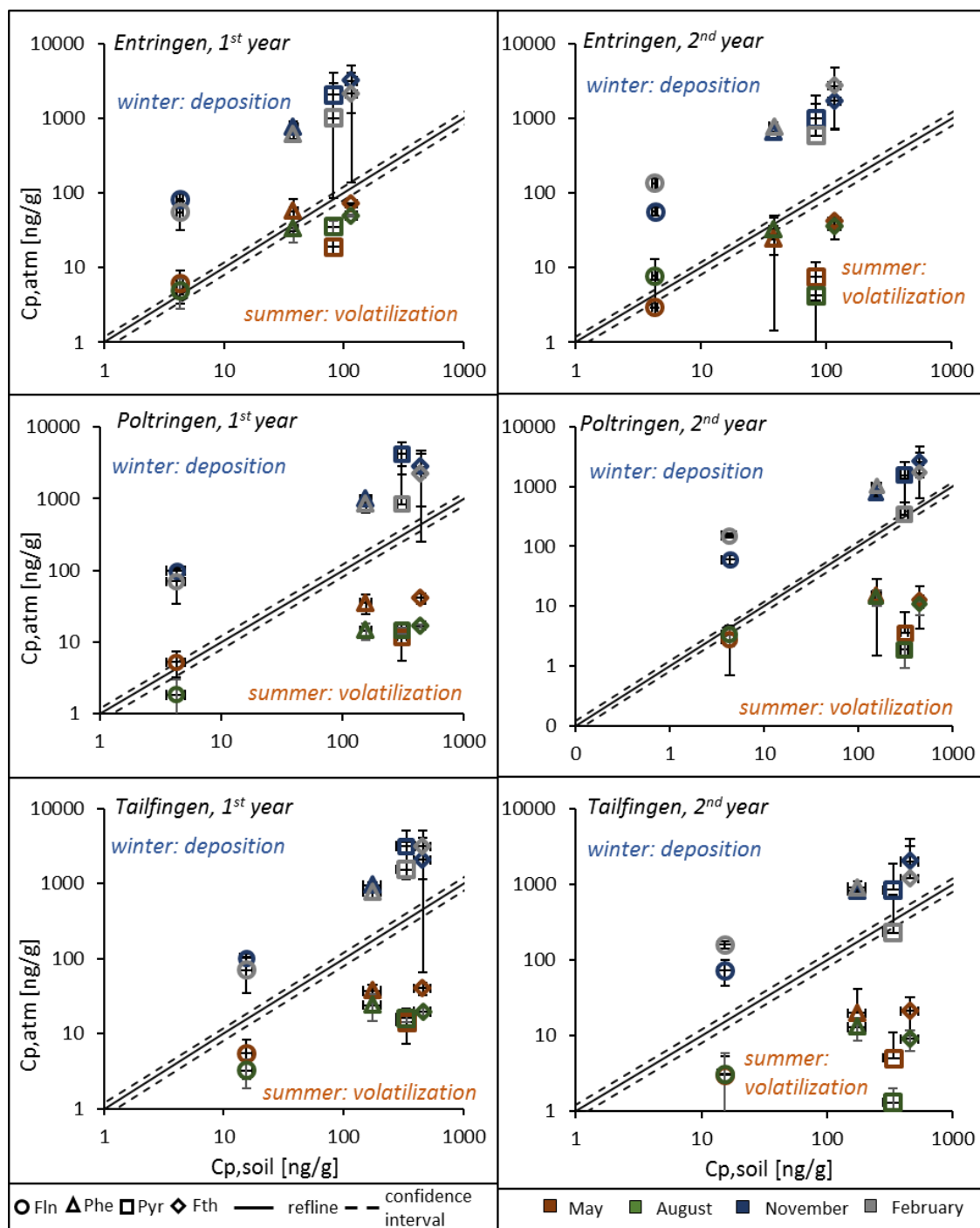


Figure A.20: Double logarithmic scatter plots of seasonal atmospheric concentrations of Fln, Phe, Fth and Pyr to estimated concentrations of the soil air in the topsoil, both based on passive samplers. Concentrations on the sampler within the atmosphere were extrapolated during November and February to obtain equilibrium conditions. Error bars indicate the measured standard deviation for triplicate samples, the reference line depicts a ratio of 1:1 and the confidence interval includes 20 % deviation.

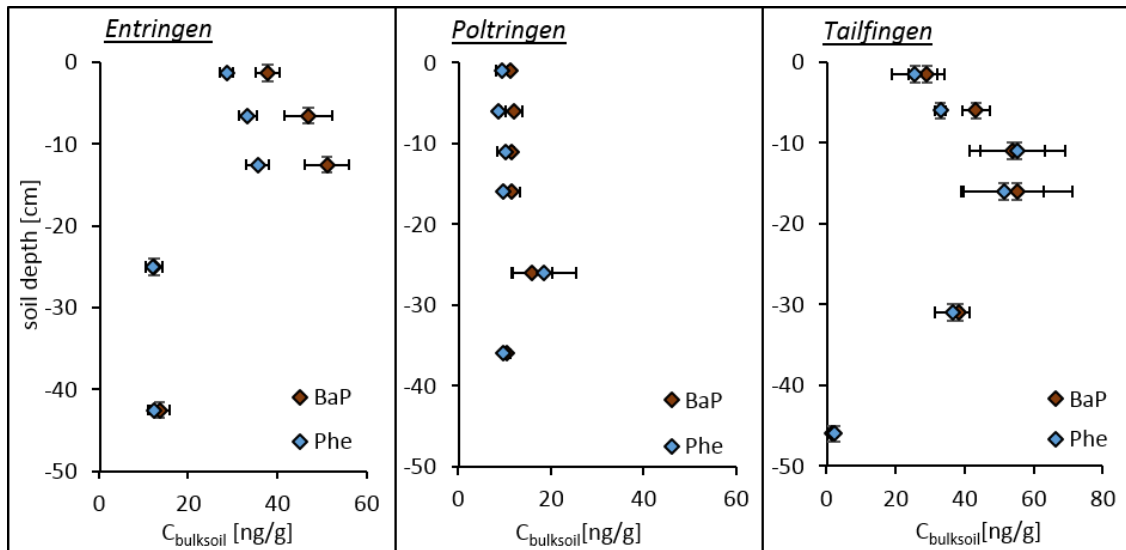


Figure A.21: Concentration profiles of BaP and Phe determined at each study site as a direct indicator on biodegradation with Phe being more biodegradable than BaP.

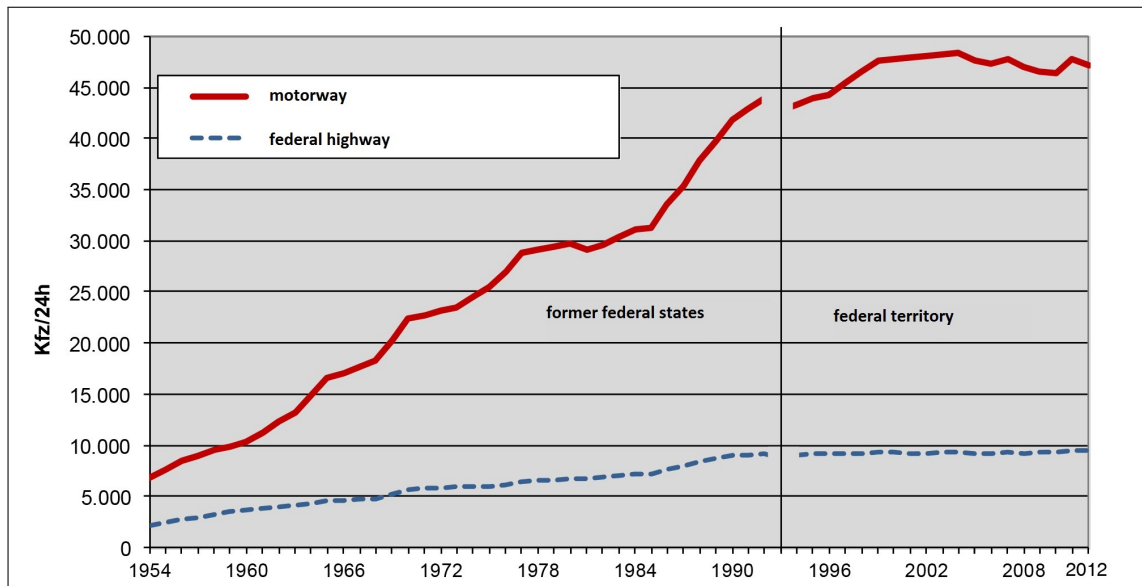


Figure A.22: Development of road traffic in Germany 1954 – 2012 (statistics provided by Federal Road Research Institute).

## Raw Data on Disc

### 1. Measured concentrations

1. Grainsize distribution
2. Organic carbon content
3. PAH concentrations in bulk soil
4. Phe concentrations of sorption tests
5. Concentrations in aqueous leachates (hot water extraction)
6. PAH concentrations on PE, during preliminary atmospheric test
7. PAH concentrations determined for day/night sampling
8. PAH concentrations determined with active sampling
9. PAH concentrations in PDMS coated jars in the atmosphere
10. PAH concentrations on PE for all seasonal atmospheric monitorings
11. Diurnal variation of Phe on PE (data adopted from Bettina Rüdiger)
12. Data from *German Weather Survey* for all seasonal monitorings, ambient and soil temperature, precipitation as well as solar radiation
13. Atmospheric bulk deposition
14. PAH concentrations measured during the batch kinetic test with PE
15. PAH concentrations in PDMS coated jars with soil slurries
16. PAH concentrations on PE from soil slurries for all soil profiles

### 2. Matlab Codes for the numerical model

1. Scripts for fitting of  $\delta_g$
2. Scripts for fitting of  $C_g$  and predicting uptake curves onto passive sampler

---

## References

- Abdel-Shafy, H. I. and Mansour, M. S. M. (2016). A review on polycyclic aromatic hydrocarbons: Source, environmental impact, effect on human health and remediation. *Egyptian Journal of Petroleum*, **25**(1), 107–123.
- Adams, R. G. ; Lohmann, R. . F. L. A. . M. J. . G. P. (2007). Polyethylene devices: Passive samplers for measuring dissolved hydrophobic organic compounds in aquatic environments. *Environ. Sci. Technol.*, **41**(4), 1317–1323.
- Aichner, B., Glaser, B., and Zech, W. (2007). Polycyclic aromatic hydrocarbons and polychlorinated biphenyls in urban soils from kathmandu, nepal. *Organic Geochemistry*, **38**(4), 700–715.
- Akyüz, M. and Çabuk, H. (2010). Gas–particle partitioning and seasonal variation of polycyclic aromatic hydrocarbons in the atmosphere of zonguldak, turkey. *Science of The Total Environment*, **408**(22), 5550–5558.
- Albuquerque, M., Coutinho, M., and Borrego, C. (2016). Long-term monitoring and seasonal analysis of polycyclic aromatic hydrocarbons (pahs) measured over a decade in the ambient air of porto, portugal. *Science of The Total Environment*, **543**, 439–448.
- Allan, I. J., Harman, C., Kringstad, A., and Bratsberg, E. (2010). Effect of sampler material on the uptake of pahs into passive sampling devices. *Chemosphere*, **79**(4), 470–5.
- Allan, I. J., Harman, C., Ranneklev, S. B., Thomas, K. V., and Grung, M. (2013). Passive sampling for target and nontarget analyses of moderately polar and nonpolar substances in water. *Environmental Toxicology and Chemistry*, **32**(8), 1718–1726.
- Allen-King, R. M., Grathwohl, P., and Ball, W. P. (2002). New modeling paradigms for the sorption of hydrophobic organic chemicals to heterogeneous carbonaceous matter in soils, sediments, and rocks. *Advances in Water Resources*, **25**(8), 985–1016.
- Alsberg, T., Håkansson, S., Strandell, M., and Westerholm, R. (1989). Profile analysis of urban air pollution. *Chemometrics and Intelligent Laboratory Systems*, **7**(1), 143–152.
- Arp, H. P., Hale, S. E., Elmquist Krusa, M., Cornelissen, G., Grabanski, C. B., Miller, D. J., and Hawthorne, S. B. (2015). Review of polyoxymethylene passive sampling methods for quantifying freely dissolved porewater concentrations of hydrophobic organic contaminants. *Environ Toxicol Chem*, **34**(4), 710–20.
- Atkinson, R.; Arey, J. (1994). Atmospheric chemistry of gas-phase polycyclic aromatic hydrocarbons: Formation of atmospheric mutagens.

## References

---

- Aydin, Y. M., Kara, M., Dumanoglu, Y., Odabasi, M., and Elbir, T. (2014). Source apportionment of polycyclic aromatic hydrocarbons (pahs) and polychlorinated biphenyls (pcbs) in ambient air of an industrial region in turkey. *Atmospheric Environment*, **97**, 271–285.
- Backe, C., Cousins, I. T., and Larsson, P. (2004). Pcb in soils and estimated soil–air exchange fluxes of selected pcb congeners in the south of sweden. *Environmental Pollution*, **128**(1), 59–72.
- Bao, Z., Haberer, C., Maier, U., Beckingham, B., Amos, R. T., and Grathwohl, P. (2015). Modeling long-term uptake and re-volatilization of semi-volatile organic compounds (svocs) across the soil-atmosphere interface. *Sci Total Environ*, **538**, 789–801.
- Bao, Z., Haberer, C. M., Maier, U., Beckingham, B., Amos, R. T., and Grathwohl, P. (2016). Modeling short-term concentration fluctuations of semi-volatile pollutants in the soil–plant–atmosphere system. *Science of The Total Environment*, **569-570**, 159–167.
- Barber, J. L., Thomas, G. O., Kerstiens, G., and Jones, K. C. (2004). Current issues and uncertainties in the measurement and modelling of air–vegetation exchange and within-plant processing of pops. *Environmental Pollution*, **128**(1), 99–138.
- Bartkow, M. E., Hawker, D. W., Kennedy, K. E., and Müller, J. F. (2004a). Characterizing uptake kinetics of pahs from the air using polyethylene-based passive air samplers of multiple surface area-to-volume ratios. *Environmental Science Technology*, **38**(9), 2701–2706.
- Bartkow, M. E., Huckins, J. N., and Müller, J. F. (2004b). Field-based evaluation of semipermeable membrane devices (spmds) as passive air samplers of polyaromatic hydrocarbons (pahs). *Atmospheric Environment*, **38**(35), 5983–5990.
- Bartkow, M. E., Booij, K., Kennedy, K. E., Muller, J. F., and Hawker, D. W. (2005). Passive air sampling theory for semivolatile organic compounds. *Chemosphere*, **60**(2), 170–6.
- Bartkow, M. E., Jones, K. C., Kennedy, K. E., Holling, N., Hawker, D. W., and Muller, J. F. (2006a). Evaluation of performance reference compounds in polyethylene-based passive air samplers. *Environ Pollut*, **144**(2), 365–70.
- Bartkow, M. E., Kennedy, K. E., Huckins, J. N., Holling, N., Komarova, T., and Muller, J. F. (2006b). Photodegradation of polyaromatic hydrocarbons in passive air samplers: field testing different deployment chambers. *Environ Pollut*, **144**(2), 371–6.
- Beckingham, B. and Ghosh, U. (2013). Polyoxymethylene passive samplers to monitor changes in bioavailability and flux of pcbs after activated carbon amendment to sediment in the field. *Chemosphere*, **91**(10), 1401–1407.



- Behymer, T. D. and Hites, R. A. (1985). Photolysis of polycyclic aromatic hydrocarbons adsorbed on simulated atmospheric particulates. Environmental Science Technology, **19**(10), 1004–1006.
- Belles, A., Alary, C., Criquet, J., Ivanovsky, A., and Billon, G. (2017). Assessing the transport of pah in the surficial sediment layer by passive sampler approach. Science of The Total Environment, **579**, 72–81.
- Bergknut, M., Sehlin, E., Lundstedt, S., Andersson, P. L., Haglund, P., and Tysklind, M. (2007). Comparison of techniques for estimating pah bioavailability: uptake in eisenia fetida, passive samplers and leaching using various solvents and additives. Environ Pollut, **145**(1), 154–60.
- Biache, C., Mansuy-Huault, L., and Faure, P. (2014). Impact of oxidation and biodegradation on the most commonly used polycyclic aromatic hydrocarbon (pah) diagnostic ratios: Implications for the source identifications. Journal of Hazardous Materials, **267**, 31–39.
- Birgöl, A., Tasdemir, Y., and Cindoruk, S. S. (2011). Atmospheric wet and dry deposition of polycyclic aromatic hydrocarbons (pahs) determined using a modified sampler. Atmospheric Research, **101**(1), 341–353.
- Booij, K. Hoedemaker, J. B. J. (2003). Dissolved pcbs, pahs and hcb in pore water and overlying waters of contaminated harbor sediments. Environ. Sci. Technol., **37**(18), 4213–4220.
- Booij, K. and van Drooge, B. L. (2001). Polychlorinated biphenyls and hexachlorobenzene in atmosphere, sea-surface microlayer, and water measured with semi-permeable membrane devices (spmDs). Chemosphere, **44**(2), 91–98.
- Booij, K., Sleiderink, H. M., and Smedes, F. (1998). Calibrating the uptake kinetics of semipermeable membrane devices using exposure standards. Environmental Toxicology and Chemistry, **17**(7), 1236–1245.
- Bozlaker, A., Muezzinoglu, A., and Odabasi, M. (2008). Atmospheric concentrations, dry deposition and air–soil exchange of polycyclic aromatic hydrocarbons (pahs) in an industrial region in turkey. Journal of Hazardous Materials, **153**(3), 1093–1102.
- Bruheim, I., Liu, X., and Pawliszyn, J. (2003). Thin-film microextraction. Analytical Chemistry, **75**(4), 1002–1010.
- Brun, G. L., Vaidya, O. C., and Léger, M. G. (2004). Atmospheric deposition of polycyclic aromatic hydrocarbons to atlantic canada: geographic and temporal distributions and trends 1980–2001. Environmental Science Technology, **38**(7), 1941–1948.

## References

---

- Brändli, R. C., Hartnik, T., Henriksen, T., and Cornelissen, G. (2008). Sorption of native polyaromatic hydrocarbons (pah) to black carbon and amended activated carbon in soil. *Chemosphere*, **73**(11), 1805–1810.
- Bucheli, T. D., Blum, F., Desaulles, A., and Gustafsson, (2004). Polycyclic aromatic hydrocarbons, black carbon, and molecular markers in soils of switzerland. *Chemosphere*, **56**(11), 1061–1076.
- Butler, J. D. and Crossley, P. (1981). Reactivity of polycyclic aromatic hydrocarbons adsorbed on soot particles. *Atmospheric Environment* (1967), **15**(1), 91–94.
- Cabrerizo, A., Dachs, J., and Barceló, D. (2009). Development of a soil fugacity sampler for determination of airsoil partitioning of persistent organic pollutants under field controlled conditions. *Environmental Science Technology*, **43**(21), 8257–8263.
- Cabrerizo, A., Dachs, J., Moeckel, C., Ojeda, M. J., Caballero, G., Barcelo, D., and Jones, K. C. (2011a). Factors influencing the soil-air partitioning and the strength of soils as a secondary source of polychlorinated biphenyls to the atmosphere. *Environ Sci Technol*, **45**(11), 4785–92.
- Cabrerizo, A., Dachs, J., Moeckel, C., Ojeda, M. J., Caballero, G., Barcelo, D., and Jones, K. C. (2011b). Ubiquitous net volatilization of polycyclic aromatic hydrocarbons from soils and parameters influencing their soil-air partitioning. *Environ Sci Technol*, **45**(11), 4740–7.
- Carmo, A. M., Hundal, L. S., and Thompson, M. L. (2000). Sorption of hydrophobic organic compounds by soil materials: application of unit equivalent freundlich coefficients. *Environmental Science Technology*, **34**(20), 4363–4369.
- Carratalá, A., Moreno-González, R., and León, V. M. (2017). Occurrence and seasonal distribution of polycyclic aromatic hydrocarbons and legacy and current-use pesticides in air from a mediterranean coastal lagoon (mar menor, se spain). *Chemosphere*, **167**, 382–395.
- Cetin, B., Yurdakul, S., Keles, M., Celik, I., Ozturk, F., and Dogan, C. (2017a). Atmospheric concentrations, distributions and air-soil exchange tendencies of pahs and pcbs in a heavily industrialized area in kocaeli, turkey. *Chemosphere*, **183**, 69–79.
- Cetin, B., Ozturk, F., Keles, M., and Yurdakul, S. (2017b). Pahs and pcbs in an eastern mediterranean megacity, istanbul: Their spatial and temporal distributions, air-soil exchange and toxicological effects. *Environmental Pollution*, **220**, 1322–1332.
- Cetin, B., Yurdakul, S., Gungormus, E., Ozturk, F., and Sofuoglu, S. C. (2018). Source apportionment and carcinogenic risk assessment of passive air sampler-derived pahs and pcbs in a heavily industrialized region. *Science of The Total Environment*, **633**, 30–41.

- Chen, Y., Feng, Y., Xiong, S., Liu, D., Wang, G., Sheng, G., and Fu, J. (2011). Polycyclic aromatic hydrocarbons in the atmosphere of shanghai, china. Environmental Monitoring and Assessment, **172**(1), 235–247.
- Chiou, C. T., Schmedding, D. W., and Manes, M. (2005). Improved prediction of octanol-water partition coefficients from liquid-solute water solubilities and molar volumes. Environmental Science Technology, **39**(22), 8840–8846.
- Cornelissen, G. and Gustafsson, (2004). Sorption of phenanthrene to environmental black carbon in sediment with and without organic matter and native sorbates. Environmental Science Technology, **38**(1), 148–155.
- Cornelissen, G., Breedveld, G. D., Kalaitzidis, S., Christanis, K., Kibsgaard, A., and Oen, A. M. P. (2006). Strong sorption of native pahs to pyrogenic and unburned carbonaceous geosorbents in sediments. Environmental Science Technology, **40**(4), 1197–1203.
- Cornelissen, G., Pettersen, A., Broman, D., Mayer, P., and Breedveld, G. D. (2008). Field testing of equilibrium passive samplers to determine freely dissolved native polycyclic aromatic hydrocarbon concentrations. Environmental Toxicology and Chemistry, **27**(3), 499–508.
- Cousins, I. T. and Jones, K. C. (1998). Air–soil exchange of semi-volatile organic compounds (socs) in the uk. Environmental Pollution, **102**(1), 105–118.
- Cousins, I. T., Beck, A. J., and Jones, K. C. (1999). A review of the processes involved in the exchange of semi-volatile organic compounds (svoc) across the air–soil interface. Science of The Total Environment, **228**(1), 5–24.
- Dachs, J. and Eisenreich, S. J. (2000). Adsorption onto aerosol soot carbon dominates gas-particle partitioning of polycyclic aromatic hydrocarbons. Environmental Science Technology, **34**(17), 3690–3697.
- Dachs, J., Glenn, T. R., Gigliotti, C. L., Brunciak, P., Totten, L. A., Nelson, E. D., Franz, T. P., and Eisenreich, S. J. (2002). Processes driving the short-term variability of polycyclic aromatic hydrocarbons in the baltimore and northern chesapeake bay atmosphere, usa. Atmospheric Environment, **36**(14), 2281–2295.
- Dat, N.-D. and Chang, M. B. (2017). Review on characteristics of pahs in atmosphere, anthropogenic sources and control technologies. Science of The Total Environment, **609**, 682–693.
- De La Torre-Roche, R. J., Lee, W.-Y., and Campos-Díaz, S. I. (2009). Soil-borne polycyclic aromatic hydrocarbons in el paso, texas: Analysis of a potential problem in the united states/mexico border region. Journal of Hazardous Materials, **163**(2), 946–958.

## References

---

- Degrendele, C., Audy, O., Hofman, J., Kučerik, J., Kukučka, P., Mulder, M. D., Příbylová, P., Prokeš, R., Šáňka, M., Schaumann, G. E., and Lammel, G. (2016). Diurnal variations of air-soil exchange of semivolatile organic compounds (pahs, pcbs, ocps, and pbdes) in a central european receptor area. *Environmental Science Technology*, **50**(8), 4278–4288.
- Demircioglu, E., Sofuoglu, A., and Odabasi, M. (2011). Particle-phase dry deposition and air–soil gas exchange of polycyclic aromatic hydrocarbons (pahs) in izmir, turkey. *Journal of Hazardous Materials*, **186**(1), 328–335.
- Desaules, A., Ammann, S., Blum, F., Brändli, R. C., Bucheli, T. D., and Keller, A. (2008). Pah and pcb in soils of switzerland—status and critical review. *Journal of Environmental Monitoring*, **10**(11), 1265–1277.
- Dickhut, R. M., Canuel, E. A., Gustafson, K. E., Liu, K., Arzayus, K. M., Walker, S. E., Edgcombe, G., Gaylor, M. O., and MacDonald, E. H. (2000). Automotive sources of carcinogenic polycyclic aromatic hydrocarbons associated with particulate matter in the chesapeake bay region. *Environmental Science Technology*, **34**(21), 4635–4640.
- DiFilippo, E. L. and Eganhouse, R. P. (2010). Assessment of pdms-water partition coefficients: Implications for passive environmental sampling of hydrophobic organic compounds. *Environmental Science Technology*, **44**(18), 6917–6925.
- Donald, C. E. and Anderson, K. A. (2017). Assessing soil-air partitioning of pahs and pcbs with a new fugacity passive sampler. *Science of The Total Environment*, **596-597**, 293–302.
- Dumanoglu, Y., Gaga, E. O., Gungormus, E., Sofuoglu, S. C., and Odabasi, M. (2017). Spatial and seasonal variations, sources, air-soil exchange, and carcinogenic risk assessment for pahs and pcbs in air and soil of kutahya, turkey, the province of thermal power plants. *Science of The Total Environment*, **580**, 920–935.
- Dvorská, A., Lammel, G., and Klánová, J. (2011). Use of diagnostic ratios for studying source apportionment and reactivity of ambient polycyclic aromatic hydrocarbons over central europe. *Atmospheric Environment*, **45**(2), 420–427.
- Endo, S., Yabuki, Y., and Tanaka, S. (2017). Comparing polyethylene and polyoxymethylene passive samplers for measuring sediment porewater concentrations of polychlorinated biphenyls: Mutual validation and possible correction by polymer-polymer partition experiment. *Chemosphere*, **184**, 358–365.
- Estoppey, N., Schopfer, A., Fong, C., Delemont, O., De Alencastro, L. F., and Esseiva, P. (2016). An in-situ assessment of low-density polyethylene and silicone rubber passive samplers using methods with and without performance reference compounds in

- the context of investigation of polychlorinated biphenyl sources in rivers. Sci Total Environ, **572**, 794–803.
- Farrar, N. J., Harner, T. J., Sweetman, A. J., and Jones, K. C. (2005a). Field calibration of rapidly equilibrating thin-film passive air samplers and their potential application for low-volume air sampling studies. Environmental Science Technology, **39**(1), 261–267.
- Farrar, N. J., Harner, T., Shoeib, M., Sweetman, A., and Jones, K. C. (2005b). Field deployment of thin film passive air samplers for persistent organic pollutants: a study in the urban atmospheric boundary layer. Environmental Science Technology, **39**(1), 42–48.
- Farrar, N. J., Prevedouros, K., Harner, T., Sweetman, A. J., and Jones, K. C. (2006). Continental scale passive air sampling of persistent organic pollutants using rapidly equilibrating thin films (pogs). Environ Pollut, **144**(2), 423–33.
- Feng, D., Liu, Y., Gao, Y., Zhou, J., Zheng, L., Qiao, G., Ma, L., Lin, Z., and Grathwohl, P. (2017). Atmospheric bulk deposition of polycyclic aromatic hydrocarbons in shanghai: Temporal and spatial variation, and global comparison. Environ Pollut, **230**, 639–647.
- Finizio, A., Mackay, D., Bidleman, T., and Harner, T. (1997). Octanol-air partition coefficient as a predictor of partitioning of semi-volatile organic chemicals to aerosols. Atmospheric Environment, **31**(15), 2289–2296.
- Franz, T. P. and Eisenreich, S. J. (1998). Snow scavenging of polychlorinated biphenyls and polycyclic aromatic hydrocarbons in minnesota. Environmental Science Technology, **32**(12), 1771–1778.
- Gao, Y., Xiong, W., Ling, W., Wang, X., and Li, Q. (2007). Impact of exotic and inherent dissolved organic matter on sorption of phenanthrene by soils. Journal of Hazardous Materials, **140**(1), 138–144.
- Garban, B., Blanchoud, H., Motelay-Massei, A., Chevreuil, M., and Ollivon, D. (2002). Atmospheric bulk deposition of pahs onto france: trends from urban to remote sites. Atmospheric Environment, **36**(34), 5395–5403.
- Ghirardello, D., Morselli, M., Semplice, M., and Di Guardo, A. (2010). A dynamic model of the fate of organic chemicals in a multilayered air/soil system: Development and illustrative application. Environmental Science Technology, **44**(23), 9010–9017.
- Ghosh, U., Kane Driscoll, S., Burgess, R. M., Jonker, M. T., Reible, D., Gobas, F., Choi, Y., Apitz, S. E., Maruya, K. A., Gala, W. R., Mortimer, M., and Beegan, C. (2014). Passive sampling methods for contaminated sediments: practical guidance

## References

---

- for selection, calibration, and implementation. Integr Environ Assess Manag, **10**(2), 210–23.
- Gigliotti, C. L., Totten, L. A., Offenberg, J. H., Dachs, J., Reinfelder, J. R., Nelson, E. D., Glenn, and Eisenreich, S. J. (2005). Atmospheric concentrations and deposition of polycyclic aromatic hydrocarbons to the mid-atlantic east coast region. Environmental Science Technology, **39**(15), 5550–5559.
- Gocht, T. (2005). Die vier Griechischen Elemente: Massenbilanzierung von polyzyklischen aromatischen Kohlenwasserstoffen (PAK) in Kleineinzugsgebieten des ländlichen Raumes. Thesis.
- Gocht, T., Klemm, O., and Grathwohl, P. (2007). Long-term atmospheric bulk deposition of polycyclic aromatic hydrocarbons (pahs) in rural areas of southern germany. Atmospheric Environment, **41**(6), 1315–1327.
- Golomb, D., Barry, E., Fisher, G., Varanusupakul, P., Koleda, M., and Rooney, T. (2001). Atmospheric deposition of polycyclic aromatic hydrocarbons near new england coastal waters. Atmospheric Environment, **35**(36), 6245–6258.
- Gouin, T., Thomas, G. O., Cousins, I., Barber, J., Mackay, D., and Jones, K. C. (2002). Airsurface exchange of polybrominated diphenyl ethers and polychlorinated biphenyls. Environmental Science Technology, **36**(7), 1426–1434.
- Gouin, T., Mackay, D., Jones, K. C., Harner, T., and Meijer, S. N. (2004). Evidence for the “grasshopper” effect and fractionation during long-range atmospheric transport of organic contaminants. Environmental Pollution, **128**(1), 139–148.
- Gouin, T., Harner, T., Blanchard, P., and Mackay, D. (2005). Passive and active air samplers as complementary methods for investigating persistent organic pollutants in the great lakes basin. Environmental Science Technology, **39**(23), 9115–9122.
- Grathwohl, P. (1990). Influence of organic matter from soils and sediments from various origins on the sorption of some chlorinated aliphatic hydrocarbons: implications on koc correlations. Environmental Science amp; Technology, **24**(11), 1687–1693.
- Grathwohl, P. (2012). Diffusion in Natural Porous Media: Contaminant Transport, Sorption/Desorption and Dissolution Kinetics. Springer US.
- Gschwend, P. M. and Hites, R. A. (1981). Fluxes of polycyclic aromatic hydrocarbons to marine and lacustrine sediments in the northeastern united states. Geochimica et Cosmochimica Acta, **45**(12), 2359–2367.
- Gschwend, P. M., MacFarlane, J. K., Reible, D. D., Lu, X., Hawthorne, S. B., Nakles, D. V., and Thompson, T. (2011). Comparison of polymeric samplers for accurately assessing pcbs in pore waters. Environ Toxicol Chem, **30**(6), 1288–96.

- Guo, X., Luo, L., Ma, Y., and Zhang, S. (2010). Sorption of polycyclic aromatic hydrocarbons on particulate organic matters. Journal of Hazardous Materials, **173**(1), 130–136.
- Halsall, C. J., Barrie, L. A., Fellin, P., Muir, D. C. G., Billeck, B. N., Lockhart, L., Rovinsky, F. Y., Kononov, E. Y., and Pastukhov, B. (1997). Spatial and temporal variation of polycyclic aromatic hydrocarbons in the arctic atmosphere. Environmental Science Technology, **31**(12), 3593–3599.
- Harmsen, J. and Rietra, R. P. J. J. (2018). 25 years monitoring of pahs and petroleum hydrocarbons biodegradation in soil. Chemosphere, **207**, 229–238.
- Harner, T. and Bidleman, T. F. (1998). Measurement of octanolair partition coefficients for polycyclic aromatic hydrocarbons and polychlorinated naphthalenes. Journal of Chemical Engineering Data, **43**(1), 40–46.
- Harner, T., Green, N. J. L., and Jones, K. C. (2000). Measurements of octanolair partition coefficients for pcdd/fs: a tool in assessing airsoil equilibrium status. Environmental Science Technology, **34**(15), 3109–3114.
- Harner, T., Bidleman, T. F., Jantunen, L. M. M., and Mackay, D. (2001). Soil—air exchange model of persistent pesticides in the united states cotton belt. Environmental Toxicology and Chemistry, **20**(7), 1612–1621.
- Harner, T., Bartkow, M., Holoubek, I., Klanova, J., Wania, F., Gioia, R., Moeckel, C., Sweetman, A. J., and Jones, K. C. (2006). Passive air sampling for persistent organic pollutants: introductory remarks to the special issue. Environ Pollut, **144**(2), 361–4.
- Harrison, R. M., Smith, D. J. T., and Luhana, L. (1996). Source apportionment of atmospheric polycyclic aromatic hydrocarbons collected from an urban location in birmingham, u.k. Environmental Science Technology, **30**(3), 825–832.
- Hawthorne, S. B., Jonker, M. T., van der Heijden, S. A., Grabanski, C. B., Azzolina, N. A., and Miller, D. J. (2011). Measuring picogram per liter concentrations of freely dissolved parent and alkyl pahs (pah-34), using passive sampling with polyoxymethylene. Anal Chem, **83**(17), 6754–61.
- Hayward, S. J., Gouin, T., and Wania, F. (2010). Comparison of four active and passive sampling techniques for pesticides in air. Environmental Science Technology, **44**(9), 3410–3416.
- Henzler, R. (2004). Quantifizierung und Modellierung der PAK Elution aus verfestigten und unverfestigten Abfallmaterialien. Thesis.

## References

---

- Herkert, N. J., Martinez, A., and Hornbuckle, K. C. (2016). A model using local weather data to determine the effective sampling volume for pcb congeners collected on passive air samplers. *Environmental Science Technology*, **50**(13), 6690–6697.
- Hippelein, M. and McLachlan, M. S. (1998). Soil/air partitioning of semivolatile organic compounds. 1. method development and influence of physical/chemical properties. *Environmental Science Technology*, **32**(2), 310–316.
- Howsam, M. and Jones, K. C. (1998). *Sources of PAHs in the Environment*, pages 137–174. Springer Berlin Heidelberg, Berlin, Heidelberg.
- Huang, W., Yu, H., and Weber, W. J. (1998). Hysteresis in the sorption and desorption of hydrophobic organic contaminants by soils and sediments: 1. a comparative analysis of experimental protocols. *Journal of Contaminant Hydrology*, **31**(1), 129–148.
- Huckins, J. N., Manuweera, G. K., Petty, J. D., Mackay, D., and Lebo, J. A. (1993). Lipid-containing semipermeable membrane devices for monitoring organic contaminants in water. *Environmental Science Technology*, **27**(12), 2489–2496.
- Huckins, J. N., Petty, J. D., Orazio, C. E., Lebo, J. A., Clark, R. C., Gibson, V. L., Gala, W. R., and Echols, K. R. (1999). Determination of uptake kinetics (sampling rates) by lipid-containing semipermeable membrane devices (spmds) for polycyclic aromatic hydrocarbons (pahs) in water. *Environmental Science Technology*, **33**(21), 3918–3923.
- Huckins, J. N., Petty, J. D., Lebo, J. A., Almeida, F. V., Booij, K., Alvarez, D. A., Cranor, W. L., Clark, R. C., and Mogensen, B. B. (2002). Development of the permeability/performance reference compound approach for in situ calibration of semipermeable membrane devices. *Environmental Science Technology*, **36**(1), 85–91.
- Hung, H., Blanchard, P., Halsall, C. J., Bidleman, T. F., Stern, G. A., Fellin, P., Muir, D. C. G., Barrie, L. A., Jantunen, L. M., Helm, P. A., Ma, J., and Konoplev, A. (2005). Temporal and spatial variabilities of atmospheric polychlorinated biphenyls (pcbs), organochlorine (oc) pesticides and polycyclic aromatic hydrocarbons (pahs) in the canadian arctic: Results from a decade of monitoring. *Science of The Total Environment*, **342**(1), 119–144.
- Hung, H., Katsoyiannis, A. A., and Guardans, R. (2016). Ten years of global monitoring under the stockholm convention on persistent organic pollutants (pops): Trends, sources and transport modelling. *Environ Pollut*, **217**, 1–3.
- Hwang, H.-M., Wade, T. L., and Sericano, J. L. (2003). Concentrations and source characterization of polycyclic aromatic hydrocarbons in pine needles from korea, mexico, and united states. *Atmospheric Environment*, **37**(16), 2259–2267.



- Jahnke, A., McLachlan, M. S., and Mayer, P. (2008). Equilibrium sampling: Partitioning of organochlorine compounds from lipids into polydimethylsiloxane. *Chemosphere*, **73**(10), 1575–1581.
- Jahnke, A., Mayer, P., and McLachlan, M. S. (2012). Sensitive equilibrium sampling to study polychlorinated biphenyl disposition in baltic sea sediment. *Environmental Science Technology*, **46**(18), 10114–10122.
- Jang, E., Alam, M. S., and Harrison, R. M. (2013). Source apportionment of polycyclic aromatic hydrocarbons in urban air using positive matrix factorization and spatial distribution analysis. *Atmospheric Environment*, **79**, 271–285.
- Jaward, F. M., Farrar, N. J., Harner, T., Sweetman, A. J., and Jones, K. C. (2004). Passive air sampling of polycyclic aromatic hydrocarbons and polychlorinated naphthalenes across europe. *Environmental Toxicology and Chemistry*, **23**(6), 1355–1364.
- Jones, K. C. (1994). Observations on long-term air-soil exchange of organic contaminants. *Environmental Science and Pollution Research*, **1**(3), 172.
- Jones, K. C., Stratford, J. A., Waterhouse, K. S., and Vogt, N. B. (1989a). Organic contaminants in welsh soils: polynuclear aromatic hydrocarbons. *Environmental Science Technology*, **23**(5), 540–550.
- Jones, K. C., Stratford, J. A., Tidridge, P., Waterhouse, K. S., and Johnston, A. E. (1989b). Polynuclear aromatic hydrocarbons in an agricultural soil: Long-term changes in profile distribution. *Environmental Pollution*, **56**(4), 337–351.
- Jonker, M. T. O. and Koelmans, A. A. (2002). Sorption of polycyclic aromatic hydrocarbons and polychlorinated biphenyls to soot and soot-like materials in the aqueous environment: mechanistic considerations. *Environmental Science Technology*, **36**(17), 3725–3734.
- Kakareka, S. V., Kukharchyk, T. I., and Khomich, V. S. (2005). Study of pah emission from the solid fuels combustion in residential furnaces. *Environmental Pollution*, **133**(2), 383–387.
- Kan, A. T., Fu, G., and Tomson, M. B. (1994). Adsorption/desorption hysteresis in organic pollutant and soil/sediment interaction. *Environmental Science Technology*, **28**(5), 859–867.
- Karickhoff, S. W. (1981). Semi-empirical estimation of sorption of hydrophobic pollutants on natural sediments and soils. *Chemosphere*, **10**(8), 833–846.
- Karickhoff, S. W., Brown, D. S., and Scott, T. A. (1979). Sorption of hydrophobic pollutants on natural sediments. *Water Research*, **13**(3), 241–248.

## References

---

- Kavouras, I. G., Koutrakis, P., Tsapakis, M., Lagoudaki, E., Stephanou, E. G., Von Baer, D., and Oyola, P. (2001). Source apportionment of urban particulate aliphatic and polynuclear aromatic hydrocarbons (pahs) using multivariate methods. *Environmental Science Technology*, **35**(11), 2288–2294.
- Kaya, E., Dumanoglu, Y., Kara, M., Altioik, H., Bayram, A., Elbir, T., and Odabasi, M. (2012). Spatial and temporal variation and air–soil exchange of atmospheric pahs and pcbs in an industrial region. *Atmospheric Pollution Research*, **3**(4), 435–449.
- Khairy, M. A. and Lohmann, R. (2012). Field validation of polyethylene passive air samplers for parent and alkylated pahs in alexandria, egypt. *Environ Sci Technol*, **46**(7), 3990–8.
- Khairy, M. A. and Lohmann, R. (2014). Field calibration of low density polyethylene passive samplers for gaseous pops. *Environ Sci Process Impacts*, **16**(3), 414–21.
- Khalili, N. R., Scheff, P. A., and Holsen, T. M. (1995). Pah source fingerprints for coke ovens, diesel and, gasoline engines, highway tunnels, and wood combustion emissions. *Atmospheric Environment*, **29**(4), 533–542.
- Kim, D., Young, T. M., and Anastasio, C. (2013). Phototransformation rate constants of pahs associated with soot particles. *Sci Total Environ*, **443**, 896–903.
- Kiss, G., Varga-Puchony, Z., Tolnai, B., Varga, B., Gelencsér, A., Krivácsy, Z., and Hlavay, J. (2001). The seasonal changes in the concentration of polycyclic aromatic hydrocarbons in precipitation and aerosol near lake balaton, hungary. *Environmental Pollution*, **114**(1), 55–61.
- Kleineidam, S., Rügner, H., Ligouis, B., and Grathwohl, P. (1999). Organic matter facies and equilibrium sorption of phenanthrene. *Environmental Science Technology*, **33**(10), 1637–1644.
- Kleineidam, S., Schüth, C., and Grathwohl, P. (2002). Solubility-normalized combined adsorption-partitioning sorption isotherms for organic pollutants. *Environmental Science Technology*, **36**(21), 4689–4697.
- Kleineidam, S., Rügner, H., and Grathwohl, P. (2004). Desorption kinetics of phenanthrene in aquifer material lacks hysteresis. *Environmental Science Technology*, **38**(15), 4169–4175.
- Klánová, J., Èupr, P., Kohoutek, J., and Harner, T. (2008). Assessing the influence of meteorological parameters on the performance of polyurethane foam-based passive air samplers. *Environmental Science Technology*, **42**(2), 550–555.

- Kobličková, M., Růžičková, P., Čupr, P., Komprda, J., Holoubek, I., and Klánová, J. (2009). Soil burdens of persistent organic pollutants: Their levels, fate, and risks. part iv. quantification of volatilization fluxes of organochlorine pesticides and polychlorinated biphenyls from contaminated soil surfaces. *Environmental Science Technology*, **43**(10), 3588–3595.
- Komprda, J., Komprdova, K., Sanka, M., Mozny, M., and Nizzetto, L. (2013). Influence of climate and land use change on spatially resolved volatilization of persistent organic pollutants (pops) from background soils. *Environ Sci Technol*, **47**(13), 7052–9.
- Kong, S., Ding, X., Bai, Z., Han, B., Chen, L., Shi, J., and Li, Z. (2010). A seasonal study of polycyclic aromatic hydrocarbons in pm2.5 and pm2.5–10 in five typical cities of liaoning province, china. *Journal of Hazardous Materials*, **183**(1), 70–80.
- Kot-Wasik, A., Zabiegala, B., Urbanowicz, M., Dominiak, E., Wasik, A., and Namiesnik, J. (2007). Advances in passive sampling in environmental studies. *Anal Chim Acta*, **602**(2), 141–63.
- Krauss, M., Wilcke, W., and Zech, W. (2000). Polycyclic aromatic hydrocarbons and polychlorinated biphenyls in forest soils: depth distribution as indicator of different fate. *Environmental Pollution*, **110**(1), 79–88.
- Kuppusamy, S., Thavamani, P., Venkateswarlu, K., Lee, Y. B., Naidu, R., and Megharaj, M. (2017). Remediation approaches for polycyclic aromatic hydrocarbons (pahs) contaminated soils: Technological constraints, emerging trends and future directions. *Chemosphere*, **168**, 944–968.
- Kurt-Karakus, P. B., Bidleman, T. F., Staebler, R. M., and Jones, K. C. (2006). Measurement of ddt fluxes from a historically treated agricultural soil in canada. *Environmental Science Technology*, **40**(15), 4578–4585.
- Larsen, R. K. and Baker, J. E. (2003). Source apportionment of polycyclic aromatic hydrocarbons in the urban atmosphere: a comparison of three methods. *Environmental Science Technology*, **37**(9), 1873–1881.
- Lee, J. and Lane, D. A. (2010). Formation of oxidized products from the reaction of gaseous phenanthrene with the oh radical in a reaction chamber. *Atmospheric Environment*, **44**(20), 2469–2477.
- Lee, R. G. M., Hung, H., Mackay, D., and Jones, K. C. (1998). Measurement and modeling of the diurnal cycling of atmospheric pcbs and pahs. *Environmental Science Technology*, **32**(14), 2172–2179.
- Lee, R. G. M., Coleman, P., Jones, J. L., Jones, K. C., and Lohmann, R. (2005). Emission factors and importance of pcdd/fs, pcbs, pcns, pahs and pm10 from the domestic

## References

---

- burning of coal and wood in the u.k. *Environmental Science Technology*, **39**(6), 1436–1447.
- Leister, D. L. and Baker, J. E. (1994). Atmospheric deposition of organic contaminants to the chesapeake bay. *Atmospheric Environment*, **28**(8), 1499–1520.
- Li, P.-h., Wang, Y., Li, Y.-h., Wai, K.-m., Li, H.-l., and Tong, L. (2016). Gas-particle partitioning and precipitation scavenging of polycyclic aromatic hydrocarbons (pahs) in the free troposphere in southern china. *Atmospheric Environment*, **128**, 165–174.
- Liang, J., Fang, H., Wu, L., Zhang, T., and Wang, X. (2016). Characterization, distribution, and source analysis of metals and polycyclic aromatic hydrocarbons (pahs) of atmospheric bulk deposition in shanghai, china. *Water, Air, Soil Pollution*, **227**(7), 234.
- Liu, B., Xue, Z., Zhu, X., and Jia, C. (2017). Long-term trends (1990-2014), health risks, and sources of atmospheric polycyclic aromatic hydrocarbons (pahs) in the u.s. *Environ Pollut*, **220**(Pt B), 1171–1179.
- Liu, F., Xu, Y., Liu, J., Liu, D., Li, J., Zhang, G., Li, X., Zou, S., and Lai, S. (2013a). Atmospheric deposition of polycyclic aromatic hydrocarbons (pahs) to a coastal site of hong kong, south china. *Atmospheric Environment*, **69**, 265–272.
- Liu, J., Li, J., Lin, T., Liu, D., Xu, Y., Chaemfa, C., Qi, S., Liu, F., and Zhang, G. (2013b). Diurnal and nocturnal variations of pahs in the lhasa atmosphere, tibetan plateau: Implication for local sources and the impact of atmospheric degradation processing. *Atmospheric Research*, **124**, 34–43.
- Liu, L.-Y., Kukučka, P., Venier, M., Salamova, A., Klánová, J., and Hites, R. A. (2014). Differences in spatiotemporal variations of atmospheric pah levels between north america and europe: Data from two air monitoring projects. *Environment International*, **64**, 48–55.
- Liu, Y., Wang, S., McDonough, C. A., Khairy, M., Muir, D. C. G., Helm, P. A., and Lohmann, R. (2016). Gaseous and freely-dissolved pcbs in the lower great lakes based on passive sampling: Spatial trends and air–water exchange. *Environmental Science Technology*, **50**(10), 4932–4939.
- Lohmann, R. (2012). Critical review of low-density polyethylene’s partitioning and diffusion coefficients for trace organic contaminants and implications for its use as a passive sampler. *Environ Sci Technol*, **46**(2), 606–18.
- Lohmann, R. and Lammel, G. (2004). Adsorptive and absorptive contributions to the gas-particle partitioning of polycyclic aromatic hydrocarbons: state of knowledge and recommended parametrization for modeling. *Environmental Science Technology*, **38**(14), 3793–3803.

- Lohmann, R., Corrigan, B. P., Howsam, M., Jones, K. C., and Ockenden, W. A. (2001). Further developments in the use of semipermeable membrane devices (spmds) as passive air samplers for persistent organic pollutants: field application in a spatial survey of pcdd/fs and pahs. *Environmental Science Technology*, **35**(12), 2576–2582.
- Lohmann, R., Dapsis, M., Morgan, E. J., Dekany, V., and Luey, P. J. (2011). Determining air-water exchange, spatial and temporal trends of freely dissolved pahs in an urban estuary using passive polyethylene samplers. *Environ Sci Technol*, **45**(7), 2655–62.
- Lu, Y. and Pignatello, J. J. (2002). Demonstration of the “conditioning effect” in soil organic matter in support of a pore deformation mechanism for sorption hysteresis. *Environmental Science Technology*, **36**(21), 4553–4561.
- Luo, X., Zheng, Y., Lin, Z., Wu, B., Han, F., Tian, Y., Zhang, W., and Wang, X. (2015). Evaluating potential non-point source loading of pahs from contaminated soils: A fugacity-based modeling approach. *Environmental Pollution*, **196**, 1–11.
- Luthy, R. G., Aiken, G. R., Brusseau, M. L., Cunningham, S. D., Gschwend, P. M., Pignatello, J. J., Reinhard, M., Traina, S. J., Weber, W. J., and Westall, J. C. (1997). Sequestration of hydrophobic organic contaminants by geosorbents. *Environmental Science Technology*, **31**(12), 3341–3347.
- Madelener, Iris; Henzler, R. G. P. (????). Material investigations to determine the leaching behaviour of pahs at elevated temperatures. In P. G. Dietrich Halm, editor, *International Workshop on Groundwater Risk Assessment at Contaminated Sites (GRACOS) and Integrated Soil and Water Protection (SOWA)*, pages 193–198.
- Mandalakis, M., Tsapakis, M., Tsoga, A., and Stephanou, E. G. (2002). Gas-particle concentrations and distribution of aliphatic hydrocarbons, pahs, pcbs and pcdd/fs in the atmosphere of athens (greece). *Atmospheric Environment*, **36**(25), 4023–4035.
- Mantis, J., Chaloulakou, A., and Samara, C. (2005). Pm10-bound polycyclic aromatic hydrocarbons (pahs) in the greater area of athens, greece. *Chemosphere*, **59**(5), 593–604.
- Marino, F., Cecinato, A., and Siskos, P. A. (2000). Nitro-pah in ambient particulate matter in the atmosphere of athens. *Chemosphere*, **40**(5), 533–537.
- Martin, H. (2000). Development of passive samplers for time-integrated deposition and groundwater monitoring: Adsorption cartridges and ceramic dosimeters. *Tübinger Geowissenschaftliche Arbeiten (TGA), Reihe C, Hydro- Ingenieur- und Umweltgeologie*, **56**.
- Masih, A., Masih, J., and Taneja, A. (2012a). Study of air-soil exchange of polycyclic aromatic hydrocarbons (pahs) in the north-central part of india – a semi arid region. *Journal of Environmental Monitoring*, **14**(1), 172–180.

## References

---

- Masih, J., Singhvi, R., Taneja, A., Kumar, K., and Masih, H. (2012b). Gaseous/particulate bound polycyclic aromatic hydrocarbons (pahs), seasonal variation in north central part of rural india. *Sustainable Cities and Society*, **3**, 30–36.
- Mayer, P., Tolls, J., L M Hermens, J., and Mackay, D. (2003). *Equilibrium sampling devices*, volume 37.
- Mayer, P., Parkerton, T. F., Adams, R. G., Cargill, J. G., Gan, J., Gouin, T., Gschwend, P. M., Hawthorne, S. B., Helm, P., Witt, G., You, J., and Escher, B. I. (2014). Passive sampling methods for contaminated sediments: scientific rationale supporting use of freely dissolved concentrations. *Integr Environ Assess Manag*, **10**(2), 197–209.
- McLachlan, M. S. and Horstmann, M. (1998). Forests as filters of airborne organic pollutants: a model. *Environmental Science Technology*, **32**(3), 413–420.
- Meijer, S. N., Shoeib, M., Jantunen, L. M. M., Jones, K. C., and Harner, T. (2003). Air-soil exchange of organochlorine pesticides in agricultural soils. 1. field measurements using a novel in situ sampling device. *Environmental Science Technology*, **37**(7), 1292–1299.
- Melymuk, L., Robson, M., Helm, P. A., and Diamond, M. L. (2011). Evaluation of passive air sampler calibrations: Selection of sampling rates and implications for the measurement of persistent organic pollutants in air. *Atmospheric Environment*, **45**(10), 1867–1875.
- Moeckel, C., Harner, T., Nizzetto, L., Strandberg, B., Lindroth, A., and Jones, K. C. (2009). Use of depuration compounds in passive air samplers: Results from active sampling-supported field deployment, potential uses, and recommendations. *Environmental Science Technology*, **43**(9), 3227–3232.
- Morgan, E. J. and Lohmann, R. (2008). Detecting air-water and surface-deep water gradients of pcbs using polyethylene passive samplers. *Environ Sci Technol*, **42**(19), 7248–53.
- Mostert, M., Ayoko, G., and Kokot, S. (2010). Application of chemometrics to analysis of soil pollutants. *Trends in Analytical Chemistry*, **29**(5), 430–445.
- Motelay-Massei, A., Ollivon, D., Garban, B., Tiphagne-Larcher, K., Zimmerlin, I., and Chevreuil, M. (2007). Pahs in the bulk atmospheric deposition of the seine river basin: Source identification and apportionment by ratios, multivariate statistical techniques and scanning electron microscopy. *Chemosphere*, **67**(2), 312–321.
- Mäenpää, K., Leppänen, M. T., Reichenberg, F., Figueiredo, K., and Mayer, P. (2011). Equilibrium sampling of persistent and bioaccumulative compounds in soil and sediment: Comparison of two approaches to determine equilibrium partitioning concentrations in lipids. *Environmental Science Technology*, **45**(3), 1041–1047.

- Nguyen, T. N. T., Jung, K.-S., Son, J. M., Kwon, H.-O., and Choi, S.-D. (2018). Seasonal variation, phase distribution, and source identification of atmospheric polycyclic aromatic hydrocarbons at a semi-rural site in ulsan, south korea. Environmental Pollution, **236**, 529–539.
- Niehus, N. C., Schafer, S., Mohlenkamp, C., and Witt, G. (2018). Equilibrium sampling of hocs in sediments and suspended particulate matter of the elbe river. Environ Sci Eur, **30**(1), 28.
- Niehus, N. C., Brockmeyer, B., and Witt, G. (2019). Bioavailability and distribution of pahs and pcbs in the sediment pore water of the german bight and wadden sea. Marine Pollution Bulletin, **138**, 421–427.
- Offenberg, J. H. and Baker, J. E. (2002). Precipitation scavenging of polychlorinated biphenyls and polycyclic aromatic hydrocarbons along an urban to over-water transect. Environmental Science Technology, **36**(17), 3763–3771.
- Pan, B., Xing, B., Tao, S., Liu, W., Lin, X., Xiao, Y., Dai, H., Zhang, X., Zhang, Y., and Yuan, H. (2007). Effect of physical forms of soil organic matter on phenanthrene sorption. Chemosphere, **68**(7), 1262–1269.
- Pankow, J. F. (1987). Review and comparative analysis of the theories on partitioning between the gas and aerosol particulate phases in the atmosphere. Atmospheric Environment (1967), **21**(11), 2275–2283.
- Peng, C., Wang, M., and Chen, W. (2016). Spatial analysis of pahs in soils along an urban–suburban–rural gradient: scale effect, distribution patterns, diffusion and influencing factors. Scientific Reports, **6**, 37185.
- Pies, C., Hoffmann, B., Petrowsky, J., Yang, Y., Ternes, T. A., and Hofmann, T. (2008). Characterization and source identification of polycyclic aromatic hydrocarbons (pahs) in river bank soils. Chemosphere, **72**(10), 1594–1601.
- Poerschmann, J., Zhang, Z., Kopinke, F.-D., and Pawliszyn, J. (1997). Solid phase microextraction for determining the distribution of chemicals in aqueous matrices. Analytical Chemistry, **69**(4), 597–600.
- Pozo, K., Harner, T., Lee, S. C., Wania, F., Muir, D. C. G., and Jones, K. C. (2009). Seasonally resolved concentrations of persistent organic pollutants in the global atmosphere from the first year of the gaps study. Environmental Science Technology, **43**(3), 796–803.
- Prevedouros, K., Brorström-Lundén, E., J. Halsall, C., Jones, K. C., Lee, R. G. M., and Sweetman, A. J. (2004). Seasonal and long-term trends in atmospheric pah concentrations: evidence and implications. Environmental Pollution, **128**(1), 17–27.

## References

---

- Qu, C., Albanese, S., Lima, A., Hope, D., Pond, P., Fortelli, A., Romano, N., Cerino, P., Pizzolante, A., and De Vivo, B. (2019). The occurrence of ocps, pcbs, and pahs in the soil, air, and bulk deposition of the naples metropolitan area, southern italy: Implications for sources and environmental processes. Environment International, **124**, 89–97.
- Ran, Y., Sun, K., Ma, X., Wang, G., Grathwohl, P., and Zeng, E. Y. (2007). Effect of condensed organic matter on solvent extraction and aqueous leaching of polycyclic aromatic hydrocarbons in soils and sediments. Environmental Pollution, **148**(2), 529–538.
- Ravindra, K., Sokhi, R., and Van Grieken, R. (2008a). Atmospheric polycyclic aromatic hydrocarbons: Source attribution, emission factors and regulation. Atmospheric Environment, **42**(13), 2895–2921.
- Ravindra, K., Wauters, E., and Van Grieken, R. (2008b). Variation in particulate pahs levels and their relation with the transboundary movement of the air masses. Science of The Total Environment, **396**(2), 100–110.
- Razzaque, M. M. and Grathwohl, P. (2008). Predicting organic carbon–water partitioning of hydrophobic organic chemicals in soils and sediments based on water solubility. Water Research, **42**(14), 3775–3780.
- Reichenberg, F. and Mayer, P. (2006). Two complementary sides of bioavailability: Accessibility and chemical activity of organic contaminants in sediments and soils. Environmental Toxicology and Chemistry, **25**(5), 1239–1245.
- Reichenberg, F., Smedes, F., Jonsson, J. A., and Mayer, P. (2008). Determining the chemical activity of hydrophobic organic compounds in soil using polymer coated vials. Chem Cent J, **2**, 8.
- Ren, J., Wang, X. P., Gong, P., and Wang, C. (2019). Characterization of tibetan soil as a source or sink of atmospheric persistent organic pollutants: Seasonal shift and impact of global warming. Environ Sci Technol.
- Ribes, S., Van Drooge, B., Dachs, J., Gustafsson, , and Grimalt, J. O. (2003). Influence of soot carbon on the soilair partitioning of polycyclic aromatic hydrocarbons. Environmental Science Technology, **37**(12), 2675–2680.
- Ringuet, J., Albinet, A., Leoz-Garziandia, E., Budzinski, H., and Villenave, E. (2012). Reactivity of polycyclic aromatic compounds (pahs, npahs and opahs) adsorbed on natural aerosol particles exposed to atmospheric oxidants. Atmospheric Environment, **61**, 15–22.



- Rogge, W. F., Hildemann, L. M., Mazurek, M. A., Cass, G. R., and Simoneit, B. R. T. (1993). Sources of fine organic aerosol. 2. noncatalyst and catalyst-equipped automobiles and heavy-duty diesel trucks. *Environmental Science Technology*, **27**(4), 636–651.
- Roux, M. V., Temprado, M., Chickos, J. S., and Nagano, Y. (2008). Critically evaluated thermochemical properties of polycyclic aromatic hydrocarbons. *Journal of Physical and Chemical Reference Data*, **37**(4), 1855.
- Rusina, T. P., Smedes, F., Klanova, J., Booiij, K., and Holoubek, I. (2007). Polymer selection for passive sampling: a comparison of critical properties. *Chemosphere*, **68**(7), 1344–51.
- Rusina, T. P., Smedes, F., and Klanova, J. (2010). Diffusion coefficients of polychlorinated biphenyls and polycyclic aromatic hydrocarbons in polydimethylsiloxane and low-density polyethylene polymers. *Journal of Applied Polymer Science*, pages NA–NA.
- Sanders, G., Jones, K. C., Hamilton-Taylor, J., and Dorr, H. (1993). Concentrations and deposition fluxes of polynuclear aromatic hydrocarbons and heavy metals in the dated sediments of a rural english lake. *Environmental Toxicology and Chemistry*, **12**(9), 1567–1581.
- Sartori, F., Wade, T. L., Sericano, J. L., Mohanty, B. P., and Smith, K. A. (2010). Polycyclic aromatic hydrocarbons in soil of the canadian river floodplain in oklahoma. *J Environ Qual*, **39**(2), 568–79.
- Schifman, L. A. and Boving, T. B. (2015). Spatial and seasonal atmospheric pah deposition patterns and sources in rhode island. *Atmospheric Environment*, **120**, 253–261.
- Schlebaum, W., Badora, A., and Schraa, G. (1998). Interactions between a hydrophobic organic chemical and natural organic matter: equilibrium and kinetic studies. *Environmental Science Technology*, **32**(15), 2273–2277.
- Schwarz, K., Gocht, T., and Grathwohl, P. (2011). Transport of polycyclic aromatic hydrocarbons in highly vulnerable karst systems. *Environ Pollut*, **159**(1), 133–139.
- Seethapathy, S. and Górecki, T. (2012). Applications of polydimethylsiloxane in analytical chemistry: A review. *Analytica Chimica Acta*, **750**, 48–62.
- Seethapathy, S., Gorecki, T., and Li, X. (2008). Passive sampling in environmental analysis. *J Chromatogr A*, **1184**(1-2), 234–53.
- Seidensticker, S., Zarfl, C., Cirpka, O. A., Fellenberg, G., and Grathwohl, P. (2017). Shift in mass transfer of wastewater contaminants from microplastics in the presence of dissolved substances. *Environmental Science Technology*, **51**(21), 12254–12263.

## References

---

- Shoeib, M. and Harner, T. (2002). Using measured octanol-air partition coefficients to explain environmental partitioning of organochlorine pesticides. Environmental Toxicology and Chemistry, **21**(5), 984–990.
- Shoeib, Mahiba; Harner, T. (2002). Characterization and comparison of three passive air samplers persistent organic pollutants. Environ. Sci. Technol., **36**(19), 4142–4151.
- Simpson, C. D., Mosi, A. A., Cullen, W. R., and Reimer, K. J. (1996). Composition and distribution of polycyclic aromatic hydrocarbon contamination in surficial marine sediments from kitimat harbor, canada. Science of The Total Environment, **181**(3), 265–278.
- Singh, K. P., Malik, A., Kumar, R., Saxena, P., and Sinha, S. (2008). Receptor modeling for source apportionment of polycyclic aromatic hydrocarbons in urban atmosphere. Environmental Monitoring and Assessment, **136**(1), 183–196.
- Smedes, F., Geertsma, R. W., Zande, T. v. d., and Booij, K. (2009). Polymerwater partition coefficients of hydrophobic compounds for passive sampling: Application of cosolvent models for validation. Environmental Science Technology, **43**(18), 7047–7054.
- Smedes, F., van Vliet, L. A., and Booij, K. (2013). Multi-ratio equilibrium passive sampling method to estimate accessible and pore water concentrations of polycyclic aromatic hydrocarbons and polychlorinated biphenyls in sediment. Environmental Science Technology, **47**(1), 510–517.
- Sobek, A., Arp, H. P. H., Wiberg, K., Hedman, J., and Cornelissen, G. (2013). Aerosol–water distribution of pcdd/fs and pcbs in the baltic sea region. Environmental Science Technology, **47**(2), 781–789.
- Sobek, A., Wiberg, K., Sundqvist, K. L., Haglund, P., Jonsson, P., and Cornelissen, G. (2014). Coastal sediments in the gulf of bothnia as a source of dissolved pcdd/fs and pcbs to water and fish. Science of The Total Environment, **487**, 463–470.
- Soclo, H. H., Garrigues, P., and Ewald, M. (2000). Origin of polycyclic aromatic hydrocarbons (pahs) in coastal marine sediments: Case studies in cotonou (benin) and aquitaine (france) areas. Marine Pollution Bulletin, **40**(5), 387–396.
- Sun, H.-W., Li, Jun-Guo Availability of pyrene in unaged and aged soils to earthworm uptake, butanol extraction and sfe. **166**(1), 353–365.
- Söderström, H. S. and Bergqvist, P.-A. (2004). Passive air sampling using semipermeable membrane devices at different wind-speeds in situ calibrated by performance reference compounds. Environmental Science Technology, **38**(18), 4828–4834.

- Tasdemir, Y., Salihoglu, G., Salihoglu, N. K., and Birgül, A. (2012). Air–soil exchange of pcbs: Seasonal variations in levels and fluxes with influence of equilibrium conditions. *Environmental Pollution*, **169**, 90–97.
- ten Hulscher, T. E. M. and Cornelissen, G. (1996). Effect of temperature on sorption equilibrium and sorption kinetics of organic micropollutants - a review. *Chemosphere*, **32**(4), 609–626.
- Terzaghi, E., Scacchi, M., Cerabolini, B., Jones, K. C., and Di Guardo, A. (2015). Estimation of polycyclic aromatic hydrocarbon variability in air using high volume, film, and vegetation as samplers. *Environ Sci Technol*, **49**(9), 5520–8.
- Thomas, G., Sweetman, A. J., Ockenden, W. A., Mackay, D., and Jones, K. C. (1998). Airpasture transfer of pcbs. *Environmental Science Technology*, **32**(7), 936–942.
- Tian, F., Chen, J., Qiao, X., Wang, Z., Yang, P., Wang, D., and Ge, L. (2009). Sources and seasonal variation of atmospheric polycyclic aromatic hydrocarbons in dalian, china: Factor analysis with non-negative constraints combined with local source fingerprints. *Atmospheric Environment*, **43**(17), 2747–2753.
- Tobiszewski, M. and Namieśnik, J. (2012). Pah diagnostic ratios for the identification of pollution emission sources. *Environmental Pollution*, **162**, 110–119.
- Tomaszewski, J. E. and Luthy, R. G. (2008). Field deployment of polyethylene devices to measure pcb concentrations in pore water of contaminated sediment. *Environ. Sci. Technol.*, **42**(16), 6086–6091.
- Trapido, M. (1999). Polycyclic aromatic hydrocarbons in estonian soil: contamination and profiles. *Environmental Pollution*, **105**(1), 67–74.
- Tuduri, L., Millet, M., Briand, O., and Montury, M. (2012). Passive air sampling of semi-volatile organic compounds. *TrAC Trends in Analytical Chemistry*, **31**, 38–49.
- Valerio, F. and Lazzarotto, A. (1985). Photochemical degradation of polycyclic aromatic hydrocarbons (pah) in real and laboratory conditions. *Int J Environ Anal Chem*, **23**(1-2), 135–51.
- Venier, M., Salamova, A., and Hites, R. A. (2016). Temporal trends of persistent organic pollutant concentrations in precipitation around the great lakes. *Environmental Pollution*, **217**, 143–148.
- Verma, P. K., Sah, D., Kumari, K. M., and Lakhani, A. (2017). Atmospheric concentrations and gas–particle partitioning of polycyclic aromatic hydrocarbons (pahs) and nitro-pahs at indo-gangetic sites. *Environmental Science: Processes Impacts*, **19**(8), 1051–1060.

## References

---

- Vrana, B. and Schüürmann, G. (2002). Calibrating the uptake kinetics of semipermeable membrane devices in water: impact of hydrodynamics. Environmental Science Technology, **36**(2), 290–296.
- Vrana, B., Allan, I. J., Greenwood, R., Mills, G. A., Dominiak, E., Svensson, K., Knutsson, J., and Morrison, G. (2005). Passive sampling techniques for monitoring pollutants in water. TrAC Trends in Analytical Chemistry, **24**(10), 845–868.
- Wang, C., Wang, X., Gong, P., and Yao, T. (2014). Polycyclic aromatic hydrocarbons in surface soil across the tibetan plateau: Spatial distribution, source and air–soil exchange. Environmental Pollution, **184**, 138–144.
- Wang, C., Wang, X., Ren, J., Gong, P., and Yao, T. (2017). Using a passive air sampler to monitor air–soil exchange of organochlorine pesticides in the pasture of the central tibetan plateau. Science of The Total Environment, **580**, 958–965.
- Wang, D., Yates, S. R., and Ernst, F. F. (1997). Calibration and testing of a dynamic flow-through chamber for field determination of methyl bromide volatilization flux. Atmospheric Environment, **31**(24), 4119–4123.
- Wang, G. and Grathwohl, P. (2009). Activation energies of phenanthrene desorption from carbonaceous materials: Column studies. Journal of Hydrology, **369**(3), 234–240.
- Wang, G., Kleineidam, S., and Grathwohl, P. (2007a). Sorption/desorption reversibility of phenanthrene in soils and carbonaceous materials. Environmental Science Technology, **41**(4), 1186–1193.
- Wang, L., Atkinson, R., and Arey, J. (2007b). Formation of 9,10-phenanthrenequinone by atmospheric gas-phase reactions of phenanthrene. Atmospheric Environment, **41**(10), 2025–2035.
- Wang, Q., Liu, M., Li, Y., Liu, Y., Li, S., and Ge, R. (2016). Dry and wet deposition of polycyclic aromatic hydrocarbons and comparison with typical media in urban system of shanghai, china. Atmospheric Environment, **144**, 175–181.
- Wang, R., Wang, Y., Li, H., Yang, M., Sun, L., Wang, T., and Wang, W. (2015a). Cloud deposition of pahs at mount lushan in southern china. Science of The Total Environment, **526**, 329–337.
- Wang, R., Liu, G., and Zhang, J. (2015b). Variations of emission characterization of pahs emitted from different utility boilers of coal-fired power plants and risk assessment related to atmospheric pahs. Sci Total Environ, **538**, 180–90.

- Wang, Y., Luo, C., Wang, S., Liu, J., Pan, S., Li, J., Ming, L., Zhang, G., and Li, X. (2015c). Assessment of the air–soil partitioning of polycyclic aromatic hydrocarbons in a paddy field using a modified fugacity sampler. Environmental Science Technology, **49**(1), 284–291.
- Wania, F., Haugen, J.-E., Lei, Y. D., and Mackay, D. (1998). Temperature dependence of atmospheric concentrations of semivolatile organic compounds. Environmental Science Technology, **32**(8), 1013–1021.
- Wania, F., Shen, L., Lei, Y. D., Teixeira, C., and Muir, D. C. G. (2003). Development and calibration of a resin-based passive sampling system for monitoring persistent organic pollutants in the atmosphere. Environmental Science Technology, **37**(7), 1352–1359.
- Weber, W. J. and Huang, W. (1996). A distributed reactivity model for sorption by soils and sediments. 4. intraparticle heterogeneity and phase-distribution relationships under nonequilibrium conditions. Environmental Science Technology, **30**(3), 881–888.
- Whitman, W. G. (1962). The two film theory of gas absorption. International Journal of Heat and Mass Transfer, **5**(5), 429–433.
- Wijayaratne, R. D. and Means, J. C. (1984). Sorption of polycyclic aromatic hydrocarbons by natural estuarine colloids. Marine Environmental Research, **11**(2), 77–89.
- Wilcke, W. (2000a). Synopsis polycyclic aromatic hydrocarbons (pahs) in soil — a review. Journal of Plant Nutrition and Soil Science, **163**(3), 229–248.
- Wilcke, Wolfgang; Amelung, W. (2000b). Persistent organic pollutants in native grassland soils along a climosquenz in north america. Soil Sci. Soc. Am. J., **64**.
- Wild, S. R. and Jones, K. C. (1995). Polynuclear aromatic hydrocarbons in the united kingdom environment: A preliminary source inventory and budget. Environmental Pollution, **88**(1), 91–108.
- Witt, G., Lang, S.-C., Ullmann, D., Schaffrath, G., Schulz-Bull, D., and Mayer, P. (2013). Passive equilibrium sampler for in situ measurements of freely dissolved concentrations of hydrophobic organic chemicals in sediments. Environmental Science Technology, **47**(14), 7830–7839.
- Wong, F., Harner, T., Liu, Q. T., and Diamond, M. L. (2004). Using experimental and forest soils to investigate the uptake of polycyclic aromatic hydrocarbons (pahs) along an urban-rural gradient. Environ Pollut, **129**(3), 387–98.
- Wu, S. C. and Gschwend, P. M. (1986). Sorption kinetics of hydrophobic organic compounds to natural sediments and soils. Environmental Science Technology, **20**(7), 717–725.

## References

---

- Wu, S.-P., Wang, X.-H., Yan, J.-M., Zhang, M.-M., and Hong, H.-S. (2010). Diurnal variations of particle-bound pahs at a traffic site in xiamen, china. Aerosol and Air Quality Research, **10**(5), 497–506.
- Xia, G. and Pignatello, J. J. (2001). Detailed sorption isotherms of polar and apolar compounds in a high-organic soil. Environmental Science Technology, **35**(1), 84–94.
- Xiao, H. and Wania, F. (2003). Is vapor pressure or the octanol–air partition coefficient a better descriptor of the partitioning between gas phase and organic matter? Atmospheric Environment, **37**(20), 2867–2878.
- Xing, B. and Pignatello, J. J. (1997). Dual-mode sorption of low-polarity compounds in glassy poly(vinyl chloride) and soil organic matter. Environmental Science Technology, **31**(3), 792–799.
- Yan, L., Li, X., Chen, J., Wang, X., Du, J., and Ma, L. (2012). Source and deposition of polycyclic aromatic hydrocarbons to shanghai, china. Journal of Environmental Sciences, **24**(1), 116–123.
- Yang, Y. and Hofmann, T. (2009). Aqueous accelerated solvent extraction of native polycyclic aromatic hydrocarbons (pahs) from carbonaceous river floodplain soils. Environmental Pollution, **157**(10), 2604–2609.
- Yang, Y., Hofmann, T., Pies, C., and Grathwohl, P. (2008). Sorption of polycyclic aromatic hydrocarbons (pahs) to carbonaceous materials in a river floodplain soil. Environmental Pollution, **156**(3), 1357–1363.
- Yang, Y., Tao, S., Zhang, N., Zhang, D. Y., and Li, X. Q. (2010a). The effect of soil organic matter on fate of polycyclic aromatic hydrocarbons in soil: A microcosm study. Environmental Pollution, **158**(5), 1768–1774.
- Yang, Y., Zhang, N., Xue, M., and Tao, S. (2010b). Impact of soil organic matter on the distribution of polycyclic aromatic hydrocarbons (pahs) in soils. Environmental Pollution, **158**(6), 2170–2174.
- Yunker, M. B., Macdonald, R. W., Vingarzan, R., Mitchell, R. H., Goyette, D., and Sylvestre, S. (2002). Pahs in the fraser river basin: a critical appraisal of pah ratios as indicators of pah source and composition. Organic Geochemistry, **33**(4), 489–515.
- Zhang, Y. and Tao, S. (2009). Global atmospheric emission inventory of polycyclic aromatic hydrocarbons (pahs) for 2004. Atmospheric Environment, **43**(4), 812–819.
- Zhang, Y., Deng, S., Liu, Y., Shen, G., Li, X., Cao, J., Wang, X., Reid, B., and Tao, S. (2011). A passive air sampler for characterizing the vertical concentration profile of gaseous phase polycyclic aromatic hydrocarbons in near soil surface air. Environmental Pollution, **159**(3), 694–699.

- Zhou, Z., Sun, H., and Zhang, W. (2010). Desorption of polycyclic aromatic hydrocarbons from aged and unaged charcoals with and without modification of humic acids. *Environ Pollut*, **158**(5), 1916–21.
- Zou, Y., Wang, L., and Christensen, E. R. (2015). Problems in the fingerprints based polycyclic aromatic hydrocarbons source apportionment analysis and a practical solution. *Environmental Pollution*, **205**, 394–402.
- Škrdlíková, L., Landlová, L., Klánová, J., and Lammel, G. (2011). Wet deposition and scavenging efficiency of gaseous and particulate phase polycyclic aromatic compounds at a central european suburban site. *Atmospheric Environment*, **45**(25), 4305–4312.